2009

Multicomponent Interdiffusion In Austenitic Ni-, Fe-ni-base Alloys And L12-ni3al Intermetallic For High-temperature Applications

Narayana Garimella
University of Central Florida

MULTICOMPONENT INTERDIFFUSION IN AUSTENITIC NI-, FE-NI-BASE ALLOYS AND $L1_2$-NI_3AL INTERMETALLIC FOR HIGH-TEMPERATURE APPLICATIONS

by

NARAYANA GARIMELLA
M.Tech., Banaras Hindu University, Varanasi, India. 2003
M.S., University of Central Florida, Orlando, USA, 2007

A dissertation submitted in partial fulfillment of the requirements
for the degree of Doctor of Philosophy
in the Department of Mechanical, Materials and Aerospace Engineering
in the College of Engineering and Computer Science
at the University of Central Florida
Orlando, Florida

Spring Term
2009

Major Professor: Yong-Ho Sohn

ABSTRACT

Interdiffusion in multicomponent-multiphase alloys is commonly encountered in many materials systems. The developments of multicomponent-multiphase alloys require control of microstructure through appropriate heat treatment, involving solid-state transformations, precipitation processes, and surface modification, where the interdiffusion processes play a major role. In addition, interdiffusion processes often control degradation and failure of these materials systems. Enhanced performance and reliable durability always requires a detailed understanding of interdiffusion.

In this study, ternary and quaternary interdiffusion in Ni-Cr-X (X = Al, Si, Ge, Pd) at 900°C and 700°C, Fe-Ni-Cr-X (X = Si, Ge) at 900°C, and Ni_3Al alloyed with Ir, Ta and Re at 1200°C were examined using solid-to-solid diffusion couples. Interdiffusion fluxes of individual components were calculated directly from experimental concentration profiles determined by electron probe microanalysis. Moments of interdiffusion fluxes were examined to calculate main and cross interdiffusion coefficients averaged over selected composition ranges from single diffusion couple experiments. Consistency in the magnitude and sign of ternary and quaternary interdiffusion coefficient were verified with interdiffusion coefficients determined by Boltzmann-Matano analysis that requires multiple diffusion couples with intersecting compositions. Effects of alloying additions, Al, Si, Ge and Pd, on the interdiffusion in Ni-Cr-X and Fe-Ni-Cr-X alloys were examined with respect to Cr_2O_3-forming ability at high temperature. Effects of Ir, Ta and Re additions on interdiffusion in Ni_3Al were examined with respect to phase stability and site-preference.

In addition, a numerically refined approach to determine average ternary interdiffusion

coefficients were developed. Concentrations and moments of interdiffusion fluxes are employed to generate multiple combinations of multicomponent interdiffusion coefficient as a function of moments. The matrix of multicomponent interdiffusion coefficients corresponds to the lowest order of the moment. It yields real and positive eigen values which provides reliable average interdiffusion coefficients for the selected composition range.

ACKNOWLEDGMENTS

I would like to express my sincere thanks to Dr. Yong-Ho Sohn, my major advisor, for his guidance and helpful discussions. It is a great privilege to work under such an expert with multitude of abilities and innovative ideas. He bears himself with the essence of profound knowledge. I highly appreciate his positive motivation and also for introducing me the concepts of thermal barrier coatings and interdiffusion before my joining in UCF. His way of teaching courses cares even the esthetics of the subject and will remain a great deal of inerasable image on the board of my memory.

Grateful appreciation is extended to my committee members:

Dr. Michael P. Brady: For providing Ni and Fe base alloys and for guiding me through emails and phone calls with complete details of information. His motivation will be remembered forever.

Dr. C. Suryanaryana: For his initial cooperation of my dream to pursue PhD. Several times, his valuable suggestions helped me in concentrating the progress of my track. His way of teaching Physical Metallurgy served a great foundation of my thinking in that subject.

Dr. Kevin Coffey: For valuable discussions about thermodynamics and kinetics of materials. Also, his teaching about trouble shooting vacuum-encapsulation system was memorable.

Dr. Helge Heinrich: For nurturing my understanding of scientific and technical part of TEM, it helped me several ways in terms of crystallography, electron diffraction and EBSD pattern analysis.

I am also grateful to National Science Foundation for funding my research. Additionally, I express sincere thanks to NIMS and Kobe Steel of Japan for providing me with the exciting project in dealing with ordered solid solution.

My current and past group members of ETMF and MCEE have all been great cooperation of my research works and in sharing several ideas. Thanks to Sreeni, Barb, Balaji, Jing and Sankar for their initial receiving and for introducing research activities. Thanks to Abby for familiarizing me with interdiffusion through the fundamentals of Matlab programming. Thanks to Manny and Travis for their help with experimental and characterization works. Thanks to Prabhakar, Mohanty and Ashley for providing help and inspiration in one or the other ways. Thanks to Carmen and Clara for their help in scanning and arranging images.

I would like to thank MCF personnel: Dr. Helge Heinrich, Mr. Kirk Scammon, Mr. Mikhail Klimov and Mr. Zia Ur Rahman for their help with materials characterization techniques. Thanks to Ms. Kari Stiles, Ms. Karen Glidewell and Ms. Cindy Harle for their help with administrative works during several times. Also, I am thankful to Ms. Jeanine Clements and Ms. Waheeda Illasarie for their administrative help during initial days.

I am highly grateful to Prof. G.V.S. Sastry for his inspiration and permission to achieve the dream of PhD. Also, I am grateful to the faculty of Metallurgical Engineering Department of Banaras Hindu University for their great encouragement of questioning and answering conversations during class and conference talks.

Teachers, classmate-friends and seniors during my Polytechnic days; Ambarnath friends during my GATE days; scientists and friends during DMRL experience, Koti and Satya along with IIT-Powai atmosphere during my undergraduate studies served a great deal of motivation in inspiring my studies and career.

The greatest cooperation and support provided by the personnel of Jhagadia Copper Limited: Mr. P.K. Sinha, Mr. Dinesh Patel, Mr. Viral Shah, Ms. Divya Pande and other staff are highly appreciated. I thank Prof. K. Baba Pai of M.S. University and Prof. B.S. Murthy of IIT-Chennai for nurturing me with career objectives during my undergraduate studies.

I would like to thank my family members for their great support and continuous motivation. They kindly allowed me to have my life as my own laboratory. My father 'Sri. Butchi Babu' and mother 'Smt. Sujata' for their inspiration to love the hard-work and teaching inspired me to proceed with care in doing things. My siblings (& families): Bhavani, Ramani and Ravi for their everlasting support and care during important times of my life and also, for their mingling with Bindu and making her as part of our association.

I am indebted to my wife Bindu, for her unconditional affection, everlasting smile and positive attitude. She successfully spent the time in pursuing MS degree. Her multiple roles in my life as friend, minister and soldier are highly appreciated. Appreciation goes to her parents for their great belief in higher studies.

Several people, including: Sri. Dhavala Lakshmi Narayana, Sri. D.V. Ramana and Sri D. Venugopala Rao and their families and so many well-wishers are behind the cheers and climbing in my way of life.

Finally, I thank all of my friends in the names of roommates, colleagues and well-wishers in Orlando. Group (Ravi/Sridhar/Balram/Vijay/Kedar/Anand/Shankar/Prabhakar), Anant, Dhaval, Sachin(s), Samar, Nidhi, Madhu and Dr. Dommeti are few to be mentioned among that complete list.

This thesis is dedicated to:

My First Teachers (Parents)

Teachers in: School, College, Industrial, University Experiences and

Teachers in: Friends, Society and in Nature.

TABLE OF CONTENTS

LIST OF FIGURES

LIST OF TABLES

CHAPTER 1: INTRODUCTION

Commercially important materials for sustaining applications consist of multicomponent systems, and it is important to understand the interactions among all components with diffusional and thermodynamic considerations. Atomic transport process's in multicomponent systems are commonly observed phenomena in various materials applications including solid-state phase transformations, oxidation, bonding, coatings, electronic packaging, etc. Multicomponent diffusion is defined [1] as the transport process, which occurs when the interdiffusion flux of a component is influenced by the concentration gradient of all independent components.

The phenomenological description of multicomponent diffusion can be expressed by Onsager's formalism [2-4], and is the important basis for experimental investigation of multicomponent systems. Experimental diffusion studies for isothermal conditions may enable the determination of interdiffusion coefficients, intrinsic diffusion coefficients, atomic mobilities and vacancy wind parameters. The Boltzmann-Matano analysis [5,6] employs independent interdiffusion couple experiments for a multicomponent system to determine interdiffusion coefficients at the intersecting composition of compositional diffusion paths. Dayananda and coworkers [7-12] developed a direct method to determine interdiffusion flux of individual components from experimental concentration profiles without the need of interdiffusion coefficients. This method paved way for a new analysis [13] to determine average interdiffusion coefficients for selected composition ranges from the single diffusion couple experiments. Numerous interdiffusion studies made use of these methods to analyze experimental concentration profiles. The experimental and numerical studies of current work mainly rely on these two techniques for the determination of ternary and quaternary interdiffusion coefficients.

Austenitic Ni-Cr and Fe-Ni-Cr based alloys are widely used in a variety of high-temperature applications because of their ability to form a protective Cr_2O_3 scale [14-21]. Alloying additions not only are intended for improving mechanical properties of these alloys, but also for their high-temperature corrosion resistance. Low amounts of alloying additions (< 6 at.%) to both Ni-Cr and Fe-Ni-Cr alloys are found to have beneficial affect in forming and retaining chromia scale [20-22]. Diffusional effects of minor alloy additions may play a significant role in formation and growth of Cr_2O_3 scale. Intermetallics have been a subject of numerous investigations [23-25]. $L1_2$ Ni_3Al is one of the well-known intermetallic phases that maintains its strength up to its melting point. Various studies on these materials mainly focus on improving its high temperature stability. This long-range ordered solution accepts a very low amount of solutes. Understanding of multicomponent diffusional interactions can provide insight to site preference of solute elements in this intermetallic.

An extended analytical method of the new analysis [13] has been developed, in which average main and cross interdiffusion coefficients are determined over selected regions in the single diffusion couple experiment from the moments (series of higher-order integrands) of interdiffusion flux and associated concentration profiles. This involves a mathematical treatment of simultaneous solutions of the zero moment interdiffusion flux flow equation with that of the higher-moment equations for the same component. Implementing this treatment for two independent components in ternary diffusion yields a series of four interdiffusion coefficients as a function of moment of the equation. These individual moments of interdiffusion quantities are treated as coefficients of linear equations in order to solve average ternary interdiffusion coefficients as variables using matrix algebra methods.

The work presented herein is in essence an analysis of diffusional interactions for high-temperature alloys for oxidation and hot-corrosion resistance. Alloys employed in this work are produced by arc-melting and drop-casting techniques. Solid-solid diffusion couples were made by diffusion annealing the polished disks together at 1200°C, 900°C and 700°C. After the isothermal treatments for designed length of time, the couple assemblies were quenched, and polished cross sections were analyzed for concentration profiles. Experimental concentration profiles were analyzed to determine interdiffusion coefficients. These interdiffusion coefficients were examined with respect to an ability to form protective oxide scales and preferential site occupation.

This dissertation is divided into several chapters starting with Chapter 2 that surveys the literature on (1) diffusion and high temperature oxidation resistance of Ni-Cr, Fe-Ni-Cr systems with the addition of active alloying elements, (2) phenomenology of isothermal interdiffusion and (3) properties and application to the Ni_3Al system. Chapter 3 presents an experimental isothermal interdiffusion investigation in Ni-Cr-X (X=Al,Si,Ge,Pd) alloys at 900°C and 700°C. Chapter 4 reports a similar work carried out for Fe-Ni-Cr-X (X=Si,Ge) alloys at 900°C. Chapter 5 presents an experimental isothermal interdiffusion study in Ni_3Al-X (X=Ir,Ta,Re) at 1200°C. Chapter 6 describes a refined analytical method to determine average ternary interdiffusion coefficients using moments of interdiffusion fluxes. Finally, Chapter 7 summarizes the findings from this work.

1.1 References

1. E.L. Cussler, Multicomponent Diffusion, Elsevier scientific publishing company, 1976.
2. L. Onsager: *Phy.Rev.,* vol. 37 (1931) pp. 405
3. L. Onsager: *Phy.Rev.,* vol. 38 (1932) pp. 2265
4. L. Onsager: *Ann. New York Acad.Sci.,* vol. 46 (1965) pp. 241.
5. L. Boltzmann, *Ann. Physik.,* vol. 53 (1894) pp. 960.
6. C. Matano, *Japan J. Phys.,* vol. 9 (1934) pp. 41.
7. M.A. Dayananda and C.W. Kim: *Metall. Trans.,* vol. 10A (1979) pp.1333.
8. M.A. Dayananda: *Metall. Trans.,* vol. 14 A (1983) pp.1851.
9. M.A. Dayananda: *Mater. Sci. Eng. A.,* vol. 121 (1989) pp. 351.
10. C.W. Kim and M.A. Dayananda: *Metall. Trans,* vol.14A, (1983) pp.857.
11. M.A. Dayananda: *Diffusion in Solids: Recent Developments,* ed. M.A. Dayananda and G.E. Murch, (1984) pp.195.
12. M.A. Dayananda: *Ordered Intermetallics-Physical Metallurgy Mechanical Behavior, ed.* C.T. Liu et al., Kluwer Academic Publisher, Dordrecht (1992) pp.465.
13. M.A. Dayananda and Y.H. Sohn: Metall. Trans. 30A (1999) 535.
14. J.L. Smialek and G.H. Meier, in: *High temperature oxidation*, edited by C.T. Sims, N.S. Stoloff, and W.C. Hagel, of Superalloy II, chapter 11, John Weley & Sons (1987) p. 293-323.
15. P. Kofstad, in: *Growth and protective properties of Chromia and Alumina scales, protective coatings*, High temperature Corrosion, Elsevier, London (1980) p. 389-404.
16. J.L. Smialek, C.A. Barrett, J.C. Schaffer, in: *Design for oxidation resistance*, edited by George E. Dieter,Vol. 20 of ASM handbook, ASM International (1997).

17. F.H. Stott, G.C. Wood, and J. Stringer : Oxi. Metals, Vol. 44 (1995), p. 113-145.
18. H.E. Evans, D.A. Hilton, R.A. Holm et al.: Oxi. Metals, Vol. 19 (No. 1-2), 1983, p. 1-18.
19. S.N.Basu, G.J.Yurek: Oxi. Metals, Vol. 36 (No. 3-4), 1991, p. 281-315.
20. A. Kumar, D.L. Douglass: Oxi. Metals, Vol. 10 (No. 1), 1976, p. 1-22.
21. D.P. Whittle, J. Stringer: Proc. R. Soc. Lond., Ser. A, Vol. 295 (1980), p.309-329.
22. G.C. Wood, F.H. Stott: Mater. Sci. Technol., Vol. 3 (1987), p. 519-530.
23. J.B. McAndrew and H.D.Kessler, J. Met., Vol. 8, 1956, p. 1348.
24. H.A. Lipsitt, High-temperature ordered intermetallic alloys I (Mater. Res. Soc. Symp. Proc. 39) p. 351
25. Y. Jinlong, X. Chuanyun, X. Shangda and W. Kelin, J. Phys.: Condens. Matter. Vol. 5, 1993, p. 6653.

CHAPTER 2: LITERATURE REVIEW

2.1 Austenitic Ni- and Fe-Ni-base alloys and their applications

Austenitic Ni- and Fe-Ni-base alloys find a wide range of applications due to their remarkable abilities to withstand oxidative and corrosive environments and also because of their versatile mechanical enduring abilities [1]. Nickel has extensive solid-solubility within the fcc γ-phase, and it readily accepts several alloying additions to form either a homogeneous solid-solution strengthened further with precipitates dispersed within the matrix [2]. It can dissolve 35 wt.% of Cr, 20 wt.% Mo, 20 wt.% W and 5 to 10 wt.% Al, Ti, Mn and V[3]. The dissolution of extensive elements within the ductile matrix of the γ-phase enables these alloys to possess excellent solid solution strengthening and corrosion and oxidation resistance characteristics [4].

Al addition together with other alloying additions provides a strong solution-hardening effect, whereas Fe and Cr additions remain weaker in this effect [2]. Unique intermetallic compounds are observed in Ni-base alloying systems. $Ni_3(Al,Ti)$, commonly known as γ'-phase, is a very significant precipitate as it provides key-strengthening effect through precipitation hardening in Ni-base superalloys [1].

Ni-Cr-base alloys are known for their corrosion and oxidation resistance during severe exposure of temperature and atmosphere [4-6]. Heating-element interconnects and high-temperature alloy applications are quite common applications for these alloys. Together, both Ni and Cr form an eutectic system with approximately 45% of Cr dissolved in the austenitic solid solution of Ni and 35% of Ni dissolved in α-solid solution of Cr at 1395°C [7]. Peritectoid reaction at 590°C temperature is responsible for the formation of the γ' phase.

Ni dissolves 11 wt.% Al in its austenitic phase at the maximum temperature of approximately 1400°C[7]. This limit drastically reduces at room temperature. Because of the great difference in the melting points of Ni (1455°C) and Al (660°C), the Ni-Al binary system incorporates several peritectic invariant reactions. NiAl, Ni_3Al and NiAl are widely-known intermetallics formed in this system. Ni dissolves up to 8 wt.% Si in austenite solution at a temperature of 1143°C. The combination of eutectic, peritectic and peritectoid reactions associated with this system explains the complexity of this system to attain an extended solid solubility based on the Hume-Rothery rule. Ni-Ge system [7] has great similarity in comparison to the Ni-Si system [7] because of the similar properties of Si and Ge belonging IVA group. Nickel dissolves Ge up to 20 wt.% at the maximum temperature of 1124°C. The combination of several invariant reactions such as eutectic, eutectoid and peritectic explains the great dissimilarities in Ni and Ge. Several intermetallics can be observed in this binary system. In accordance with Hume-Rothery rules, Ni and Pd a noble metal exhibit complete solubility in both solid and liquid states.

Fe-Ni-base alloys are very common and can be considered are economical substitution to Ni-base alloys in several aspects [7]. Most of the versatility factors of Ni base alloys are reflected in these alloys provided 25 wt.% minimum of Ni is dissolved in. Complete solubility of Fe and Ni can be observed in between 900 to 1400°C as fcc austenitic phase. This system provides the basis for stainless steels and other ferrous alloys to combat mainly corrosion related problems. The evolution of various Fe-Ni-base alloys is shown in Figure 2.1[8], with reference to 304 stainless steel.

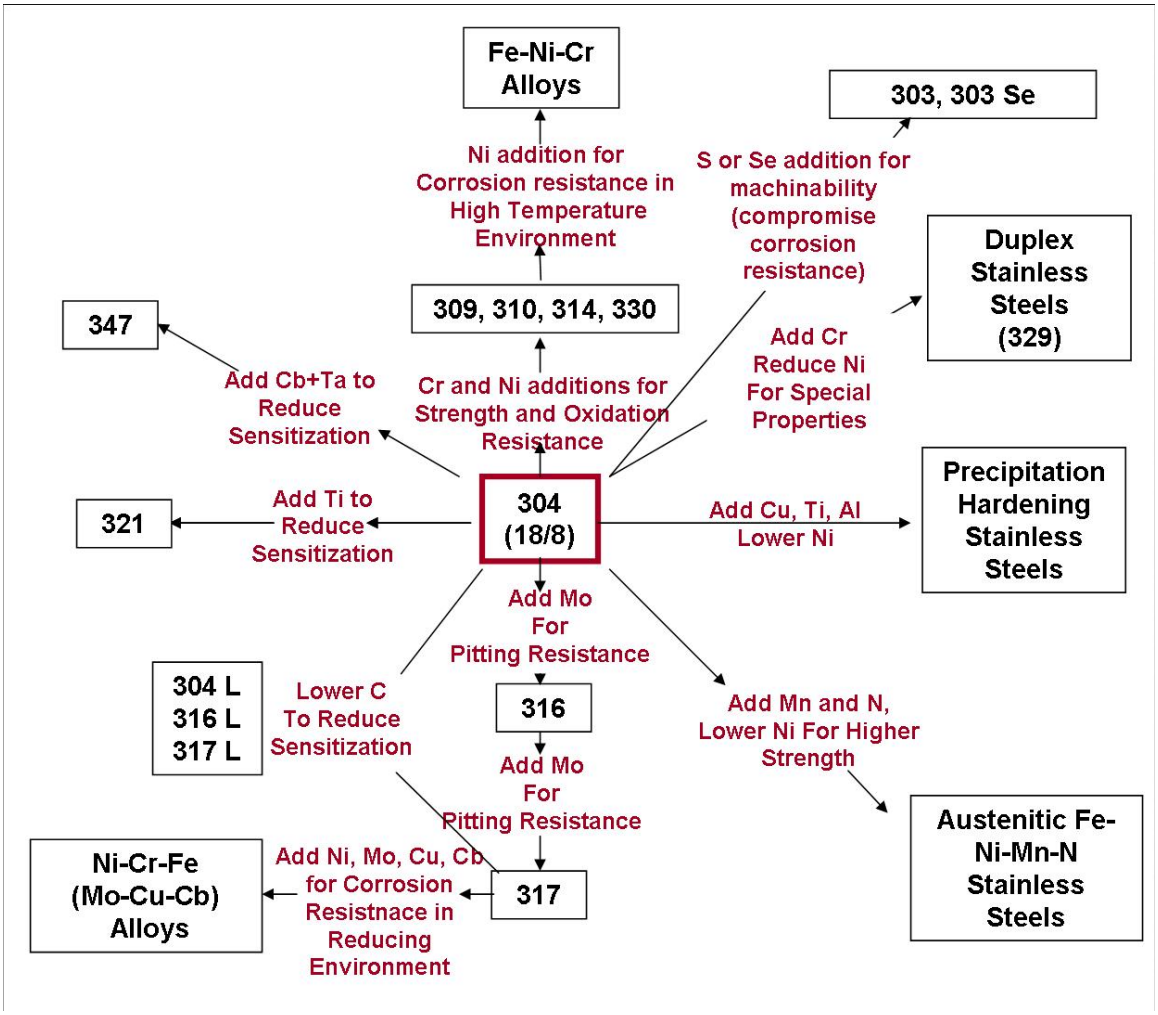

Figure 2.1: Evolution of Fe-Ni-Cr Alloys due to several requirements.[8]

The Fe-Cr system has been a basis for many engineering alloys for high-strength, corrosion-resistant applications. Cr is an bcc α-stabilizer, and it suppresses the fcc γ-phase (e.g., γ-loop). Oxidation of Fe-Cr alloys has been widely studied under different atmospheres [4-6]. Fe-Ni-Cr alloys offer excellent corrosion resistance properties in severe environments due to the well maintained impervious Cr_2O_3 scale formation. With a proper amount of Ni content, these alloys can operate at a maximum temperature of 1200°C. The application of Fe-Ni-Cr alloys

ranges from petrochemical environments to sulphurous atmospheres accompanied by high temperature.

2.2 Oxidation and Hot-Corrosion Resistance of Ni and Fe-Ni-base Alloys

Different types of corrosion or degradation of these alloys are mainly due to operation environments that include oxidation, carburization, nitridation, sulfidation and halogenation[3]. Addition of alloying elements has different influence on each of the corrosive environment. Most heat resistant alloys have sufficient amounts of Cr (with or without Al or Si) to form Cr_2O_3, Al_2O_3 or SiO_2 protective oxide scales which provide resistance to environmental degradation.

Cr-addition improves oxidation, carburization and sulfidation resistance of Ni- and Fe-Ni-base alloys below 950°C. Ni- and Fe-Ni-base alloys with Cr addition can serve well against degradation by oil ash corrosion and molten glass. However, the addition of Cr does not provide any protection against fluorine and nitriding environment. Si-addition to Ni- and Fe-Ni-base improves resistance against oxidation, nitridation, sulfidation and carburization, and synergistically improves the scale resilience with Cr addition. However, Ni- and Fe-Ni-base alloys with Si addition degrades under chlorination environment. Al-addition to Ni- and Fe-Ni-base alloys independently and synergistically (e.g., with Cr) improves the oxidation resistance, and helps against sufidizing and carburization, but does not improve nitridation resistance.

2.3 Ni_3Al Intermetallic and Its Properties

Ni_3Al is known as γ' phase, and finds a wide range of high-temperature applications including precipitation strengthening constituents in Ni-base superalloys [4]. These Ni_3Al precipitates can be spherical or cuboidal. Alloying additions can further enhance its high-temperature strength, environmental stability and room-temperature toughness [9]. The compatibility of Ni_3Al phase in terms of crystal structure and lattice parameter with an fcc Ni allows homogeneous nucleation of precipitates with low surface energy and extraordinary stability. Ni_3Al precipitates contribute to remarkable strengthening in Ni-base superalloys by interaction with dislocations. In addition, the strength of Ni_3Al increases as temperature increases [4].

Figure 2.2(a) illustrates the crystal structure of Ni_3Al[10]. Elemental additions to Ni_3Al with high electronegativity tend to occupy Ni sites, whereas electropositive ones occupy the Al sites [4]. The coordination number of this $L1_2$ structure in terms of atoms surrounding Ni and Al are illustrated in Figure 2.2(b) and Figure 2.2(c) respectively. Ni has eight number of nearest neighboring sites to facilitate the substitutional exchange mechanism. On the other hand, Al is surrounded by 12 Ni atoms. For this reason, Ni and Ni-replacing alloying additions tend to have higher magnitude of interdiffusion coefficients than for Al and Al-replacing alloying elements.

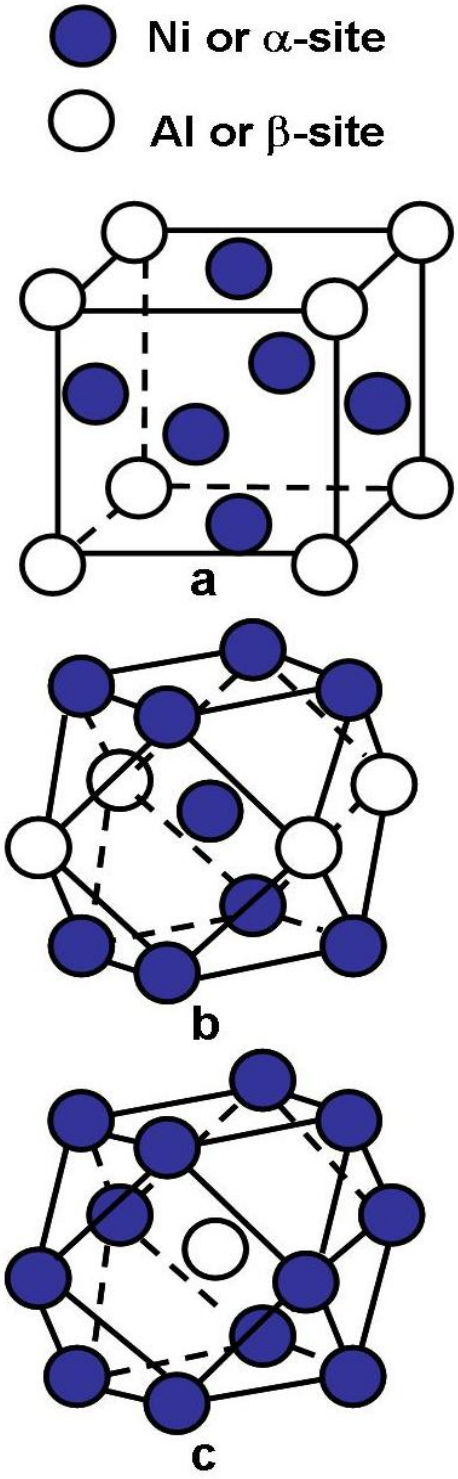

Figure 2.2 : Unit cell of Ni_3Al and nearest neighboring atoms surrounding Ni and Al sites.

2.4 Multicomponent Interdiffusion

The phenomenology of multicomponent interdiffusion can be understood from Fick's law [11]. The interdiffusion flux ($\tilde{J}_i$) of component (i) is directly proportional to its concentration gradient, $\partial C_i/\partial x$:

$$\tilde{J}_i = -\tilde{D}_i \frac{\partial C_i(x,t)}{\partial x} \tag{2.1}$$

where D_i is called interdiffusion coefficient of component i. The negative sign indicates the nature of diffusion to occur down the concentration gradient.

The phenomenological description of interdiffusion in multicomponent systems expressed on the basis of Onsager's Formalism [12-14]. This requires (n-1) number of independent components to obtain $(n-1)^2$ interdiffusion coefficients. Accordingly, interdiffusion flux for an independent components 'i' can be expressed as:

$$\tilde{J}_i = -\sum_{j=1}^{n-1} \tilde{D}_{ij}^{n} \frac{\partial C_j(x,t)}{\partial x} (i = 1,2,.....,n-1) \tag{2.2}$$

The above equation requires (n-1) number of concentration gradients in the form of $\partial C_i/\partial x$, to relate $(n-1)^2$ numbers of interdiffusion coefficients in the form of $\tilde{D}_{ij}^{n}$. Concentration dependent interdiffusion coefficients can be determined in ternary systems using the Boltzmann-Matano analysis [15, 16].

Eq. (2.2) can be used to express interdiffusion flux in a ternary system:

$$\tilde{J}_i = -\overline{\overline{\tilde{D}}}^{3}_{i1} \frac{\partial C_1}{\partial x} - \overline{\overline{\tilde{D}}}^{3}_{i2} \frac{\partial C_2}{\partial x} \qquad (i=1,2) \qquad (2.3)$$

where $\overline{\overline{\tilde{D}}}^{3}_{i1}$ and $\overline{\overline{\tilde{D}}}^{3}_{i2}$ refer to the average main and cross-interdiffusion coefficients (for the component i), respectively. Component 3 serves as dependent concentration variable.

Implementing Eq. (2.3) for the interdiffusion fluxes of both independent components will yield two equations. Finding another such set of ternary interdiffusion flux equations for another independent diffusion couple experiment of the same ternary system, provided the diffusion paths of both these separate experiments have a common intersecting composition will enable determination of all the four interdiffusion coefficients. This analysis is known as Boltzmann-Matano analysis. Figure (2.3) illustrates series of such independent intersecting diffusion paths with one common path of AB. This illustrates one way of Boltzmann-Matano analysis to determine interdiffusion coefficients along one direction of composition points.

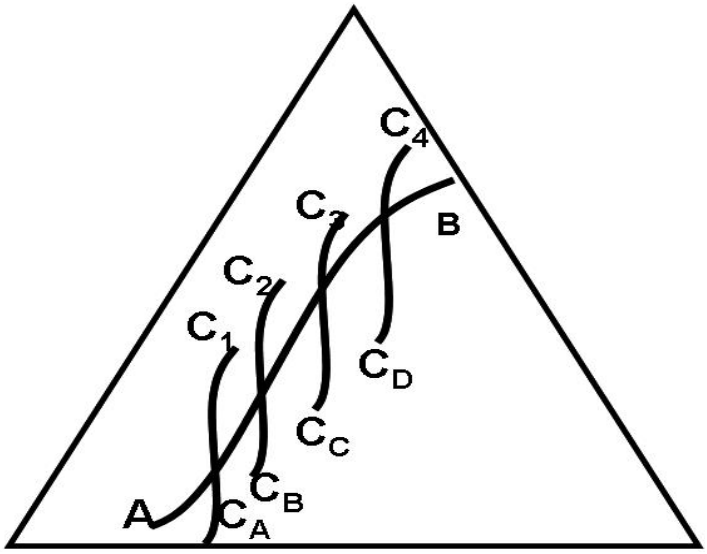

Figure 2.3 :Exemplifying composition dependency of interdiffusion coefficients determination using Boltzmann-Matano Analysis.

A method of direct determination of interdiffusion fluxes for all components of the concentration profiles without invoking the interdiffusion coefficients has been developed [17-19] on the basis of an integration of the continuity equation:

$$\left(\frac{\partial C_i}{\partial t}\right)_x = -\left(\frac{\partial \tilde{J}_i}{\partial x}\right)_t \tag{2.4}$$

where t is the time of diffusion annealing, $\tilde{J}_i$ is the interdiffusion flux and x is the diffusion distance that is perpendicular to the bonding interface of two solid materials. Figure 2.2 (a) represents a schematic concentration profile for a component 'i' that develops in a solid-solid diffusion couple in an n-component system. The interdiffusion flux at any section x of this concentration profile can be calculated directly using the relation [20-25]:

$$\tilde{J}_i = \frac{1}{2t} \int_{C_i^{-\infty} \text{ or } C_i^{+\infty}}^{C_i(x)} (x - x_0) dC_i \qquad (i = 1,2,\ldots,n) \tag{2.5}$$

where $C_i^{-\infty}$ and $C_i^{+\infty}$ are the terminal concentrations and x_o refers to the location of the Matano plane. The determination of x_o is based on the mass balance of individual behavior of the concentration profiles, using [11,25,26]:

$$\int_{C_i^{-\infty}}^{C_i^{+\infty}} (x - x_o) dC_i = 0 \qquad (i=1, 2, 3) \tag{2.6}$$

The integral in Eq. (2.6) for a selected value of x is given by the hatched area S_1 as shown in Figure 2.4(a). The interdiffusion flux $\tilde{J}_i$ of component 'i' determined as a function of x from Eq. (2.5) is shown schematically in Figure 2.4(b). The direct determination of interdiffusion fluxes enables assessing of diffusional behavior of the components to understand the concepts such as zero-flux-planes and flux-reversals [28-32].

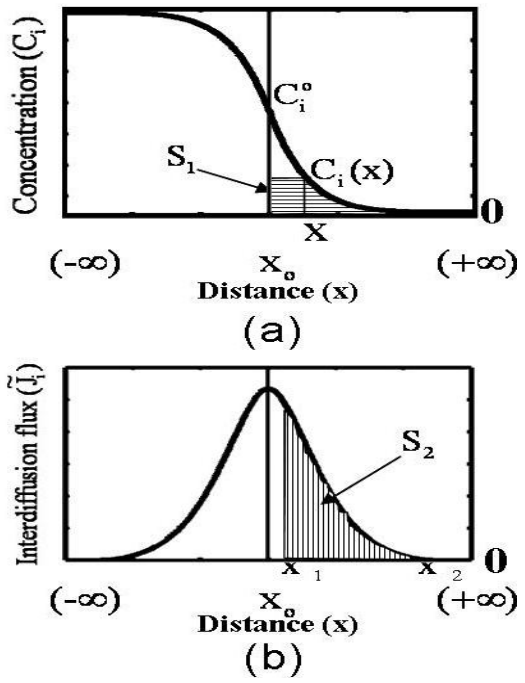

Figure 2.4: A schematic concentration profile (a) for component i in a solid-solid diffusion couple and (b) the corresponding interdiffusion flux profile. C_i^o and $\left(\tilde{J}_i\right)_{x_o}$ refer to the concentration and the interdiffusion flux, respectively, at the Matano plane. The hatched area S in (a) corresponds to the term $\int_{C_i^+}^{C_i(x)} (x - x_o)dC_i$ and the cross-hatched area in (b) corresponds to the term $\int_{x_o}^{+\infty} \tilde{J}_i dx$ for a component i.

2.5 High-temperature oxidation

High temperature oxidation of metals and alloys is very common phenomena where the combination of elevated temperature, oxygen, air and any oxide prevailing atmospheres are unavoidable. Oxidation between metal (M) and oxygen (O_2) in its gaseous form can be expressed as:

$$M(s) + O_2\,(g) = MO_2(s) \qquad (2.7)$$

The equilibrium partial pressure of oxygen that associates with the metal system can be related to the standard free energy of oxidation reaction as below.

$$\Delta G^o = -RT \ln(a_{MO_2} / a_{Mp(O_2)}) \tag{2.8}$$

where $a_{(MO2)}$ and $a_{(M)}$ are the activities of the oxide and the metal respectively and $p_{(O2)}$ is the partial pressure of the oxygen gas.

As metal and metal oxide are solid phases in the Eq. (2.7), the activities of these phases can be assumed as unities, then, Eq. (2.8) can be expressed as:

$$\Delta G^o = RT \ln(p_{O_2}) \tag{2.9}$$

$$p_{O_2} = \exp(\Delta G^o / RT) \tag{2.10}$$

Therefore, standard free energy of formation is required to use Eq. (2.10) to in order to determine partial pressure of oxygen.

The change in this work function can be expressed using second law of thermodynamics as:

$$\Delta G^o = \Delta H^o - T\Delta S^o \tag{2.11}$$

where $\Delta H^o and \Delta S^o$ are changes in standard enthalpy and entropy respectively.

The Ellingham diagram[33] makes use of Eq. (2.11) to express standard free energies of oxide formation to predict the predominant influence of oxides over each other. For the current oxidation work in Ni-Cr-X and Fe-Ni-Cr-X alloys, this information of standard oxide formation is expressed in Figure 2.5. From this figure it is evident that oxides of Al and Si are more stable than Cr, Ni and Fe. For this reason Ni and Fe-Ni are considered as solvents of these alloys expecting less tendency of formation of these oxides. The medium tendency of chromia formation is compensated by considering higher amount of Cr to expect predominance of this oxide on the alloy system.

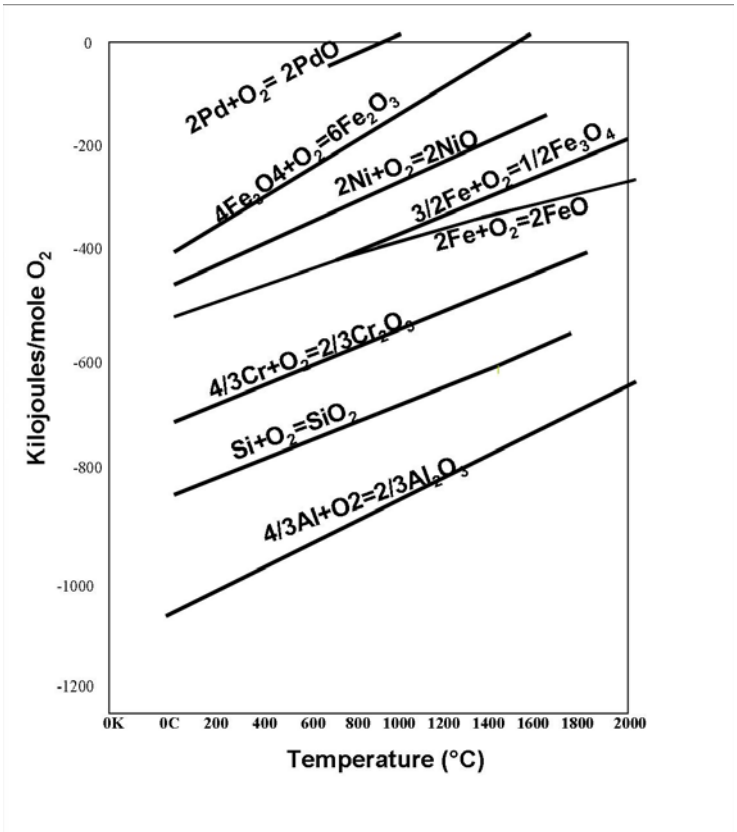

Figure 2.5 : Ellingham diagram of oxides pertaining to current studies.

The Ellingham diagram is of only thermodynamic help in assessing the stability of oxides, kinetics of oxide formation are also very important to find out the extent of the reaction required to form the required oxide and also to estimate thickness and hierarchy of oxides

forming on the alloy system. The kinetics of oxidation follow either a logarithmic law or a parabolic law or a linear law or the combination of any of them in deciding the rate of oxide growth depending on the composition (partial pressure) and temperature combinations. However, the parabolic law is considered more relevant for high temperature oxidation. Figure 2.6 [21], illustrates the parabolic growth rate constant values of few oxides[4]. The lower the position of oxide, the more it will be beneficial in terms of providing slow-growth rate.

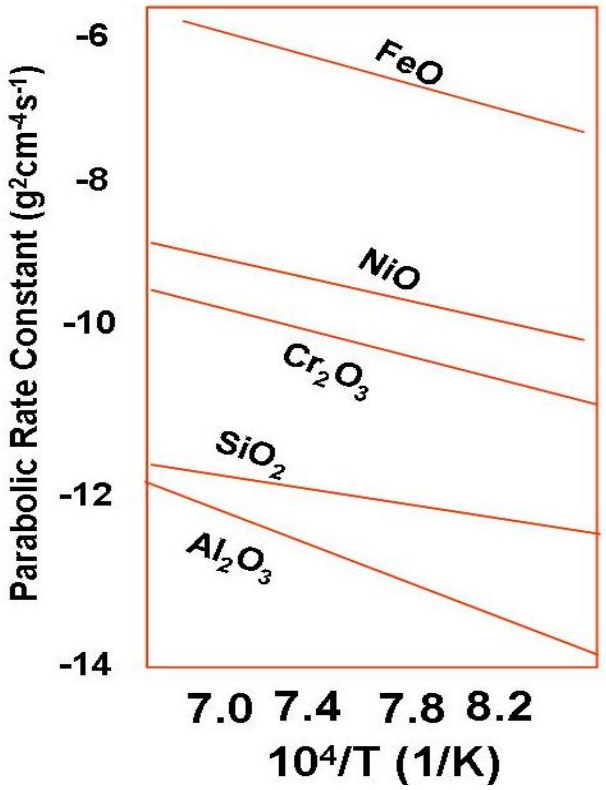

Figure 2.6 : Kinetics of metal oxides at high temperatures.

According to the parabolic rate law of oxidation, the oxide growth proceeds with the continuos decrease in oxidation rate. Therefore, the rate of oxidation is inversely proportional to the scale thickness or weight of the oxide formed.

$$\frac{dx}{dt} = \frac{K_p}{x} \tag{2.12}$$

$$\Rightarrow x^2 = 2K_p t + C \tag{2.13}$$

Most of the alloys obey the parabolic law of oxidation at elevated temperatures. The diffusion of ions or electrons through the initially formed oxide scale is the characteristic feature of this oxidation.

According to Wagner [34], when a metal is exposed to high temperature, oxidation proceeds in two steps. Figure 2.7 illustrates Wagner's application of metal oxidation [35]. The first is to form a monolayer of oxide and second is its growth. Both these steps require transfer of metals ions from the substrate or oxygen ions from the atmospheric gaseous phase. Metal-oxide and Gas-oxide interfaces move relatively opposite to each other. Diffusion is the rate controlling step and is mainly due to the defect structure of the oxide. For thick scale formation ions have to move a larger distance whereas for thinner scales this distance decreases. The kinetics of oxide formation is parabolic in nature. Wagner's model of parabolic oxidation rate obeys the following assumptions [4].

1. The oxide scale is dense and impervious.

2. Transport of ions, charged species or electrons is the rate controlling step.
3. Thermodynamic equilibrium is established at metal-oxide and oxide-metal interfaces.
4. Thermodynamic equilibrium is established thought the scale.
5. The oxide follows negligible deviation from stoichiometry.
6. The metal contains only negligible amount of oxide dissolved in it.
7. The scale size is thicker than the distances required for space charges.

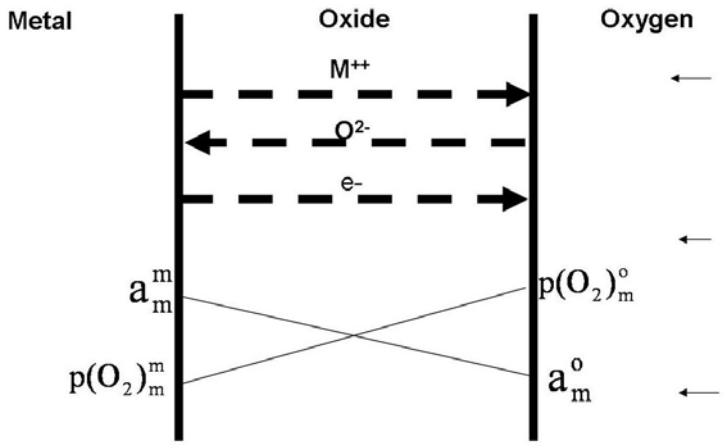

Figure 2.7: Wagner's illustration of metal oxidation [36].

As a thermodynamic equilibrium prevails at interfaces of metal-oxide and oxide-oxygen phases, activity depletion of the metal from the metal-oxide interface to oxygen-oxide interface and a reduction in partial pressure of oxygen from the oxide-oxygen interface to the metal-oxide interface complement each other. This consequently leads to ion migration. Thereby, both chemical and electrical potential gradients develop to provide a driving force for the oxidation. The result of this whole phenomenology can be expressed as a parabolic rate constant [4]:

$$k' = \frac{1}{RT}\int_{\mu_0'}^{\mu_0''}\left(D_o + \frac{Z_M D_M}{2}\right)d\mu_o \tag{2.14}$$

where D_M and D_O are diffusivities of metal and oxygen respectively, in the oxide, and Z_M is the metal volume, and u and u are the chemical potentials of oxygen at the metal-oxide and oxide-oxygen interfaces, respectively.

Oxidation of alloys is more complex than the oxidation of metals, and Wagner classified alloys into following groups: (1) base solute alloying additions in noble solvent, and (2) base solute with base solvent alloy. As shown in Figure 2.8, in this case element B is more reactive than element A. Depending on the amount of B, two sub-cases exist as shown in figure. In first sub-case, B is dilute in amount and tends to form dispersions of internal oxide within the matrix of selected A rich region. But, in the second sub-case when the B content is sufficient enough to form its own oxide, no discontinuous regions are observed. The critical amount of B to form continuous oxide can be expressed, according to [4] as:

$$B_{Critical} \geq [0.3N_o(D_O / D_B)(V_m / V_{mO})]^{1/2} \tag{2.15}$$

Where, D_O, D_B are the diffusivities of O and B respectively in the alloy. V_m and V_{mO} are molar volumes of metal and oxide formed, and N_O is the solubility of oxygen in the alloy. But, it is possible to form continuous oxide of B at its lower concentration, provided N_O, D_O and V_m are low and D_B and V_{mO} are high.

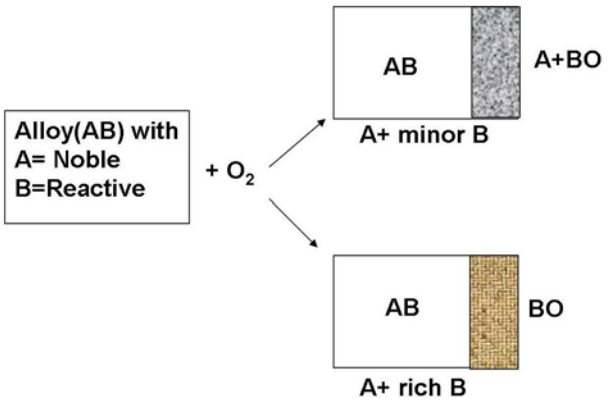

Figure 2.8 : Oxidation of Binary alloy consisting reactive B and noble A elements [35].

As shown in Figure 2.9, in this second case, though both elements A and B are reactive, BO is more stable than AO. When B content is not sufficient enough, it leads to the first sub-case, where AO forms externally with BO remaining as internal oxide. On the other hand, with the availability of sufficient B, external BO only forms on the alloy surface. This second sub-case is commonly used in designing alloys to withstand high temperature oxidation resistance. Also, this manifests parabolic oxide growth rate.

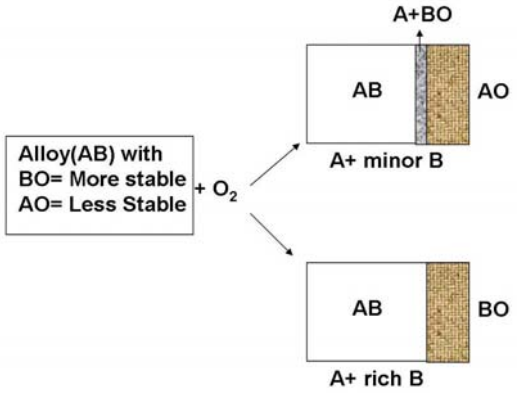

Figure 2.9: Oxidation of Binary alloy, consisting oxide of B (BO) more stable than oxide of A (AO)[35].

In 1937, Griffiths and Pfeil [37] showed that rare earth addition to Ni-20Cr alloys had

beneficial effects in enhancing the life time of these alloys under cycling conditions for the application of heating elements. The presence of minor amount of an elemental constituent can induce changes in properties: physical, mechanical, chemical and quite out of proportion to the amount added. The beneficial effect of active elements on the oxidation behavior of high temperature NiCr and FeNiCr alloys has been observed for the last 5 decades and minor additions of active elements are now used with various MCrAl alloys (M= Fe and/or Ni), which include Cr_2O_3-as well as Al_2O_3 forming alloys. Active elements can be incorporated in one or the other forms with the substrate alloys.

1. Dissolving minor element and form an alloy by melting.
2. As an oxide dispersion on substrate surface.
3. Ion implantation.

The active elements promote the formation of a protective scale reduce the rate of continuing scale growth or inhibit the scale failure process. The major effect of alloying is to improve scale adherence. Different theories [38-44] have been proposed to explain the effects of minor alloying elements. These theories mainly incorporate:

1. Active element oxides act as nucleation sites and promote selective oxidation of the protective-scale forming element, thereby curtailing the transient stage of oxidation.
2. Modify growth mechanism of the oxide, especially applicable to Cr_2O_3 forming alloys.
3. Modification of scale morphology and structure.
4. Improvement of the scale plasticity by refining grain size.
5. Formation of an secondary or intermediate scale.
6. Forming oxide pegs internally to key the surface oxide along with the substrate.

7. Act as vacancy sinks.
8. Establish chemical bonding.
9. Prevent segregation of impurities.

Some of the important parameters those can greatly help in designing alloys for high temperature protective oxide scales are:

- Free energy of oxides of the alloying elements.
- Crystallographic structure of oxides.
- Pilling and Bedworth ratio of oxide compounds.
- Solubility of elements in both substrate and coating systems.
- Diffusivity of active elements in oxide scale and alloy.
- Valencies of active elements and their atomic or ion radii.
- Thermal conductivities of oxides.

Active element addition can promote selective oxidation of Cr in alloy [43], and thereby initially protective Cr_2O_3 forms and prevents forming the other base metal oxides. The most possible mechanism [44] is shown Figure [2.8]. In this, the dispersed active element oxide particles form at the alloy surface and act as heterogeneous nucleation sites for the initially-forming oxides, thereby reducing the spacing between nuclei. It minimizes time required for subsequent lateral growth processes to connect nuclei to form a protective Cr_2O_3 scale. This mechanism is proven to be reasonable and consistent with further similar studies of oxidation.

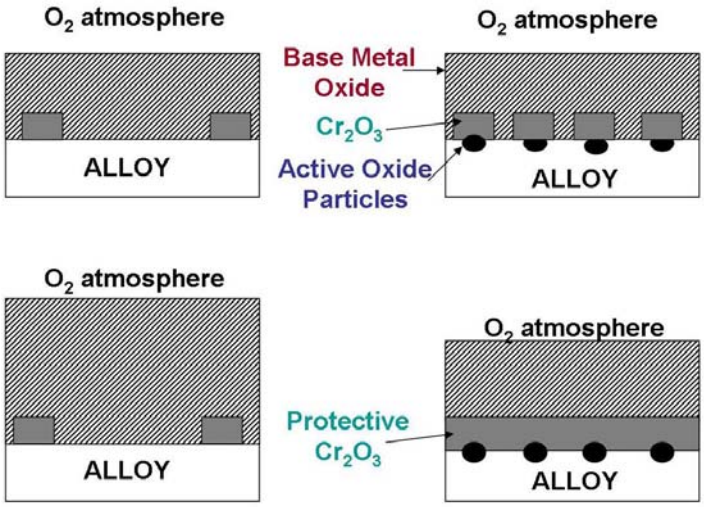

Figure 2.10: Schematic representation of role of active element oxide particles in providing heterogeneous nucleation sites and in favoring further oxidation.

2.6 References

1. *ASM Handbook, 10th Ed., Vol. 3, Alloy Phase Diagrams*, (Materials Park, OH: ASM Int., 1992), p. 178.
2. R.F.Decker, Strengthening Mechanisms in Nickel-Base Superalloys, Climax Molybdenum Company Symposium, Zurich, May 5-6, 1969.
3. Nickel, cobalt and their alloys *ASM Specialty Handbook* 2000, (Metals Park, OH: ASM International) p. 45.
4. C.T. Sims, N.S. Stoloff, W.C. Hagel, Superalloys II, John Wiley and Sons, 1987.
5. P. Kofsted, 'Growth and protective properties of Chromia (Cr_2O_3) and Alumina (Al_2O_3) scales, protective coatings', High temperature Corrosion, Elsevier, London, 1980, p. 389.
6. J.L. Smialek, C.A. Barrett, J.C. Schaffer, Design for oxidation resistance, ASM handbook, George E. Dieter, Ed., ASM International, 1997, p. 589.

7. *ASM Handbook, 10th Ed., Vol. 3, Alloy Phase Diagrams*, (Materials Park, OH: ASM Int., 1992), p. 178.
8. A.J. Sedriks. In: (3rd edn ed.),*Corrosion of Stainless Steels*, John Wiley and Sons, NY (1979), p. 12.
9. R. D. Rawling and A. Staton-Bevan, J. Mater. Sci. Vol. 10, 1975, p. 505.
10. H. Numakura, T. Ikeda, H. Nakajima and M. Koiwa, Mater. Sci. Eng. A 312 (2001), p. 109.
11. P. Shewmon, "Diffusion in Solids, 2nd ed.," The Minerals, Metals and Materials Society, Warrendale, PA (1989).
12. L. Onsager: *Phy.Rev.,* vol. 37 (1931) pp. 405
13. L. Onsager: *Phy.Rev.,* vol. 38 (1932) pp. 2265
14. L. Onsager: *Ann. New York Acad.Sci.,* vol. 46 (1965) pp. 241.
15. L. Boltzmann, *Ann. Physik.,* vol. 53 (1894) pp. 960.
16. C. Matano, *Japan J. Phys.,* vol. 9 (1934) pp. 41.
17. J.R. Manning, "Diffusion Kinetics for Atoms in Crystals," D. Van Nostrand Co., Inc. (1968)
18. J.S. Kirkaldy and D.J. Young, "Diffusion in the Condensed state," The Institute of Metals, London (1987).
19. J. Philibert, "Atom Movement-Diffusion and Mass Transport in Solids", Les Editions de Physique, Paris (1991).
20. M.A. Dayananda and C.W. Kim: *Metall. Trans.,* vol. 10A (1979) pp.1333.
21. M.A. Dayananda: *Metall. Trans.,* vol. 14 A (1983) pp.1851.
22. M.A. Dayananda: *Mater. Sci. Eng. A.,* vol. 121 (1989) pp. 351.
23. C.W.Kim and M.A. Dayananda: *Metall. Trans,* vol.14A, (1983) pp.857.

24. M.A. Dayananda: *Diffusion in Solids: Recent Developments,* ed. M.A. Dayananda and G.E. Murch, (1984) pp.195.

25. M.A. Dayananda: *Ordered Intermetallics-Physical Metallurgy Mechanical Behavior, ed.* C.T. Liu et al., Kluwer Academic Publisher, Dordrecht (1992) pp.465.

26. J.S. Kirkaldy and D.J. Young: *Diffusion in the Condensed state,* The Inst. Of Metals, London, 1987, pp. 226-72.

27. M.E. Glicksman: *Diffusion in Solids, John Wiley & Sons, New York, NY, 2000.*

28. M.A. Dayananda and C.W. Kim: *Metall. Trans.,* vol. 10A (1979) pp.1333.

29. M.A. Dayananda: *Metall. Trans.,* vol. 14 A (1983) pp.1851.

30. M.A. Dayananda: *Mater. Sci. Eng. A.,* vol. 121 (1989) pp. 351.

31. C.W.Kim and M.A. Dayananda: *Metall. Trans,* vol.14A, (1983) pp.857.

32. M.A. Dayananda: *Diffusion in Solids: Recent Developments,* ed. M.A. Dayananda and G.E. Murch, (1984) pp.195.

33. F.D. Richardson and J.J.E. Jeffes, J. Iron Steel Inst., The Metals Society, 1948, 160, 261.

34. C. Wagner, Ber. Bunsenges Phys. Chem., Vol. 63, 1959, p. 772.

35. S.Bose, High Temperature Coatings, Elsevier, 2007.

36. A.S. Khanna, High temperature oxidation and corrosion, ASM International, 2002.

37. WT Griffiths and LB Pfeil, UK Patent no. 459848 (1937).

38. D.P. Whittle and J.Stringer, phil. Trans. Roy. Soc. London, 1980, A295, 309.

39. D.G. Lees, Oxid. Met., Vol. 27, 1987, p.75.

40. K.L. Luthra and C.L.Briant, Oxid. Met., Vol. 30,1988, p. 257.

41. J.G. Smeggil, N.S. Bornstein and M.A.Decrescente, Oxid. Met., Vol.30, 1988, p.259.

42. D.G. Lees, Oxid. Met., Vol.30, 1988, p. 267.

43. D.P. Whittle and J. Stringer, Phil. Trans. R. Soc. Lond. A., 1980, 295, p.309

44. J. Stringer, B.A. Wilcox and R.I. Jaffee, Oxid. Met., Vol.5, 1972, p.11.

CHAPTER 3: INTERDIFFUSION IN NI-CR-X ALLOYS AT 900°C AND 700°C

3.1 Introduction

Nickel-chromium base alloys are widely used in a variety of high-temperature applications due to their combination of good oxidation resistance and excellent high-temperature strength, and are the basis for a number of commercial superalloy families [1-3]. Oxidation resistance in these alloys is derived from a continuous, slow-growing, adherent C_2O_3-base oxide scale [1-3]. In particular, composition in the range of Ni alloyed with 20~30 wt.% Cr have been extensively studied as a model material for Cr_2O_3 scale formation [4-13].

Minor alloying additions (< 5wt.%) can significantly improve the oxidation resistance of Ni-base Cr_2O_3-forming alloys [14-16]. Effects include: (1) establishment of continuous Cr_2O_3 scale formation at reduced Cr concentrations; (2) a decrease in the growth rate of Cr_2O_3; and (3) enhanced scale adherence [1,14,17]. For example, the addition of Si in Ni-28wt.%Cr promoted formation of both Cr_2O_3 and SiO_2 [13], in which a continuous inner SiO_2 layer acted as a diffusion barrier, and reduced the isothermal oxidation rate by suppressing cation transport through the Cr_2O_3 scale [6,13,17-20]. However, the same inner SiO_2 layer can also reduce the spallation resistance, dependent on the level of Si and the continuity and thickness of the inner SiO_2 layer formed [21].

Diffusional effects of minor alloy additions may play a significant role in the initial establishment of a continuous protective oxide scale [2,14,16,22,23]. It can also play a significant role in maintaining protective scale growth. For example, the growth of Cr_2O_3 can locally deplete Cr from the alloy in the subsurface region [24]. If the scale is locally damaged or

spalled, such a depletion can prevent the reformation of the Cr_2O_3 scale, and result in a transition to less-protective or non-protective oxidation behavior. Understanding of diffusional interactions in Ni-Cr-X alloys where X represents minor alloying additions can help design Ni base Cr_2O_3-forming alloys with improved resistance against environmental degradation [25].

In this work, interdiffusion in Ni-22at.%Cr-X (fcc γ phase) alloys with small additions of X (X = Al, Si, Ge, or Pd) is investigated using solid-to-solid diffusion couples annealed at 900°C for 168 hours and 700°C for 720 hours. This information can be used as a part of a larger study whose goal is to better elucidate the effects of minor alloying additions on oxidation of Cr_2O_3-forming alloys. Addition of Si was selected because it has long been known to be beneficial to Cr_2O_3 scale formation [17] via both establishment of an inner layer of SiO_2 and possibility enhanced diffusivity of Cr. To help probe these effects, additions of Ge were also selected. Germanium is thermochemically similar to Si in many regards, but does not form a protective oxide scale as does Si. Additions of Al at levels > 3~4wt.% can improve the oxidation via the formation of a protective Al_2O_3 scale [2,14,16,26]. At subcritical levels (2~3wt.%), Al may also be beneficial to the oxidation resistance of Ni-Cr alloys, in part via the formation of semi-continuous inner region of Al_2O_3 particles [26,27]. Palladium was chosen for the study because it is a noble alloying addition, and would be expected to accumulate at the alloy/scale interface during oxidation and may improve the oxide/metal adhesion [28,29].

In this ternary interdiffusion study at 900°C and 700°C, the experimental concentration profiles were used to calculate interdiffusion fluxes of individual components, and to determine average effective interdiffusion coefficients $\tilde{D}_i^{eff}$ and average ternary interdiffusion coefficients

$\tilde{\tilde{D}}_{ij}^{Ni}$ (i,j=Cr,X). Values of $\tilde{D}_{Cr}^{eff}$ and $\tilde{\tilde{D}}_{CrX}^{Ni}$ are examined to assess the effects of alloying additions on the interdiffusion behavior of Cr, and the Cr_2O_3-forming ability in Ni-Cr-X alloys.

3.2 Determination of Interdiffusion Fluxes and Coefficients

Onsager's formalism for the interdiffusion flux $\tilde{J}_i$ of component i in a ternary system can be written as [30]:

$$\tilde{J}_i = -\tilde{D}_{i1}^3 \frac{\partial C_1}{\partial x} - \tilde{D}_{i2}^3 \frac{\partial C_2}{\partial x} \quad (i, j = 1,2) \tag{3.1}$$

where $\partial C_1/\partial x$ and $\partial C_2/\partial x$ are the two independent concentration gradients, and $\tilde{D}_{i1}^3$ and $\tilde{D}_{i2}^3$ refer to the ternary interdiffusion coefficients. An experimental determination of the four concentration-dependent interdiffusion coefficients requires the use of the Boltzmann-Matano analysis with two independent diffusion couples that develop a common composition in the diffusion zone. Instead, the interdiffusion fluxes $\tilde{J}_i$ of all components can be determined directly from their concentration profiles of an infinite diffusion couple without the need of the interdiffusion coefficients on the basis of the relation [31]:

$$\tilde{J}_i = \frac{1}{2t} \int_{C_i^- \text{ or } C_i^+}^{C_i(x)} (x - x_o) dC_i \quad (i = 1, 2, ..., n) \tag{3.2}$$

where t is the time, C_i^- and C_i^+ are the terminal concentrations of the alloys employed for the

couple and x_o refers to the location of the Matano plane.

The interdiffusion flux $\tilde{J}_i$, determined from Eq. (3.2) can be integrated with respect to position x to define average effective interdiffusion coefficient $\tilde{D}_i^{eff}$ [32]:

$$\tilde{D}_i^{eff} = \frac{\int_{x_1}^{x_2} \tilde{J}_i dx}{C_i^{x_2} - C_i^{x_1}} \qquad (i = 1,2,3) \tag{3.3}$$

This effective interdiffusion coefficient incorporates all multicomponent diffusional interactions for the system to provide an effective value for the interdiffusion of a component species as defined by:

$$\tilde{D}_i^{eff} = \tilde{D}_{ii}^{n} + \sum_j \frac{\tilde{D}_{ij}^{n} \partial C_j / \partial x}{\partial C_i / \partial x} \quad (i \neq j) \tag{3.4}$$

The interdiffusion flux $\tilde{J}_i$, determined from Eq. (3.2) as a function of x, can be multiplied by $(x-x_o)^n$ and integrated over a selected region, x_1 to x_2; in the light of Eq. (3.1), one gets [33]:

$$\int_{x_1}^{x_2} \tilde{J}_i (x - x_o)^n dx = -\overline{\tilde{D}}_{i1}^{3} \int_{C_1(x_1)}^{C_1(x_2)} (x - x_o)^n dC_1 - \overline{\tilde{D}}_{i2}^{3} \int_{C_2(x_1)}^{C_2(x_2)} (x - x_o)^n dC_2 \qquad (i, j = 1,2) \tag{3.5}$$

where $\overline{\tilde{D}}_{ij}^{3}$ $(i,j = 1,2)$ coefficients are the average values of main and cross-interdiffusion coefficients treated as constants over the selected composition range. Eq. (3.5) can provide four

equations involving the $\tilde{\bar{D}}_{ij}^{3}$ interdiffusion coefficients (n = 0, 1 or 2) and can be set up from interdiffusion fluxes calculated on the basis of Eq. (3.2) from the concentration profiles of a single diffusion couple. The $\tilde{\bar{D}}_{ij}^{3}$ coefficients, characteristic of the diffusion path, can be determined over selected composition ranges that include nonlinear segment of the profiles [33]. Determination of ternary interdiffusion coefficients by using Eq. (3.5) do not require the use of concentration gradients (i.e., $\partial C_i/\partial x$), and significantly reduces the uncertainty involved on the determination of interdiffusion coefficients arising from microprobe measurement and concentration smoothening procedure [33].

3.3 Experimental Procedure

Binary and ternary alloys with compositions reported in Table 3.1 were prepared with 99.9% pure Ni, Cr, Al, Si, Ge and Pd by arc melting under an argon atmosphere. The alloys were chill-cast by water-cooled copper mold into rods with approximately vacuum 12 mm in diameter. The alloy rods were placed in a quartz tube, evacuated to a pressure less than 10^{-6} torr, and flushed with hydrogen. This hydrogen-flushing procedure was repeated several times and Ar was filled into a quartz capsule before the final seal. They were homogenized at 900˚C for 168 hours in a horizontal Lindberg™ 3-zone tube furnace and water-quenched to preserve the high temperature microstructure. The microstructures and compositions of the alloys were examined by optical microscopy, scanning electron microscopy (SEM), energy dispersive spectroscopy (EDS) and electron microprobe analysis (EMPA). No measurable variation in the alloy compositions was observed and all alloys consisted of fcc Ni solid solution (γ-phase).

Table 3.1: Compositions of Ni-Cr-X alloys employed for solid-to-solid diffusion couples.

Alloy Identification	Composition (atom fraction)			Composition (weight fraction)		
	Ni	Cr	X	Ni	Cr	X
Ni	100.0	-	-	100	-	-
NiCr (X = None)	78.0	22.0	-	80	20	-
NiCrAl (X = Al)	72.5	21.3	6.2	77	20	3
NiCrSi (X = Si)	74.0	22.0	4.0	78	20	2
NiCrGe (X = Ge)	76.3	22.1	1.6	78	20	2
NiCrPd (X = Pd)	76.1	22.3	1.6	77	20	3

Diffusion disks with approximate thickness of 2 mm were cut from the rods of alloys and prepared metallographically by polishing through 0.25 μm diamond paste. Table 3.2 presented ternary diffusion coupes that were assembled with the disks held together in Invar™ steel jig consisting of two end plates and three threaded rods. The couples were placed in quartz capsules, which were sealed at one end, and evacuated to a pressure less than 10^{-6} torr and flushed with hydrogen several times. Ar was filled into a capsule before the final sealing. The capsules containing the couples were annealed in a horizontal Lindberg 3-zone furnace at 900˚C for 168 hours and at 700˚C for 720 hours. After the anneal, the couples were quenched in water to preserve the high temperature microstructures.

Table 3.2: List of Ni vs. Ni-Cr-X and NiCr vs. Ni-Cr-X solid-to-solid diffusion couples annealed at 900°C for 168 hours and at 700°C for 720 hours.

Series	Diffusion Couples
I	Ni vs. Ni-Cr
II	Ni vs. Ni-Cr-Al
	Ni vs. Ni-Cr-Si
	Ni vs. Ni-Cr-Ge
	Ni vs. Ni-Cr-Pd
III	Ni-Cr vs. Ni-Cr-Al
	Ni-Cr vs. Ni-Cr-Si
	Ni-Cr vs. Ni-Cr-Ge
	Ni-Cr vs. Ni-Cr-Pd

The diffusion assembly was then mounted, sectioned, metallographically prepared for microstructural observations. Excellent bonding within all diffusion couples was observed. Then, cross-section surface was repolished with 1μm diamond paste for electron microprobe analysis. The concentration profiles of Ni, Cr, Al, Si, Ge, and Pd for the diffusion couples were determined with a JEOL™ 733 microprobe by point-to-point counting techniques using pure Ni, Cr, Al, Si, Ge, and Pd as standards. Intensities of K_α x-radiations were measured and converted to concentrations of Ni, Cr, Al, Si, Ge, and L_α x-radiations for that of Pd with appropriate ZAF corrections. Concentration profiles obtained from microprobe was smoothened by weighted-spline-tool using MatLab™. It should be noted that the analytical method employed in this study to determine interdiffusion coefficients by integration of interdiffusion fluxes, *vis.* Eq. (3.5), do not require the use of concentration gradients. This method significantly reduces the influence of smoothening procedure on the determination of interdiffusion coefficients.

3.4. Interdiffusion in Ni-Cr-X Alloys at 900°C

Figure 3.1 presents optical micrographs obtained from the diffusion couples Ni vs. Ni-Cr-Al and Ni vs. Ni-Cr-Si that was annealed at 900°C for 168 hours. Excellent bonding was achieved during the diffusion anneal for all diffusion couples. Figure 3.2 presents an example of experimental and smoothened concentration profiles that were used for the determination of interdiffusion coefficients. Scatters in the concentration profiles for all diffusion couples were minimum and within the experimental uncertainty associated with EPMA. Experimental concentration profiles were smoothened with weighted-spline routine by using MatLab™.

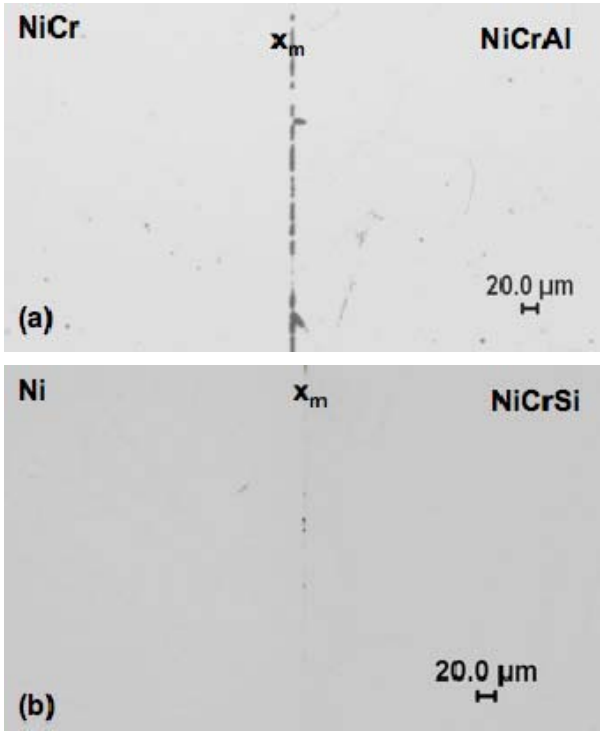

Figure 3.1. Typical optical micrographs of solid-to-solid diffusion couples etched with Kallings reagent: (a) Ni-Cr vs. Ni-Cr-Al, (b) Ni vs. Ni-Cr-Si annealed at 900°C for 168 hours. Specimens were slightly over-etched to clearly distinguish the experimental contact plane, x_m.

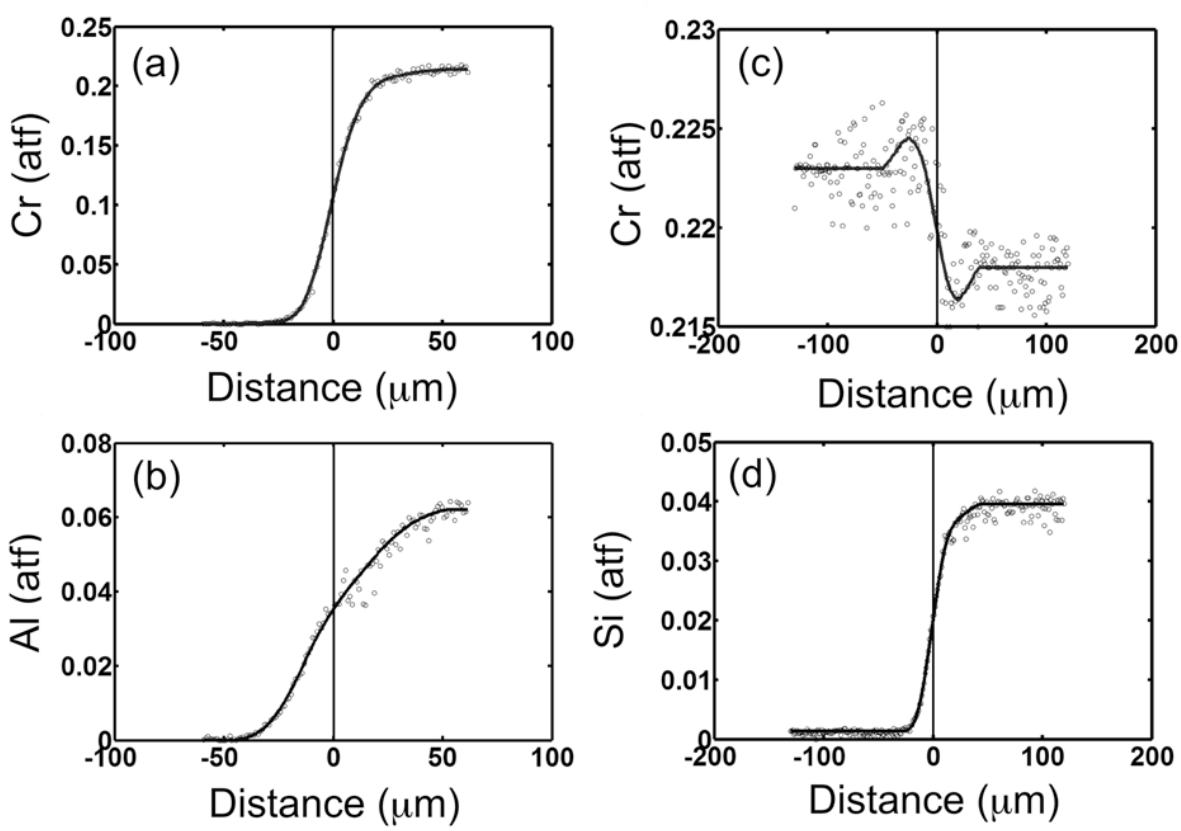

Figure 3.2: Typical experimental and smoothened concentration profiles measured from solid-to-solid diffusion couples (a,b) Ni vs. Ni-Cr-Al and (c,d) Ni-Cr vs. Ni-Cr-Si, annealed at 900°C for 168 hours.

From concentration profiles obtained from series I and II diffusion couples (i.e., Ni vs. Ni-Cr, and Ni vs. Ni-Cr-X), average effective interdiffusion coefficients $\tilde{D}_i^{eff}$'s on either side of the Matano plane were determined using Eq. (3.3). They are reported in Table 3.3. In general, $\tilde{D}_i^{eff}$ was higher on the $\left(C_i^o \sim C_i^{+\infty}\right)$ composition range with higher Cr concentration relative to the other side of the Matano plane. Table 3.3 also reports that Al addition to NiCr alloy can increase or decrease the $\tilde{D}_{Cr}^{eff}$ as a function of composition. This indicates appreciable variation in interdiffusion coefficients as a function of composition: specifically, Al increased $\tilde{D}_{Cr}^{eff}$ on the $\left(C_i^o \sim C_i^{+\infty}\right)$ composition range with higher Cr concentration. $\tilde{D}_{Cr}^{eff}$ was observed to increase with

Si addition to NiCr alloy especially on the $\left(C_i^o \sim C_i^{+\infty}\right)$ side with higher Cr concentration. According to Table 3.3, Ge does not change $\tilde{D}_{Cr}^{eff}$ significantly, while Pd addition to Ni-Cr alloy increased $\tilde{D}_{Cr}^{eff}$, quite significant on the $\left(C_i^o \sim C_i^{+\infty}\right)$ range with higher Cr concentration.

Table 3.3 : Average effective interdiffusion coefficients determined from Ni vs. Ni-Cr-X diffusion couples annealed at 900°C for 168 hours.

Diffusion Couple	Composition Range	$\tilde{D}_{Cr}^{eff}$ (10^{-16} m^2/s)	$\tilde{D}_{X}^{eff}$ (10^{-16} m^2/s)	$\tilde{D}_{Ni}^{eff}$ (10^{-16} m^2/s)
Ni vs. Ni-Cr (X = None)	$\left(C_i^{-\infty} \sim C_i^o\right)$	1.40	-	1.40
	$\left(C_i^o \sim C_i^{+\infty}\right)$	1.53	-	1.53
Ni vs. Ni-Cr-Al (X = Al)	$\left(C_i^{-\infty} \sim C_i^o\right)$	0.91	3.31	1.83
	$\left(C_i^o \sim C_i^{+\infty}\right)$	1.58	4.68	2.19
Ni vs. Ni-Cr-Si (X = Si)	$\left(C_i^{-\infty} \sim C_i^o\right)$	1.68	5.74	2.26
	$\left(C_i^o \sim C_i^{+\infty}\right)$	3.00	6.91	3.57
Ni vs. Ni-Cr-Ge (X = Ge)	$\left(C_i^{-\infty} \sim C_i^o\right)$	1.30	3.09	1.40
	$\left(C_i^o \sim C_i^{+\infty}\right)$	1.44	3.47	1.61
Ni vs. Ni-Cr-Pd (X = Pd)	$\left(C_i^{-\infty} \sim C_i^o\right)$	1.77	1.19	1.74
	$\left(C_i^o \sim C_i^{+\infty}\right)$	4.09	2.07	3.92

From concentration profiles obtained from diffusion couple series II (i.e., Ni vs. Ni-Cr-X), average ternary interdiffusion coefficients $\overline{\tilde{D}}_{ij}^{Ni}(i,j = Cr,X)$ were determined on either side of the Matano plane using Eq. (3.5). These are reported in Table 3.4. It should be noted that these diffusion couples were designed to yield the same sign of $\partial C_{Cr}/\partial x$ and $\partial C_X/\partial x$. Thus, positive and negative $\overline{\tilde{D}}_{CrX}^{Ni}$ indicates an increase and a decrease in $\tilde{J}_{Cr}$, respectively. In general, larger magnitudes of $\overline{\tilde{D}}_{CrCr}^{Ni}$ and $\overline{\tilde{D}}_{XX}^{Ni}$ were observed on the $\left(C_i^o \sim C_i^{+\infty}\right)$ composition range with higher Cr concentration. Al addition in the Ni-Cr alloy yielded positive $\overline{\tilde{D}}_{CrAl}^{Ni}$, and increased $\tilde{J}_{Cr}$ in

accordance with previous work by Nesbitt [25] and Morral [34]. The magnitude of $\overline{\tilde{D}}^{Ni}_{CrAl}$ was quite large as reported in Table 3.4 on the $\left(C_i^o \sim C_i^{+\infty}\right)$ with higher Cr concentration. Similarly, Si, Ge and Pd additions to Ni-Cr alloy increased $\tilde{J}_{Cr}$ with positive $\overline{\tilde{D}}^{Ni}_{CrX}$. This effect was, again, stronger when Cr concentration is high on the $\left(C_i^o \sim C_i^{+\infty}\right)$ particularly for Si and Pd.

Table 3.4: Average ternary interdiffusion coefficients determined from Ni vs. Ni-Cr-X diffusion couples (series II) annealed at 900°C for 168 hours.

Diffusion Couple	Composition Range	$\overline{\tilde{D}}^{Ni}_{CrCr}$ (10^{-16} m^2/s)	$\overline{\tilde{D}}^{Ni}_{CrX}$ (10^{-16} m^2/s)	$\overline{\tilde{D}}^{Ni}_{XCr}$ (10^{-16} m^2/s)	$\overline{\tilde{D}}^{Ni}_{XX}$ (10^{-16} m^2/s)
Ni vs. Ni-Cr-Al (X = Al)	$\left(C_i^{-\infty} \sim C_i^o\right)$	0.78	0.31	0.40	1.99
	$\left(C_i^o \sim C_i^{+\infty}\right)$	1.11	1.72	0.43	2.84
Ni vs. Ni-Cr-Si (X = Si)	$\left(C_i^{-\infty} \sim C_i^o\right)$	1.23	0.15	0.44	2.92
	$\left(C_i^o \sim C_i^{+\infty}\right)$	2.05	4.88	0.57	3.35
Ni vs. Ni-Cr-Ge (X = Ge)	$\left(C_i^{-\infty} \sim C_i^o\right)$	1.08	0.36	0.07	1.73
	$\left(C_i^o \sim C_i^{+\infty}\right)$	1.24	0.89	0.10	1.99
Ni vs. Ni-Cr-Pd (X = Pd)	$\left(C_i^{-\infty} \sim C_i^o\right)$	1.43	4.06	0.01	0.98
	$\left(C_i^o \sim C_i^{+\infty}\right)$	3.49	4.86	0.01	1.76

Diffusion couple series III was designed with initial $\partial C_{Cr}/\partial x = 0$, so that $\tilde{J}_{Cr}$ is largely due to $\partial C_X/\partial x$, and depends on the magnitude and sign of $\overline{\tilde{D}}^{Ni}_{CrX}$. $\tilde{J}_X$ has caused an uphill-diffusion of Cr in the direction of $\tilde{J}_X$ with positive $\overline{\tilde{D}}^{Ni}_{CrX}$ for Al and Si. This suggests that Al and Si increase the thermodynamic activity of Cr in Ni-Cr alloys. On the other hand, $\tilde{J}_{Ge}$ and $\tilde{J}_{Pd}$ did not caused any measurable redistribution of Cr ($\tilde{J}_{Cr} \approx 0$). Average ternary interdiffusion coefficients determined from diffusion couples series III are reported in Table 3.5. It should be

noted that Ge and Pd have lower contents in the Ni-Cr-X alloys than Al and Si, as reported in Table 3.1.

Table 3.5: Average ternary interdiffusion coefficients determined from Ni-Cr vs. Ni-Cr-X diffusion couples annealed at 900°C for 168 hours.

Diffusion Couple	Composition Range	$\overline{\tilde{D}}^{Ni}_{CrCr}$ (10^{-16} m^2/s)	$\overline{\tilde{D}}^{Ni}_{CrX}$ (10^{-16} m^2/s)	$\overline{\tilde{D}}^{Ni}_{XCr}$ (10^{-16} m^2/s)	$\overline{\tilde{D}}^{Ni}_{XX}$ (10^{-16} m^2/s)
Ni-Cr vs. Ni-Cr-Al (X = Al)	$\left(C_i^{-\infty} \sim C_i^o\right)$	0.23	0.12	0.01	0.67
	$\left(C_i^o \sim C_i^{+\infty}\right)$	1.20	0.44	0.13	1.17
Ni-Cr vs. Ni-Cr-Si (X = Si)	$\left(C_i^{-\infty} \sim C_i^o\right)$	2.58	1.73	0.01	0.68
	$\left(C_i^o \sim C_i^{+\infty}\right)$	1.39	0.63	1.78	1.97
Ni-Cr vs. Ni-Cr-Ge (X = Ge)	$\left(C_i^{-\infty} \sim C_i^o\right)$	$\Delta C_{Cr}/\Delta x = 0$ and cannot be determined.			
	$\left(C_i^o \sim C_i^{+\infty}\right)$				
Ni-Cr vs. Ni-Cr-Pd (X = Pd)	$\left(C_i^{-\infty} \sim C_i^o\right)$				

Based on average effective interdiffusion coefficients and average ternary interdiffusion coefficients determined in this study, alloying additions of Al, Si, Ge and Pd have all increased $\tilde{D}^{eff}_{Cr}$ and yielded positive $\overline{\tilde{D}}^{Ni}_{CrX}$ particularly at high Cr content (~22at.%). Therefore, the Cr_2O_3-forming ability of Ni-20at.%Cr-base alloy should improve with these alloying additions by establishing Cr_2O_3 scale, maintaining protective Cr_2O_3 scale formation, and in reformation of Cr_2O_3 on spallation. It should be noted that positive $\overline{\tilde{D}}^{Ni}_{XCr}$ reported in Tables 3.4 and 3.5 should also promote the formation of other scales (Al_2O_3, SiO_2) in the γ (fcc) Ni-Cr alloy, which may reduce the rate of scale growth and/or change the thermo-mechanical properties of the scale.

3.5. Interdiffusion in Ni-Cr-X Alloys at 700°C

Excellent diffusion bonding was achieved in all diffusion couples as shown by Figure 3.3 that presents a typical optical micrograph obtained by etching (Kalling's reagent) the polished surface of the diffusion couple.

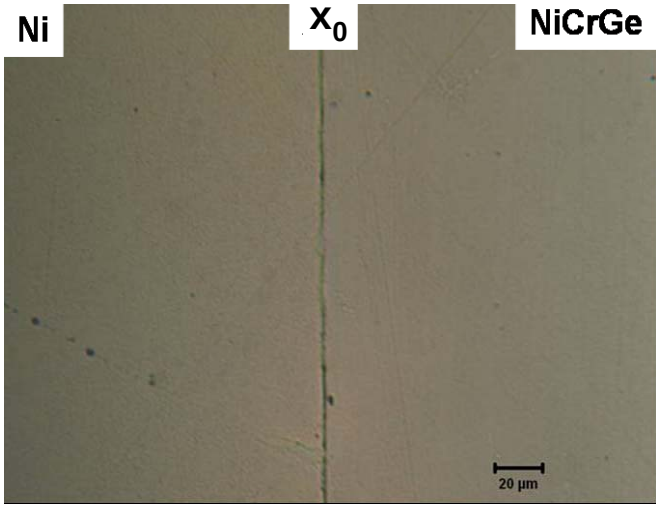

Figure 3.3 Typical optical micrograph of solid-to-solid diffusion couple Ni vs. Ni-Cr-Ge annealed at 700°C for 720 hours.

Figure 3.4 presents an example of experimental and smoothened concentration profiles that were used for the determination of interdiffusion fluxes and interdiffusion coefficients. The scatters in the concentration profiles for all diffusion couples were within the experimental uncertainty associated with EPMA. Experimental concentration profiles were smoothened with a smoothing-spline approximation by using MatLab. Consistency in experimental and smoothened concentration profiles of Cr in series III (see for example Figure 3.4), owing to similar terminal concentration was examined by multiple EPMA acquisitions (e.g., independent Cr concentration) and by close examination of concentration profiles for Ni and X ternary alloying additions (e.g.,

dependent Cr concentrations). *Consistency in terms of repeatable assessment of all concentration profiles was obtained for determination of interdiffusion fluxes and interdiffusion coefficients.*

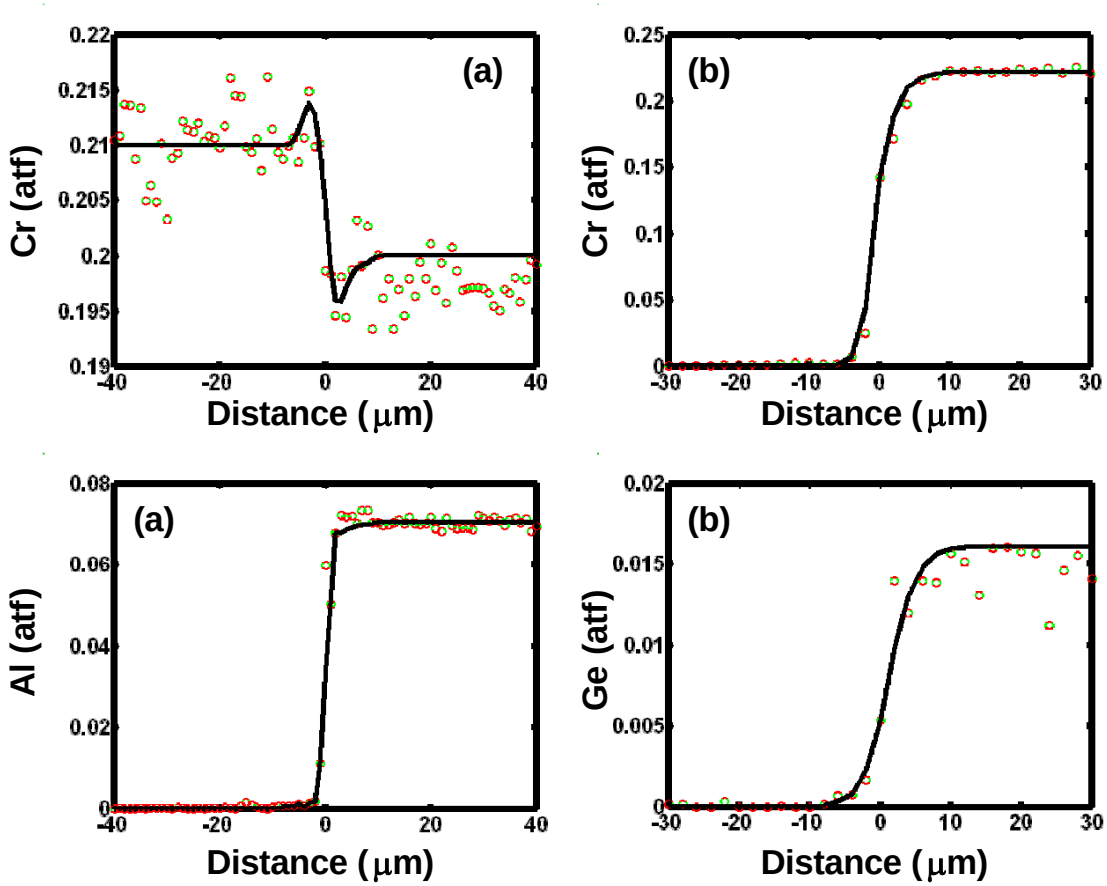

Figure 3.4: Typical experimental and smoothened concentration profiles measured from solid-to-solid diffusion couples (a) Ni-Cr vs. Ni-Cr-Al and (b) Ni vs. Ni-Cr-Ge annealed at 700°C for 720 hours. Note that concentration is given in atf, which stands for atomic fraction.

Using Eq. (3.5), average effective interdiffusion coefficients, $\tilde{D}_i^{eff}$'s on either side of the Matano plane were determined from the concentration profiles obtained from series I and II diffusion couples (i.e., Ni vs. Ni-Cr and Ni vs. Ni-Cr-X). They are reported in Tables 3.6. These average effective interdiffusion coefficients are two orders of magnitude lower than those

determined at 900°C. $\tilde{D}_i^{eff}$ was generally higher on the $\left(C_i^o \sim C_i^{+\infty}\right)$ composition range with higher Cr concentration relative to the other side.

Table 3.6:Average effective interdiffusion coefficients determined from Ni vs. Ni-Cr-X diffusion couples annealed at 700°C for 720 hours.

Diffusion Couple	Composition Range	$\tilde{D}_{Cr}^{eff}$ [10^{-18} m^2/s]	$\tilde{D}_X^{eff}$ [10^{-18} m^2/s]	$\tilde{D}_{Ni}^{eff}$ [10^{-18} m^2/s]
Ni vs. Ni-Cr (X = None)	$\left(C_i^{-\infty} \sim C_i^o\right)$	1.98	-	1.98
	$\left(C_i^o \sim C_i^{+\infty}\right)$	2.34	-	2.34
Ni vs. Ni-Cr-Al (X = Al)	$\left(C_i^{-\infty} \sim C_i^o\right)$	0.50	0.40	0.47
	$\left(C_i^o \sim C_i^{+\infty}\right)$	0.61	0.86	0.68
Ni vs. Ni-Cr-Si (X = Si)	$\left(C_i^{-\infty} \sim C_i^o\right)$	1.22	2.08	1.27
	$\left(C_i^o \sim C_i^{+\infty}\right)$	1.95	2.26	1.99
Ni vs. Ni-Cr-Ge (X = Ge)	$\left(C_i^{-\infty} \sim C_i^o\right)$	1.39	2.38	1.43
	$\left(C_i^o \sim C_i^{+\infty}\right)$	2.74	5.17	2.97
Ni vs. Ni-Cr-Pd (X = Pd)	$\left(C_i^{-\infty} \sim C_i^o\right)$	6.91	6.06	6.85
	$\left(C_i^o \sim C_i^{+\infty}\right)$	9.86	5.41	9.57

Table 3.6 also reports that Al, Si and Ge diffuse faster than Ni in γ-phase Ni-Cr-X alloys. In the case of Ni vs. Ni-Cr-Pd, $\tilde{D}_i^{eff}$'s for Ni, Cr and Pd are similar. These results are in general, analogues observations made at 900°C. At 700°C, Table 3.6 shows that Al and Si additions to Ni-Cr alloy reduced $\tilde{D}_{Cr}^{eff}$, but Pd additions to Ni-Cr alloy increased $\tilde{D}_{Cr}^{eff}$ significantly, especially in the composition range of $\left(C_i^o \sim C_i^{+\infty}\right)$.

Concentration profiles obtained from diffusion couple series II and III (i.e., Ni vs. Ni-Cr-X and NiCr vs. Ni-Cr-X) were employed to determine average ternary interdiffusion coefficients, $\overline{\tilde{D}}_{ij}^{Ni}$ on either side of the Matano plane using Eq. (3.5). These are reported in Tables 3.7 and 3.8. The magnitude of these interdiffusion coefficients is approximately two orders lower than those

determined at 900°C. The sign of the cross interdiffusion coefficients remained the same with those determined at 900°C.

Series II diffusion couples were designed to yield the same sign of $\partial C_{Cr}/\partial x$ and $\partial C_{X}/\partial x$ where a positive and negative $\tilde{\bar{D}}^{Ni}_{CrX}$ indicates an increase and a decrease in $\tilde{J}_{Cr}$, respectively. In general, higher magnitude of $\tilde{\bar{D}}^{Ni}_{CrCr}$ and $\tilde{\bar{D}}^{Ni}_{XX}$ was observed on the $\left(C_i^o \sim C_i^{+\infty}\right)$ composition range with higher Cr concentration. The Al addition in the Ni-Cr alloy yielded positive $\tilde{\bar{D}}^{Ni}_{CrAl}$, and increased $\tilde{J}_{Cr}$ in agreement with the previous work by Nesbitt [14], Thomson [15] and observation made at 900°C in this study.

Table 3.7. Average ternary interdiffusion coefficients determined from Ni-Cr vs. Ni-Cr-X diffusion couples annealed at 700°C for 720 hours.

Diffusion Couple	Composition Range	$\tilde{\bar{D}}^{Ni}_{CrCr}$ [10^{-18} m^2/s]	$\tilde{\bar{D}}^{Ni}_{CrX}$ [10^{-18} m^2/s]	$\tilde{\bar{D}}^{Ni}_{XCr}$ [10^{-18} m^2/s]	$\tilde{\bar{D}}^{Ni}_{XX}$ [10^{-18} m^2/s]
Ni vs. Ni-Cr-Al (X = Al)	$\left(C_i^{-\infty} \sim C_i^o\right)$	0.48	0.53	0.06	0.42
	$\left(C_i^o \sim C_i^{+\infty}\right)$	0.54	0.02	0.10	0.35
Ni vs. Ni-Cr-Si (X = Si)	$\left(C_i^{-\infty} \sim C_i^o\right)$	0.96	0.58	0.03	1.20
	$\left(C_i^o \sim C_i^{+\infty}\right)$	1.42	0.05	0.05	1.30
Ni vs. Ni-Cr-Ge (X = Ge)	$\left(C_i^{-\infty} \sim C_i^o\right)$	0.67	5.44	Negligible	2.51
	$\left(C_i^o \sim C_i^{+\infty}\right)$	0.93	5.84	Negligible	2.88
Ni vs. Ni-Cr-Pd (X = Pd)	$\left(C_i^{-\infty} \sim C_i^o\right)$	6.49	4.92	Negligible	5.84
	$\left(C_i^o \sim C_i^{+\infty}\right)$	7.59	5.83	Negligible	5.58

The Si, Ge and Pd additions to Ni-Cr alloy also increased $\tilde{J}_{Cr}$ with positive $\overline{\tilde{D}}^{Ni}_{CrX}$. This effect was stronger when Cr concentration was high on the $\left(C_i^o \sim C_i^{+\infty}\right)$ side, particularly for Ge and Pd. At 900°C, $\overline{\tilde{D}}^{Ni}_{CrGe}$ was not significant to this extent. The Si, Ge and Pd additions to Ni-Cr alloy also increased $\tilde{J}_{Cr}$ with positive $\overline{\tilde{D}}^{Ni}_{CrX}$. This effect was stronger when Cr concentration is high on the $\left(C_i^o \sim C_i^{+\infty}\right)$ side, particularly for Ge and Pd. Also at 900°C [9], $\overline{\tilde{D}}^{Ni}_{CrGe}$ was not significant while $\overline{\tilde{D}}^{Ni}_{CrSi}$ and $\overline{\tilde{D}}^{Ni}_{CrPd}$ were significantly large. This study at 700°C finds that $\overline{\tilde{D}}^{Ni}_{CrGe}$ and $\overline{\tilde{D}}^{Ni}_{CrPd}$ are large positive values while $\overline{\tilde{D}}^{Ni}_{CrSi}$ is not so significant.

Table 3.8. Average ternary interdiffusion coefficients determined from NiCr vs. Ni-Cr-X diffusion couples annealed at 700°C for 720 hours.

Diffusion Couple	Composition Range	$\overline{\tilde{D}}^{Ni}_{CrCr}$ [10^{-18} m^2/s]	$\overline{\tilde{D}}^{Ni}_{CrX}$ [10^{-18} m^2/s]	$\overline{\tilde{D}}^{Ni}_{XCr}$ [10^{-18} m^2/s]	$\overline{\tilde{D}}^{Ni}_{XX}$ [10^{-18} m^2/s]
Ni-Cr vs. Ni-Cr-Al (X = Al)	$\left(C_i^{-\infty} \sim C_i^o\right)$	1.98	0.73	1.97	0.78
	$\left(C_i^o \sim C_i^{+\infty}\right)$	2.65	1.00	1.01	0.76
Ni-Cr vs. Ni-Cr-Si (X = Si)	$\left(C_i^{-\infty} \sim C_i^o\right)$	6.91	5.87	0.11	0.62
	$\left(C_i^o \sim C_i^{+\infty}\right)$	2.59	2.22	0.16	1.35
Ni-Cr vs. Ni-Cr-Ge (X = Ge)	$\Delta C_{Cr}/\Delta x \approx 0$ and cannot be determined				
Ni-Cr vs. Ni-Cr-Ge (X = Ge)					

Diffusion couple series III was designed so that the initial $\partial C_{Cr}/\partial x \approx 0$. Therefore, $\tilde{J}_{Cr}$ is mainly due to $\partial C_X/\partial x$, and the magnitude and sign of $\overline{\tilde{D}}^{Ni}_{CrX}$. $\tilde{J}_{Al}$ and $\tilde{J}_{Si}$ have caused an uphill-diffusion of Cr owing to positive $\overline{\tilde{D}}^{Ni}_{CrAl}$ and $\overline{\tilde{D}}^{Ni}_{CrSi}$, respectively. On the other hand, $\tilde{J}_{Ge}$ and $\tilde{J}_{Pd}$ did not cause any measurable redistribution of Cr ($\tilde{J}_{Cr} \approx 0$). However, Ge and Pd are lower in

concentration than those of Al and Si, in the Ni-Cr-X alloys, as reported in Table 3.1. Based on average effective interdiffusion coefficients and average ternary interdiffusion coefficients determined at 700°C, alloying additions of Al, Si, Ge and Pd have yielded positive $\overline{\tilde{D}}_{CrX}^{Ni}$. Therefore, Cr_2O_3-forming ability of Ni-22at.%Cr alloy should improve with these alloying additions.

3.6 Summary

From experimental solid-to-solid diffusion couples, small addition of Al, Si, Ge, or Pd was observed to increase the overall interdiffusion flux of Cr in Ni-22at.%Cr-X (fcc γ phase) alloys. Experimental concentration profiles, measured after annealing at 900°C and 700°C in a three-zone tube furnace for 168 and 720 hours, respectively, were employed to determine interdiffusion fluxes, average effective interdiffusion coefficients and average ternary interdiffusion coefficients. In general, $\tilde{D}_i^{eff}$ was observed to increase with higher Cr concentration. Also, $\overline{\tilde{D}}_{CrX}^{Ni}$ coefficients were determined to be positive with alloying additions of Al, Si, Ge, or Pd. These results suggest that these alloying additions can help the formation of Cr_2O_3-scale for initial scale formation, maintaining scale homogeneity during prolonged high-temperature exposure, and reformation after scale-spallation.

3.7 References

1. C.T. Sims, N.S. Stoloff, W.C. Hagel, Superalloys II, John Wiley and Sons, 1987.
2. P. Kofsted, 'Growth and protective properties of Chromia (Cr_2O_3) and Alumina (Al_2O_3) scales, protective coatings', High temperature Corrosion, Elsevier, London, 1980, p. 389.
3. J.L. Smialek, C.A. Barrett, J.C. Schaffer, Design for oxidation resistance, ASM handbook, George E. Dieter, Ed., ASM International, 1997, p. 589.
4. F.H. Stott, G.C. Wood, M.G. Hobby, A comparison of the oxidation behavior of Fe-Cr-Al, NI-Cr-Al and Co-Cr-Al alloys, *Oxi. Metals*, Vol. 3, 1971, p. 103.

5. C.E. Lowell, A scanning electron microscope study of the surface morphology of TD-NiCr oxidized at 800°C to 1200°C, *Oxi. Metals*, Vol. 5, 1972, p. 205.
6. C.E. Lowell, Cyclic and isothermal oxidation behavior on some Ni-Cr alloys, *Oxid. Metals*, Vol. 7, 1973, p. 95.
7. G.M. Ecer, G.H. Meier, Oxidation of high-chromium Ni-Cr alloys, *Oxi. Metals*, Vol. 13, 1979, p. 119.
8. G. Benabderrazik, G. Moulin, A.M. Huntz, Relation between impurities and oxide-scale growth mechanisms on Ni-34Cr and Ni-20Cr alloys – I. Influence of C, Mn, and Si, *Oxi. Metals*, Vol. 33, 1990, p. 191.
9. J. F. Schmitt, N. Pacia, P. Pigeat, B. Weber, Study of the initial oxidation of a Ni-20Cr alloy in the temperature range 550–830°C: Influence of mechanical deformation, *Oxid. Metals*, Vol. 44, 1995, p 429.
10. C.K. Kim, L.W. Hobbs, Microstructural evidence for short-circuit oxygen diffusion paths in the oxidation of a dilute Ni-Cr alloy, *Oxid. Metals*, Vol. 45, 1996, p. 247.
11. B. Ahmad, P. Fox, STEM analysis of the transient oxidation of a Ni-20Cr alloy at high temperature, *Oxi. Metals*, Vol. 52, 1998, p. 113.
12. J.R. Nicholls, M.J. Bennett, Cyclic oxidation-guidelines for test standardization, aimed at the assessment of service behavior, Mater. High Temp., Vol. 17, 2000, p 413.
13. B. Li, B.Gleeson, Effect of Silicon on Oxidation Behavior of Ni-base chromia-forming alloys, *Oxi. Metals*, 2006, in press.
14. F.H. Stott, G.C. Wood, J. Stringer, The influence of alloying elements on the development and maintenance of protective scales, Oxi. Metals, Vol. 44, 1995, p. 113.

15. D.P. Whittle, J. Stringer, Improvements in high temperature oxidation resistance by additions of reactive elements or oxide dispersions, Proc. Royal Soc. Lond. A, Vol. 295, 1980, p. 309.
16. G.C. Wood: Oxidation of Metals, Mater. Sci. Technol., Vol. 3, 1987, p. 519.
17. G.C. Wood, J.A. Richards, M.G. Hobby, J. Boustead, Identification of thin healing layers at based of oxide scale on Fe-Cr base alloys, Corr. Sci. Vol. 9, 1969, p. 659.
18. A.G. Revsz, F.P. Fehlner, The role of noncrystalline films in the oxidation and corrosion of metals, Oxid. Metals, Vol. 15, 1981, p. 297.
19. M.J. Bennett, J.A. Desport, P.A. Labun, Analytical electron microscopy of a selective oxide scale formed on 20% Cr-25% Ni-Nb stainless steel, Oxi. Metals, Vol. 22, 1984, p. 291.
20. M.J. Bennett, J.A. Despota, P.A. Labun, Transverse microstructue of an oxide scale formed on a 20%Cr-25%Ni-Nb stabilized stainless steel, Proc. Royal Soc. London, Seiries A – Math. Phys. Eng. Sci., Vol. 412, 1987, p. 223.
21. R.C. Lobb, J.A. Sasse, H.E. Evans, Dependence of oxidation behavior on Silicon content of 20%Cr Austenitic steels, Mater. Sci. Technol., Vol. 5, 1989, p. 828.
22. W.C. Hagel, Oxidation of Iron Nickel and Cobalt-base alloys containing Aluminum, Corr., Vol. 21, 1965, p. 316.
23. J.A. Nesbitt, Numerical modeling of high-temperature corrosion processes, Oxi. Metals, Vol. 44, 1995 p. 309.
24. H.E. Evans, A.T. Donaldson, T.C. Gilmour, Mechanisms of breakaway oxidation and application to a chromia-forming steel, Oxi. Metals, Vol. 52, 1999, p. 379.
25. J.A. Nesbitt, R.W. Heckel, Interdiffusion in Ni-Rich, Ni-Cr-Al alloys at 1100 and 1200°C: Part I. Diffusion paths and Microstructures., *Metall. Trans. A*, Vol. 18A, 1987, p 2061.

26. C.S. Giggin, F.S. Pettit, Oxidation of Ni-Cr-Al alloys between 1000 and 1200C, J. Electrochem. Soc., Vol. 118, 1971, p. 1782.
27. B.A. Pint, J.R. Keiser, Alloy selection for high temperature heat exchangers, NACE Paper 06-469, Houston, TX, 2006; Presented at NACE Corrosion 2006, San Diego, CA, March, 2006.
28. M.P. Brady, B. Gleeson, I.G. Wright, Alloy design strategies for promoting protective oxide scale formation, JOM, Vol. 52, 2000, p. 16.
29. D.J. Young, B. Gleeson: Alloy phase transformations driven by high temperature corrosion processes, Corr. Sci., Vol. 44, 2002, p. 345.
30. L. Onsager, Theories and problems of liquid diffusion, *Ann. NY Acad. Sci*., Vol. 46 1965, p. 241.
31. M.A. Dayananda, C.W. Kim, Zero-flux planes and flux reversals in Cu-Ni-Zn diffusion couples, *Metall. Trans. A*, Vol. 10A, 1979, p. 1333.
32. M.A. Dayananda, Y.H. Sohn, Average effective interdiffusion coefficients and their applications for isothermal multicomponent diffusion couples, *Scr. Mater.*, Vol. 40, 1996, p. 683.
33. M.A. Dayananda, Y.H. Sohn, A new approach for the determination of interdiffusion coefficients in ternary systems, Metall. Mater. Trans. A, Vol. 30A, 1999, p. 535.
34. M.S. Thompson, J.E. Morral, A.D. Romig, Jr., Applications of the square root diffusivity to diffusion in Ni-Al-Cr alloys, Metall. Trans. A, Vol. 21A, 1990, p. 2679.

CHAPTER 4: TERNARY AND QUATERNARY INTERDIFFUSION IN FE-NI-CR-X ALLOYS AT 900°C

4.1 Introduction

Austenitic (fcc-γ) Cr_2O_3 forming Fe-Ni-Cr alloys are of potential interest for many applications due to their combination of good oxidation/corrosion resistance and high temperature strength [1-7]. Minor alloying additions (< 5 wt.%) on these alloys are found to increase the oxidation resistance by forming a slowly growing, adherent, continuous and impervious layer of Cr_2O_3 [4,8,9]. In this work, effects of Si and Ge alloying additions on the interdiffusion behavior of quaternary Fe-Ni-Cr-X (X = Si, Ge) alloys (fcc γ-phase) were studied by using solid-to-solid diffusion couples with due respect for the formation and growth kinetics of protective Cr_2O_3 scale of these alloys.

Ternary and quaternary interdiffusion coefficients are important tools to explain the effects of minor alloying additions on the oxidation of Cr_2O_3-forming alloys. In this work, interdiffusion in Fe-24at.%Ni-22at.%Cr-X (fcc γ phase) alloys (X = Si, Ge) was examined using solid-to-solid diffusion couples annealed at 900°C for 168 hours. The selection criteria of minor alloying additions (e.g., Si, Ge) for the case of Ni-Cr alloys has been described in earlier interdiffusion studies carried out at 900°C and 700°C [10,11]. Experimental concentration profiles are employed to calculate interdiffusion fluxes of individual components, and determine average effective interdiffusion coefficients and average ternary and quaternary interdiffusion coefficients. Interdiffusion coefficients are examined to assess effects of alloying additions on the interdiffusion behavior of Cr in promoting Cr_2O_3-formation in Fe-24at.%Ni-22at.%Cr-X alloys.

4.2 Determination of Interdiffusion Coefficients

In this study, the interdiffusion fluxes $\tilde{J}_i$ of all components were determined directly from their concentration profiles using Eq. (3.2). Based on the integration of interdiffusion fluxes described in section 3.2, average effective interdiffusion coefficients, $\tilde{D}_i^{eff}$ were calculated using Eq. (3.3) for individual components. Average ternary interdiffusion coefficients, as defined and described in section 3.2 were determined using Eq. (3.5) for ternary Fe-Cr-X alloys while those for quaternary Fe-Ni-Cr-X alloys were determined using the expression:

$$\int_{x_1}^{x_2} \tilde{J}_i (x - x_o)^n dx = -\overline{\tilde{D}}_{i1}^4 \int_{C_1(x_1)}^{C_1(x_2)} (x - x_o)^n dC_1 - \overline{\tilde{D}}_{i2}^4 \int_{C_2(x_1)}^{C_2(x_2)} (x - x_o)^n dC_2 - \overline{\tilde{D}}_{i3}^4 \int_{C_2(x_1)}^{C_2(x_2)} (x - x_o)^n dC_3 \quad (i = 1,2,3) \tag{4.1}$$

Eq. (3.5) provides four equations involving the $\overline{\tilde{D}}_{ij}^3$ interdiffusion coefficients (n = 0, 1) and can be set up from interdiffusion fluxes calculated using Eq. (3.2) from the concentration profiles of a single diffusion couple of the ternary system. Similarly, Eq. (4.1) provides nine equations involving nine $\overline{\tilde{D}}_{ij}^4$ interdiffusion coefficients (n = 0, 1 and 2) from the single diffusion couple in a quaternary system. The $\overline{\tilde{D}}_{ij}^k$ coefficients, characteristic of the diffusion path, can be determined over selected composition ranges that include nonlinear segment of the profiles [15].

4.3 Experimental Procedure

Ternary and quaternary alloys of Fe-Ni-Cr-X (fcc γ phase) system with compositions reported in Table 4.1 were prepared with 99.9% pure Fe, Ni, Cr, Si and Ge by arc melting under an argon atmosphere. These alloys were chill-cast by water-cooled copper molds into rods with approximately 12 mm in diameter. The alloy rods were placed in a quartz capsule, evacuated to pressure below 10^{-6} torr, and flushed with hydrogen. The hydrogen-flush procedure was repeated several times, and Ar was finally filled into the capsule before the final encapsulation. They were homogenized at 900°C for 168 hours in a horizontal Lindberg™ 3-zone tube furnace, and water-quenched to retain the high temperature microstructure. The microstructures and compositions of the alloys were examined by optical microscopy, scanning electron microscopy (SEM), energy dispersive spectroscopy (EDS) and electron microprobe analysis (EMPA). No measurable variation in the alloy compositions was found, and all alloys consisted single-phase fcc solid solution (γ-phase).

Table 4.1Nominal compositions of Fe-Ni-Cr-X alloys employed for solid-to-solid diffusion couple studies. Values in parenthesis are standard deviation.

Alloy Identification	Composition (atom percent)			
	Fe	Ni	Cr	X
Fe-Ni	76.3 (0.7)	23.7 (0.7)	-	-
Fe-Ni-Cr	55.5 (0.7)	23.1 (0.4)	21.4 (0.4)	-
Fe-Ni-Cr-Si (X = Si)	52.2 (0.7)	22.3 (0.4)	21.4 (0.3)	4.1 (0.4)
Fe-Ni-Cr-Ge (X = Ge)	53.4 (0.3)	22.3 (0.4)	21.9 (0.3)	1.4 (0.3)

Alloy disks of approximately 2 mm in thickness were sliced from the rods of alloys, and prepared metallographically by polishing through 0.25 μm diamond paste. Table 4.2 presents ternary and quaternary diffusion coupes that were assembled with the disks held together in Invar™ steel jig consisting of two end plates and three threaded rods. The couples were placed in quartz capsules, which were sealed at one end, and evacuated to a pressure less than 10^{-6} torr and flushed with hydrogen several times. Ar was filled into a capsule before the final sealing. The capsules containing the couples were annealed at 900˚C in a horizontal Lindberg 3-zone furnace for 168 hours. After the diffusion anneal, the couples were quenched in water to preserve the high temperature composition and/or microstructure.

Table 4.2 : List of solid-to-solid diffusion couples annealed at 900ºC for 168 hours.

Series	Diffusion Couples
Fe-Ni vs. Fe-Ni-Cr-X (Si,Ge)	Fe-Ni vs. Fe-Ni-Cr
	Fe-Ni vs. Fe-Ni-Cr-Si
	Fe-Ni vs. Fe-Ni-Cr-Ge

The diffusion couple assembly was then mounted, sectioned and metallographically prepared for microstructural observations. Excellent diffusion bonding in all couples was observed. Then, cross-section surface was polished with 1μm diamond paste for electron microprobe analysis (EPMA). The concentration profiles of Fe, Ni, Cr, Si and Ge for the diffusion couples were determined with a JEOL 733 (Tokyo, Japan) microprobe by point-to-point counting techniques using pure standards of all the constituent alloying elements. Intensities of K_α X-radiations were measured and converted to concentrations of Fe, Ni, Cr, Si and Ge with appropriate ZAF (atomic number, Z; absorption, A; fluorescence, F) corrections.

Concentration profiles obtained from EPMA were smoothened by a smoothening-spline-tool using MatLab (The Math Works, Natick, MA). The analytical method used in this study to determine interdiffusion coefficients is by the integration of interdiffusion fluxes (e.g. Eqs. 3.5 and 4.1) only. It does not require the determination of concentration gradients that significantly reduces the influence of a smoothening procedure on the determination of interdiffusion coefficients.

4.4. Results and Discussions

Figures 4.1 and 4.2 present examples of experimental and smoothened concentration profiles that were used for the determination of interdiffusion fluxes and interdiffusion coefficients. The scatters in the concentration profiles for all diffusion couples were minimal and within the experimental uncertainty associated with EPMA. Consistency in experimental and smoothened concentration profiles of Ni, owing to similar terminal concentration was examined by multiple EPMA acquisitions (e.g., independent Ni concentration) and by close examination of concentration profiles for Cr and X ternary alloying additions (e.g., dependent Ni concentrations).

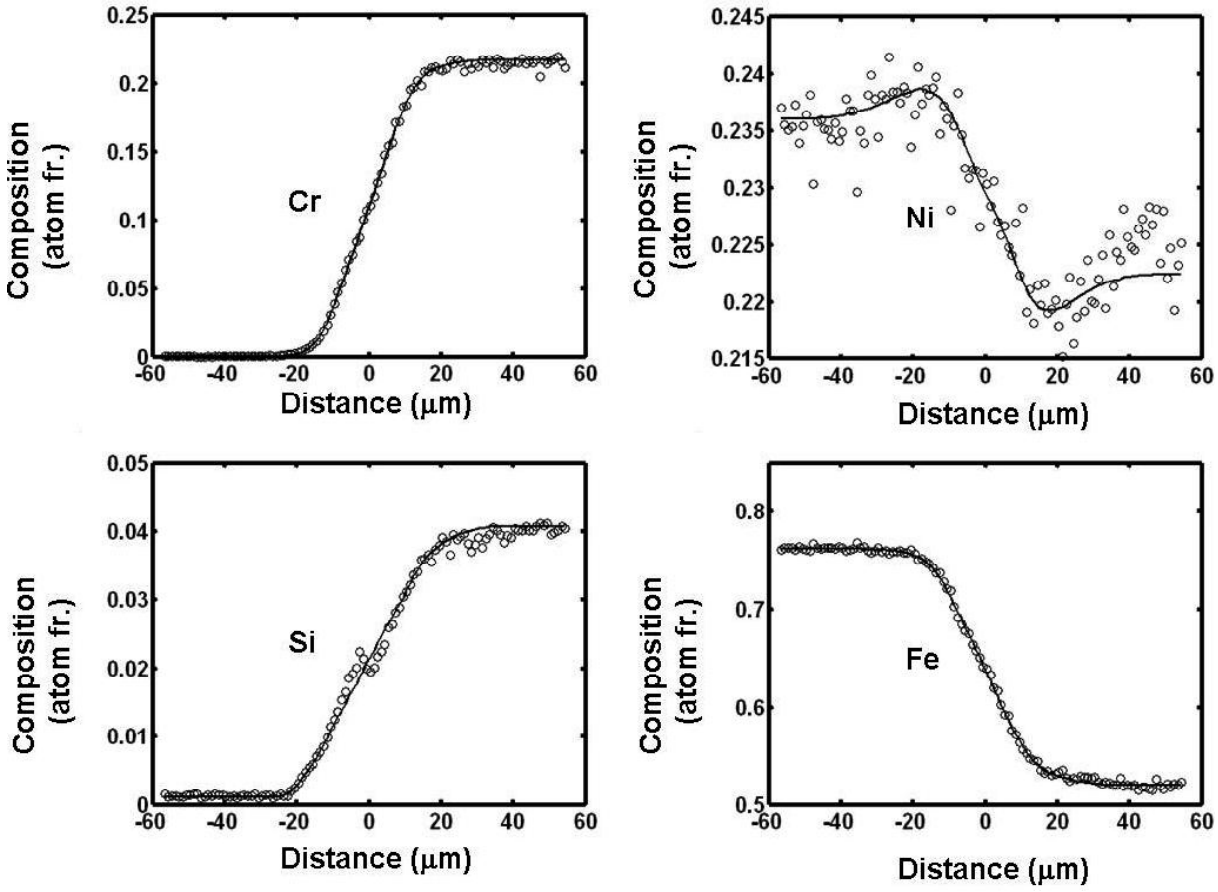

Figure 4.1 : Typical experimental and smoothened concentration profiles from solid-to-solid diffusion couple, Fe-Ni vs. Fe-Ni-Cr-Si annealed at 900°C for 168 hours.

From concentration profiles obtained from diffusion couples, average effective interdiffusion coefficients $\tilde{D}_i^{eff}$'s on either side of the Matano plane were determined using Eq. 3.2, and are reported in Table 4.3. Fe-Ni vs. Fe-Ni-Cr is considered as a reference to compare and contrast the diffusional interactions of alloying elements Si and Ge. Average effective interdiffusion coefficients reported in Table 4.3 are comparable in magnitude to those determined for Ni-Cr-X (Si, Ge) alloys at 900°C [12]. Alloying additions have increased the

magnitude of average effective interdiffusion coefficients of Cr and Fe on the $\left(C_i^o \sim C_i^{+\infty}\right)$ side with X (X = Si or Ge) alloying additions.

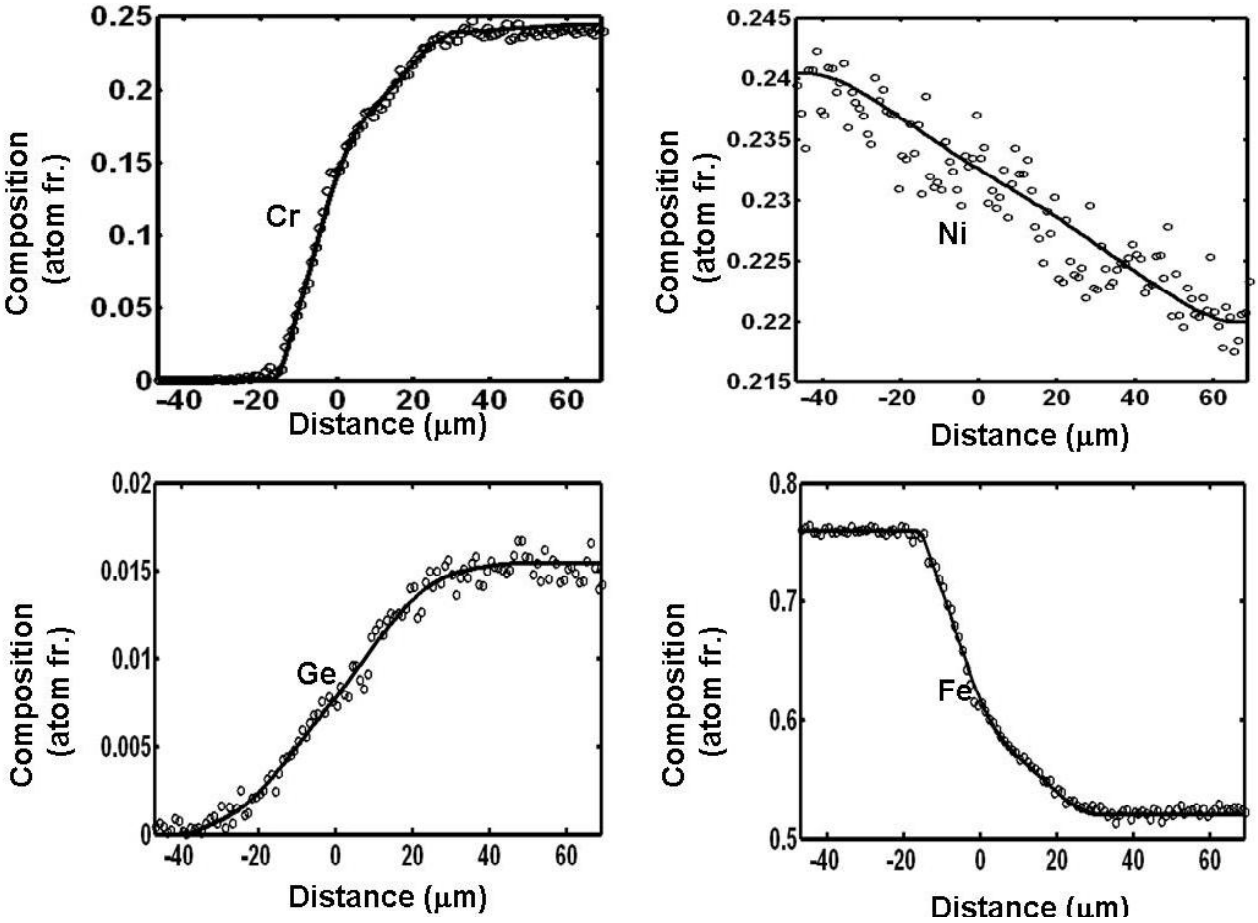

Figure 4.2 : Typical experimental and smoothened concentration profiles from solid-to-solid diffusion couple, Fe-Ni vs. Fe-Ni-Cr-Ge annealed at 900°C for 168 hours.

Table 4.3 : Average effective interdiffusion coefficients determined from Fe-Ni vs. Fe-Ni-Cr-X (Si, Ge) diffusion couples annealed at 900°C for 168 hours. (Units: 10^{-16} m^2/s)

Diffusion Couple	Composition Range	$\tilde{D}_{Cr}^{eff}$	$\tilde{D}_{X}^{eff}$	$\tilde{D}_{Ni}^{eff}$	$\tilde{D}_{Fe}^{eff}$
Fe-Ni vs. Fe-Ni-Cr	$\left(C_i^{-\infty} \sim C_i^{o}\right)$	0.6	N/A	N/A	0.6
	$\left(C_i^{o} \sim C_i^{+\infty}\right)$	0.3	N/A	N/A	0.3
Fe-Ni vs. Fe-Ni-Cr-Si (X = Si)	$\left(C_i^{-\infty} \sim C_i^{o}\right)$	0.7	1.3	-2.8	0.9
	$\left(C_i^{o} \sim C_i^{+\infty}\right)$	0.8	1.2	-2.3	1.0
Fe-Ni vs. Fe-Ni-Cr-Ge (X = Ge)	$\left(C_i^{-\infty} \sim C_i^{o}\right)$	0.7	2.8	3.9	0.7
	$\left(C_i^{o} \sim C_i^{+\infty}\right)$	1.8	2.7	2.9	1.7

Note: $\tilde{D}_{Ni}^{eff}$ could not be determined since there was no observable development of concentration gradient (i.e., pseudo-binary).

Duh's [16] study for interdiffusion in Fe-Ni-Cr alloys at 1100°C reported a decrease in $\tilde{D}_{CrCr}^{Fe}$ values with an increase in Cr at constant Ni concentration. Similar observation was made in this study from Fe-Ni vs. Fe-Ni-Cr diffusion couple where $\tilde{D}_{Cr}^{eff}$ was observed to decrease on the $\left(C_i^{o} \sim C_i^{+\infty}\right)$ region with higher Cr content. However, the influence of Si and Ge alloying additions on quaternary diffusion couples altered this trend by increasing the $\tilde{D}_{Cr}^{eff}$ on the $\left(C_i^{o} \sim C_i^{+\infty}\right)$ side where the contents of both Cr and X (X = Si or Ge) are higher. $\tilde{J}_{Si}$ caused an uphill-diffusion of Ni as shown in Figure 4.1, which yielded a negative average effective interdiffusion coefficients of Ni, $\tilde{D}_{Ni}^{eff}$, reported in Table 4.3. This indicates a significant diffusional interaction between Ni and Si in austenitic Fe-based alloys where $\tilde{J}_{Ni}$ would be significantly influence by the concentration gradient of Si, $\partial C_{Si}/\partial x$. There was no "noticeably-unusual" redistribution of Ni in Fe-Ni vs. Fe-Ni-Cr-Ge diffusion couple as shown in Figure 4.2. However, a higher magnitude of $\tilde{D}_{Ni}^{eff}$ in Table 4.3 is noted for all concentration ranges within this diffusion couple.

Concentration profiles obtained from diffusion couples were employed to determine the average quaternary interdiffusion coefficients $\overline{\tilde{D}}_{ij}^{Fe}(i,j=Cr,Ni,X)$ on either side of the Matano plane using Eq. (4.1). They are reported in Table 4.4. Table 4.4 reports that the magnitude of these interdiffusion coefficients are comparable to those obtained for Ni-Cr-X alloys at 900°C [11]. These diffusion couples were designed with initial $\partial C_{Ni}/\partial x \approx 0$, and to yield the same sign of $\partial C_{Cr}/\partial x$ and $\partial C_X/\partial x$, so that a positive and negative $\overline{\tilde{D}}_{CrX}^{Fe}$ indicates an increase and a decrease in $\tilde{J}_{Cr}$, respectively. Also, the initial $\partial C_{Ni}/\partial x \approx 0$ implies that, $\tilde{J}_{Ni}$ is mainly due to $\partial C_{Cr}/\partial x$ and/or $\partial C_X/\partial x$, and the magnitude and sign of $\overline{\tilde{D}}_{NiCr}^{Fe}$ and/or $\overline{\tilde{D}}_{NiX}^{Fe}$.

Table 4.4 : Average quaternary interdiffusion coefficients determined from Fe-Ni vs. Fe-Ni-Cr-X (X = Si or Ge) diffusion couples annealed at 900°C for 168 hours. (Units: 10^{-16} m^2/s)

Couple	Composition Range	$\overline{\tilde{D}}_{CrCr}^{Fe}$	$\overline{\tilde{D}}_{CrNi}^{Fe}$	$\overline{\tilde{D}}_{CrX}^{Fe}$	$\overline{\tilde{D}}_{NiCr}^{Fe}$	$\overline{\tilde{D}}_{NiNi}^{Fe}$	$\overline{\tilde{D}}_{NiX}^{Fe}$	$\overline{\tilde{D}}_{XCr}^{Fe}$	$\overline{\tilde{D}}_{XNi}^{Fe}$	$\overline{\tilde{D}}_{XX}^{Fe}$
Fe-Ni vs. Fe-Ni-Cr-Si (X=Si)	$(C_i^{-\infty} \sim C_i^o)$	1.1	0.3	-2.1	-0.1	2.7	2.7	0.2	Neg.	0.1
	$(C_i^o \sim C_i^{+\infty})$	1.0	0.3	-1.1	-0.3	1.6	4.2	0.1	Neg.	0.3
Fe-Ni vs. Fe-Ni-Cr-Ge (X=Ge)	$(C_i^{-\infty} \sim C_i^o)$	0.8	-0.1	0.4	-0.3	4.3	4.3	0.1	-0.6	0.1
	$(C_i^o \sim C_i^{+\infty})$	1.6	-0.4	2.9	-0.3	3.2	3.3	Neg.	-0.3	1.5

Note: "Neg." refers to magnitude less than 0.1 x 10^{-16} m^2/s.

The $\tilde{D}_{CrNi}^{Fe}$ and $\tilde{D}_{NiCr}^{Fe}$ cross coefficients have been reported small in magnitude and both positive and negative signs in literature [16-18] for Fe-Ni-Cr alloys. This holds true for quaternary cross coefficients, $\overline{\tilde{D}}_{CrNi}^{Fe}$ and $\overline{\tilde{D}}_{NiCr}^{Fe}$ reported in Table 4.4. This implies that there is no

significant influence of Ni and Cr on each other in austenitic Fe alloys. The magnitude of $\overline{\tilde{D}}^{Fe}_{SiSi}$ is lower than that of both $\overline{\tilde{D}}^{Fe}_{NiNi}$ and $\overline{\tilde{D}}^{Fe}_{CrCr}$ coefficients for Fe-Ni-Cr-Si alloys. However, the magnitude of $\overline{\tilde{D}}^{Fe}_{CrSi}$ and $\overline{\tilde{D}}^{Fe}_{NiSi}$ coefficients is comparable to that of $\overline{\tilde{D}}^{Fe}_{CrCr}$ and $\overline{\tilde{D}}^{Fe}_{NiNi}$ coefficients. The large magnitude of $\overline{\tilde{D}}^{Fe}_{NiSi}$ would have caused an uphill-diffusion of Ni. The magnitude of $\overline{\tilde{D}}^{Fe}_{GeGe}$ coefficient is comparable with that of $\overline{\tilde{D}}^{Fe}_{CrCr}$, and slightly lower than that of $\overline{\tilde{D}}^{Fe}_{NiNi}$ coefficient. Even though the magnitude of $\overline{\tilde{D}}^{Fe}_{NiGe}$ is large, an apparent uphill-diffusion of Ni is be absent due to a large $\overline{\tilde{D}}^{Fe}_{NiNi}$ despite a very small $\partial C_{Ni}/\partial x$.

4.5. Summary

Interdiffusion in Fe-Ni-Cr (fcc γ phase) alloys with small additions of Si and Ge was studied using solid-to-solid diffusion couples annealed at 900°C for 168 hours. Alloying addition of Si or Ge altered diffusional behavior of Ni and Cr in austenitic Fe-Ni-Cr alloys. Large magnitude of cross coefficients, $\overline{\tilde{D}}^{Fe}_{CrSi}$, $\overline{\tilde{D}}^{Fe}_{CrGe}$, $\overline{\tilde{D}}^{Fe}_{NiSi}$ and $\overline{\tilde{D}}^{Fe}_{NiGe}$ were observed in Fe-Ni-Cr-X (X=Si or Ge) alloys. The Si addition has caused on uphill-diffusion of Ni while there was no measurable uphill diffusion of Ni due to an increase in $\overline{\tilde{D}}^{Fe}_{NiNi}$ in Fe-Ni-Cr-Ge alloy, despite the large positive $\overline{\tilde{D}}^{Fe}_{NiGe}$.

4.6 References

[1] J.L. Smialek and G.H.Meier, in: *High temperature oxidation*, edited by C.T. Sims, N.S. Stoloff, and W.C. Hagel, of Superalloy II, chapter 11, John Weley & Sons (1987) p. 293-323.

[2] P. Kofstad, in: *Growth and protective properties of Chromia and Alumina scales, protective coatings*, High temperature Corrosion, Elsevier, London (1980) p. 389-404.

[3] J.L. Smialek, C.A. Barrett, J.C. Schaffer, in: *Design for oxidation resistance*, edited by George E. Dieter,Vol. 20 of ASM handbook, ASM International (1997).

[4] F.H. Stott, G.C. Wood, and J. Stringer : Oxi. Metals, Vol. 44 (1995), p. 113-145.

[5] H.E. Evans, D.A. Hilton, R.A. Holm et al.: Oxi. Metals, Vol. 19 (No. 1-2), 1983, p. 1-18.

[6] S.N.Basu, G.J.Yurek: Oxi. Metals, Vol. 36 (No. 3-4), 1991, p. 281-315.

[7] A. Kumar, D.L. Douglass: Oxi. Metals, Vol. 10 (No. 1), 1976, p. 1-22.

[8] D.P. Whittle, J. Stringer: Proc. R. Soc. Lond., Ser. A, Vol. 295 (1980), p.309-329.

[9] G.C. Wood, F.H. Stott: Mater. Sci. Technol., Vol.3 (1987), p. 519-530.

[10] N. Garimella, M.P. Brady, Y.H. Sohn: Defects and Diffusion Forum, Vol. 266, (2007), p. 191-198.

[11] N. Garimella, M.P. Brady, Y.H. Sohn: Journal of Phase Equilibria and Diffusion, Vol. 27, (2006), p. 665-670.

[12] L.Onsager, Ann. N.Y.Acad. Sci., Vol. 46 (1965), p. 241-265.

[13] M.A. Dayananda, C.W. Kim: Metall. Trans. A, Vol. 10A (1979), p. 1333-1339.

[14] M.A. Dayananda, Y.H. Sohn: Scr. Mater., Vol. 40 (1996), p. 683-688.

[15] M.A. Dayananda, Y.H. Sohn: Metall. Trans. A, Vol. 30A (1999), p 535-543.

[16] J.G. Duh: Ph.D. Thesis, Purdue University, West Lafayette, IN, U.S.A. (1983).

[17] M.A. Krishtal, P.N. Zakharov, A.P. Mokrov et al.: Izv. Akad. Nauk SSSR, Met., No. 2 (1972) p. 75-78.

[18] A.P. Mokrov, V.K. Akimov and P.N. Zakharov: Izv. Akad. Nauk SSSR, Met., No. 1 (1979), p. 234- 238.

CHAPTER 5: EFFECTS OF IR, TA AND RE ALLOYING ON INTERDIFFUSION OF L12-NI3AL AT 1200°C

5.1. Introduction

Nickel-base superalloys are extensively used in both aviation and land-based gas turbines, and many studies have been devoted to improve their mechanical properties and microstructural stability [1]. Ni-base superalloys are typically composed of $L1_2$ γ'-phase (Ni_3Al) coherently precipitated in an fcc γ-phase matrix. The diffusion mobility database for Ni-base superalloys is available for fcc phase [2]. Although γ' is the strengthening phase of Ni-base superalloys, a limited number of studies exists on interdiffusion of the γ'-phase [3-9], particularly when alloyed with other constituents in superalloys. An understanding of multicomponent diffusion processes in these alloys is very important because it is essential to achieve a durable microstructure for strength and oxidation resistance at high temperature. This study is also fueled by recent conceptual development of refractory based superalloys with $L1_2$ precipitates and refractory-modified aluminide coatings [10-15] for optimized oxidation resistance along with reduced interdiffsion between oxidation resistant coatings and structural superalloy substrate (e.g. to mitigate the formation of deleterious phases due to interdiffusion at the interface).

The crystal structure of Ni_3Al is derived from an fcc based Cu_3Au prototype lattice with face centered sublattice sites (α-sites) occupied by Ni-atoms and corner sublattice sites (β-sites) by Al-atoms. In general, highly electronegative substitutional elements (e.g. Pt, Cu and Co) occupy the α sites, where as highly electropositive ones (e.g. Ti, Ta and Nb) occupy the β sites in Ni_3Al [1]. The relative site-preference for ternary alloying elements can be best illustrated

from the direction of the solubility lobes for the γ' phase within the ternary isotherm of Ni-Al-X (X = alloying addition) system at 1273K as shown by Figure 1 [16]. Site preference of ternary alloying additions to Ni_3Al has attracted significant interest, as this true solid solution accepts considerable amount of third elements into solution [17-19].

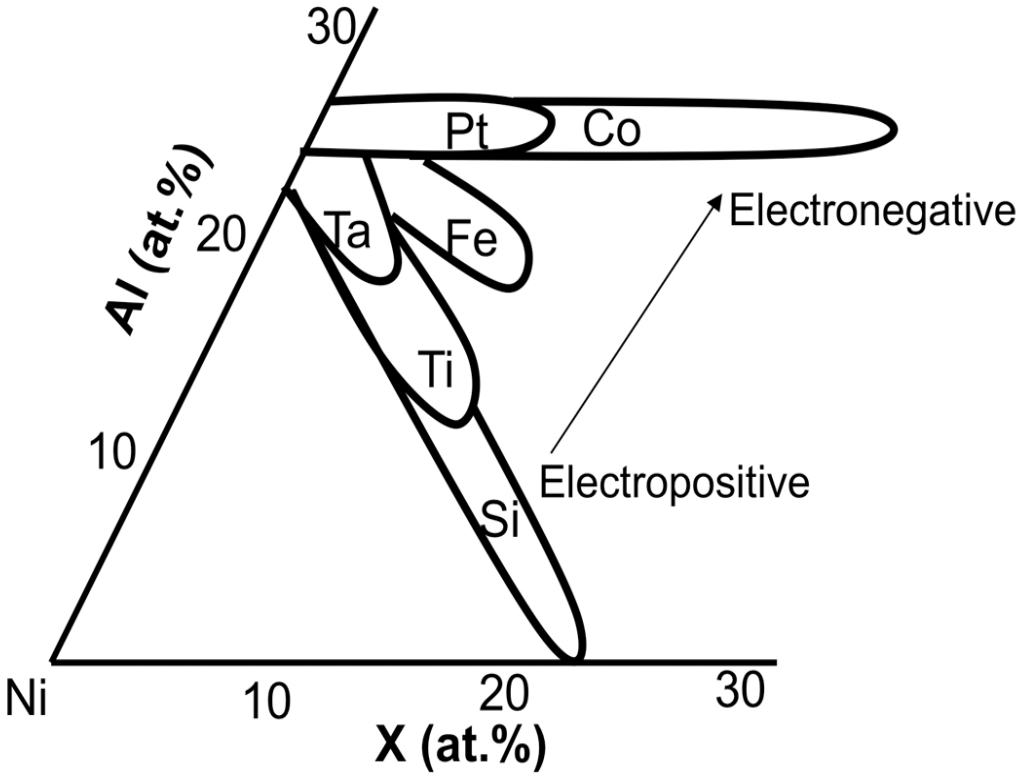

Figure 5.1 : Solubility ranges of selected ternary alloying additions in Ni3Al (adopted from Ochiai [16]) at 1273K.

The alloying phenomenon plays an important role in enhancing the mechanical properties and high temperature oxidation resistance of this intermetallic [18-25]. The behavior of ternary substitutional alloying additions to Ni_3Al was first reported by Guard and Westbrook [17] as Ni-occupiers, Al-occupiers or Ni-and-Al-occupiers. Several studies [26-28] have predicted the change in site preference of alloying elements as a function of temperature and chemical composition of Ni_3Al.

Diffusional interactions of a ternary alloying addition to Ni_3Al can be a tool to examine the site preference. The diffusion mechanism in ordered alloys is recognized to be more complex than for disordered solid solutions [29]. In the case of $L1_2$ structure, the diffusion mechanism is even more complex than that for B2 structure. Diffusion can occur through α or β site where Ni or Al atoms mainly occupy, respectively, and the diffusion coefficient largely depends on the alloy composition, namely the degrees of order [30-32]. While tracer diffusion studies in γ' Ni_3Al are difficult since ^{26}Al is not readily available, self-diffusion of Ni and chemical/impurity diffusion in Ni_3Al binary and Ni_3Al-X ternary alloys (X= Co, Cu, Pt, Ti, Si, W, Ge, In, V, Mb, Cr, Fe, Mn) have been studied [3-5]. The temperature dependency of the diffusion for a ternary alloying addition is evident from Arrhenius rate law [5, 33-35]. The β-site occupiers have been observed to diffuse slower than the α-site occupiers [29,36]. This is attributed to the fact that, in $L1_2$-ordered structure, each Ni atom is surrounded by 4 Al atoms and 8 Ni atoms, where as an Al atom is surrounded by 12 Ni atoms. Therefore, the activation enthalpy of alloying element increases mainly due to the antisite-defect formation [36].

For an additional insight to understand the diffusion process in $L1_2$ structure, to enhance microstructural stability of Ni-base superalloys, and to develop refractory-modified aluminide

oxidation resistant coatings, we examined the ternary diffusional interaction of Ir, Ta and Re additions to the $L1_2$ Ni_3Al phase. Solid-to-solid diffusion couples were assembled and annealed at 1473K for 5 hours. Based on concentration profiles obtained by electron probe microanalysis, average ternary interdiffusion coefficients from an integration of interdiffusion fluxes, and ternary interdiffusion coefficients via Boltzmann-Matano analysis were determined to assess how Ir, Ta and Re additions influence interdiffusion behavior of Ni and Al in $L1_2$ Ni_3Al phase. Additional estimates of binary interdiffusion coefficients in Ni_3Al, and tracer diffusion coefficients of Ir, Ta and Re in Ni_3Al were made.

5.2. Determination of ternary interdiffusion coefficients

From Onsager's formalism [37,38] and Fick's law [39], the interdiffusion flux $\tilde{J}_i$ of component i in a ternary system can be expressed in terms of two independent concentration gradients $\partial C_j/\partial x$ by:

$$\tilde{J}_i = -\tilde{D}^3_{i1}\frac{\partial C_1}{\partial x} - \tilde{D}^3_{i2}\frac{\partial C_2}{\partial x} \qquad (i = 1,2) \tag{5.1}$$

where $\tilde{D}^3_{ij}$'s refer to the ternary interdiffusion coefficients. An experimental determination of the four concentration-dependent interdiffusion coefficients is generally carried out by the use of Boltzmann-Matano analysis with two independent diffusion couples that develop a common composition in the diffusion zone where the interdiffusion coefficients can be evaluated [40,41].

Alternatively, the interdiffusion fluxes of individual components can be determined directly from their concentration profiles without the need or use of the interdiffusion coefficients. The interdiffusion flux at any section x can be calculated directly from the concentration profile from the relation [42,43]:

$$\tilde{J}_i = \frac{1}{2t} \int_{C_i^- \text{ or } C_i^+}^{C_i(x)} (x - x_o)\, dC_i \qquad (i = 1,2,\ ...,\ n) \tag{5.2}$$

where t is the time, C_i^- and C_i^+ are the terminal concentrations, and x_o refers to the location of the Matano plane. Based on the direct determination of interdiffusion fluxes, diffusional behavior of components can be examined, and observations of zero-flux-planes (ZFPs) and flux-reversals have been reported for individual components in isothermal ternary interdiffusion studies [42-45]. Furthermore, the calculated interdiffusion fluxes can be related to interdiffusion parameters which can be employed to generate and characterize concentration profiles developed in ternary diffusion couples [46-49].

The interdiffusion flux $\tilde{J}_i$ determined from Eq. (5.2) as a function of x can be integrated over a selected region, x_1 to x_2, to yield an expression based on Eq. (5.1) [49]:

$$\begin{aligned} \int_{x_1}^{x_2} \tilde{J}_i dx &= -\int_{C_1(x_1)}^{C_1(x_2)} \tilde{D}_{i1}^3 dC_1 - \int_{C_2(x_1)}^{C_2(x_2)} \tilde{D}_{i2}^3 dC_2 \qquad (i = 1,2) \\ &= \overline{\tilde{D}}_{i1}^3 \left[C_1(x_1) - C_1(x_2)\right] + \overline{\tilde{D}}_{i2}^3 \left[C_2(x_1) - C_2(x_2)\right] \qquad (i = 1,2) \end{aligned} \tag{5.3}$$

where $\overline{\tilde{D}}_{ij}^{3}$'s correspond to the average values of main and cross interdiffusion coefficients. With $\overline{\tilde{D}}_{ij}^{3}$'s taken as constants, Eq. (5.1) is re-written as:

$$\tilde{J}_i = -\overline{\tilde{D}}_{i1}^{3}\frac{\partial C_1}{\partial x} - \overline{\tilde{D}}_{i2}^{3}\frac{\partial C_2}{\partial x} \qquad (i=1,2) \tag{5.4}$$

If both sides of Eq. (5.4) are multiplied by $(x-x_o)^m$ and integrated over the diffusion zone between x_1 and x_2, one obtains in general [49]:

$$\int_{x_1}^{x_2}\tilde{J}_i(x-x_o)^m dx = -\overline{\tilde{D}}_{i1}^{3}\int_{C_1(x_1)}^{C_1(x_2)}(x-x_o)^m dC_1 - \overline{\tilde{D}}_{i2}^{3}\int_{C_2(x_1)}^{C_2(x_2)}(x-x_o)^m dC_2 \qquad (i=1,2) \tag{5.5}$$

If the exponent m is chosen to be zero, Eq. (5.5) becomes identical to Eq. (5.3). For m=1, Eq. (5.5) yields [49]:

$$\begin{aligned}\int_{x_1}^{x_2}\tilde{J}_i(x-x_o)dx &= -\overline{\tilde{D}}_{i1}^{3}\int_{C_1(x_1)}^{C_1(x_2)}(x-x_o)dC_1 - \overline{\tilde{D}}_{i2}^{3}\int_{C_2(x_1)}^{C_2(x_2)}(x-x_o)dC_2 \\ &= 2t\left\{\overline{\tilde{D}}_{i1}^{3}\left[\tilde{J}_1(x_1)-\tilde{J}_1(x_2)\right]+\overline{\tilde{D}}_{i2}^{3}\left[\tilde{J}_2(x_1)-\tilde{J}_2(x_2)\right]\right\} \qquad (i=1,2)\end{aligned} \tag{5.6}$$

Eqs. (5.3) and (5.6) provide four equations involving the $\overline{\tilde{D}}_{11}^{3}$, $\overline{\tilde{D}}_{12}^{3}$, $\overline{\tilde{D}}_{21}^{3}$ and $\overline{\tilde{D}}_{22}^{3}$ interdiffusion coefficients and can be easily set up from experimental concentrations and the

corresponding interdiffusion fluxes. Hence, from the concentration profiles of a single diffusion couple, $\overline{\tilde{D}}_{ij}^{3}$ $(i,j=1,2)$ coefficients, characteristic of the diffusion path, can be determined by using Eqs. (5.3) and (5.6) over selected composition ranges in the diffusion zone [49]. Eqs. (5.3) and (5.6) provide independent relations when the composition ranges are selected to include non-linear segments of the profiles. This analysis method to determine average ternary interdiffusion coefficients has been directly employed in various studies [3, 50-59]. In addition, the independence of Eq. (5.3) and (5.5) in solving the average ternary interdiffusion coefficients for the concentration profiles obtained in this study is demonstrated in section 5.4.2. In this paper, the analysis applied to the concentration profiles of experimental ternary diffusion couples in $L1_2$ Ni-Al-X (X = Ir or Ta) intermetallics is carried out for 2 segments, one on either side of the Matano plane; the two chosen composition ranges are $\left(C_i^- - C_i^o\right)$ and $\left(C_i^o - C_i^+\right)$, where C_i^o refers to the concentration at the Matano plane. The average ternary interdiffusion coefficients, $\overline{\tilde{D}}_{ij}^{3}$, determined on either side of the Matano plane are employed to simulate experimental concentration profiles using error-function solution for infinite ternary systems from Fujita and Gosting [60]. For Ni-Al vs. Ni-Al-Ir diffusion couples, the average ternary interdiffusion coefficients, $\overline{\tilde{D}}_{ij}^{3}$, are found to be consistent with ternary interdiffusion coefficients, $\tilde{D}_{ij}^{3}$, determined by Boltzmann-Matano analysis [40,41].

5.3. Experimental Details

Ni-Al, Ni-Al-Ir, Ni-Al-Ta and Ni-Al-Re alloys were prepared by the vacuum arc melting of 99.97 wt.% Ni, 99.9 wt.% Al, 99.2 wt.% Ir, 99.2 wt.% Ta, and 99.2 wt. Re according to the

compositions presented in Table 5.1. The alloys were cast into a semi-cylindrical mold with the diameter of 8 mm in an arc furnace. The alloy rods were homogenized at 1473K for 137 hours in the vacuum furnace evacuated to a pressure less than 10^{-2} Pa. The homogenized alloys were then sectioned into discs with the height of 1.5 mm. The surfaces of alloy discs were polished metallographically up to 1200-grit and cleaned thoroughly prior to diffusion couple assembly.

Table 5.1 : Nominal composition of alloys employed for diffusion couple studies.

Alloy Identification	Composition (atom percent)			Composition (weight percent)		
	Ni	Al	Ir, Ta or Re	Ni	Al	Ir, Ta or Re
Ni-24.5Al	76.0	24.0	0	59.3	40.7	0.0
Ni-25Al	75.0	25.0	0	58.0	42.0	0.0
Ni-26Al	74.5	25.5	0	57.3	42.7	0.0
Ni-23.5Al-1Ir	75.5	23.5	1.0	59.5	40.3	0.2
Ni-24.5Al-1Ir	74.5	24.5	1.0	58.2	41.6	0.2
Ni-23Al-2Ir	74.5	23.5	2.0	59.0	40.5	0.5
Ni-23Al-3Ir	74.0	23.0	3.0	59.2	40.0	0.7
Ni-23Al-1.5Ta	75.5	23.0	1.5	59.9	39.7	0.4
Ni-23.5Al-0.5Re	76.0	23.5	0.5	59.7	40.2	0.1
Ni-23.5Al-0.7Re	75.8	23.5	0.7	59.6	40.2	0.2

Table 5.2 presents diffusion couples that were assembled and analyzed in this study. Coupled alloys were put into a Si_3N_4 jig and annealed at 1473K for 0.5 hour in a vacuum furnace to promote initial bonding. Since the metal discs have larger thermal expansion coefficients than the Si_3N_4 jig, the discs can adhere to each other due to the compression during the annealing treatment. Each diffusion couple fabricated in this manner was then sealed in an evacuated transparent quartz capsule, and annealed at 1473K for 4.5 hours in an atmosphere furnace. All diffusion couples were water quenched after the high-temperature anneal to preserve high temperature microstructure and concentrations. In this study, the time required for the diffusion bonding treatment (0.5 hour) was added to the total annealing time. Thus, concentration profiles from all diffusion couples were analyzed with diffusion anneal time of 5 hours.

Table 5.2 : Diffusion couples assembled and analyzed after anneal at 1473Kfor 5 hours.

Series	Diffusion Couples
Ni-Al vs. Ni-Al-Ir	Ni-25Al vs. Ni-23.5Al-1Ir
	Ni-24.5Al vs. Ni-24.5Al-1Ir
	Ni-26Al vs. Ni-23Al-2Ir
	Ni-24Al vs. Ni-24Al-2Ir
	Ni-25Al vs. Ni-23Al-3Ir
	Ni-25Al vs. Ni-23Al-2Ir
Ni-Al vs. Ni-Al-Ta	Ni-24Al vs. Ni-23Al-1.5Ta
	Ni-25Al vs. Ni-23Al-1.5Ta
	Ni-26Al vs. Ni-23Al-1.5Ta
Ni-Al vs. Ni-Al-Re	Ni-24.5Al vs. Ni-23.5Al-0.5Re
	Ni-24.5Al vs. Ni-23.5Al-0.7Re
	Ni-25Al vs. Ni-23.5Al-0.5Re
	Ni-26Al vs. Ni-23.5Al-0.7Re

Microstructures and concentration profiles of the annealed diffusion couples were analyzed by JEOL-JXA-8900 electron probe microanalyzer (EPMA). An accelerating voltage of 20 kV, a beam current of 50 nA, and a probe diameter of 1 μm were employed for data acquisition of Ni K_α x-radiation peak using LIF crystal, Al K_α x-radiation peak using TAP crystal, Ir L_α x-radiation using LIFH crystal, and Ta L_α x-radiation using LIFH crystal. Pure element standards of Ni, Al, Ir, Ta, along with ZAF correction [61], were used for quantification of concentrations via point-to-point count technique.

5.4. Results and Analysis

5.4.1 Profiles of concentrations and interdiffusion fluxes

Figures 5.2, 5.3 and 5.4 present typical concentration profiles obtained by EPMA measurements from diffusion couples, Ni-26Al vs. Ni-23Al-2Ir, Ni-24.5Al vs. Ni-23Al-1.5Ta, and Ni-25Al vs. Ni-23.5Al-0.5Re, respectively, annealed at 1473K for 5 hours. The x-axis represents the distance from the Matano plane and the open circles are EPMA measurement. Scatter in the concentration profiles for all diffusion couples were minimum and within the experimental uncertainty associated with EPMA. The interdiffusion fluxes of individual components were then determined using Eq. (5.2) from experimental concentration profiles that were smoothend with a series of weighted splines.

While no zero-flux plane was observed, a significant diffusional interactions between Ni and Ir, Al and Ta, and Al and Re were observed when Ni_3Al was diffusion annealed against Ni_3Al alloyed with Ir, Ta, and Re respectively, as shown in Figures 5.2, 5.3, and 5.4. Clearly, the interdiffusion of Ni was greatly enhanced by the interdiffusion of Ir down the Ir gradient, while

Al exhibited an uphill diffusion against its own gradient due to the interdiffusion of Ta. In addition, interdiffusion of Al was reduced by the interdiffusion of Re against the gradient of Al. However, diffusional influences of Ir on Al, Ta on Ni, and Re on Ni are difficult to ascertain from the profiles presented in Figures 5.2, 5.3, and 5.4. Determination of ternary interdiffusion coefficients can quantify the extent and magnitude of these diffusional interactions, and provide competent approaches to compositional design, modification of alloys and protective coatings.

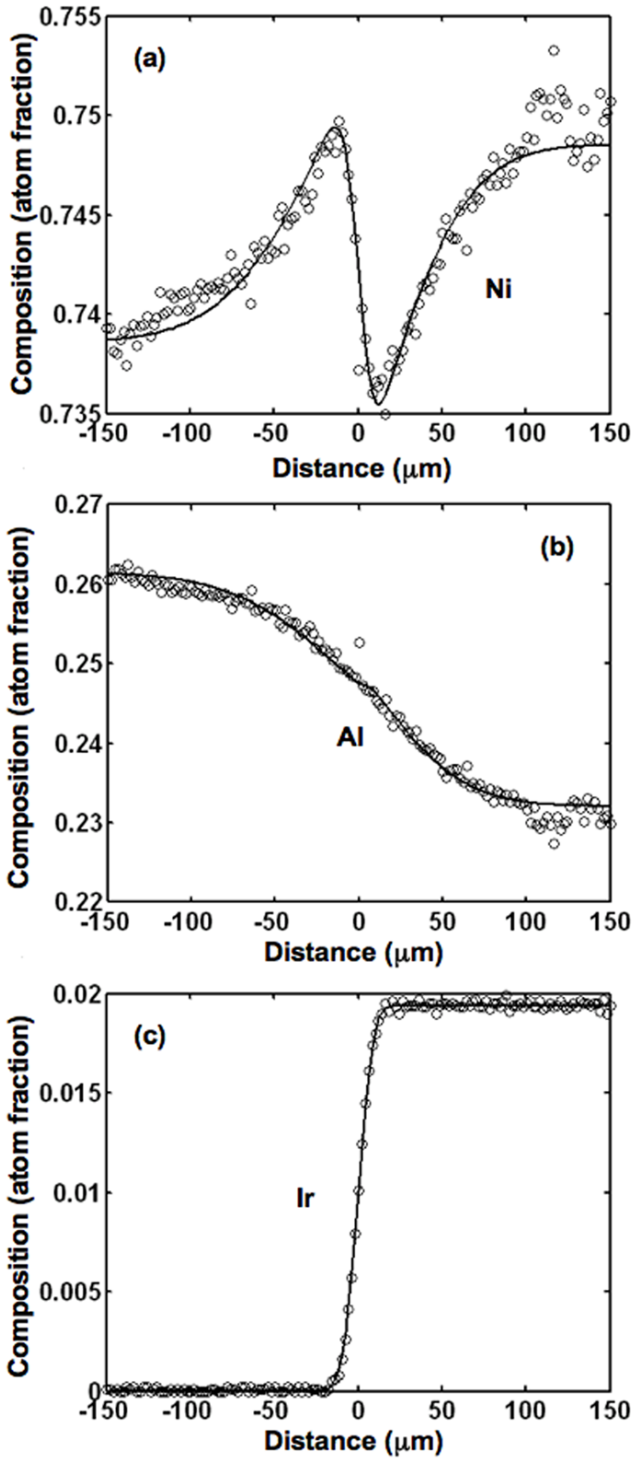

Figure 5.2 : Concentration profiles of (a) Ni, (b) Al and (c) Ir obtained from diffusion couple Ni-26Al vs. Ni-23Al-2Ir annealed at 1473K for 5 hours. Open circles and solid lines represent EPMA measurement and calculated concentration profiles, respectively.

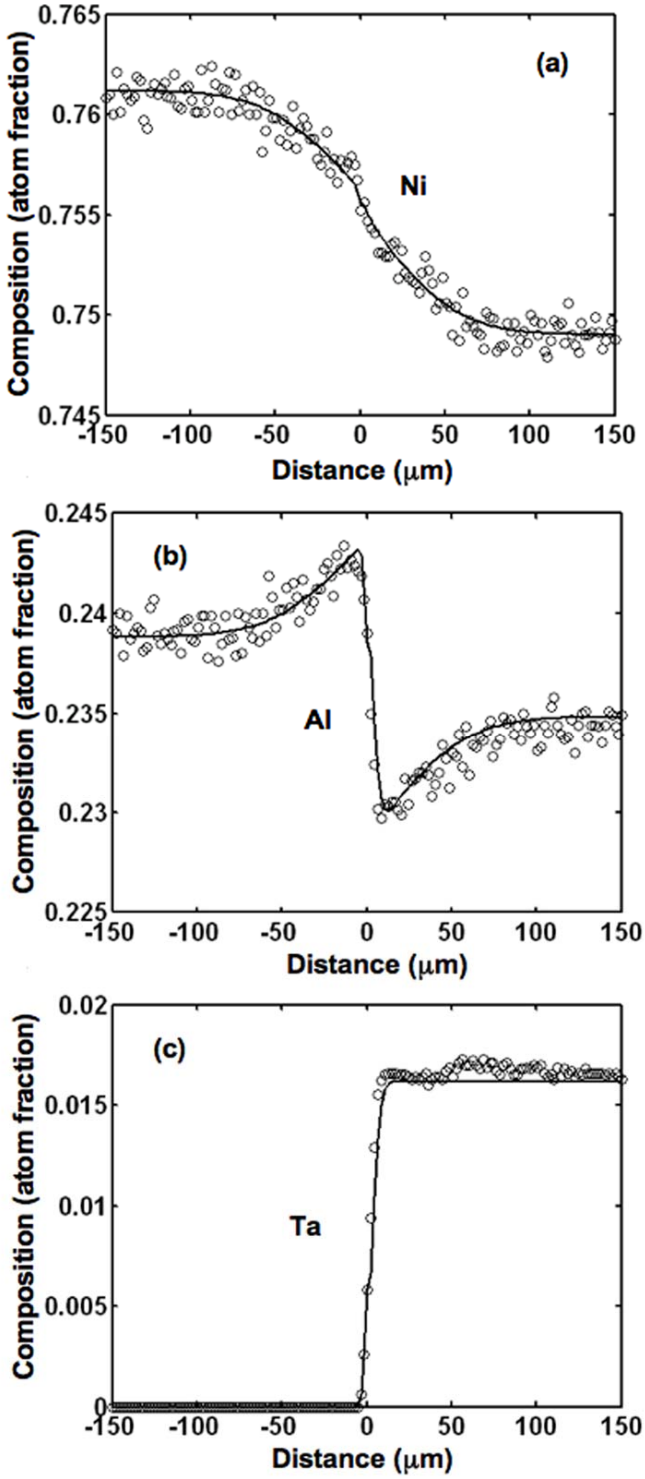

Figure 5.3 : Concentration profiles of (a) Ni, (b) Al and (c) Ta obtained from diffusion couple Ni-24.5Al vs. Ni-23Al-1.5Ta annealed at 1473K for 5 hours. Open circles and solid lines represent EPMA measurement and calculated concentration profiles, respectively.

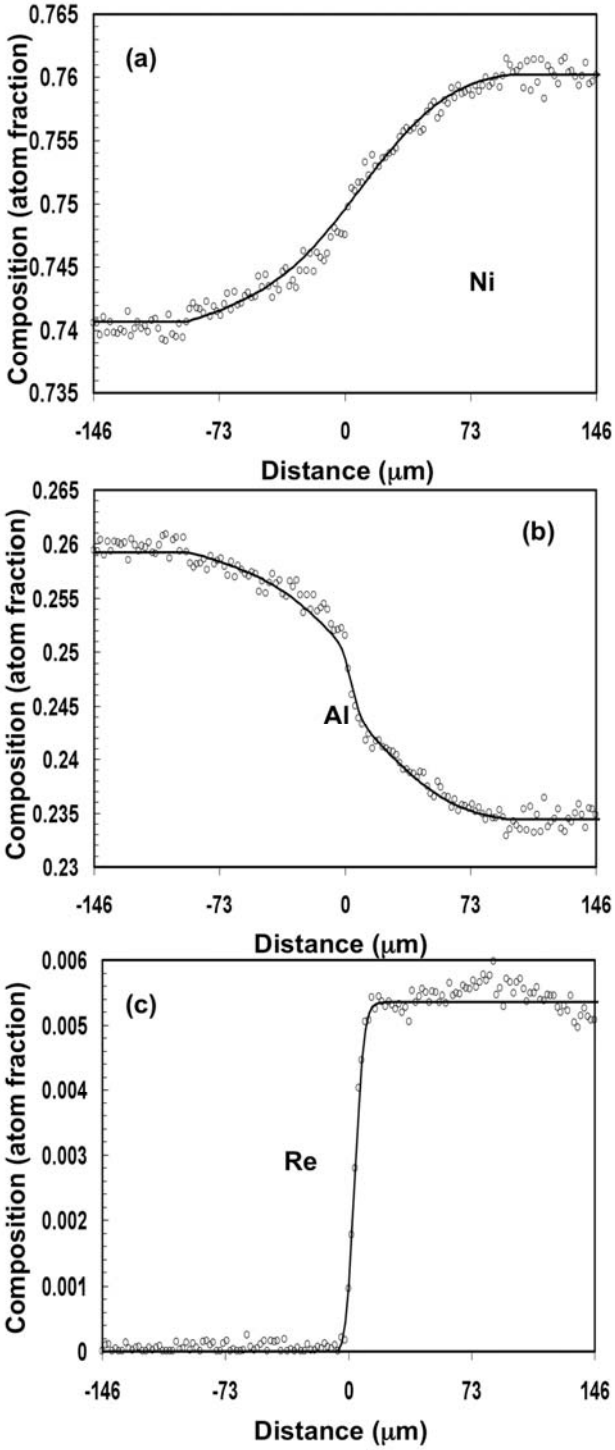

Figure 5.4 : Concentration profiles of (a) Ni, (b) Al and (c) Re obtained from diffusion couple Ni-25Al vs. Ni-23.5Al-0.5Re annealed at 1473K for 5 hours. Open circles and solid lines represent EPMA measurement and calculated concentration profiles, respectively.

5.4.2 Average ternary interdiffusion coefficients

From profiles of concentration and interdiffusion fluxes in Ni-Al vs Ni-Al-Ir diffusion couples, average ternary interdiffusion coefficients, $\overline{\tilde{D}}_{ij}^{Ni}(i,j=Al,Ir)$ and $\overline{\tilde{D}}_{ij}^{Al}(i,j=Ni,Ir)$, were determined on either side of the Matano plane using Eqs. (5.3) and (5.6). Use of Eqs. (5.3) and (5.6) provides independent relations for the determination of average ternary interdiffusion coefficients as presented in Figure 5.5. In this Figure, for diffusion couple Ni-26Al vs. Ni-23Al-2Ir whose concentration profiles are presented in Figure 5.2, the variation of $\overline{\tilde{D}}_{ij}^{Al}(i,j=Ni,Ir)$ in Eq. (5.5) where m = 0, equivalent to Eq. (5.3), and m = 1, equivalent to Eq. (5.6), is presented. The two lines generated by Eqs. (5.3) and (5.6) are sufficiently independent to obtain an unique solution of $\overline{\tilde{D}}_{ij}^{Al}(i,j=Ni,Ir)$ coefficients that are reported in Table 5.3.

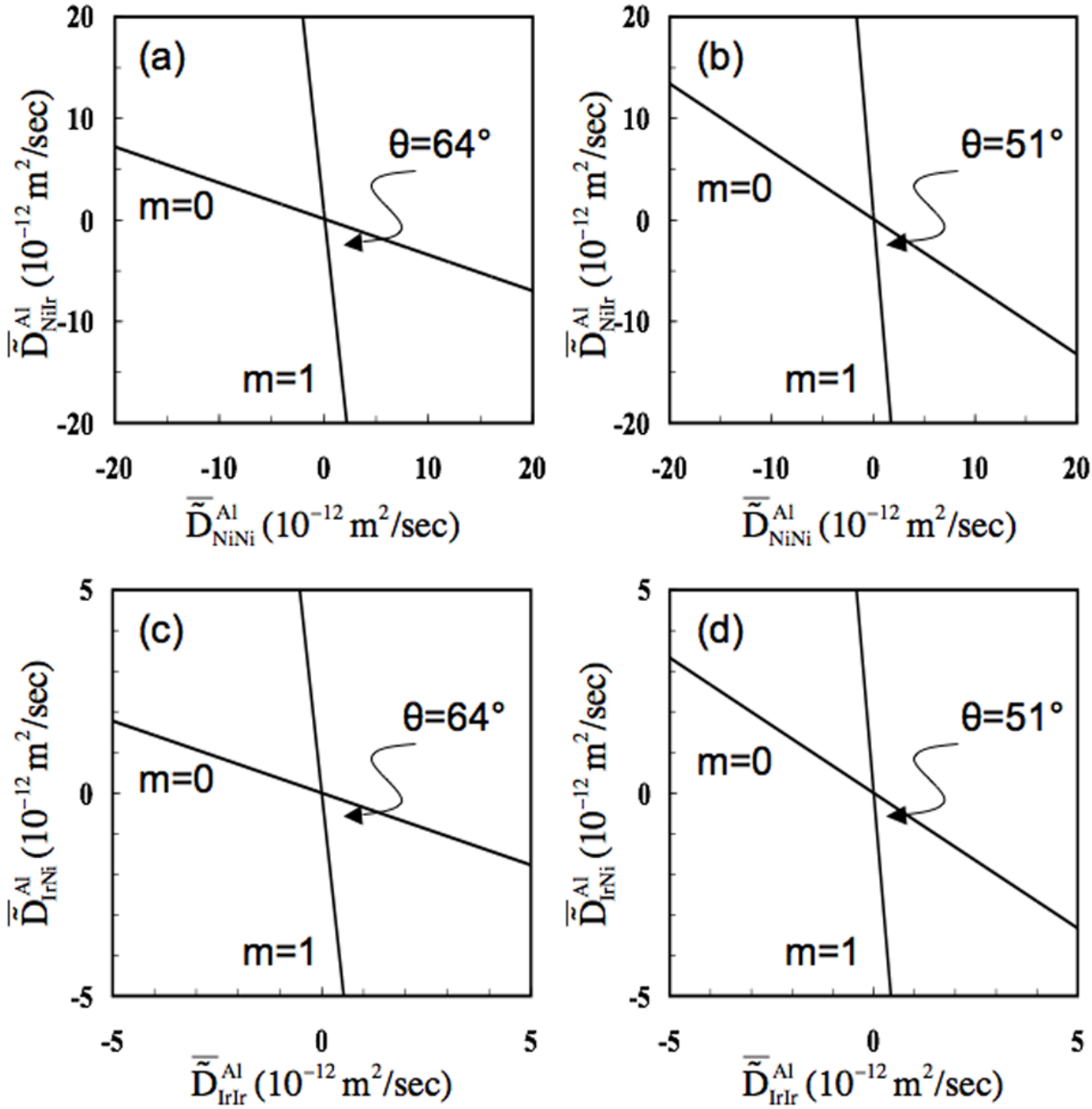

Figure 5.5 : Variation of $\tilde{\bar{D}}^{Al}_{ij}(i,j=Ni,Ir)$ coefficients in Eq. (5.3), equivalent to Eq. (5.5) when m = 0, and (5.6) equivalent to Eq. (5.5) when m = 1. The two lines generated by Eqs. (5.3) and (5.6) are sufficiently independent to obtain an unique solution of $\tilde{\bar{D}}^{Al}_{ij}(i,j=Ni,Ir)$ coefficients that are reported for the composition ranges of $(C_i^- - C_i^o)$ and $(C_i^o - C_i^+)$ in Table 5.3.

Table 5.3 : Average ternary interdiffusion coefficients (10^{-16} m^2/s) determined from Ni-Al vs. Ni-Al-Ir diffusion couples annealed at 1473K for 5 hours.

Diffusion Couple	Composition Range	$\overline{\widetilde{D}}^{Ni}_{AlAl}$	$\overline{\widetilde{D}}^{Ni}_{AlIr}$	$\overline{\widetilde{D}}^{Ni}_{IrAl}$	$\overline{\widetilde{D}}^{Ni}_{IrIr}$
Ni-25Al vs. Ni-23.5Al-1Ir	$(C_i^{-\infty} \sim C_i^{o})$	623.7	-117.2	Ngl.	13.6
	$(C_i^{o} \sim C_i^{+\infty})$	511.6	-166.6	Ngl.	11.2
Ni-24.5Al vs. Ni-24.5Al-1Ir	$(C_i^{-\infty} \sim C_i^{o})$	541.0	-84.7	Ngl.	10.5
	$(C_i^{o} \sim C_i^{+\infty})$	816.9	-75.7	Ngl.	19.1
Ni-26Al vs. Ni-23Al-2Ir	$(C_i^{-\infty} \sim C_i^{o})$	871.4	-52	Ngl.	15.4
	$(C_i^{o} \sim C_i^{+\infty})$	591.5	-117.3	Ngl.	13.0
Ni-25Al vs. Ni-23Al-2Ir	$(C_i^{-\infty} \sim C_i^{o})$	522	-107.3	Ngl.	16.4
	$(C_i^{o} \sim C_i^{+\infty})$	494	-116.6	Ngl.	15.9
Ni-25Al vs. Ni-23Al-3Ir	$(C_i^{-\infty} \sim C_i^{o})$	440.9	-92.8	Ngl.	15.1
	$(C_i^{o} \sim C_i^{+\infty})$	441.2	-135.5	Ngl.	19.3
Ni-24Al vs. Ni-24Al-2Ir	$(C_i^{-\infty} \sim C_i^{o})$	267.2	14.1	Ngl.	11.8
	$(C_i^{o} \sim C_i^{+\infty})$	318.0	9.8	Ngl.	14.8
Diffusion Couple	Composition Range	$\overline{\widetilde{D}}^{Al}_{NiNi}$	$\overline{\widetilde{D}}^{Al}_{NiIr}$	$\overline{\widetilde{D}}^{Al}_{IrNi}$	$\overline{\widetilde{D}}^{Al}_{IrIr}$
Ni-25Al vs. Ni-23.5Al-1Ir	$(C_i^{-\infty} \sim C_i^{o})$	623.7	727.3	Ngl.	13.6
	$(C_i^{o} \sim C_i^{+\infty})$	511.6	667.0	Ngl.	11.2
Ni-24.5Al vs. Ni-24.5Al-1Ir	$(C_i^{-\infty} \sim C_i^{o})$	541.0	615.2	Ngl.	10.5
	$(C_i^{o} \sim C_i^{+\infty})$	816.9	873.5	Ngl.	19.1
Ni-26Al vs. Ni-23Al-2Ir	$(C_i^{-\infty} \sim C_i^{o})$	871.4	908.0	Ngl.	15.4
	$(C_i^{o} \sim C_i^{+\infty})$	591.5	695.8	Ngl.	13.0
Ni-25Al vs. Ni-23Al-2Ir	$(C_i^{-\infty} \sim C_i^{o})$	522	612.9	Ngl.	16.4
	$(C_i^{o} \sim C_i^{+\infty})$	494	594.7	Ngl.	15.9
Ni-25Al vs. Ni-23Al-3Ir	$(C_i^{-\infty} \sim C_i^{o})$	440.9	518.6	Ngl.	15.1
	$(C_i^{o} \sim C_i^{+\infty})$	441.2	557.4	Ngl.	19.3
Ni-24Al vs. Ni-24Al-2Ir	$(C_i^{-\infty} \sim C_i^{o})$	267.2	241.3	Ngl.	11.8
	$(C_i^{o} \sim C_i^{+\infty})$	318.0	293.4	Ngl.	14.8

Note: Ngl refers to magnitude less than 0.1 x 10^{-16} m^2/sec.

The main diffusion coefficients, $\overline{\tilde{D}}^{Ni}_{AlAl}$ and $\overline{\tilde{D}}^{Al}_{NiNi}$, correspond well to the interdiffusion coefficients of Al and Ni reported in literature for binary Ni_3Al at 1473K [3-9]. Estimation of binary interdiffusion coefficients from the ternary diffusion couples and the comparison to the interdiffusion coefficients of Al and Ni reported in literature for binary Ni_3Al are presented in detail in section 5.4.4. The magnitude of these main coefficients for Al and Ni are observed to be larger with higher Al content as well. The main interdiffusion coefficient of Ir, $\overline{\tilde{D}}_{IrIr}$, is 20 to 40 times lower in magnitude than the main coefficients of Ni and Al. Table 5.3 reports that $\overline{\tilde{D}}^{Ni}_{AlIr}$ coefficients are negative, and smaller in magnitude than $\overline{\tilde{D}}^{Ni}_{AlAl}$ coefficients, and $\overline{\tilde{D}}^{Ni}_{IrAl}$ coefficients are negligibly small (< 0.1 x 10^{-16} m^2/sec). Thus the interdiffusion flux of Al can be influenced only slightly by the interdiffusion of Ir. However, $\overline{\tilde{D}}^{Al}_{NiIr}$ coefficients are positive and large (e.g., larger than the $\overline{\tilde{D}}^{Al}_{NiNi}$ coefficients in some cases), while $\overline{\tilde{D}}^{Al}_{IrNi}$ coefficients are negligibly small (< 0.1 x 10^{-16} m^2/sec). The large positive $\overline{\tilde{D}}^{Al}_{NiIr}$ coefficient corresponds well with an enhanced interdiffusion of Ni (e.g., down the gradient of Ir). Against the concentration gradient of Ir, the large positive $\overline{\tilde{D}}^{Al}_{NiIr}$ coefficient can therefore reduce the interdiffusion of Ni. The average ternary interdiffusion coefficients reported in Table 5.3 indicate a strong diffusional interaction between Ni and Ir, both occupying the α-site in $L1_2$ lattice structure.

The average ternary interdiffusion coefficients, $\overline{\tilde{D}}^{Ni}_{ij}(i,j = Al,Ta)$ and $\overline{\tilde{D}}^{Al}_{ij}(i,j = Ni,Ta)$, determined on either side of the Matano plane for Ni-Al vs. Ni-Al-Ta couples are reported in Table 5.4. For diffusion couple Ni-24.5Al vs. Ni-23Al-1.5Ta whose concentration profiles are presented in Figure 5.3, the variation of $\overline{\tilde{D}}^{Ni}_{ij}(i,j = Al,Ta)$ in Eq. (5.3), equivalent to Eq. (5.5) where m = 0, and Eq. (5.6), equivalent to Eq. (5.5) where m = 1 is presented in Figure 5.6. The

two lines generated by Eqs. (5.3) and (5.6) are again sufficiently independent to obtain an unique solution of $\overline{\tilde{D}}_{ij}^{Ni}(i,j = Al,Ta)$ coefficients that are reported in Table 5.4.

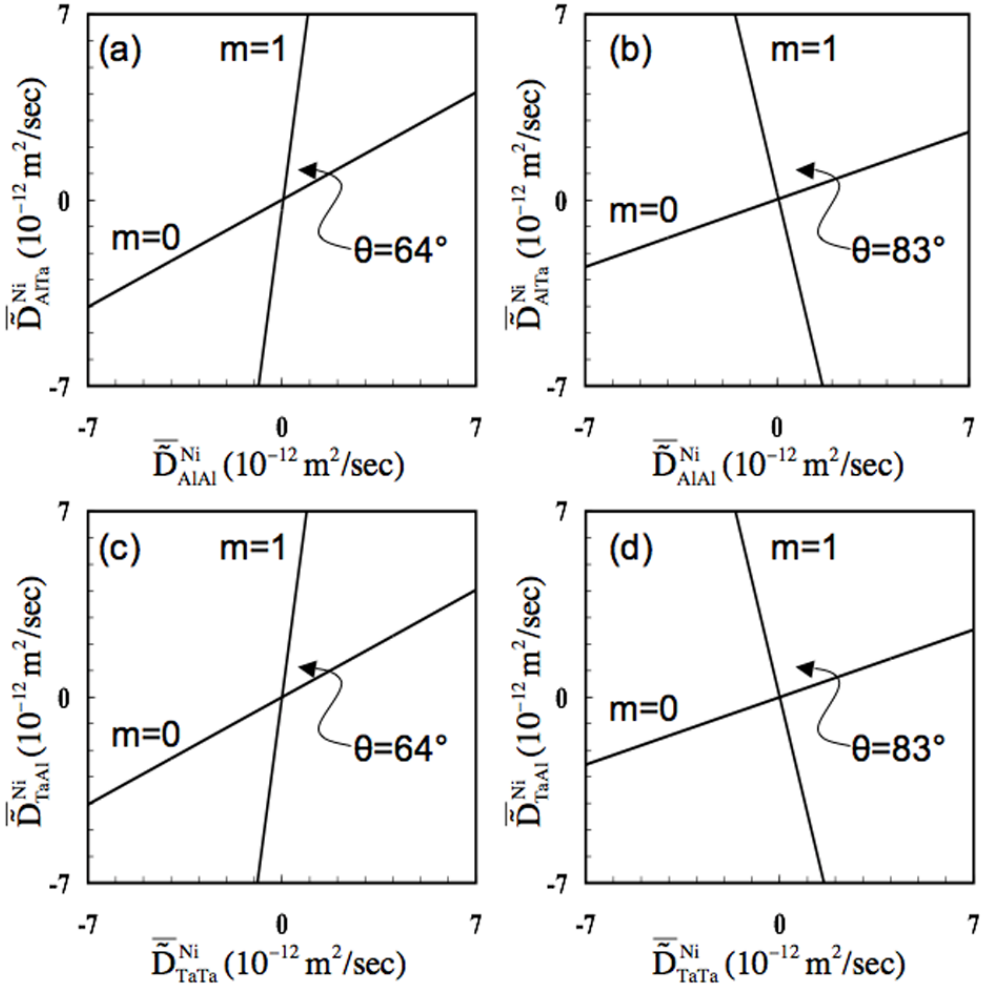

Figure 5.6 : Variation of $\overline{\tilde{D}}_{ij}^{Ni}(i,j = Al,Ta)$ coefficients in Eq. (5.3), equivalent to Eq. (5.5) when m = 0, and (5.6) equivalent to Eq. (5.5) when m = 1. The two lines generated by Eqs. (5.3) and (5.6) are sufficiently independent to obtain an unique solution of $\overline{\tilde{D}}_{ij}^{Ni}(i,j = Al,Ta)$ coefficients that are reported for the composition ranges of $(C_i^- - C_i^o)$ and $(C_i^o - C_i^+)$ in Table 5.4.

Table 5.4 : Average ternary interdiffusion coefficients (10^{-16} m^2/s) determined from Ni-Al vs. Ni-Al-Ta diffusion couples annealed at 1473K for 5 hours.

Diffusion Couple	Composition Range	$\overline{\tilde{D}}^{Ni}_{AlAl}$	$\overline{\tilde{D}}^{Ni}_{AlTa}$	$\overline{\tilde{D}}^{Ni}_{TaAl}$	$\overline{\tilde{D}}^{Ni}_{TaTa}$
Ni-24.5Al vs. Ni-23Al-1.5Ta	$\left(C_i^{-\infty} \sim C_i^{o}\right)$	561	501.3	Ngl.	3.2
	$\left(C_i^{o} \sim C_i^{+\infty}\right)$	482.6	451.8	Ngl.	1.8
Ni-25Al vs. Ni-23Al-1.5Ta	$\left(C_i^{-\infty} \sim C_i^{o}\right)$	810.4	807.1	Ngl.	3.4
	$\left(C_i^{o} \sim C_i^{+\infty}\right)$	652.7	580.5	Ngl.	1.9
Ni-26Al vs. Ni-23Al-1.5Ta	$\left(C_i^{-\infty} \sim C_i^{o}\right)$	313.2	333.6	Ngl.	3.7
	$\left(C_i^{o} \sim C_i^{+\infty}\right)$	445	391.9	Ngl.	5.6
Diffusion Couple	Composition Range	$\overline{\tilde{D}}^{Al}_{NiNi}$	$\overline{\tilde{D}}^{Al}_{NiTa}$	$\overline{\tilde{D}}^{Al}_{TaNi}$	$\overline{\tilde{D}}^{Al}_{TaTa}$
Ni-24.5Al vs. Ni-23Al-1.5Ta	$\left(C_i^{-\infty} \sim C_i^{o}\right)$	561	56.5	Ngl.	3.2
	$\left(C_i^{o} \sim C_i^{+\infty}\right)$	482.6	29	Ngl.	1.8
Ni-25Al vs. Ni-23Al-1.5Ta	$\left(C_i^{-\infty} \sim C_i^{o}\right)$	810.4	Ngl.	Ngl.	3.4
	$\left(C_i^{o} \sim C_i^{+\infty}\right)$	652.7	70.3	Ngl.	1.9
Ni-26Al vs. Ni-23Al-1.5Ta	$\left(C_i^{-\infty} \sim C_i^{o}\right)$	313.2	-24.1	Ngl.	3.7
	$\left(C_i^{o} \sim C_i^{+\infty}\right)$	445	47.5	Ngl.	5.6

Note: Ngl refers to magnitude less than 0.1 x 10^{-16} m^2/sec.

The main diffusion coefficients, $\overline{\tilde{D}}^{Ni}_{AlAl}$ and $\overline{\tilde{D}}^{Al}_{NiNi}$, again correspond well to the interdiffusion coefficients of Al and Ni reported in literature [3-9] for Ni_3Al at 1473K. Aforementioned, estimation of binary interdiffusion coefficients from the ternary diffusion couples along with the comparison to the interdiffusion coefficients of Al and Ni reported in literature for binary Ni_3Al are presented in detail in section 5.4.4. The main interdiffusion coefficient of Ta, $\overline{\tilde{D}}_{TaTa}$, is 10 to 40 times lower in magnitude than the main coefficients of Ni and Al. Table 5.4 reports that $\overline{\tilde{D}}^{Ni}_{AlTa}$ coefficients are positive, and comparable in magnitude to

$\overline{\tilde{D}}^{Ni}_{AlAl}$ coefficients, while $\overline{\tilde{D}}^{Ni}_{TaAl}$ coefficients are negligibly small (< 0.1 x 10^{-16} m^2/sec). Thus, the large positive $\overline{\tilde{D}}^{Ni}_{AlTa}$ coefficient corresponds well with an interdiffusion flux of Al (e.g., uphill diffusion) against the gradient of Ta. The $\overline{\tilde{D}}^{Al}_{NiTa}$ coefficients are positive, but much smaller than the $\overline{\tilde{D}}^{Al}_{NiNi}$ coefficients, and $\overline{\tilde{D}}^{Al}_{TaNi}$ coefficients are negligibly small (< 0.1 x 10^{-16} m^2/sec). Thus the interdiffusion flux of Ni can be influenced only slightly by the interdiffusion flux of Ta. The average ternary interdiffusion coefficients reported in Table 5.4 indicate a strong diffusional interaction between Al and Ta, both occupying the β-site in $L1_2$ lattice structure.

From profiles of concentration and interdiffusion fluxes in Ni-Al vs. Ni-Al-Re diffusion couples, average ternary interdiffusion coefficients, $\overline{\tilde{D}}^{Ni}_{ij}(i, j = Al, Re)$ and $\overline{\tilde{D}}^{Al}_{ij}(i, j = Ni, Re)$, were determined on either side of the Matano plane using Eqs. (5.3) and (5.6). They are reported in Table 5.5. The magnitudes of main diffusion coefficients, $\overline{\tilde{D}}^{Ni}_{AlAl}$ and $\overline{\tilde{D}}^{Al}_{NiNi}$ are similar to the interdiffusion coefficients of Al and Ni reported in literature for binary Ni_3Al at 1473K [3-10]. Estimation of binary interdiffusion coefficients from the ternary diffusion couples and the comparison to the interdiffusion coefficients of Al and Ni reported in literature for binary Ni_3Al are presented in detail in section 5.4.4. The main interdiffusion coefficient, $\overline{\tilde{D}}_{ReRe}$ is approximately 100 times smaller in magnitude than $\overline{\tilde{D}}^{Ni}_{AlAl}$ and $\overline{\tilde{D}}^{Al}_{NiNi}$. Table 5.5 reports that $\overline{\tilde{D}}^{Ni}_{AlRe}$'s are positive and comparable to the magnitude of $\overline{\tilde{D}}^{Ni}_{AlAl}$, while $\overline{\tilde{D}}^{Ni}_{ReAl}$ coefficients are negligibly small (< 0.1 x 10^{-16} m^2/sec). Thus the interdiffusion of Al can be strongly influenced by the interdiffusion of Re. The $\overline{\tilde{D}}^{Al}_{NiRe}$ coefficients are also positive, but only 2 to 13 times smaller in magnitude than the $\overline{\tilde{D}}^{Al}_{NiNi}$'s.

Table 5.5 : Average ternary interdiffusion coefficients (10^{-16} m^2/s) determined from Ni-Al vs. Ni-Al-Re diffusion couples annealed at 1473K for 5 hours.

Diffusion Couple	Composition Range	$\overline{\tilde{D}}^{Ni}_{AlAl}$	$\overline{\tilde{D}}^{Ni}_{AlRe}$	$\overline{\tilde{D}}^{Ni}_{ReAl}$	$\overline{\tilde{D}}^{Ni}_{ReRe}$
Ni-24.5Al vs. Ni-23.5Al-0.5Re	$\left(C_i^{-\infty} \sim C_i^{o}\right)$	417.7	380.2	Ngl.	3.8
	$\left(C_i^{o} \sim C_i^{+\infty}\right)$	265.1	191.0	Ngl.	4.0
Ni-24.5Al vs. Ni-23.5Al-0.7Re	$\left(C_i^{-\infty} \sim C_i^{o}\right)$	509.9	463.4	Ngl.	4.5
	$\left(C_i^{o} \sim C_i^{+\infty}\right)$	362.8	304.1	Ngl.	3.4
Ni-25Al vs. Ni-23.5Al-0.5Re	$\left(C_i^{-\infty} \sim C_i^{o}\right)$	463.2	294.6	Ngl.	3.8
	$\left(C_i^{o} \sim C_i^{+\infty}\right)$	668.3	477.4	Ngl.	2.4
Ni-26Al vs. Ni-23.5Al-0.7Re	$\left(C_i^{-\infty} \sim C_i^{o}\right)$	449.9	336.6	Ngl.	5.8
	$\left(C_i^{o} \sim C_i^{+\infty}\right)$	298.9	123	Ngl.	4.7
Diffusion Couple	Composition Range	$\overline{\tilde{D}}^{Al}_{NiNi}$	$\overline{\tilde{D}}^{Al}_{NiRe}$	$\overline{\tilde{D}}^{Al}_{ReNi}$	$\overline{\tilde{D}}^{Al}_{ReRe}$
Ni-24.5Al vs. Ni-23.5Al-0.5Re	$\left(C_i^{-\infty} \sim C_i^{o}\right)$	417.7	33.7	Ngl.	3.8
	$\left(C_i^{o} \sim C_i^{+\infty}\right)$	265.1	70.1	Ngl.	4.0
Ni-24.5Al vs. Ni-23.5Al-0.7Re	$\left(C_i^{-\infty} \sim C_i^{o}\right)$	509.9	42.0	Ngl.	4.5
	$\left(C_i^{o} \sim C_i^{+\infty}\right)$	362.8	55.3	Ngl.	3.4
Ni-25Al vs. Ni-23.5Al-0.5Re	$\left(C_i^{-\infty} \sim C_i^{o}\right)$	463.2	164.8	Ngl.	3.8
	$\left(C_i^{o} \sim C_i^{+\infty}\right)$	668.3	188.5	Ngl.	2.4
Ni-26Al vs. Ni-23.5Al-0.7Re	$\left(C_i^{-\infty} \sim C_i^{o}\right)$	449.9	107.5	Ngl.	5.8
	$\left(C_i^{o} \sim C_i^{+\infty}\right)$	298.9	171.2	Ngl.	4.7

Note: Ngl refers to magnitude less than 0.1 x 10^{-16} m^2/sec.

The average ternary interdiffusion coefficients reported in Tables 5.3, 5.4 and 5.5 were employed to generate concentration profiles using error-function solution provided by Fujita and Gosting [60]. Excellent agreement between EPMA measurement and calculated concentration profiles were found for all couples. Typical examples are presented in Figures 5.2, 5.3 and 5.4 where open circles are the EPMA measurements and solid lines are the calculated concentration profile.

5.4.3 Ternary interdiffusion coefficients determined by Boltzmann-Matno analysis

For the diffusion couples Ni-Al vs. Ni-Al-Ir and Ni-Al vs. Ni-Al-Re, several intersecting compositions were found among the diffusion paths. Intersecting diffusion paths shown in Figures 5.7 and 5.8 represent typical challenges in determining the interdiffusion coefficients by Boltzmann-Matano analysis for ordered intermetallics with ternary alloying addition. Two diffusion paths can intersect at a shallow angle or with negligible Ir and Re concentration gradient. In order to determine the ternary interdiffusion coefficients at these compositions, Boltzmann-Matano analysis was employed using a range of concentrations and distance that are certain with respect to EPMA measurement. The values of ternary interdiffusion coefficients estimated in this study are reported in Tables 5.6 and 5.7, and correspond well to the average ternary interdiffusion coefficients for either side of the Matano plane reported in Tables 5.3 and 5.5, respectively. Slight deviation in values and change in signs of the $\overline{\widetilde{D}}^{Al}_{NiRe}$ coefficients are attributed to the uncertainty in concentration gradient of Re.

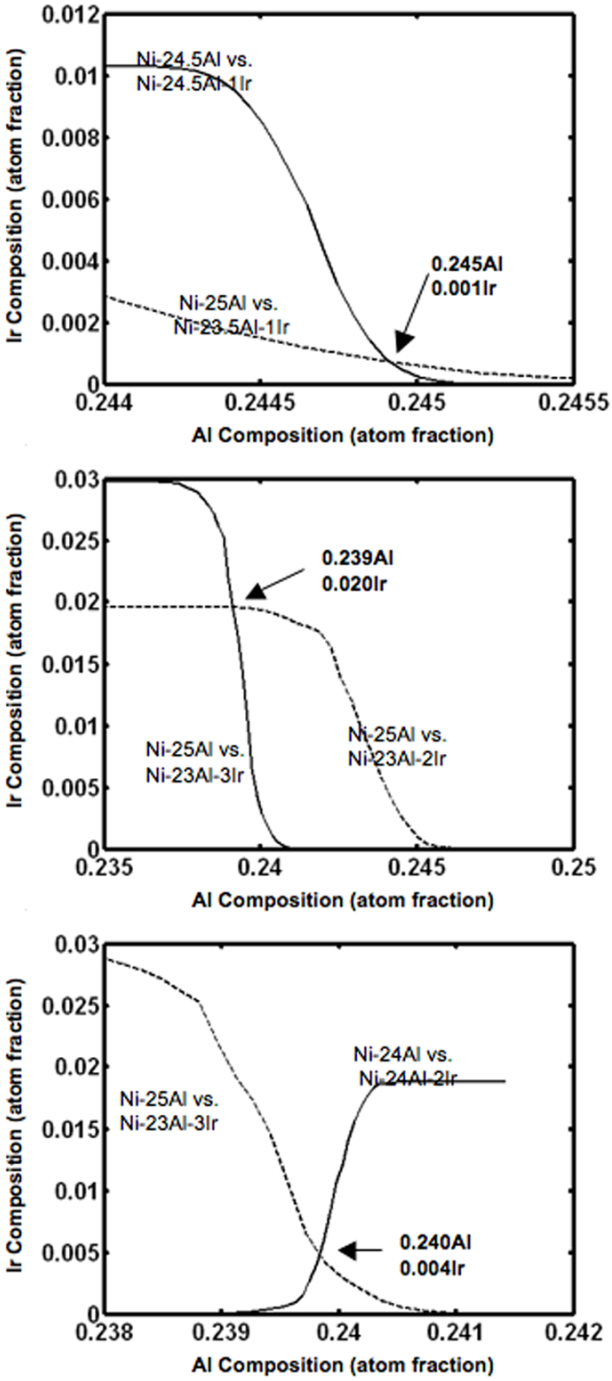

Figure 5.7 : Typical intersecting diffusion paths of Ni-Al vs. Ni-Al-Ir diffusion couples annealed at 1473K for 5 hours. Compositions at these intersections were employed for the determination of ternary interdiffusion coefficients based on Boltzmann-Matano analysis.

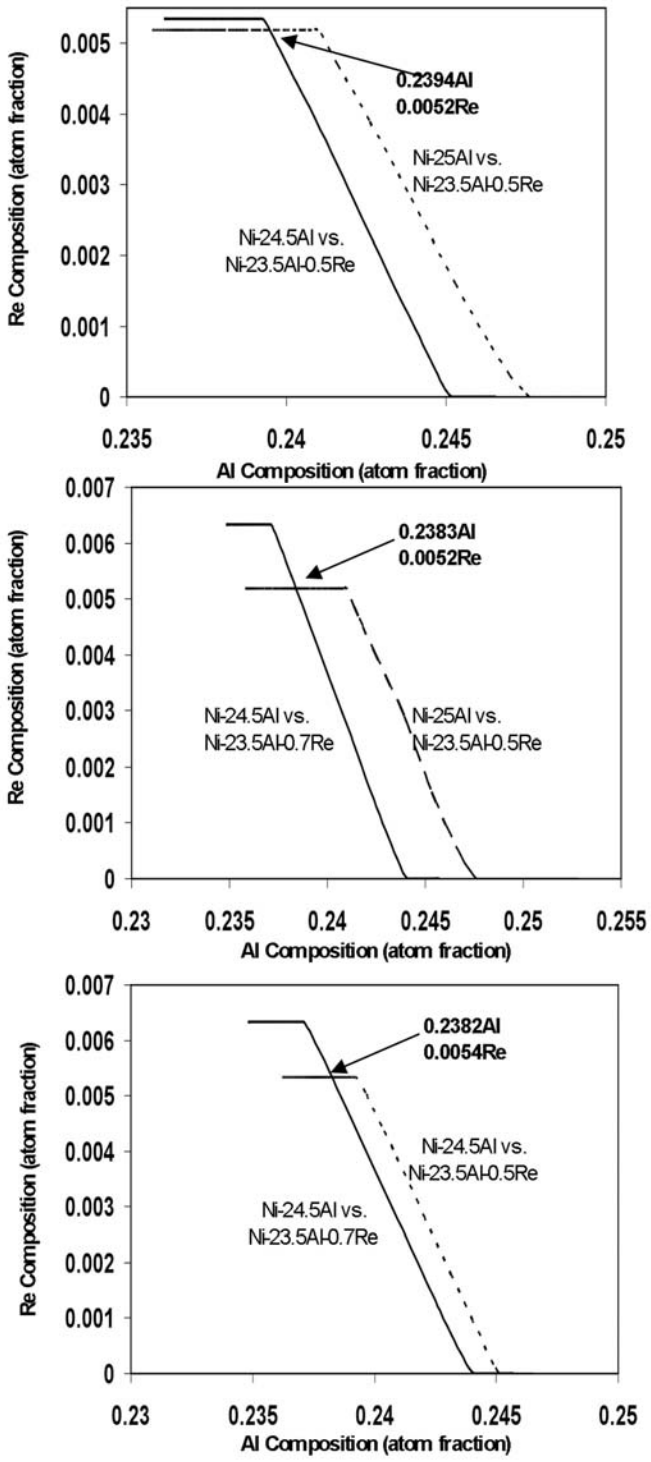

Figure 5.8 : Typical intersecting diffusion paths of Ni-Al vs. Ni-Al-Re diffusion couples annealed at 1473K for 5 hours. Compositions at these intersections were employed for the determination of ternary interdiffusion coefficients based on Boltzmann-Matano analysis.

Table 5.6 : Ternary interdiffusion coefficients (10^{-16} m^2/s) determined by Boltzmann-Matano analysis from Ni-Al vs. Ni-Al-Ir diffusion couples annealed at 1473K for 5 hours.

Diffusion Couples with Intersecting Diffusion Paths	Intersecting Composition (atom fraction)	$\widetilde{D}^{Ni}_{AlAl}$	$\widetilde{D}^{Ni}_{AlIr}$	$\widetilde{D}^{Ni}_{IrAl}$	$\widetilde{D}^{Ni}_{IrIr}$
Ni-25Al vs. Ni-23Al-3Ir Ni-24Al vs. Ni-24Al-2Ir	Al: 0.24 Ir: 0.005	1021.3	-15.0	-39.9	12.5
Ni-25Al vs. Ni-23Al-2Ir Ni-25Al vs. Ni-23Al-3Ir	Al: 0.239 Ir: 0.019	494.7	-36.3	Ngl.	17.2
Ni-26Al vs. Ni-23Al-2Ir Ni-25Al vs. Ni-23Al-3Ir	Al: 0.239 Ir: 0.020	563.9	-33.0	Ngl.	17.3
Ni-24Al vs. Ni-24Al-2Ir Ni-25Al vs. Ni-23.5Al-1Ir	Al: 0.240 Ir: 0.001	634.5	-3.4	Ngl.	11.5
Ni-24Al vs. Ni-24Al-2Ir Ni-25Al vs. Ni-23Al-2Ir	Al: 0.241 Ir: 0.019	419.3	-117.6	Ngl.	25.9
Ni-25Al vs. Ni-23Al-2Ir Ni-24.5Al vs. Ni-24.5Al-1Ir	Al: 0.243 Ir: 0.001	594.0	-38.5	-15.0	11.0
Ni-25Al vs. Ni-23Al-2Ir Ni-24.5Al vs. Ni-24.5Al-1Ir	Al: 0.245 Ir: 0.017	827.3	28.1	Ngl.	15.2
Ni-25Al vs. Ni-23Al-3Ir Ni-25Al vs. Ni-23.5Al-1Ir	Al: 0.240 Ir: 0.010	623.0	-26.9	Ngl.	13.7
Ni-25Al vs. Ni-23.5Al-1Ir Ni-24.5Al vs. Ni-24.5Al-1Ir	Al: 0.245 Ir: 0.0002	644.4	-73.2	Ngl.	12.0
Diffusion Couples with Intersecting Diffusion Paths	Intersecting Composition (atom fraction)	$\widetilde{D}^{Al}_{NiNi}$	$\widetilde{D}^{Al}_{NiIr}$	$\widetilde{D}^{Al}_{IrNi}$	$\tilde{D}^{Al}_{IrIr}$
Ni-25Al vs. Ni-23Al-3Ir Ni-24Al vs. Ni-24Al-2Ir	Al: 0.24 Ir: 0.005	981.4	983.9	39.9	52.4
Ni-25Al vs. Ni-23Al-2Ir Ni-25Al vs. Ni-23Al-3Ir	Al: 0.239 Ir: 0.019	493.0	512.2	Ngl.	18.8
Ni-26Al vs. Ni-23Al-2Ir Ni-25Al vs. Ni-23Al-3Ir	Al: 0.239 Ir: 0.020	564.0	580.0	Ngl.	17.3
Ni-24Al vs. Ni-24Al-2Ir Ni-25Al vs. Ni-23.5Al-1Ir	Al: 0.240 Ir: 0.001	634.5	626.4	Ngl.	11.6
Ni-24Al vs. Ni-24Al-2Ir Ni-25Al vs. Ni-23Al-2Ir	Al: 0.241 Ir: 0.019	419.3	511.0	Ngl.	25.9
Ni-25Al vs. Ni-23Al-2Ir Ni-24.5Al vs. Ni-24.5Al-1Ir	Al: 0.243 Ir: 0.001	579.0	606.6	15.0	26.0
Ni-25Al vs. Ni-23Al-2Ir Ni-24.5Al vs. Ni-24.5Al-1Ir	Al: 0.245 Ir: 0.017	827.3	784.1	Ngl.	15.2
Ni-25Al vs. Ni-23Al-3Ir Ni-25Al vs. Ni-23.5Al-1Ir	Al: 0.240 Ir: 0.010	623.0	636.2	Ngl.	13.7
Ni-25Al vs. Ni-23.5Al-1Ir Ni-24.5Al vs. Ni-24.5Al-1Ir	Al: 0.245 Ir: 0.0002	644.4	705.6	Ngl.	12.1

Note: Ngl refers to magnitude less than 0.1 x 10^{-16} m^2/sec.

Table 5.7 : Ternary interdiffusion coefficients (10^{-16} m^2/s) determined by Boltzmann-Matano analysis from Ni-Al vs. Ni-Al-Re diffusion couples annealed at 1473K for 5 hours.

Diffusion Couples with Intersecting Diffusion Paths	Intersecting Composition (atom fraction)	$\tilde{D}^{Ni}_{AlAl}$	$\tilde{D}^{Ni}_{AlRe}$	$\tilde{D}^{Ni}_{ReAl}$	$\tilde{D}^{Ni}_{ReRe}$
Ni-24.5Al vs. Ni-23.5Al-0.5Re Ni-25Al vs. Ni-23.5Al-0.5Re	Al: 0.239 Re: 0.005	832.5	926.5	Ngl.	2.8
Ni-24.5Al vs. Ni-23.5Al-0.5Re Ni-24.5Al vs. Ni-23.5Al-0.7Re	Al: 0.2382 Re: 0.005	244.2	216.0	Ngl.	3.1
Ni-25Al vs. Ni-23.5Al-0.5Re Ni-24.5Al vs. Ni-23.5Al-0.7Re	Al: 0.2393 Re: 0.005	726.1	734.9	Ngl.	3.1
Diffusion Couples with Intersecting Diffusion Paths	Intersecting Composition (atom fraction)	$\tilde{D}^{Al}_{NiNi}$	$\tilde{D}^{Al}_{NiRe}$	$\tilde{D}^{Al}_{ReNi}$	$\tilde{D}^{Al}_{ReRe}$
Ni-24.5Al vs. Ni-23.5Al-0.5Re Ni-25Al vs. Ni-23.5Al-0.5Re	Al: 0.239 Re: 0.005	832.5	-96.8	Ngl.	2.8
Ni-24.5Al vs. Ni-23.5Al-0.5Re Ni-24.5Al vs. Ni-23.5Al-0.7Re	Al: 0.2382 Re: 0.005	244.2	25.0	Ngl.	3.1
Ni-25Al vs. Ni-23.5Al-0.5Re Ni-24.5Al vs. Ni-23.5Al-0.7Re	Al: 0.2393 Re: 0.005	726.1	-11.9	Ngl.	3.1

Note: Ngl refers to magnitude less than 0.1 x 10^{-16} m^2/sec.

Several relative maxima and minima in concentration profiles (e.g., $\partial C_i/\partial x = 0$) were also observed for Ni in Ni-Al vs. Ni-Al-Ir couples and for Al in Ni-Al vs. Ni-Al-Ta couples as shown in Figures 5.2 and 5.3. Ternary interdiffusion coefficients at these compositions were also determined since one of the terms in Eq. (5.1) becomes zero. These values are reported in Table 5.8 for Ni-Al vs. Ni-Al-Ir couples, and correspond well to the average ternary interdiffusion coefficients on either side of the Matano plane reported in Table 5.3, and ternary interdiffusion coefficients determined by Boltzmann-Matano analysis reported in Table 5.6. Unfortunately, for Ni-Al vs. Ni-Al-Ta couples, the concentration and its gradient for Ta, where the concentration gradient of Al became zero (e.g., relative maxima and minima of Al), were uncertain (e.g., $C_{Ta} \approx 0$ and $\partial C_{Ta}/\partial x \approx 0$) to determine any ternary interdiffusion coefficients. The relative maxima and minima in concentration profiles were not observed in any Ni-Al vs. Ni-Al-Re diffusion couples.

Table 5.8 : Ternary interdiffusion coefficients (10^{-16} m^2/s) determined at relative maxima and minima of concentration profiles in Ni-Al vs. Ni-Al-Ir diffusion couples annealed at 1473K for 5 hours.

Couple	Extrema Composition (atom fraction)	Ternary Interdiffusion Coefficinets at Extrema	
		$\widetilde{D}^{Al}_{NiIr}$	$\widetilde{D}^{Al}_{IrIr}$
Ni-25Al vs. Ni-23.5Al-1Ir	Al: 0.2452 Ir: 0.00037	737.4	12.5
	Al: 0.2420 Ir: 0.0091	675	34.4
Ni-24.5Al vs. Ni-24.5Al-1Ir	Al: 0.2451 Ir: 0.00005	1190.4	12.0
	Al: 0.2443 Ir: 0.0102	922.3	43.7
Ni-26Al vs. Ni-23Al-2Ir	Al: 0.2501 Ir: 0.001	656.5	18.9
	Al: 0.245 Ir: 0.0186	617.6	22.2
Ni-25Al vs. Ni-23Al-2Ir	Al: 0.2453 Ir: 0.00045	552.2	12.4
	Al: 0.2408 Ir: 0.0187	499.6	25.9
Ni-25Al vs. Ni-23Al-3Ir	Al: 0.2409 Ir: 0.00011	1195.6	8.8
	Al: 0.2374 Ir: 0.0296	778.7	26.8

5.4.4 Estimation of binary interdiffusion coefficients in Ni_3Al

The ternary interdiffusion coefficients $\tilde{D}^{Ni}_{AlAl}$ and $\tilde{D}^{Al}_{NiNi}$ approach the binary $\tilde{D}_i$ for Ni_3Al as the concentration of Ir, Ta or Re decreases to zero. Hence, values of $\tilde{D}_i$ ($i = Ni$ or Al) were estimated from ternary diffusion couples where Ir, Ta or Re concentration was negligibly small in segments of the diffusion zone (e.g., Fick's law for substitutional binary alloys). Such regions were found in all couples since $\overline{\tilde{D}}_{IrIr}$, $\overline{\tilde{D}}_{TaTa}$, and $\overline{\tilde{D}}_{ReRe}$ coefficients are much smaller than $\overline{\tilde{D}}^{Ni}_{AlAl}$ and $\overline{\tilde{D}}^{Al}_{NiNi}$. The $\tilde{D}_i$ values extrapolated from the ternary couples with large enough concentration

difference (e.g., ΔC_{Al} or ΔC_{Ni} > 2 at.%) in terminal alloys are presented in Figures 5.9 and 5.10. The magnitude of $\tilde{D}_i$ appears consistent with the available binary diffusion data [3-9] for Ni_3Al. However, the composition-dependence could not be evaluated correctly since this estimation is carried out near the terminal end of the concentration profiles with high uncertainty in the magnitude of concentration gradient for Al, and assumes that the Ir, Ta and Re concentration, less than 2 at.%, do not influence the value of $\tilde{D}_i$.

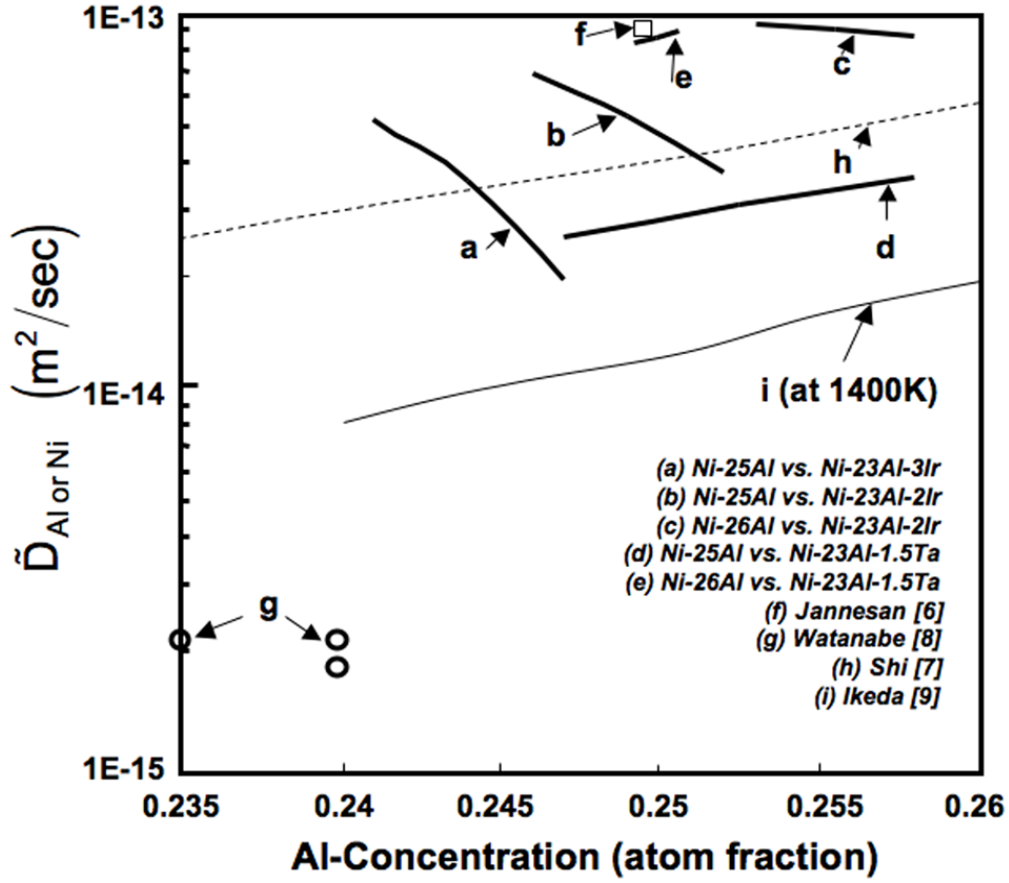

Figure 5.9 : Interdiffusion coefficients of Ni or Al in Ni_3Al at 1473K compiled from this investigation and literature review.

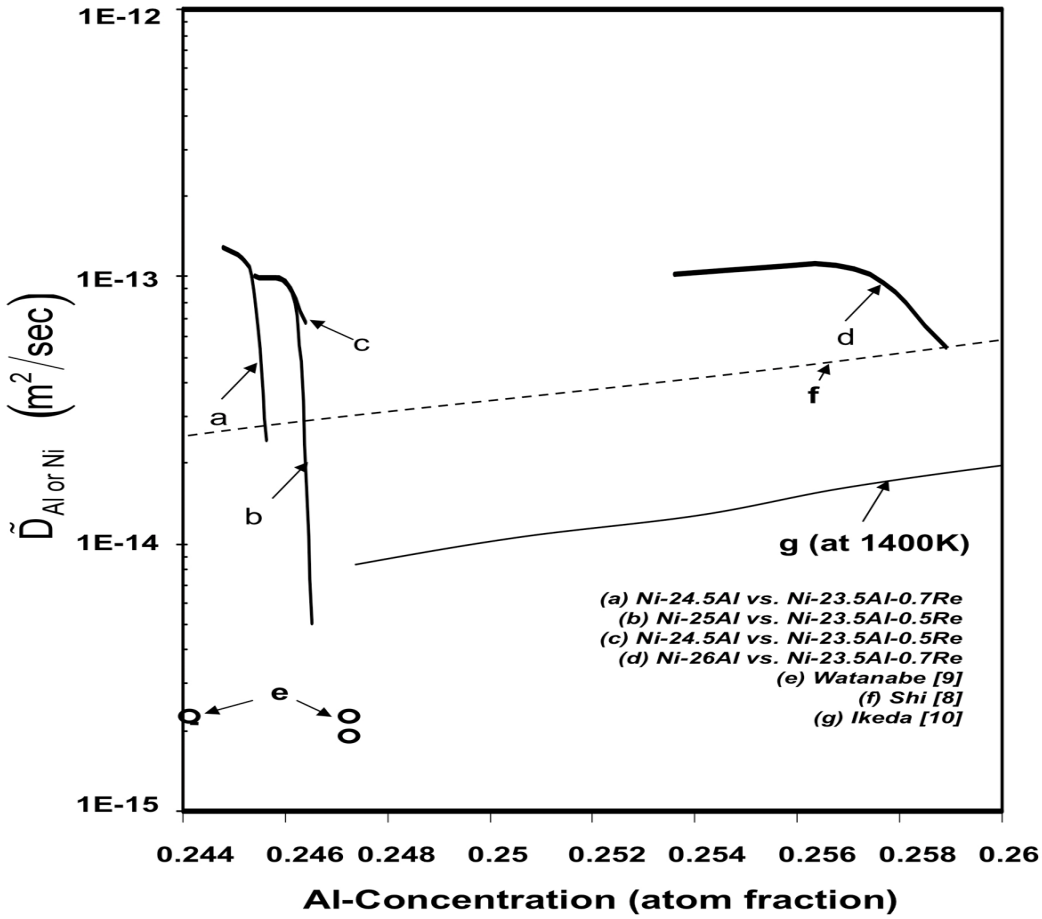

Figure 5.10 : Interdiffusion coefficients of Ni or Al in Ni_3Al at 1473K compiled from this investigation and literature review.

5.4.5 Estimation of tracer diffusion coefficient of Ir and Ta in Ni_3Al

For component i diffusing into a binary alloy j-k, the cross interdiffusion coefficient $\tilde{D}_{ij}^{k}$ $(i \neq j)$ becomes negligible at infinite dilution of component i in a j-k alloy [62]. Then the value of the main coefficient $\tilde{D}_{ii}$ approaches that of the tracer diffusion coefficient D_i^* for component i:

$$C_i \to 0 \quad \tilde{J}_i = -\tilde{D}_{ii}^{k} \frac{\partial C_i}{\partial x} \cong -D_{i(jk)}^{*} \frac{\partial C_i}{\partial x} \tag{5.7}$$

Thus, the tracer diffusion coefficients of Ir, Ta and Re in Ni_3Al alloy can be estimated from the main interdiffusion coefficient of Ir, $\tilde{D}_{IrIr}^{Ni}$ or $\tilde{D}_{IrIr}^{Al}$, Ta, $\tilde{D}_{TaTa}^{Ni}$ or $\tilde{D}_{TaTa}^{Al}$, and Re, $\tilde{D}_{ReRe}^{Ni}$ or $\tilde{D}_{ReRe}^{Al}$ using Eq. (5.7), provided that the concentration of Ir or Ta or Re approaches zero within the diffusion zone so that the cross interdiffusion coefficients, $\tilde{D}_{IrAl}^{Ni}$ or $\tilde{D}_{IrNi}^{Al}$, $\tilde{D}_{TaAl}^{Ni}$ or $\tilde{D}_{TaNi}^{Al}$, and $\tilde{D}_{ReAl}^{Ni}$ or $\tilde{D}_{ReNi}^{Al}$ become negligible. Such regions were found in all couples since $\overline{\tilde{D}}_{IrIr}$, $\overline{\tilde{D}}_{TaTa}$ and $\overline{\tilde{D}}_{ReRe}$ coefficients are much smaller than $\overline{\tilde{D}}_{AlAl}^{Ni}$ and $\overline{\tilde{D}}_{NiNi}^{Al}$. Values of tracer diffusion coefficients of Ir, D_{Ir}^*, Ta, D_{Ta}^*, and Re, D_{Re}^* were extrapolated from the main interdiffusion coefficients, $\tilde{D}_{IrIr}^{Ni}$ or $\tilde{D}_{IrIr}^{Al}$, $\tilde{D}_{TaTa}^{Ni}$ or $\tilde{D}_{TaTa}^{Al}$, and $\tilde{D}_{ReRe}^{Ni}$ or $\tilde{D}_{ReRe}^{Al}$ as the concentration of Ir, Ta, and Re, respectively, becomes zero. The extrapolations for D_{Ir}^*, D_{Ta}^* and D_{Re}^* from the ternary interdiffusion coefficients on the basis of Eq. (5.7) are presented in Figures 5.11, 5.12, and 5.13, respectively. The estimated values of D_{Ir}^* and D_{Ta}^* are reported in Table 5.9.

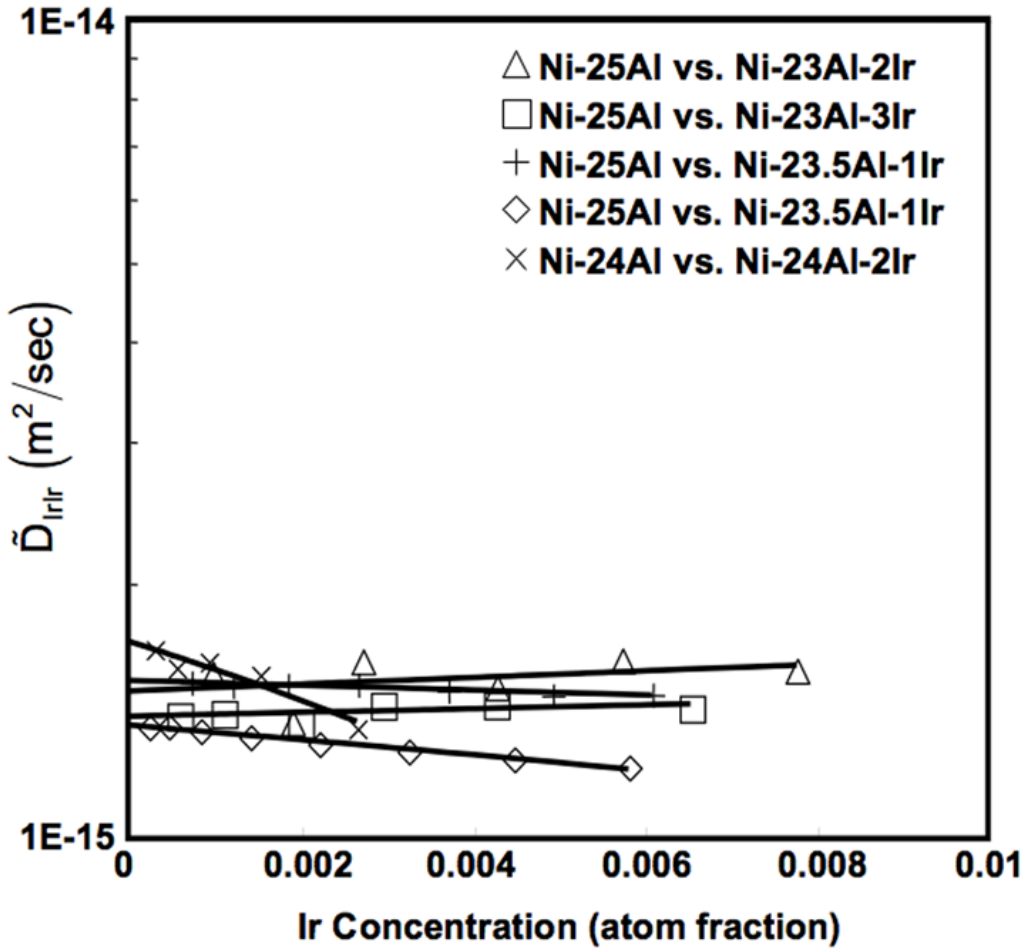

Figure 5.11 : Extrapolation of $\tilde{D}_{IrIr}$ coefficient for the estimation of tracer diffusion coefficient of Ir in Ni_3Al at 1473K.

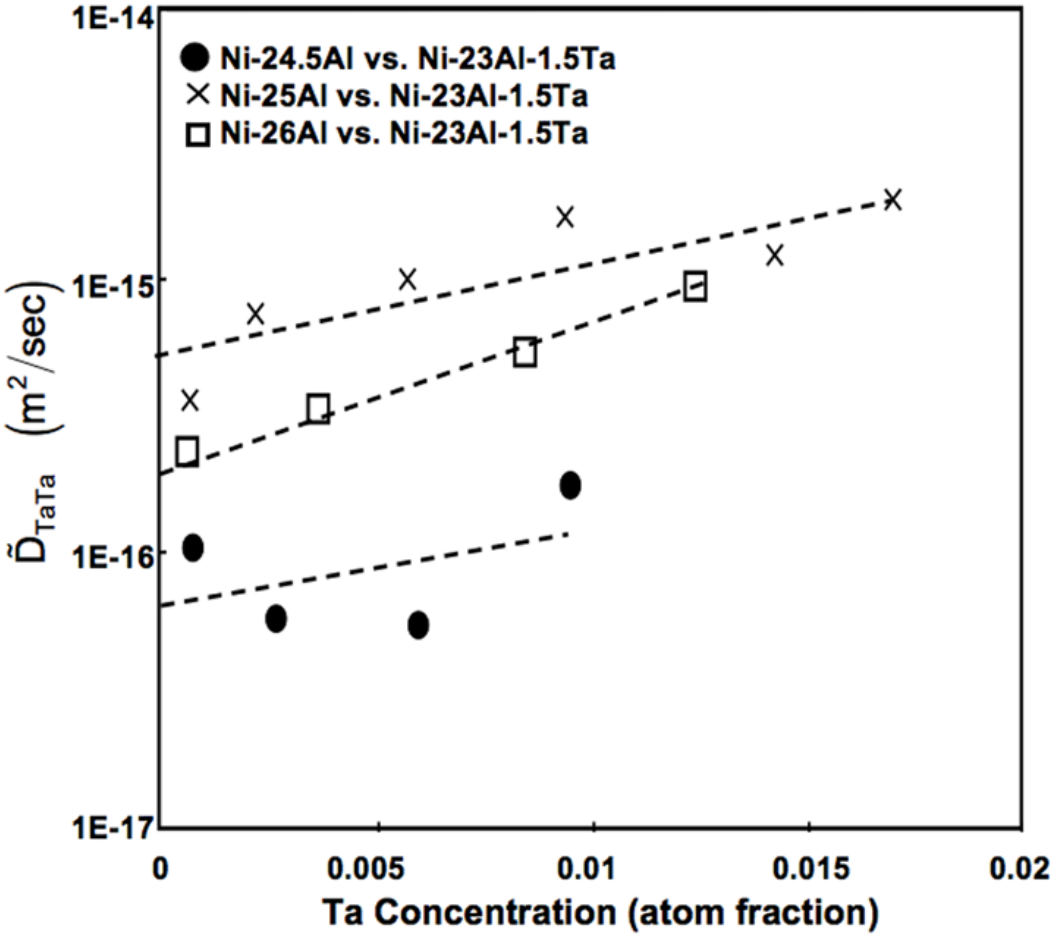

Figure 5.12 : Extrapolation of $\tilde{D}_{TaTa}$ coefficient for the estimation of tracer diffusion coefficient of Ta in Ni_3Al at 1473K.

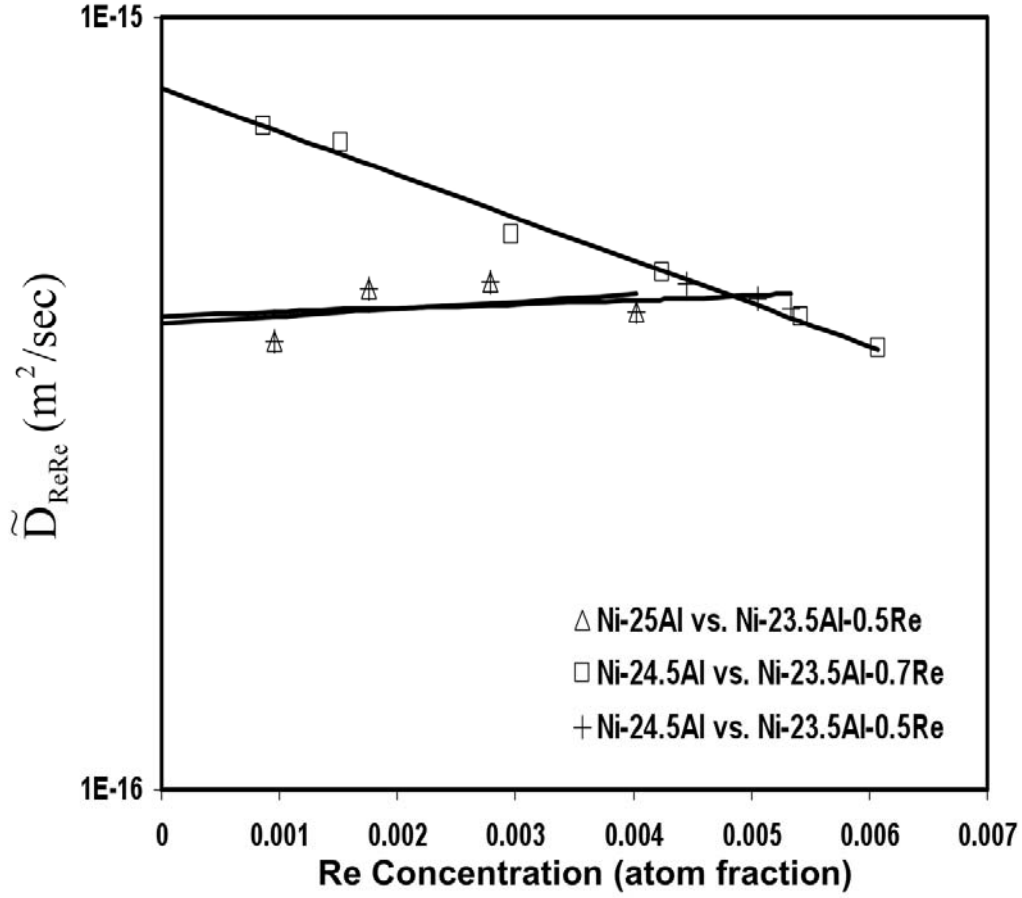

Figure 5.13 : Extrapolation of $\tilde{D}_{ReRe}$ coefficient for the estimation of tracer diffusion coefficient of Re in Ni_3Al at 1473K.

Table 5.9 : Tracer diffusion coefficients (10^{-16} m^2/s) of Ir, Ta and Re in Ni_3Al extrapolated from concentration profiles of ternary diffusion couples at 1473K.

Composition	Tracer Component	D_i^* (10^{-16} m^2/sec)
75.4Ni-24.6Al	Ir	15.1
75.3Ni-24.7Al	Ir	14.6
75.5Ni-24.5Al	Ir	13.3
76.1Ni-24.1Al	Ir	13.6
76.2Ni-23.8Al	Ir	16.9
Average Value for Ir		**14.7 ± 1.4**
75.6Ni-24.3Al	Ta	0.6
75.1Ni-24.8Al	Ta	5.3
74.2Ni-25.8Al	Ta	2.0
Average Value for Ta		**2.6 ± 2.4**
75.2Ni-24.8Al	Re	4.0
75.6Ni-24.4Al	Re	8.1
75.5Ni-24.5Al	Re	4.1
Average Value for Re		**5.4 ± 2.3**

At these dilute concentration of Ir, Ta, Re the magnitude of tracer diffusion coefficients of Ir, Ta and Re are very similar to their respective main ternary interdiffusion coefficients. The estimated tracer diffusion coefficient for the β-site-occupying Ta ($2.6 \times 10^{-16} \pm 2.4 \times 10^{-16}$ m^2/sec) is lower than that for the α-site-occupying Ir ($14.7 \times 10^{-16} \pm 1.4 \times 10^{-16}$ m^2/sec). The tracer diffusion coefficient of Re ($5.4 \times 10^{-16} \pm 2.3 \times 10^{-16}$ m^2/sec) falls between the two tracer diffusion coefficients for Ir and Ta.

5.5. Summary

Ternary interdiffusion interactions of Ir and Ta addition on the $L1_2$ Ni_3Al phase were examined using solid-to-solid diffusion couples annealed at 1473K for 5 hours. Average ternary interdiffusion coefficients were determined from an integration of interdiffusion fluxes for

individual components. The magnitude of $\tilde{\bar{D}}^{Al}_{NiNi}$ and $\tilde{\bar{D}}^{Ni}_{AlAl}$ coefficients was determined to be much larger than that of $\tilde{\bar{D}}_{IrIr}$, $\tilde{\bar{D}}_{TaTa}$, and $\tilde{\bar{D}}_{ReRe}$ coefficients. The $\tilde{\bar{D}}^{Al}_{NiIr}$ coefficient was determined to be positive and large in magnitude; Ir substitutes in Ni-site and influences the interdiffusion of Ni significantly. The $\tilde{\bar{D}}^{Ni}_{AlTa}$ coefficient was positive and large in magnitude; Ta substitutes in Al-site and influences the interdiffusion of Al significantly. The $\tilde{\bar{D}}^{Ni}_{AlRe}$ coefficient was determined to be positive and large in magnitude; Re substitutes in Al-site and influences the interdiffusion of Al significantly. Ternary interdiffusion coefficients were also determined at compositions of intersecting diffusion paths, and at relative maxima and minima in concentration profiles for Ir-alloyed Ni_3Al. Consistency among ternary interdiffusion coefficients was observed. Profiles of concentrations were also examined to estimate binary interdiffusion coefficients in Ni_3Al. The results agreed well with published values. Tracer diffusion coefficients of Ir, Ta and Re in Ni_3Al were also estimated as $D^*_{Ir} = 14.7 \times 10^{-16} \pm 1.4 \times 10^{-16}$ m^2/sec, $D^*_{Ta} = 2.6 \times 10^{-16} \pm 2.4 \times 10^{-16}$ m^2/sec, and $D^*_{Re} = 5.4 \times 10^{-16} \pm 2.3 \times 10^{-16}$ m^2/sec at 1473K.

The experiment and analysis reported herein demonstrates the practical use of analytical technique for multicomponent interdiffusion based on the determination and an integration of interdiffusion fluxes. The large magnitude of $\tilde{\bar{D}}^{Al}_{NiIr}$, $\tilde{\bar{D}}^{Ni}_{AlTa}$, and $\tilde{\bar{D}}^{Ni}_{AlRe}$ coefficients also signifies a correlation in ternary diffusional interactions and site-preference of ordered ternary intermetallic alloys. In practical applications such as γ'-Ni_3Al containing oxidation resistant coatings, Ir can substitute for Ni to reduce the interdiffusion fluxes of Ni from the Ni-rich superalloy substrate into the Al-rich oxidation resistant coatings [10-15]. Presence of Ta and Re in Ni-base superalloy

substrate can also reduce the interdiffusion fluxes of Al from the Al-rich coatings into the superalloy substrate. Microstructural stability of Ni-base superalloy can also improve by appropriate partitioning of Ir, Ta and Re in γ'-Ni_3Al precipitates and fcc-Ni matrix.

5.6 References

1. C.T. Sims, N.S. Stoloff, W.C. Hagel: Superalloys II, John Wiley & Sons, New York, NY, 1987, pp. 3–131.
2. C.E. Campbell, W.J. Boettinger, U.R. Kattner, Development of a diffusion mobility database for Ni-base superalloys, Acta Mater. 50 (2002) 775–92.
3. J. Cermak, V. Rothova, Concentration dependence of ternary interdiffusion coefficients in Ni_3Al/Ni_3Al–X couples with X=Cr, Fe, Nb and Ti, Acta Mater. 51 (2003) 4411–21.
4. V. Rothova, J. Cermak, Bulk and grain boundary diffusion of ^{67}Ga in Ni_3Al—influence of composition , Intermetallics. 13 (2005) 113-20.
5. Y. Minamino, H. Yoshida, S.B. Jung, K. Hirao, T. Yamane, Diffusion of platinum and molybdenum in Ni and Ni3Al, Defect Diff. Forum. 143-147 (1997) 257–62.
6. M.M.P. Janssen, Diffusion in the Nickel-rich part of the Ni-Al system at 1000° to 1300°C, Ni_3Al layer growth, diffusion coefficients and interface concentrations, Metall. Trans., 4 (1973) 1623–33.
7. Y.Shi, G. Frohberg, H. Wever, Diffusion of Ni and In in the γ′-phase Ni_3Al, Phys. Status Solidi A. 152 (1995) 361–375.
8. M. Watanabe, Z. Horita, D. J. Smith, M.R. McCartney, T. Sano, M. Nemoto, Electron microscopy study of Ni/Ni[3]Al diffusion-couple interface. II: Diffusivity measurement

Acta Metall. Mater, 42 (1994) 3389–96.

9. T. Ikeda, A. Almazouzi, H. Numakura, M. Koiwa, W. Sprengel, H. Nakajima, Single-phase interdiffusion in Ni_3Al, Acta Mater. 46 (1998) 5369–76.

10. Y.N.A. Wu, J. Tsukuba, A. Yamaguchi, J. Tsukuba, S. Kuroda, Role of Iridium in hot corrosion resistance of Pt-Ir modified aluminide coatings with Na_2SO_4-NaCl Salt at 1173 K, Mater. Trans. 47 (2006) 1918–21.

11. T. Abe, M. Ode, H. Murakami, C.S. Oh, C. Kocer, Y. Yamabe-Mitarai, H. Onodera, A thermodynamic description of the Al-Ir system, Mater. Sci. Forum, 539–543 (2007) 2389–94.

12. H. Murakami, A. Yamaguchi, Y.N. Wu, S. Kuroda, Effect of Hf addition on high temperature properties of Ir-containing alloy coatings, Mater. Sci. Forum. 546–549 (2007) 1689–94.

13. Y.N. Wu, A. Yamaguchi, H. Murakami, S. Kuroda, Hot corrosion behavior of Pt-Ir modified aluminide coatings on the nickel-base single crystal superalloy TMS-82+, J. Mater. Res. 22 (2007) 206–16.

14. Y. Yamabe-Mitarai, T. Aoyagi, K. Nishida, H. Aoki, T. Abe, H. Murakami, Phase Equilibria between the B2, $L1_2$, and fcc phases in the Ir-Ni-Al System. Intermetallics. 15 (2007) 479–88.

15. A. Suzuki, Y.N. Wu, A. Yamaguchi, H. Murakami, C.M.F. Rae, Oxidation Behavior of Pt–Ir Modified Aluminized Coatings on Ni-base Single Crystal Superalloy TMS-82+, Oxi. Metals. 68 (2007) 53–64.

16. S. Ochiai, Y. Oya, T. Suzuki, Alloying behaviour of Ni_3Al, Ni_3Ga, Ni_3Si and Ni_3Ge, Acta Metall. 32 (1984) 289–98.

17. R.W. Guard, J.H. Westbrook, Alloying behaviour of Ni_3Al (γ'phase), Trans. TMS-AIME. 215 (1959) 807–14.

18. R.F. Decker, J.R. Mihalisin, Coherency strains in γ hardened nickel alloys, Trans. ASM, 62 (1969) 481–89.

19. R.D. Rawlings, A.E. Staton-Bevan, The alloying behaviour and mechanical properties of polycrystalline Ni_3Al (γ′ phase) with ternary additions, J. Mater. Sci. 10 (1975) 505–14.

20. A. Chiba, D. Shindo, S. Watanabe, Site occupation determination of Pd in Ni_3Al, Acta Metall. Mat., 39 (1991) 13–18.

21. A. Chiba, S. Hanada, S. Watanabe, Effect of γ and γ' former doping on ductility of Ni_3Al, Scripta Metall., 25 (1991) 303–07.

22. A. Chiba, S. Hanada, S. Watanabe, Correlation between ductility and ordering energy of Ni_3Al, Materials Transactions, JIM. 31 (1990) 824–27.

23. A. Chiba, S. Hanada, S.Watanabe, Ductilization of Ni_3 by microalloying with Ag, Scripta Mater., 26 (1992) 1031–36.

24. A. Chiba, S. Hanada, S.Watanabe, Improvement in ductility of Ni_3Al by γ former doping Mater. Sci. Eng. A, 152 (1992)108–13.

25. B. Gleeson, W. Wang, S. Hayashi, D. Sordelet, Effects of Platinum on the interdiffusion and oxidation behavior of Ni-Al-based alloys, 461-464 (2004) 213-22.

26. M.H.F. Sluiter, Y. Kawazoe, Site preference of ternary additions in Ni_3Al, Phys. Rev. B, 51 (1995) 4062–73.

27. A.V. Ruban, H.L. Skriver, Calculated site substitution in ternary γ′-Ni_3Al: Temperature and composition effects. Phys. Rev. B, 55 (1997) 8801–07.

28. M. Enomoto, H. Harada, Analysis of γ′/γ equilibrium in Ni−Al−X alloys by the Cluster

Variation Method With the Lennard−Jones Potential, Met. Trans. A. 1989, vol. 20A, pp.649–64.

29. H. Mehrer, Diffusion in intermetallics, Mater. Trans. JIM, 37 (1996) 1259–80.
30. H. Numakura, T. Ikeda, M. Koiwa, A. Almazouzi, Physics of condensed matter, structure, defects and mechanical properties, Phil. Mag. A, 77 (1998) 887–909.
31. S.V. Divinski, S. Frank, U. Sodervall, C. Herzig, Solute diffusion of Al-substituting elements in Ni_3Al and the diffusion mechanism of the minority component, Acta Mater.46 (1998) 4369-80.
32. H. Numakura, T. Ikeda, H. Nakajima, M. Koiwa, Diffusion in Ni_3Al, Ni_3Ga and Ni_3Ge, Mater. Sci. Eng. A, 312 (2001)109–17.
33. Y. Minamino, S.B. Jung, T. Yamane, K. Hirao, Diffusion of Cobalt, Chromium, and Titanium in Ni_3Al. Met. Trans. A. 23 (1992) 2783–90.
34. Y. Minamino, T. Yamane, S. Saji, K. Hirao, S.B. Jung, T. Kohira, Diffusion of Copper, Iron and Silicon in $L1_2$-Type intermetallic compound Ni_3Al, J. Jap. Inst. Metals. 58 (1994) 397–403.
35. S.B. Jung, Y. Minamino, T. Yamane, Diffusion of Mn in Ni and Ni_3Al, J. Mater. Sci. Lett. 18 (1999) 1063-66.
36. J. Cermak, A. Gazda, V. Rothova, Interdiffusion in ternary Ni_3Al/Ni_3Al-X diffusion couples with X=Cr, Fe, Nb and Ti, Intermetallics, 11 (2003) 939–46.
37. L. Onsager, Reciprocal relations in irreversible processes, Phys. Rev. 37 (1931) 405–26 and 38 (1932) 2265–79.
38. L. Onsager, The Diffusion of Electrolytes and Macromolecules in Solution, Ann. NY Acad. Sci. 46 (1965) 241–65.

39. A. Fick, Uber diffusion, Phil. Mag. 10 (1855), 30–39.

40. J.S. Kirkaldy, Diffusion in multicomponent metallic systems. I. Phenomenological theory for substitutional solid-solution alloys, Can. J. Phys. 36 (1958) 899–906.

41. J.S. Kirkaldy, D.J. Young, Diffusion in the Condensed State, The Institute of Metals, London, 1987, pp. 226–72.

42. M.A. Dayananda, C.W. Kim, Zero-flux planes and flux reversals in copper-nickel-zinc diffusion couples, Metall. Trans. A. 10A (1979) 1333–39.

43. M.A. Dayananda, An analysis of concentration profiles for fluxes, diffusion depths, and zero-flux planes in multicomponent diffusion, Metall. Trans. A, 14A (1983) 1851–58.

44. C.W. Kim, M.A. Dayananda, Identification of zero-flux planes and flux reversals in several studies of ternary diffusion, Metall. Trans. A. 14A (1983) 857–64.

45. C.W. Kim, M.A. Dayananda, Zero-flux planes and flux reversals in the copper-nickel-zinc system at 775°, Metall. Trans. A. 15A (1984) 649–59.

46. M.A. Dayananda, D.A. Behnke, Effective interdiffusion coefficients and penetration depths, Scripta Metall. 25 (1991) 2187–91.

47. M.A. Dayananda, Average effective interdiffusion coefficients and the Matano plane composition, Metal. Mater. Trans. A. 27A (1996) 2504–09.

48. M.A. Dayananda, Y.H. Sohn, Average effective interdiffusion coefficients and their applications for isothermal multicomponent diffusion couples, Scripta Mater. 35 (1996) 683–88.

49. M.A. Dayananda, Y.H. Sohn, A new analysis for the determination of ternary interdiffusion coefficients from a single diffusion couple, Metall. Mater. Trans. A. 30A (1999) 535-43.

50. M.S.A. Karunaratne, P. Carter, R.C. Reed, On the diffusion of Aluminum and Titanium in the Ni-rich Ni–Al–Ti system between 900 and 1200° C, Acta Mater. 49 (2001) 861-75.

51. T. Morimura, M. Hasaka, A. Nagata, Ordered phase formation and diffusion composition path in Cu3Au/Pd couple, J. Alloys Compounds. 347 (2002) 141-48.

52. R. Bouchet, R. Mevrel, A numerical inverse method for calculating the interdiffusion coefficients along a diffusion path in ternary systems, Acta Mater. 50 (2002) 4887-900.

53. T. Morimura, M. Hasaka, A. Nagata, Ordered phase formation and diffusion composition path in Cu_3Au/Pd couple, J. Alloys. Comp. 347 (2002) 141-48.

54. R. Bachorczyk, M. Danielewski, R. Filipek, Interdiffusion under the Chemical Potential Gradient; Comparison of Onsager and Darken Models, Defect Diff. Forum. 216-217 (2003) 141-47.

55. J. Moon, P. Wynblatt, S. Garoff, R. Suter, Pseudopartial wetting and precursor film growth in immiscible metal systems. Surf Sci. 559 (2004) 149-57.

56. P. Dawah-Tankeu, L. Dorer, G. Borchardt, K. Gomann, W.M. Pragnell, H.E. Evans, and J. L. Coze, Concentration dependence of the ternary interdiffusivities in the FeCrAl System at 1100C, Mater. High Temp. 22 (2005) 375-84.

57. N. Garimella, M.P. Brady, Y.H. Sohn, Interdiffusion in γ (face-centered cubic) Ni-Cr-X (X =Al, Si, Ge, or Pd) alloys at 900 °C, J. Phase. Equil. Diff. 27 (2006) 665-70.

58. S. Kim, J.H. Perepezko, Interdiffusion kinetics in the Mo_5SiB_2 (T_2) phase, J. Phase. Equil. Diff., 27 (2006) 605-13.

59. L.R. Ram-Mohan, M.A. Dayananda, A transfer matrix method for the calculation of concentrations and fluxes in multicomponent diffusion couples, Acta Mater. 54 (2006) 2325-34.

60. H. Fujita, L.J. Gosting, An exact solution of the equations for free diffusion in three-component systems with interacting flows, and its use in evaluation of the diffusion coefficients, J. Am. Chem. Soc. 78 (1956) 1099–106.

61. J.L. Pouchou, F. Pchoir, A new model for quantitative X-ray microanalysis. I Application to the analysis of homogeneous samples, Recherche Aerospatiale (English Edition). 3 (1984) 13-38.

62. T.O. Ziebold, R.E. Ogilvie, Ternary diffusion in copper-silver-gold alloys, Trans. TMS-AIME. 239 (1967) 942–53.

CHAPTER 6: DETERMINATION OF AVERAGE TERNARY INTERDIFFUSION COEFFICIENTS USING MOMENTS OF INTERDIFFUSION FLUX AND CONCENTRATION PROFILES

6.1 Introduction

The analysis of multicomponent diffusion often requires nonlinear fitting procedures with careful attention required even for the near-linear segments. Determination of composition dependent interdiffusion coefficients from concentration profiles obtained from diffusion couples can become a highly complex process. Consequently, reporting unquestionable values even within a single-phase region of the diffusion couple experiment can pose challenges. The objective of this work is to present an extended analytical method of a analytical approach [1], wherein average main and cross interdiffusion coefficients are determined over selected regions from a single diffusion couple experiment using moments (series of higher order integrands) of interdiffusion flux. For a ternary system, implementing this analytical technique yields the four interdiffusion coefficients as a function of interdiffusion-flux-moments for two independent components. The analysis is applied to selected single-phase isothermal diffusion couples including hypothetical A vs. B, and experimental ones in Ni_3Al-Ir [2] and Fe-Ni-Al [3] systems.

6.2 Description of a Refined Approach

From phenomenological description of ternary diffusion based on Onsager's formalism of Fick's law [4-6], an average ternary interdiffusion coefficients [1] can be employed to express

the interdiffusion flux $\tilde{J}_i$ of a component i in terms of two independent concentration gradients $\partial C_j/\partial x\,(j=1,2)$ by:

$$\tilde{J}_i = -\overline{\tilde{D}}^3_{i1}\frac{\partial C_1}{\partial x} - \overline{\tilde{D}}^3_{i2}\frac{\partial C_2}{\partial x} \qquad (i=1,2) \tag{6.1}$$

where $\overline{\tilde{D}}^3_{i1}$ and $\overline{\tilde{D}}^3_{i2}$ refer to the average main and cross-interdiffusion coefficients, respectively. The interdiffusion flux at any section x can be calculated directly from the experimental concentration profile using the relation [7]:

$$\tilde{J}_i = -\frac{1}{2t}\int_{C_i^- \text{ or } C_i^+}^{C_i(x)} (x - x_o)\,dC_i \qquad (i=1,\ 2) \tag{6.2}$$

where t is the time, C_i^- and C_i^+ are the terminal concentrations, and x_o refers to the location of the Matano plane. Figure 6.1(a) illustrates a typical concentration profile, and Figure 6.1(b) shows the corresponding interdiffusion flux profile determined using Eq. (6.2).

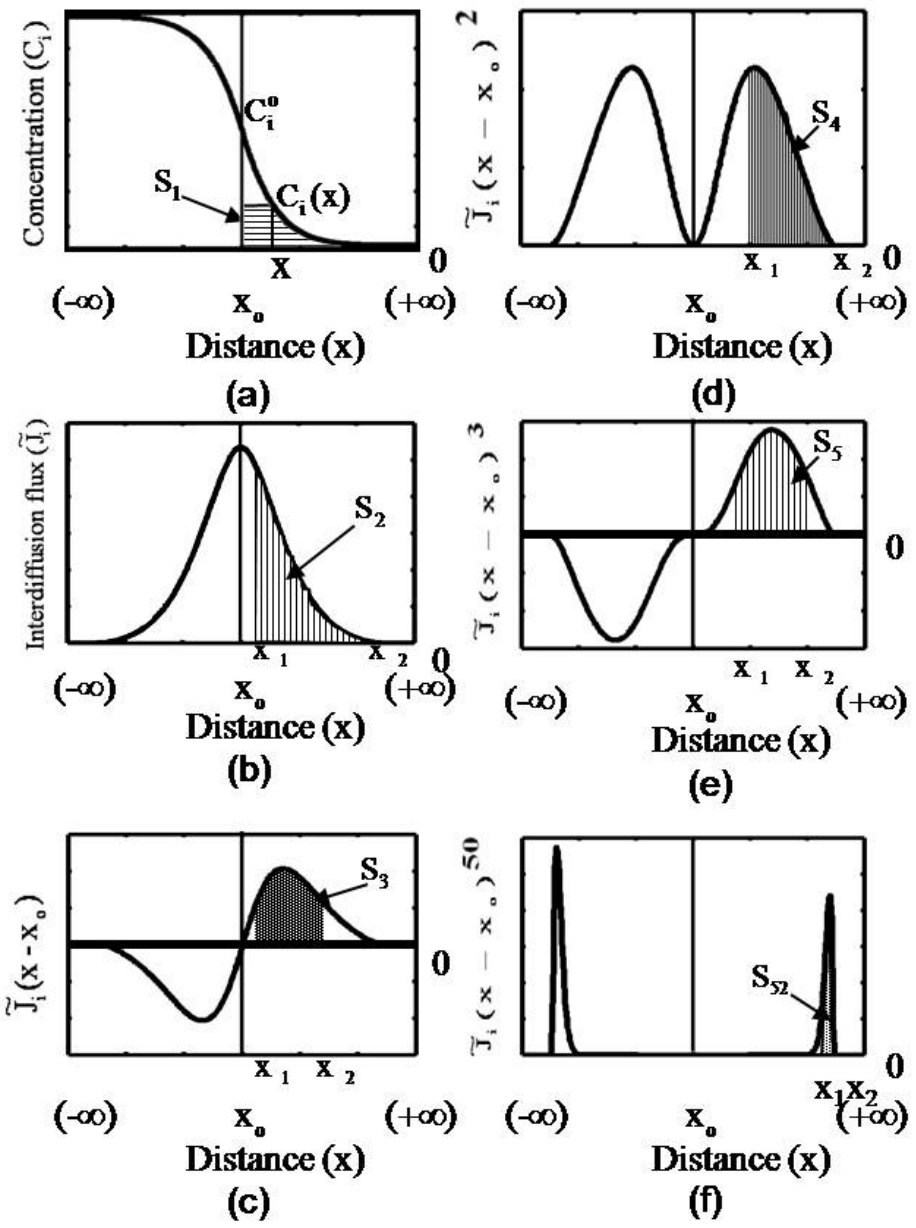

Figure 6.1 : Schematic profiles of (a) concentration Ci, (b) interdiffusion flux $\widetilde{J}_i$, (c) $\widetilde{J}_i(x-x_o)$, (d) $\widetilde{J}_i(x-x_o)^2$, (e) $\widetilde{J}_i(x-x_o)^3$, and (f) $\widetilde{J}_i(x-x_o)^{50}$ for a solid-solid diffusion couple. Area S1 S2, S3, S4, S5 and S50 correspond to $\int_{C_i^- \text{or } C_i^+}^{C_i(x)}(x-x_o)dC_i$, $\int_{x_1}^{x_2}\widetilde{J}_i dx$, $\int_{x_1}^{x_2}\widetilde{J}_i(x-x_0)dx$, $\int_{x_1}^{x_2}\widetilde{J}_i(x-x_0)^2dx$, $\int_{x_1}^{x_2}\widetilde{J}_i(x-x_0)^3dx$ and $\int_{x_1}^{x_2}\widetilde{J}_i(x-x_0)^{50}dx$, respectively. C1, C2 and x1, x2 are arbitrarily chosen limits of concentration and distance, respectively.

The interdiffusion flux $\tilde{J}_i$ for 'm' number of moments can be determined from Eq. (6.2) as a function of x, by multiplying both sides of Eq. (6.1) with $(x\text{-}x_o)^m$. An integration over a selected region, x_1 to x_2, yields [1]:

$$M(m) = \int_{x_1}^{x_2} \tilde{J}_i (x - x_o)^m dx = -\overline{\tilde{D}}_{i1}^3 \int_{C_1(x_1)}^{C_1(x_2)} (x - x_o)^m dC_1 - \overline{\tilde{D}}_{i2}^3 \int_{C_2(x_1)}^{C_2(x_2)} (x - x_o)^m dC_2 \quad (i = 1,2) \quad (6.3)$$

Eq. (6.3) is the recursion equation [8], and also can be referred as "Modified Onsager's Flow Equation" that involves moments of interdiffusion fluxes. By varying the m values from m = 0 to m = ∞ for the two independent components (e.g., 1 and 2), Eq. (6.3) can be written to provide infinite number for set of four equations to solve for the four $\overline{\tilde{D}}_{ij}^3$ interdiffusion coefficients. Solving each combination of these equations provides values of individual series for all the four average ternary interdiffusion coefficients.

Variation of $\int_{x_1}^{x_2} \tilde{J}_i (x - x_0)^m dx$ integral is presented in Figures 1(b) through 1(f). For the moments m = 0, 1 and 2 Eq. (6.3) can be written as:

$$M(0) = \int_{x_1}^{x_2} \tilde{J}_i dx = -\overline{\tilde{D}}_{i1}^3 \int_{C_1(x_1)}^{C_1(x_2)} dC_1 - \overline{\tilde{D}}_{i2}^3 \int_{C_2(x_1)}^{C_2(x_2)} dC_2 \quad (i = 1,2) \quad (6.4)$$

$$M(1) = \int_{x_1}^{x_2} \tilde{J}_i (x - x_o) dx = -\overline{\tilde{D}}_{i1}^3 \int_{C_1(x_1)}^{C_1(x_2)} (x - x_o) dC_1 - \overline{\tilde{D}}_{i2}^3 \int_{C_2(x_1)}^{C_2(x_2)} (x - x_o) dC_2 \quad (i = 1,2) \quad (6.5)$$

$$M(2) = \int_{x_1}^{x_2} \tilde{J}_i (x - x_o)^2 dx = -\overline{\tilde{D}}_{i1}^3 \int_{C_1(x_1)}^{C_1(x_2)} (x - x_o)^2 dC_1 - \overline{\tilde{D}}_{i2}^3 \int_{C_2(x_1)}^{C_2(x_2)} (x - x_o)^2 dC_2 \quad (i = 1,2) \quad (6.6)$$

Eq. (6.4) is a statement of mass conservation, Eq. (6.5) is proportional to the centroid or the mean of the distribution in terms of concentration integral of the diffusion distance, and Eq. (6.6) is proportional to moment of inertia or dispersion [8]. Eqs. (6.4), (6.5) and (6.6) and all higher order equations can provide linearly independent equations that can yield unique solution at the intersection of any two equations.

6.3 Thermodynamic Criteria of Interdiffusion Coefficients

Numerical requirement of ternary interdiffusion coefficients based on Fickian behavior and thermodynamic stability of the solid solutions are presented by Eq. (6.7) and Eqs. (6.8) through (6.10), respectively [9]. These can be used as selection criteria to identify the representing values of the average ternary interdiffusion coefficients in a single-phase region. Use of these selection criteria will ensure real positive eigen-values of the diffusivity matrix, which then can be employed for the generation of concentration profiles based on analytical error function solution given by Fujita and Gosting [10].

$$\overline{\widetilde{D}}^{3}_{11} > 0 \qquad \overline{\widetilde{D}}^{3}_{22} > 0 \tag{6.7}$$

$$\overline{\widetilde{D}}^{3}_{11} + \overline{\widetilde{D}}^{3}_{22} > 0 \tag{6.8}$$

$$(\overline{\widetilde{D}}^{3}_{11}\overline{\widetilde{D}}^{3}_{22} - \overline{\widetilde{D}}^{3}_{12}\overline{\widetilde{D}}^{3}_{21}) \geq 0 \tag{6.9}$$

$$(\overline{\widetilde{D}}^{3}_{11} + \overline{\widetilde{D}}^{3}_{22})^{2} - 4(\overline{\widetilde{D}}^{3}_{11}\overline{\widetilde{D}}^{3}_{22} - \overline{\widetilde{D}}^{3}_{12}\overline{\widetilde{D}}^{3}_{21}) \geq 0 \tag{6.10}$$

6.4. Application of the Method

The interdiffusion coefficients determined at the lowest possible m-value that satisfy all the above requirements and constraints represent the average interdiffusion coefficients of a particular composition range within the diffusion couple. In most cases, solving Eq. (6.4) where m = 0 and Eq. (6.5) where m = 1 yields reliable ternary interdiffusion coefficients. Aforementioned, extrapolating polynomial curves of all 4 interdiffusion coefficients determined as a function of m, to the m = 0 will further improve the accuracy of the interdiffusion coefficients. But for cases where Eqs. (6.4) and (6.5) do not satisfy the above mentioned requirements and constraints, *vis.* Eqs. (6.7) through (6.10), higher order combinations (e.g., m = 0 and m > 1) may provide values of average ternary interdiffusion coefficients.

In Table 6.1 are listed solid-to-solid isothermal diffusion couples in the A-B, $(Ni,Ir)_3Al$ and Fe-Ni-Al systems selected from literature [2,3]. Hypothetical A vs. B couple has been chosen to verify the accuracy in obtaining parent interdiffusion coefficient to regenerate the concentration profiles. These initial values are chosen such that they obey all requirements and constraints given in Eqs. (6.7) through (6.10). Concentration profiles from Ni-26.0Al *vs.* Ni-23.0Al-2Ir diffusion couple exhibits an relative maximum and minimum for Ni with a strong diffusional interaction with Ir. The β_8 vs. β_9 couple from the Fe-Ni-Al system presents "near-linear" segments in Ni and Al concentration profiles.

Table 6.1 : Selected hypothetical and experimental ternary diffusion couples investigated in various systems.

Diffusion Couples and Terminal Compositions (At. Pct)	Diffusion Annealing Parameters		Reference
	Temperature (°C)	Time (hours)	
A ($0C_1$-$0C_2$-$100C_3$) *vs.* B ($60C_1$-$40C_2$-$0C_3$)	N/A	100	N.A.
Ni-26.0Al *vs.* Ni-23.0Al-2Ir	1200	5	[2]
β_8 (18.0Fe-51.0Ni-20.9Al) *vs.* β_9 (37.9Fe-39.0Ni-23.1Al)	1000	96	[3]

The hypothetical and experimental concentration profiles of selected ternary diffusion couples listed in Table 6.1 are presented in Figures 6.2(a), 6.3(a) and 6.4(a). Thick lines represent parent or experimental concentration profiles where as thin lines correspond to calculated profiles. Interdiffusion fluxes of individual components were calculated using Eq. (6.2). Average ternary interdiffusion coefficients $\widetilde{\overline{D}}_{ij}^{3}$ were determined by solving two equations of Eq. (6.3) with m = 0 and Eq. (6.2) with m = 1, 2, 3,…,50 on either side of the Matano plane. Variation in $\widetilde{\overline{D}}_{ij}^{3}$'s as a function of m values in second equation was examined as presented in Figure 6.2(b), 6.3(b) and 6.4(b). The variation was extrapolated to m = 0 using polynomial extrapolation. Requirement given by Eq. (6.7) can then be addressed from Figures 6.2(b), 6.3(b) and 6.4(b). The average ternary interdiffusion coefficients determined were also examined by utilizing thermodynamic constraints given by Eq. (6.8) denoted as constraint 1, Eq. (6.9) denoted as constraint 2, and Eq. (6.10) denoted as constraint 3. Figures 6.2(c), 6.3(c) and 6.4(c) presents left-hand-side of Eq. (6.8), Eq. (6.9) and Eq. (6.10) plotted against non-zero "m" value used for the determination of average ternary interdiffusion coefficients.

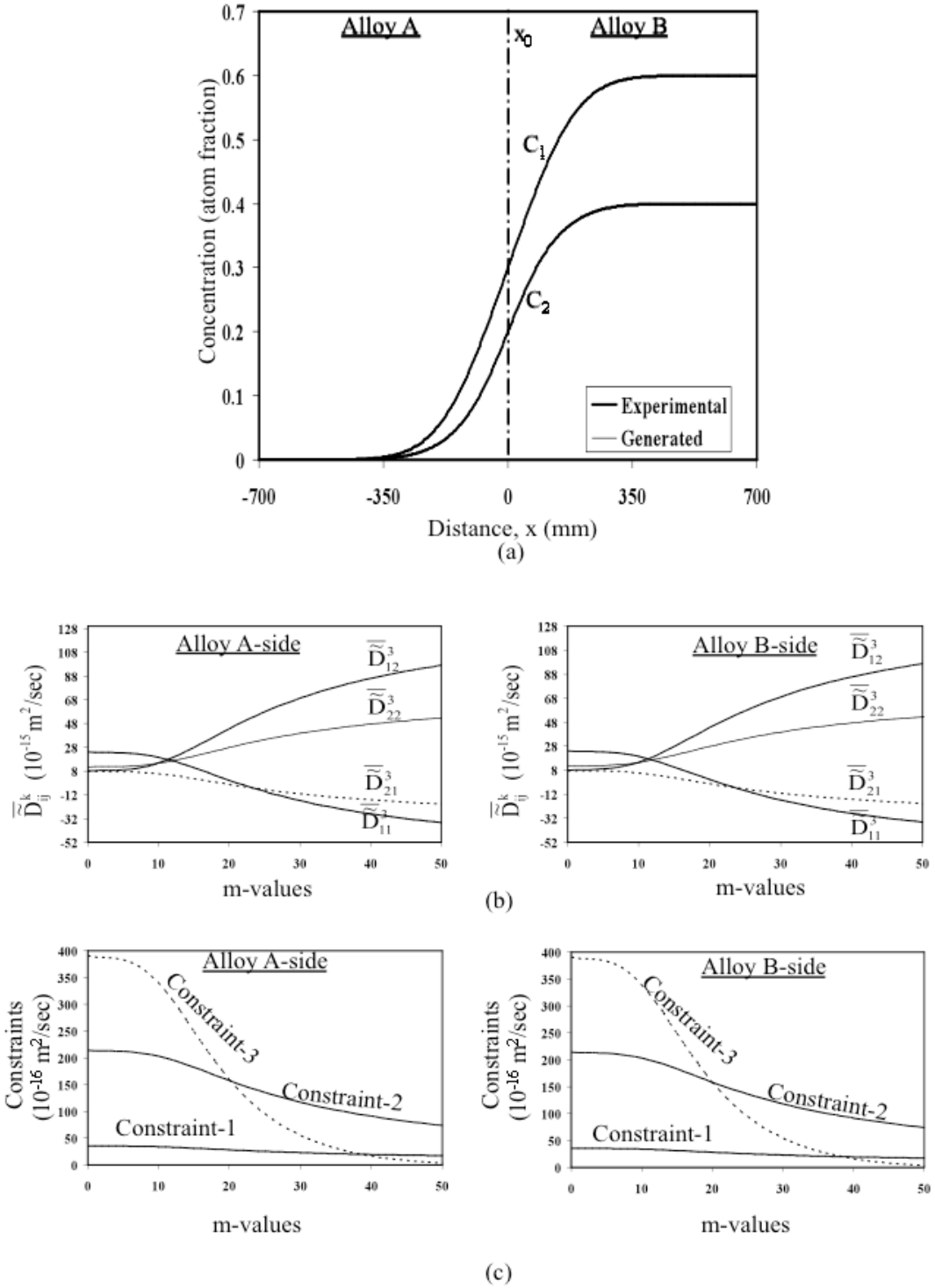

Figure 6.2 : (a) Hypothetical and calculated concentration profiles in diffusion couple A vs. B with chosen annealing time of 100 hours. (b) Variation in $\widetilde{\overline{D}}^3_{ij}$'s as a function of m on either side of the Matano plane x_o (c) Thermodynamic constraints of interdiffusion coefficients as a function of m on either side of the Matano plane x_o.

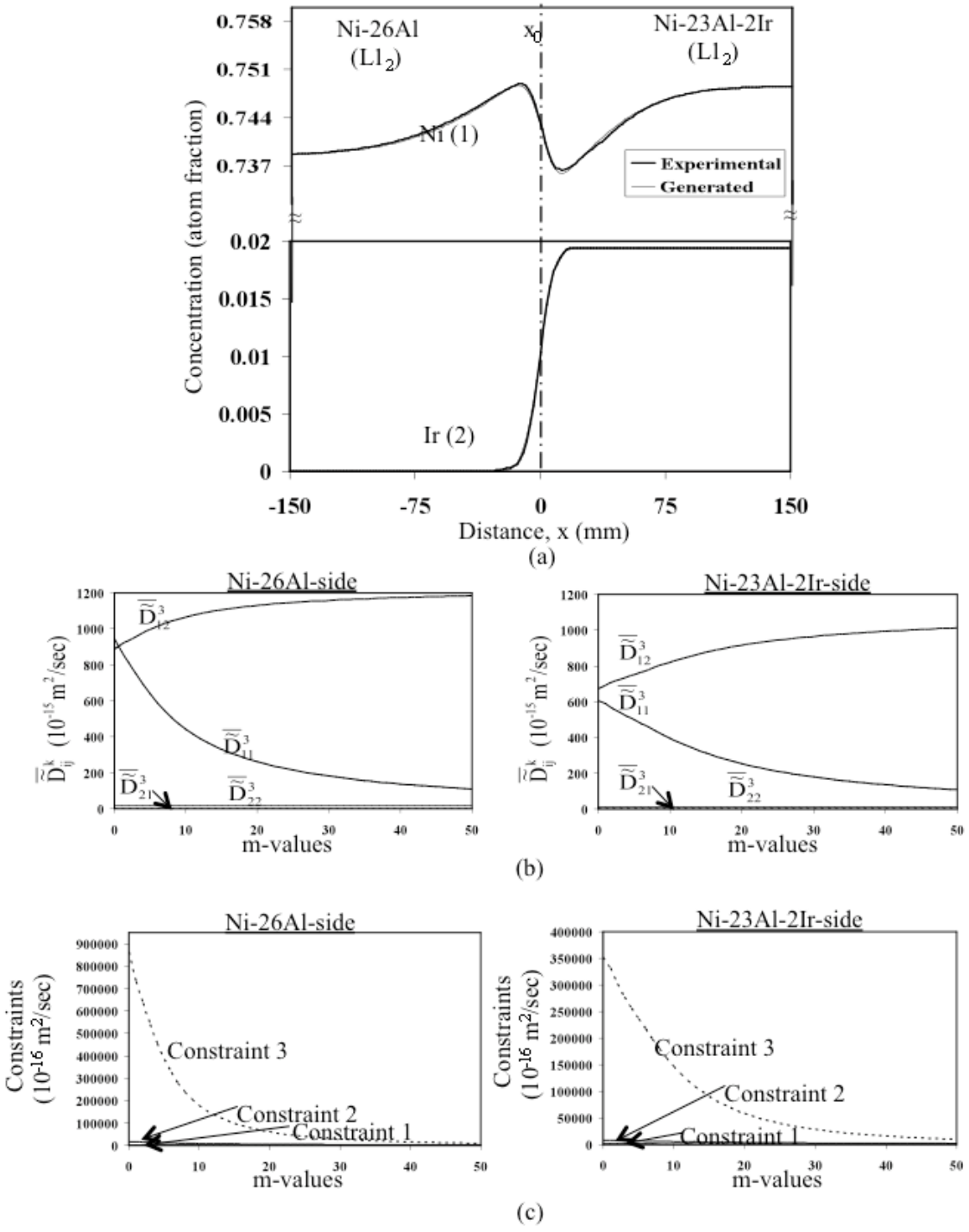

Figure 6.3 : (a) Experimental and calculated concentration profiles for Ni-Al-Ir ($L1_2$) diffusion couple Ni_3Al vs. Ni_3Al-Ir annealed at 1200ºC for 5 hours. (b) Variation in $\widetilde{\overline{D}}^3_{ij}$'s as a function of m on either side of the Matano plane xo (c) Thermodynamic constraints of interdiffusion coefficients as a function of m on either side of the Matano plane x_o.

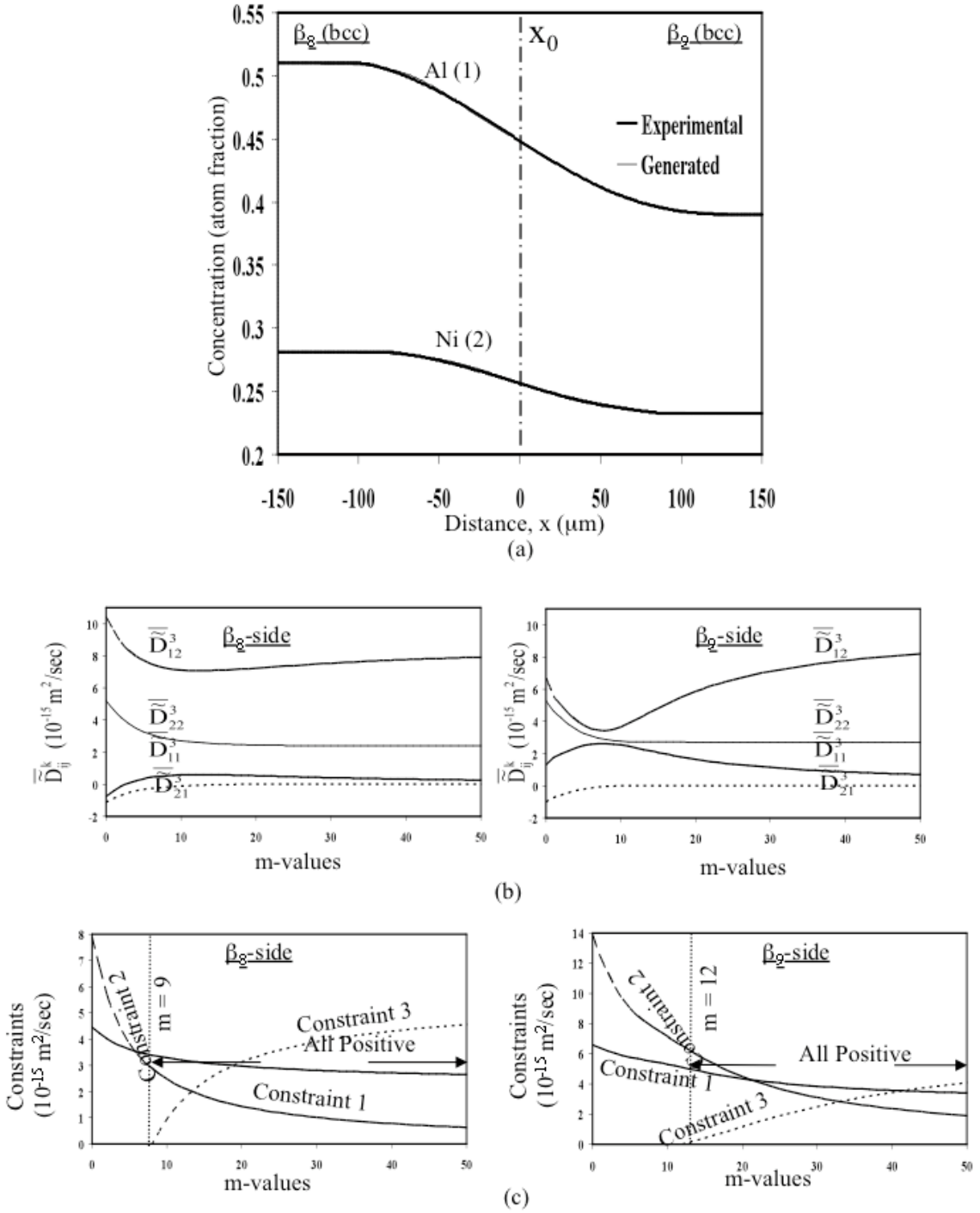

Figure 6.4 : (a) Experimental and calculated concentration profiles for Fe-Ni-Al (B2) diffusion couple β_8 vs. β_9 annealed at 1000ºC for 96 hours. (b) Variation in $\widetilde{\overline{D}}^3_{ij}$'s as a function of m on either side of the Matano plane x_o (c) Thermodynamic constraints of interdiffusion coefficients as a function of m on either side of the Matano plane x_o.

Values of average ternary interdiffusion coefficients determined by extrapolation to m = 0 was the most accurate for couples A vs. B and Ni-26.0Al *vs.* Ni-23.0Al-2Ir. Table I shows the excellent agreement between the "input" $\overline{\widetilde{D}}_{ij}^{3}$'s with calculated $\overline{\widetilde{D}}_{ij}^{3}$'s for the hypothetical diffusion couple A vs. B. This comparison proves that extrapolation to m = 0 for the determination of $\overline{\widetilde{D}}_{ij}^{3}$ coefficients removes the uncertainty (i.e., ± 5%) observed in backcalculated values by Dayananda and Sohn [1]. For the case of β_8 vs. β_9 couple, use of Eqs. (6.4) where m = 0 and (6.5) where m = 1 does not provide $\overline{\widetilde{D}}_{ij}^{3}$ coefficients that satisfy Eqs. (6.7) through (6.10). This is due to the fact that the concentration profiles seen in Figure 6.4 consist mostly of "linear" segments. For β_8 vs. β_9 couple, use of Eq. (6.4) where m = 0 and Eq. (6.3) where m=9 yielded $\overline{\widetilde{D}}_{ij}^{3}$ coefficients that satisfy Eqs. (6.7) through (6.10) on the concentration range of ($C^{-\infty}$-C^{o}). Similarly use of Eq. (6.4) where m = 0 and Eq. (6.3) where m = 11 yielded $\overline{\widetilde{D}}_{ij}^{3}$ coefficients that satisfy Eqs. (6.7) through (6.10) on the concentration range of side (C^{o}-$C^{+\infty}$). The average ternary interdiffusion coefficients determined for β_8 vs. β_9 couple can be utilized for generation of concentration profiles as well. It should be noted that $\overline{\widetilde{D}}_{ij}^{3}$ coefficients determined in this study correspond well to those determined by Boltzmann-Matano analysis [2,3].

Table 6.2 : A comparison between the "input" $\overline{\widetilde{D}}_{ij}^{3}$'s with calculated $\overline{\widetilde{D}}_{ij}^{3}$'s on either side of the Matano plane for the hypothetical ternary diffusion couple A vs. B, and experimental diffusion copules Ni-26.0Al *vs.* Ni-23.0Al-2Ir and β_8 *vs.* β_9.

Couple	Average ternary interdiffusion coefficients (calculated)						Average ternary interdiffusion coefficients [1]			
	Composition Range	m	$\overline{\widetilde{D}}_{ij}^{3}$ ($X10^{-15}$ m^2/s)				$\overline{\widetilde{D}}_{ij}^{3}$ ($X10^{-15}$ m^2/s)			
			$\overline{\widetilde{D}}_{11}^{3}$	$\overline{\widetilde{D}}_{12}^{3}$	$\overline{\widetilde{D}}_{21}^{3}$	$\overline{\widetilde{D}}_{22}^{3}$	$\overline{\widetilde{D}}_{11}^{3}$	$\overline{\widetilde{D}}_{12}^{3}$	$\overline{\widetilde{D}}_{21}^{3}$	$\overline{\widetilde{D}}_{22}^{3}$
A *vs.* B	($C^{-\infty}$-C^{o})	0	23.7	8.1	7.4	11.5	23.7	8.1	7.4	11.5
	(C^{o}-$C^{+\infty}$)	0	23.7	8.1	7.4	11.5	23.7	8.1	7.4	11.5
Ni-26Al *vs.* Ni-23Al-2Ir	($C^{-\infty}$-C^{o})	0	94.5	88.6	Ng.	1.7	87.1	90.8	Ng.	1.5
	(C^{o}-$C^{+\infty}$)	0	60.6	67.0	Ng.	1.2	59.1	69.6	Ng.	1.3
β_8 *vs.* β_9	($C^{-\infty}$-C^{o})	9	0.6	7.1	Ng.	2.8	Cannot determine due to linear segments in concentration profiles.			
	(C^{o}-$C^{+\infty}$)	12	2.4	4.1	Ng.	2.7				

Note: For Ni-26Al *vs.* Ni-23Al-2Ir, *1=Ni, 2=Ir, 3=Al ; For* β_8 *vs.* β_9, *1=Al*, *2=Ni*, *3=Fe;* * Ng. refers to magnitudes less than $0.1X10^{-15}$ m^2/sec.

6.5. Summary

A refined analysis is developed to determine average ternary interdiffusion coefficients in single-phase diffusion couples and successfully implemented to selected hypothetical and experimental data. This technique allows determination of interdiffusion coefficients in ternary alloys even from concentration profiles with linear segments, and are comparable to those measured by Boltzmann-Matano Analysis. This approach can be applied to near-linear segment of the concentration profiles and higher order alloy systems within the single-phase regions.

6.6 References

[1] M.A. Dayananda and Y.H. Sohn: Metall. Trans. 30A (1999) 535.

[2] N. Garimella, M. Ikeda, M. Ode, H. Mukarami, Y.H. Sohn, Intermetallics, In Press.

[3] T.D. Moyer and M.A. Dayananda: Metall. Trans. A, 7A (1976) 1035.

[4] L. Onsager: Phy.Rev. 37 (1931) 405.

[5] L. Onsager: Phy.Rev. 38 (1932) 2265.

[6] L. Onsager: Ann. New York Acad.Sci. 46 (1945) 241.

[7] M.A. Dayananda and C.W. Kim: Metall. Trans., 10A (1979)1333.

[8] Ghez R, Fehribach JD, Ochrlein GS. J.Electrochem Soc. 11 (1985) 2759.

[9] J.S. Kirkaldy, D. Weichert, and Z.U. Haq: Can. J.Phys, 41 (1963) 2166.

[10] H. Fujita and L.J. Gosting: J.Am. Chem. Soc. 78 (1956)1099.

CHAPTER 7: SUMMARY

Interdiffusion in Ni-Cr (fcc γ phase) alloys with small additions of Al, Si, Ge, or Pd was investigated using solid-to-solid diffusion couples annealed at 900°C and 700°C for 168 and 720 hours, respectively. Ni-Cr-X alloys having compositions of Ni-22at.%Cr, Ni-21at.%Cr-6.2at.%Al, Ni-22at.%Cr-4.0at.%Si, Ni-22at.%Cr-1.6at.%Ge and Ni-22at.%Cr-1.6at.%Pd were cast using arc-melting and homogenized at 900°C for 168 hours. The diffusion couples were assembled in an Invar™ steel jig, encapsulated in Ar after several hydrogen purges, and annealed at 900°C and 700°C in a three-zone tube furnace for 168 and 720 hours, respectively. Experimental concentration profiles were determined from polished cross-section of these couples by using electron probe microanalysis with pure element standards. Interdiffusion fluxes of individual components were calculated directly from the experimental concentration profiles, and the moments of interdiffusion fluxes were examined to determine average ternary interdiffusion coefficients. In general, $\tilde{D}_i^{eff}$ was observed to increase with higher Cr concentration. Also, $\widetilde{\overline{D}}_{CrX}^{Ni}$ coefficients were determined to be positive with alloying additions of Al, Si, Ge, or Pd. The results suggest that these alloying additions can help the formation of Cr_2O_3-scale for initial scale formation, maintaining scale homogeneity during prolonged high-temperature exposure, and reformation after scale-spallation.

A similar experimental investigation for interdiffusion in Fe-Ni-Cr (fcc γ phase) alloys with small additions of Si and Ge at 900°C was also studied using solid-to-solid diffusion couples. Alloy rods, Fe-24 at.%Ni, Fe-24 at.%Ni-22at.%Cr, Fe-24 at.%Ni-22at.%Cr-4at.%Si and Fe-24 at.%Ni-22at.%Cr-1.7at.%Ge were cast using arc-melt, and homogenized at 900°C for 168

hours and diffusion couples from these alloys were annealed at 900°C for 168 hours. Large magnitudes of cross coefficients, $\overline{\tilde{D}}^{Fe}_{CrSi}$, $\overline{\tilde{D}}^{Fe}_{CrGe}$, $\overline{\tilde{D}}^{Fe}_{NiSi}$ and $\overline{\tilde{D}}^{Fe}_{NiGe}$ were observed in Fe-Ni-Cr-X (X=Si or Ge) alloys. The Si addition has caused on uphill-diffusion of Ni while there was no measurable uphill diffusion of Ni due to an increase in $\overline{\tilde{D}}^{Fe}_{NiNi}$ in Fe-Ni-Cr-Ge alloy, despite the large positive $\overline{\tilde{D}}^{Fe}_{NiGe}$.

Ternary interdiffusion in $L1_2$-Ni_3Al with ternary alloying additions of Ir, Ta and Re was investigated at 1473K using solid-to-solid diffusion couples. Average ternary interdiffusion coefficients were determined from an integration of interdiffusion fluxes calculated directly from experimental concentration profiles. The magnitude of $\overline{\tilde{D}}_{NiNi}$ and $\overline{\tilde{D}}_{AlAl}$ coefficients was determined to be much larger than that of $\overline{\tilde{D}}_{IrIr}$, $\overline{\tilde{D}}_{TaTa}$, and $\overline{\tilde{D}}_{ReRe}$ coefficients. Ir substituting in Ni-site influenced the interdiffusion of Ni significantly, and $\overline{\tilde{D}}^{Al}_{NiIr}$ coefficients were determined to be large and positive. Similar observations was made for Re with large positive $\overline{\tilde{D}}^{Ni}_{AlRe}$ coefficients. On the other hand Ta substituting for Al influenced the interdiffusion of Al significantly, and $\overline{\tilde{D}}^{Ni}_{AlTa}$ coefficients were determined to be large and positive. An excellent agreement was found with ternary interdiffusion coefficients determined by Boltzmann-Matano analysis. Profiles of concentrations and interdiffusion fluxes were also examined to estimate binary interdiffusion coefficients in Ni_3Al, and tracer diffusion coefficients of Ir ($14.7 \times 10^{-16} \pm 1.4 \times 10^{-16}$ m^2/sec), Ta ($2.6 \times 10^{-16} \pm 2.4 \times 10^{-16}$ m^2/sec) and Re ($5.4 \times 10^{-16} \pm 2.3 \times 10^{-16}$ m^2/sec) in Ni_3Al.

Finally, a refined approach to determine average ternary interdiffusion coefficients was developed using Onsager's flow equations with moments of the interdiffusion-parameter

integrands. The new analysis [1] developed by Dayananda and Sohn is the basis for this refined approach. The interdiffusion coefficients determined by this method are more accurate and can be applied to concentration profiles that contains linear segments.

APPENDIX A : LIST OF PUBLICATIONS AND REPRINTS

During the course of study for Ph.D. in materials science and engineering, the following papers were published.

1. N. Garimella, M.P. Brady, Y.H. Sohn, "Determination of Average Ternary Interdiffusion Coefficients using Moments of Interdiffusion Fluxes and Concentration Profiles," Scripta Materialia, in Preparation.
2. N. Garimella, M. Ikeda, M. Ode, H. Mukarami, Y.H. Sohn, "Effects of Ternary Alloying Addition of Re on Interdiffusion of L12-Ni3Al at 1200ºC," Journal of Phase Equilibria and Diffusion, Submitted, Setpember, 2008.
3. N. Garimella, M. Ikeda, M. Ode, H. Mukarami, Y.H. Sohn, "Effects of Ternary Alloying Addition of Ir and Ta on Interdiffusion of L12-Ni3Al at 1200ºC," Intermetallics, Vol. 16 (2008) pp. 1095–1103.
4. N. Garimella, M.P. Brady, Y.H. Sohn, "Ternary and Quaternary Interdiffusion in g (fcc) Fe-Ni-Cr-X (X = Si, Ge) Alloys at 900°C," Materials Science Forum, Vols. 595-598 (2008) pp. 1145-1152.
5. M. Ikeda, N. Garimella, M. Ode, H. Mukarami, Y.H. Sohn, "Ternary Interdiffusion in Ni3Al with Ir Addition," Defects and Diffusion Forum, Vol. 273-276 (2008) pp. 637-642.
6. N. Garimella, M.P. Brady, Y.H. Sohn, "Interdiffusion in g (fcc) Ni-Cr-X (Al, Si, Ge or Pd) Alloys at 900ºC," Defects and Diffusion Forum, Vol. 266 (2007) pp. 191-198.
7. J.W. Byeon, J. Liu, M. Hopkins, W. Fischer, N. Garimella, K.B. Park, M.P. Brady, M. Radovic, T. El-Raghy, Y.H. Sohn, "Microstructure and Residual Stress of Alumina Scale Formed on Ti2AlC at High Temperature in Air," Oxidation of Metals, Vol. 68 (2007) pp. 97-111.

8. Y.H. Sohn, N. Garimella, E. Perez, R. Mohanty, J. Liu, “Integrated, Effective and Average and Their Applications in Multicomponent Alloys for Energy Production Systems,” Defects and Diffusion Forum, Vol. 258-260 (2007) pp. 346-359.
9. N.Garimella, M. Brady, Y.H. Sohn, “Interdiffusion in g (fcc) Ni-Cr-X (Al, Si, Ge or Pd) Alloys at 900ºC,” Journal of Phase Equilibria and Diffusion, Vol. 27 (2006) pp. 6

JPEDAV (2006) 27:665-670
DOI: 10.1361/154770306X153710
1547-7037/$19.00 ©ASM International

Interdiffusion in (Face-Centered Cubic) Ni-Cr-*X* (*X* = Al, Si, Ge, or Pd) Alloys at 900 °C

Narayana Garimella, and M.P. Brady, and Yongho Sohn

(Submitted April 3, 2006; in revised form July 19, 2006)

Interdiffusion in nickel (Ni)-chromium (Cr) (face-centered cubic phase) alloys with small additions of aluminum (Al), silicon (Si), germanium (Ge), or palladium (Pd) was investigated using solid-to-solid diffusion couples. Ni-Cr-*X* alloys having compositions of Ni-22at.%Cr, Ni-21at.%Cr-6.2at.%Al, Ni-22at.%Cr-4.0at.%Si, Ni-22at.%Cr-1.6at.%Ge, and Ni-22at.%Cr-1.6at.%Pd were manufactured by arc casting. The diffusion couples were assembled in an Invar steel jig, encapsulated in Ar after several hydrogen purges, and annealed at 900 °C in a three-zone tube furnace for 168 h. Experimental concentration profiles were determined from polished cross sections of these couples by using electron probe microanalysis with pure element standards. Interdiffusion fluxes of individual components were calculated directly from the experimental concentration profiles, and the moments of interdiffusion fluxes were examined to determine the average ternary interdiffusion coefficients. The effects of ternary alloying additions on the diffusional behavior of Ni-Cr-X alloys are presented in the light of the diffusional interactions and the formation of a protective Cr_2O_3 scale.

Keywords Boltzmann/Matano analysis, diffusion couples, diffusivity coefficient, experimental study, interdiffusion, multicomponent diffusion, ternary system

1. Introduction

Nickel (Ni)-chromium (Cr)-base alloys are widely used in a variety of high-temperature applications due to their combination of good oxidation resistance and excellent high-temperature strength, and are the basis for a number of commercial superalloy families.[1-3] Oxidation resistance in these alloys is derived from a continuous, slow-growing, adherent C_2O_3-base oxide scale.[1,3] In particular, composition in the range of Ni alloyed with 20-30 wt.% Cr have been extensively studied as a model material for Cr_2O_3 scale formation.[4-13]

Minor alloying additions (<5 wt.%) can significantly improve the oxidation resistance of Ni-base Cr_2O_3-forming alloys.[14-16] Effects include: the establishment of continuous Cr_2O_3 scale formation at reduced Cr concentrations; a decrease in the growth rate of Cr_2O_3; and enhanced scale adherence.[1,14,16] For example, the addition of silicon (Si) in Ni-28wt.%Cr promoted the formation of both Cr_2O_3 and SiO_2,[e.g., 13] in which a continuous inner SiO_2 layer acted as a diffusion barrier, and reduced the isothermal oxidation rate by suppressing cation transport through the Cr_2O_3 scale.[6,13,17-20] However, the same inner SiO_2 layer can also reduce the spallation resistance, which is dependent on the level of Si and on the continuity and thickness of the inner SiO_2 layer formed.[e.g., 21]

Diffusional effects of minor alloy additions may play a significant role in the initial establishment of a continuous protective oxide scale.[2,14,16,22,23] It can also play a significant role in maintaining protective scale growth. For example, the growth of Cr_2O_3 can locally deplete Cr from the alloy in the subsurface region.[e.g., 24] If the scale is locally damaged or spalled, such depletion can prevent the reformation of the Cr_2O_3 scale and result in a transition to less protective or nonprotective oxidation behavior. An understanding of diffusional interactions in Ni-Cr-*X* alloys, where *X* represents minor alloying additions, can help to design Ni-base Cr_2O_3-forming alloys with improved resistance against environmental degradation.[25]

In this work, interdiffusion in Ni-22at.%Cr-*X* [face-centered cubic (fcc) phase] alloys with small additions of *X* [*X* aluminum (Al), Si, germanium (Ge), or palladium (Pd)] is investigated using solid-to-solid diffusion couples at 900 °C for 168 h. This information will be used as a part of a larger study, the goal of which is to better elucidate the effects of minor alloying additions on the oxidation of Cr_2O_3-forming alloys. Additions of Si were selected because it has long been known to be beneficial to Cr_2O_3 scale formation[e.g., 17] via both the establishment of an inner layer of SiO_2 and the possibility of the enhanced diffusivity of Cr. To help probe these effects, additions of Ge were also selected. Ge is thermochemically similar to Si in many regards

This article was presented at the Multicomponent-Multiphase Diffusion Symposium in Honor of Mysore A. Dayananda, which was held during TMS 2006, the 135th Annual Meeting and Exhibition, March 12–16, 2006, in San Antonio, TX. The symposium was organized by Yongho Sohn of University of Central Florida, Carelyn E. Campbell of National Institute of Standards and Technology, Richard D. Sisson, Jr., of Worcester Polytechnic Institute, and John E. Morral of Ohio State University.

Narayana Garimella and **Yongho Sohn,** Advanced Materials Processing and Analysis Center and Department of Mechanical, Materials and Aerospace Engineering, University of Central Florida, Orlando, FL; and **M.P. Brady,** Materials Science and Technology Division, Oak Ridge National Laboratory, Oak Ridge, TN. Contact e-mail: ysohn@mail.ucf.edu.

but does not form a protective oxide scale as does Si. Additions of Al at levels > 3-4 wt.% can improve the oxidation via the formation of a protective Al_2O_3 scale.[2,4,14,16] At subcritical levels (2-3 wt.%), Al may also be beneficial to the oxidation resistance of Ni-Cr alloys, in part via the formation of semicontinuous inner region of Al_2O_3 particles.[26,27] Pd was chosen for the study because it is a noble alloying addition and would be expected to accumulate at the alloy-scale interface during oxidation.[e.g., 28,29]

In this ternary interdiffusion study at 900 °C, the experimental concentration profiles were used to calculate interdiffusion fluxes of individual components, and to determine the average effective interdiffusion coefficients $\tilde{D}_i^{\text{eff}}$ and the average ternary interdiffusion coefficients $\tilde{D}_{ij}^{\text{Ni}}$ (i,j Cr,X). Values of $\tilde{D}_{\text{Cr}}^{\text{eff}}$ and $\tilde{D}_{\text{CrX}}^{\text{Ni}}$ are examined to assess the effects of alloying additions on the interdiffusion behavior of Cr, and the Cr_2O_3-forming ability in Ni-Cr-X alloys.

2. Determination of Interdiffusion Coefficients From Ternary Isothermal Diffusion Couples

Onsager's[30] formalism for the interdiffusion flux $\tilde{J}_i$ of component i in a ternary system can be written as:

$$\tilde{J}_i = \tilde{D}_{i1}^{3}\frac{C_1}{x} \quad \tilde{D}_{i2}^{3}\frac{C_2}{x} \quad i,j = 1, 2 \qquad \text{(Eq 1)}$$

where C_1/x and C_2/x are the two independent concentration gradients, and $\tilde{D}_{i1}^{3}$ and $\tilde{D}_{i2}^{3}$ refer to the ternary interdiffusion coefficients. An experimental determination of the four concentration-dependent interdiffusion coefficients requires the use of the Boltzmann-Matano analysis with two independent diffusion couples that develop a common composition in the diffusion zone. Instead, the interdiffusion fluxes $\tilde{J}_i$ of all components can be determined directly from their concentration profiles of an infinite diffusion couple without the need of the interdiffusion coefficients on the basis of the relation:[31]

$$\tilde{J}_i = \frac{1}{2t}\int_{C_i \text{ or } C_i^{+}}^{C_i x} x \quad x_o \, dC_i \quad i = 1, 2, \ldots, n \qquad \text{(Eq 2)}$$

where t is the time, C_i^{-} and C_i^{+} are the terminal concentrations of the alloys used for the couple, and x_o refers to the location of the Matano plane.

The interdiffusion flux $\tilde{J}_i$, determined from Eq 2 can be integrated with respect to position x to define the average effective interdiffusion coefficient $\tilde{D}_i^{\text{eff}}$:[32]

$$\tilde{D}_i^{\text{eff}} = \frac{\int_{x_1}^{x_2} \tilde{J}_i dx}{C_i^{x_2} \quad C_i^{x_1}} \quad i = 1, 2, 3 \qquad \text{(Eq 3)}$$

This effective interdiffusion coefficient incorporates all multicomponent diffusional interactions for the system to provide an effective value for the interdiffusion of a component species as defined by:

$$\tilde{D}_i^{\text{eff}} = \tilde{D}_{ii}^{n} + \sum_{j} \frac{\tilde{D}_{ij}^{n} \, C_j \quad x}{C_i \quad x} \quad i \quad j \qquad \text{(Eq 4)}$$

The interdiffusion flux $\tilde{J}_i$, determined from Eq 2 as a function of x, can be multiplied by $(x - x_o)^n$ and integrated over a selected region, x_1 to x_2, in the light of Eq 1, one gets:[33]

$$\int_{x_1}^{x_2} \tilde{J}_i \, x \quad x_o \, ^n dx = \int_{C_1 x_1}^{C_1 x_2} \tilde{D}_{i1}^{3} \quad x \quad x_o \, ^n dC_1 + \int_{C_2 x_1}^{C_2 x_2} \tilde{D}_{i2}^{3} \quad x \quad x_o \, ^n dC_2 \quad i,j = 1, 2 \qquad \text{(Eq 5)}$$

where $\tilde{D}_{ij}^{3}$ (i, j 1,2) coefficients are the average values of main and cross-interdiffusion coefficients treated as constants over the selected composition range. Equation 5 can provide four equations involving the $\tilde{D}_{ij}^{3}$ interdiffusion coefficients (n 0, 1, or 2) and can be set up from interdiffusion fluxes calculated on the basis of Eq 2 from the concentration profiles of a single diffusion couple. The $\tilde{D}_{ij}^{3}$ coefficients, characteristic of the diffusion path, can be determined over selected composition ranges that include the nonlinear segment of the profiles.[33] The determination of ternary interdiffusion coefficients by using Eq 5 does not require the use of concentration gradients (i.e., C_i/x), and significantly reduces the uncertainty involved in the determination of interdiffusion coefficients arising from microprobe measurement and the concentration smoothening procedure.[33]

Table 1 Compositions of Ni-Cr-X alloys employed for solid-to-solid diffusion couples

Alloy identification	Composition, atom fraction			Composition, weight fraction		
	Ni	Cr	X	Ni	Cr	X
Ni	100.0	...	...	100	...	...
NiCr (X None)	78.0	22.0	...	80	20	...
NiCrAl (X Al)	72.5	21.3	6.2	77	20	3
NiCrSi (X Si)	74.0	22.0	4.0	78	20	2
NiCrGe (X Ge)	76.3	22.1	1.6	78	20	2
NiCrPd (X Pd)	76.1	22.3	1.6	77	20	3

3. Experimental Procedure

Binary and ternary alloys with compositions reported in Table 1 were prepared with 99.9% pure Ni, Cr, Al, Si, Ge, and Pd by arc melting under an argon (Ar) atmosphere. The alloys were chill-cast by water-cooled copper mold into

Table 2 List of Ni versus Ni-Cr-X and NiCr versus Ni-Cr-X solid-to-solid diffusion couples annealed at 900 °C for 168 h

Series	Diffusion couples
I	Ni vs. Ni-Cr
II	Ni vs. Ni-Cr-Al
	Ni vs. Ni-Cr-Si
	Ni vs. Ni-Cr-Ge
	Ni vs. Ni-Cr-Pd
III	Ni-Cr vs. Ni-Cr-Al
	Ni-Cr vs. Ni-Cr-Si
	Ni-Cr vs. Ni-Cr-Ge
	Ni-Cr vs. Ni-Cr-Pd

rods with a vacuum 12 mm in diameter. The alloy rods were placed in a quartz tube, evacuated to a pressure $<10^{-6}$ torr, and flushed with hydrogen. This hydrogen-flushing procedure was repeated several times, and a quartz capsule was filled with Ar before the final seal. They were homogenized at 900 °C for 168 h in a horizontal Lindberg three-zone tube furnace and water-quenched to preserve the high-temperature microstructure. The microstructures and compositions of the alloys were examined by optical microscopy, scanning electron microscopy, energy dispersive spectroscopy, and electron microprobe analysis (EPMA). No measurable variation in the alloy compositions was observed, and all alloys consisted of face-centered cubic (fcc) Ni solid solution (phase).

Diffusion disks with approximate thicknesses of 2 mm were cut from the rods of alloys and were prepared metallographically by polishing with 0.25 m diamond paste. Table 2 presented ternary diffusion couples that were assembled with the disks held together in an Invar steel jig consisting of two end plates and three threaded rods. The couples were placed in quartz capsules, which were sealed at one end, evacuated to a pressure $<10^{-6}$ torr, and flushed with hydrogen several times. A capsule was filled with Ar before the final sealing. The capsules containing the couples were annealed at 900 °C in a horizontal Lindberg three-zone furnace for 168 h. After the anneal, the couples were quenched in water to preserve the high-temperature microstructures.

The diffusion assembly was then mounted, sectioned, and metallographically prepared for microstructural observations. Excellent bonding within all diffusion couples was observed. Then, the cross section surface was repolished with 1 m diamond paste for EPMA. The concentration profiles of Ni, Cr, Al, Si, Ge, and Pd for the diffusion couples were determined with a JEOL 733 (Tokyo, Japan) microprobe by point-to-point counting techniques using pure Ni, Cr, Al, Si, Ge, and Pd as standards. Intensities of K *X*-radiation were measured and converted to concentrations of Ni, Cr, Al, Si, Ge, and L *X*-radiation for that of Pd with appropriate ZAF (atomic number, Z; absorption, A; fluorescence, F) corrections. Concentration profiles obtained from EPMA was smoothened by a weighted spline tool using MatLab (The Math Works, Natick, MA). It

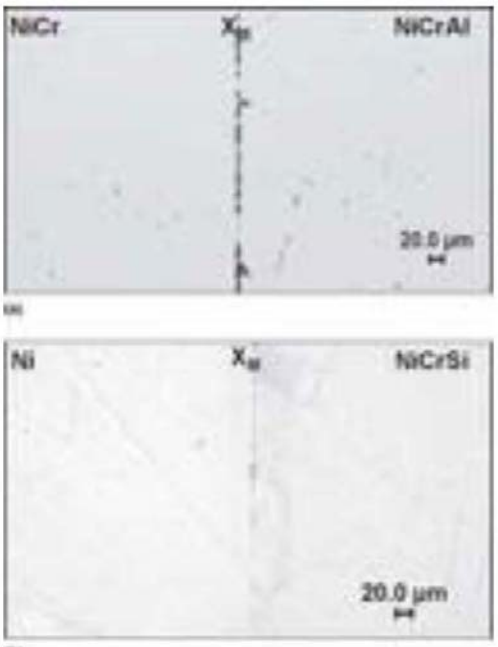

Fig. 1 Typical optical micrographs of solid-to-solid diffusion couples etched with Kallings reagent: (a) Ni-Cr versus Ni-Cr-Al and (b) Ni versus Ni-Cr-Si annealed at 900 °C for 168 h. Specimens were slightly overetched to clearly distinguish the experimental contact plane x_m.

should be noted that the analytical method used in this study to determine interdiffusion coefficients by the integration of interdiffusion fluxes (e.g., Eq 5) do not require the use of concentration gradients. This method significantly reduces the influence of a smoothening procedure on the determination of interdiffusion coefficients.

4. Results and Discussion

Figure 1 presents an optical micrograph obtained from the diffusion couples Ni versus Ni-Cr-Al and Ni versus Ni-Cr-Si that was annealed at 900 °C for 168 h. Excellent bonding was achieved during the diffusion anneal for all diffusion couples. Figure 2 presents an example of the experimental and smoothened concentration profiles that were used for the determination of interdiffusion coefficients. The scatters in the concentration profiles for all diffusion couples were minimal and within the experimental uncertainty associated with EPMA. Experimental concentration profiles were smoothened with a weighted-spline routine by using MatLab.

From concentration profiles obtained from series I and II diffusion couples (i.e., Ni versus Ni-Cr, and Ni versus

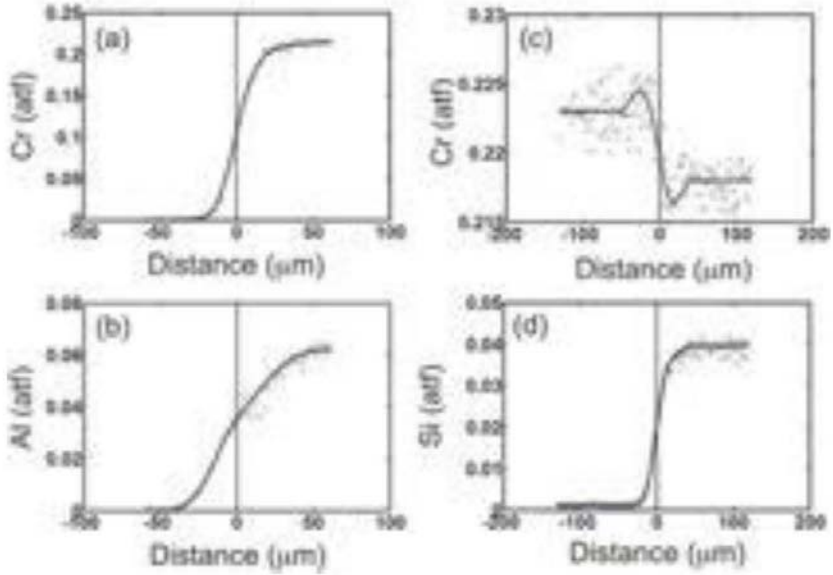

Fig. 2 Typical experimental and smoothened concentration profiles measured from solid-to-solid diffusion couples (a, b) Ni vs. Ni-Cr-Al and (c, d) Ni-Cr vs. Ni-Cr-Si, annealed at 900 °C for 168 h

Ni-Cr-X, respectively), the average effective interdiffusion coefficients $\tilde{D}_i^{\text{eff}}$ on either side of the Matano plane were determined using Eq 3. In general, $\tilde{D}_i^{\text{eff}}$ was higher on the (C_i° C_i^{+}) composition range with a higher Cr concentration relative to the other side of the Matano plane. Table 3 also reports that an Al addition to a NiCr alloy can increase or decrease the $\tilde{D}_{\text{Cr}}^{\text{eff}}$ as a function of composition. This indicates appreciable variation in interdiffusion coefficients as a function of composition: specifically, Al increased $\tilde{D}_{\text{Cr}}^{\text{eff}}$ on the (C_i° C_i^{+}) composition range with a higher Cr concentration. $\tilde{D}_{\text{Cr}}^{\text{eff}}$ was observed to increase with an Si addition to a NiCr alloy, especially on the (C_i° C_i^{+}) side with higher Cr concentration. According to Table 3, Ge does not change $\tilde{D}_{\text{Cr}}^{\text{eff}}$ significantly, while a Pd addition to an Ni-Cr alloy increased $\tilde{D}_{\text{Cr}}^{\text{eff}}$, which is quite significant on the (C_i° C_i^{+}) range with a higher Cr concentration.

From concentration profiles obtained from diffusion couple series I and II (i.e., Ni versus Ni-Cr, and Ni versus Ni-Cr-X, respectively), average ternary interdiffusion coefficients $\tilde{D}_{ij}^{\text{Ni}}(i,j$ Cr, $X)$ were determined on either side of the Matano plane using Eq 5. These diffusion couples are reported in Table 4. It should be noted that these diffusion couples were designed to yield the same sign of C_{Cr}/x and C_X/x. Thus, positive and negative $\tilde{D}_{\text{Cr}X}^{\text{Ni}}$ indicates an increase and a decrease in $\tilde{J}_{\text{Cr}}$, respectively. In general, larger magnitudes of $\tilde{D}_{\text{CrCr}}^{\text{Ni}}$ and $\tilde{D}_{XX}^{\text{Ni}}$ were observed on the (C_i° C_i^{+}) composition range with higher Cr concentration. The Al addition in the Ni-Cr alloy yielded positive $\tilde{D}_{\text{CrAl}}^{\text{Ni}}$, and increased $\tilde{J}_{\text{Cr}}$ in accordance with previous work by Nesbitt and Heckel[25] and Thompson et al.[34] The magnitude of $\tilde{D}_{\text{CrAl}}^{\text{Ni}}$ was quite large, as reported in Table 4 on the (C_i° C_i^{+}) with higher Cr concentration. Similarly, Si, Ge, and Pd additions to the Ni-Cr alloy increased J_{Cr} with positive $\tilde{D}_{\text{Cr}X}^{\text{Ni}}$. This effect was, again, stronger when the Cr concentration was high on the (C_i° C_i^{+}), particularly for Si and Pd.

Table 3 Average effective interdiffusion coefficients determined from Ni vs. Ni-Cr-X diffusion couples annealed at 900 °C for 168 h

Diffusion couple	Composition range	$\tilde{D}_{\text{Cr}}^{\text{eff}}$, 10^{-16} m²/s	$\tilde{D}_{X}^{\text{eff}}$, 10^{-16} m²/s	$\tilde{D}_{\text{Ni}}^{\text{eff}}$, 10^{-16} m²/s
Ni vs. Ni-Cr	(C_i^{-} C_i°)	1.40	...	1.40
(X None)	(C_i° C_i^{+})	1.53	...	1.53
Ni vs. Ni-Cr-Al	(C_i^{-} C_i°)	0.91	3.31	1.83
(X Al)	(C_i° C_i^{+})	1.58	4.68	2.19
Ni vs. Ni-Cr-Si	(C_i^{-} C_i°)	1.68	5.74	2.26
(X Si)	(C_i° C_i^{+})	3.00	6.91	3.57
Ni vs. Ni-Cr-Ge	(C_i^{-} C_i°)	1.30	3.09	1.40
(X Ge)	(C_i° C_i^{+})	1.44	3.47	1.61
Ni vs. Ni-Cr-Pd	(C_i^{-} C_i°)	1.77	1.19	1.74
(X Pd)	(C_i° C_i^{+})	4.09	2.07	3.92

Diffusion couple series III was designed with initial C_{Cr}/x 0, so that $\tilde{J}_{\text{Cr}}$ is largely due to C_X/x, and depends on the magnitude and sign of $\tilde{D}_{\text{Cr}X}^{\text{Ni}}$. $\tilde{J}_X$ has caused an uphill diffusion of Cr in the direction of J_X with positive $\tilde{D}_{\text{Cr}X}^{\text{Ni}}$ for Al and Si. This indicates that Al and Si should increase the thermodynamic activity of Cr in Ni-Cr alloys.

Table 4 Average ternary interdiffusion coefficients determined from Ni vs. Ni-Cr-X diffusion couples annealed at 900 °C for 168 h

Diffusion couple	Composition range	$\tilde{D}^{Ni}_{CrCr}$, 10^{-16} m^2/s	$\tilde{D}^{Ni}_{CrX}$, 10^{-16} m^2/s	$\tilde{D}^{Ni}_{XCr}$, 10^{-16} m^2/s	$\tilde{D}^{Ni}_{XX}$, 10^{-16} m^2/s
Ni vs. Ni-Cr-Al (X Al)	(C_i^- C_i^o)	0.78	0.31	0.40	1.99
	(C_i^o C_i^+)	1.11	1.72	0.43	2.84
Ni vs. Ni-Cr-Si (X Si)	(C_i^- C_i^o)	1.23	0.15	0.44	2.92
	(C_i^o C_i^+)	2.05	4.88	0.57	3.35
Ni vs. Ni-Cr-Ge (X Ge)	(C_i^- C_i^o)	1.08	0.36	0.07	1.73
	(C_i^o C_i^+)	1.24	0.89	0.10	1.99
Ni vs. Ni-Cr-Pd (X Pd)	(C_i^- C_i^o)	1.43	4.06	0.01	0.98
	(C_i^o C_i^+)	3.49	4.86	0.01	1.76

Table 5 Average ternary interdiffusion coefficients determined from Ni-Cr vs. Ni-Cr-X diffusion couples annealed at 900 °C for 168 h

Diffusion couple	Composition range	$\tilde{D}^{Ni}_{CrCr}$, 10^{-16} m^2/s	$\tilde{D}^{Ni}_{CrX}$, 10^{-16} m^2/s	$\tilde{D}^{Ni}_{XCr}$, 10^{-16} m^2/s	$\tilde{D}^{Ni}_{XX}$, 10^{-16} m^2/s
Ni-Cr vs. Ni-Cr-Al (X Al)	(C_i^- C_i^o)	0.23	0.12	0.01	0.67
	(C_i^o C_i^+)	1.20	0.44	0.13	1.17
Ni-Cr vs. Ni-Cr-Si (X Si)	(C_i^- C_i^o)	2.58	1.73	0.01	0.68
	(C_i^o C_i^+)	1.39	0.63	1.78	1.97
Ni-Cr vs. Ni-Cr-Ge (X Ge)	(C_i^- C_i^o)				
	(C_i^o C_i^+)				
Ni-Cr vs. Ni-Cr-Pd (X Pd)	(C_i^- C_i^o)				

C_{Cr}/ x 0 and cannot be determined.

On the other hand, $\tilde{J}_{Ge}$ and $\tilde{J}_{Pd}$ did not cause any measurable redistribution of Cr (J_{Cr} 0). It should be noted that Ge and Pd have lower contents in the Ni-Cr-X alloys than Al and Si, as reported in Table 1.

Based on the average effective interdiffusion coefficients and average ternary interdiffusion coefficients determined in this study, alloying additions of Al, Si, Ge, and Pd have all increased $\tilde{D}^{eff}_{Cr}$ and yielded positive $\tilde{D}^{Ni}_{CrX}$ particularly with high Cr content (22 at.%). Therefore, the Cr_2O_3-forming ability of the Ni-20at.%Cr-based alloy should improve with these alloying additions by establishing Cr_2O_3 scale, by maintaining protective Cr_2O_3 scale formation, and in reformation of Cr_2O_3 on spallation. It should be noted that the positive $\tilde{D}^{Ni}_{XCr}$ reported in Tables 4 and 5 should also promote the formation of other scales (Al_2O_3, SiO_2) in the (fcc) Ni-Cr alloy, which may reduce the rate of scale growth and/or change the thermomechanical properties of the scale.

5. Summary

Based on experimental solid-to-solid diffusion couples, a small addition of Al, Si, Ge, or Pd was observed to increase the overall interdiffusion flux of Cr in Ni-22at.%Cr-X (fcc phase) alloys. Experimental concentration profiles, measured after annealing at 900 °C in a three-zone tube furnace for 168 h, were used to determine interdiffusion fluxes, average effective interdiffusion coefficients, and average ternary interdiffusion coefficients. In general, $\tilde{D}^{eff}_{i}$ was observed to increase with a higher Cr concentration. Also, $\tilde{D}^{Ni}_{CrX}$ coefficients were determined to be positive with alloying additions of Al, Si, Ge, or Pd. These results suggest that these alloying additions can help the formation of Cr_2O_3 scale for initial scale formation, maintaining scale homogeneity during prolonged high-temperature exposure, and for reformation after scale spallation.

Acknowledgments

This work was supported by the National Science Foundation CAREER Award under the grant DMR-0238356 (Y.H. Sohn) and U.S. Department of Energy, Fossil Energy Advanced Research Materials (ARM) program. Oak Ridge National Laboratory is managed by UT-Battelle, LLC, for the U.S. Department of Energy under contract DE-AC05-00OR22725.

References

1. C.T. Sims, N.S. Stoloff, and W.C. Hagel, *Superalloys II*, John Wiley and Sons, 1987
2. P. Kofsted, Growth and Protective Properties of Chromia (Cr_2O_3) and Alumina (Al_2O_3) Scales, Protective Coatings, *High Temperature Corrosion*, Elsevier, London, 1980, p 389-423
3. J.L. Smialek, C.A. Barrett, and J.C. Schaffer, Design for Oxidation Resistance, *ASM Handbook, Vol. 20, Materials Selection and Design*, George E. Dieter, Ed., ASM International, 1997, p 589-602
4. F.H. Stott, G.C. Wood, and M.G. Hobby, A Comparison of the

Oxidation Behavior of Fe-Cr-Al, Ni-Cr-Al and Co-Cr-Al Alloys, *Oxid. Met.*, 1971, **3**, p 103-113
5. C.E. Lowell, A Scanning Electron Microscope Study of the Surface Morphology of TD-NiCr Oxidized at 800 °C to 1200 °C, *Oxid. Met.*, 1972, **5**, p 205-220
6. C.E. Lowell, Cyclic and Isothermal Oxidation Behavior on Some Ni-Cr Alloys, *Oxid. Met.*, 1973, **7**, p 95-115
7. G.M. Ecer and G.H. Meier, Oxidation of High-Ehromium Ni-Cr Alloys, *Oxid. Met.*, 1979, **13**, p 119-158
8. G. Benabderrazik, G. Moulin, and A.M. Huntz, Relation Between Impurities and Oxide-Scale Growth Mechanisms on Ni-34Cr and Ni-20Cr Alloys: I. Influence of C, Mn, and Si, *Oxid. Met.*, 1990, **33**, p 191-235
9. J.F. Schmitt, N. Pacia, P. Pigeat, and B. Weber, Study of the Initial Oxidation of a Ni-20Cr Alloy in the Temperature Range 550–830 °C: Influence of Mechanical Deformation, *Oxid. Met.*, 1995, **44**, p 429-452
10. C.K. Kim and L.W. Hobbs, Microstructural Evidence for Short-Circuit Oxygen Diffusion Paths in the Oxidation of a Dilute Ni-Cr Alloy, *Oxid. Met.*, 1996, **45**, p 247-265
11. B. Ahmad and P. Fox, STEM Analysis of the Transient Oxidation of a Ni-20Cr Alloy at High Temperature, *Oxid. Met.*, 1998, **52**, p 113-138
12. J.R. Nicholls and M.J. Bennett, Cyclic Oxidation-Guidelines for Test Standardization, Aimed at the Assessment of Service Behavior, *Mater. High Temp.*, 2000, **17**, p 413-428
13. B. Li and B. Gleeson, Effect of Silicon on Oxidation Behavior of Ni-Base Chromia-Forming Alloys, *Oxid. Met.*, 2006, **65**, p 101-122
14. F.H. Stott, G.C. Wood, and J. Stringer, The Influence of Alloying Elements on the Development and Maintenance of Protective Scales, *Oxid. Met.*, 1995, **44**, p 113-145
15. D.P. Whittle and J. Stringer, Improvements in High Temperature Oxidation Resistance by Additions of Reactive Elements or Oxide Dispersions, *Proc. R. Soc. Lond., Ser. A*, 1980, **295**, p 309-329
16. G.C. Wood and F.H. Scott, Oxidation of Metals, *Mater. Sci. Technol.*, 1987, **3**, p 519-530
17. G.C. Wood, J.A. Richards, M.G. Hobby, and J. Boustead, Identification of Thin Healing Layers at Based of Oxide Scale on Fe-Cr Base Alloys, *Corros. Sci.*, 1969, **9**, p 659-671
18. A.G. Revsz and F.P. Fehlner, The Role of Noncrystalline Films in the Oxidation and Corrosion of Metals, *Oxid. Met.*, 1981, **15**, p 297-321
19. M.J. Bennett, J.A. Desport, and P.A. Labun, Analytical Electron Microscopy of a Selective Oxide Scale Formed on 20% Cr-25% Ni-Nb Stainless Steel, *Oxid. Met.*, 1984, **22**, p 291-306
20. M.J. Bennett, J.A. Despota, and P.A. Labun, Transverse Microstructue of an Oxide Scale Formed on a 20%Cr-25%Ni-Nb Stabilized Stainless Steel, *Proc. R. Soc. Lond., Ser. A*, 1987, **412**, p 223-230
21. R.C. Lobb, J.A. Sasse, and H.E. Evans, Dependence of Oxidation Behavior on Silicon Content of 20%Cr Austenitic Steels, *Mater. Sci. Technol.*, 1989, **5**, p 828-834
22. W.C. Hagel, Oxidation of Iron Nickel and Cobalt-Base Alloys Containing Aluminum, *Corrosion*, 1965, **21**, p 316-326
23. J.A. Nesbitt, Numerical Modeling of High-Temperature Corrosion Processes, *Oxid. Met.*, 1995, **44**, p 309-338
24. H.E. Evans, A.T. Donaldson, and T.C. Gilmour, Mechanisms of Breakaway Oxidation and Application to a Chromia-Forming Steel, *Oxid. Met.*, 1999, **52**, p 379-402
25. J.A. Nesbitt and R.W. Heckel, Interdiffusion in Ni-Rich, Ni-Cr-Al Alloys at 1100 and 1200 °C: Part I. Diffusion Paths and Microstructures, *Metall. Trans. A*, 1987, **18A**, p 2061-2086
26. C.S. Giggin and F.S. Pettit, Oxidation of Ni-Cr-Al Alloys Between 1000 and 1200 °C, *J. Electrochem. Soc.*, 1971, **118**, p 1782-1790
27. B.A. Pint, J.R. Keiser, "Alloy Selection for High Temperature Heat Exchangers," NACE Paper 06-469, presented at NACE Corrosion 2006 (San Diego, CA), NACE International, March 2006
28. M.P. Brady, B. Gleeson, and I.G. Wright, Alloy Design Strategies for Promoting Protective Oxide Scale Formation, *JOM*, 2000, **52**, p 16-21
29. D.J. Young and B. Gleeson, Alloy Phase Transformations Driven by High Temperature Corrosion Processes, *Corros. Sci.*, 2002, **44**, p 345-357
30. L. Onsager, Theories and Problems of Liquid Diffusion, *Ann. N. Y. Acad. Sci.*, 1965, **46**, p 241-265
31. M.A. Dayananda and C.W. Kim, Zero-Flux Planes and Flux Reversals in Cu-Ni-Zn Diffusion Couples, *Metall. Trans. A*, 1979, **10A**, p 1333-1339
32. M.A. Dayananda and Y.H. Sohn, Average Effective Interdiffusion Coefficients and Their Applications for Isothermal Multicomponent Diffusion Couples, *Ser. Mater.*, 1996, **40**, p 683-688
33. M.A. Dayananda and Y.H. Sohn, A New Approach for the Determination of Interdiffusion Coefficients in Ternary Systems, *Metall. Mater. Trans. A*, 1999, **30A**, p 535-543
34. M.S. Thompson, J.E. Morral, and A.D. Romig Jr., Applications of the Square Root Diffusivity to Diffusion in Ni-Al-Cr Alloys, *Metall. Trans. A*, 1990, **21A**, p 2679-2685

Defect and Diffusion Forum Vols. 258-260 (2006) pp 346-359
online at http://www.scientific.net

Online available since 2006/Oct/15

Integrated, Effective and Average Interdiffusion Coefficients and Their Applications in Multicomponent Alloys for Energy Production Technologies

Y.H. Sohn[1,a], N. Garimella[1,b], E. Perez[1,c], R. Mohanty[1,d], J. Liu[1,e]

[1]Advanced Materials Processing and Analysis Center and Department of Mechanical, Materials and Aerospace Engineering, University of Central Florida, Orlando, FL 32816

[a]ysohn@mail.ucf.edu, [b]ga825540@pegasus.cc.ucf.edu, [c]em168604@pegasus.cc.ucf.edu, [d]rmohanty@mail.ucf.edu, [e]ji181643@pegasus.cc.ucf.edu

Keywords: Interdiffusion, Microstructure, Multicomponent Alloys, Interdiffusion Coefficients, Thermal Barrier Coatings, NiCoCrAlY, Nickel Aluminides, Superalloys, Metallic Nuclear Fuels

Abstract. Solid-state diffusion is a subject of great interest for many intellectual merits and practical applications. It also provides excellent educational studies with cross-fertilization of science and technology. This paper examines the importance of multicomponent-multiphase interdiffusion with specific examples from materials and coatings for components in advanced energy production systems, including gas turbines and nuclear reactors. Results and analysis from laboratory experiments are presented in terms of interdiffusion fluxes, integrated interdiffusion coefficients, effective interdiffusion coefficients, and average multicomponent interdiffusion coefficients. Applications are highlighted for materials and coatings for components in advanced energy production technologies. Additional consideration is given to the refined approach to assess composition-dependent interdiffusion coefficients in multicomponent alloys.

Interdiffusion in Gas Turbine and Nuclear Reactor Components

Interdiffusion in multicomponent-multiphase alloys is commonly encountered in many materials systems employed in gas turbine and nuclear reactor environment. The developments of multicomponent-multiphase alloys require control of microstructure through appropriate heat treatment, involving solid-state transformations, precipitation processes, and surface modification, where the interdiffusion processes play a major role. In addition, interdiffusion processes often control degradation and failure of these materials systems, and enhanced performance and reliable durability always requires a detailed understanding of interdiffusion.

For example, hot section components such as blades and vanes of turbine engines for propulsion and utilities are generally coated with oxidation resistant coatings (e.g., NiCoCrAlY or NiAl) and insulating-ceramic thermal barrier coatings (TBCs) to protect load-bearing superalloys [1-5]. For TBCs, the NiCoCrAlY or NiAl-based coatings are also known as bond coats. TBCs are in general air plasma sprayed or electron beam physical vapor deposited ZrO_2-8wt.Y_2O_3 (YSZ) as presented in Fig. 1. In a typical gas turbine application, TBCs degrade by many diffusion-controlled phenomena including: sintering of YSZ, phase transformation (e.g., non-equilibrium tetragonal to equilibrium cubic and equilibrium monoclinic) of YSZ, formation of thermally grown oxide (TGO) due to oxidation of bond coats, polymorphic and phase transformations within the TGO scale, phase transformations in bond coats due to oxidation and interdiffusion with superalloys substrates, coarsening of precipitates in superalloys, phase transformations (e.g., TCP) in superalloys and creep of superalloys. A typical example of microstructural degradation in a NiCoCrAlY bond coat due

to oxidation and interdiffusion with superalloy underneath is presented in Fig. 2, where Al-rich β-NiAl phase gets dissolved by depletion of Al via interdiffusion [6].

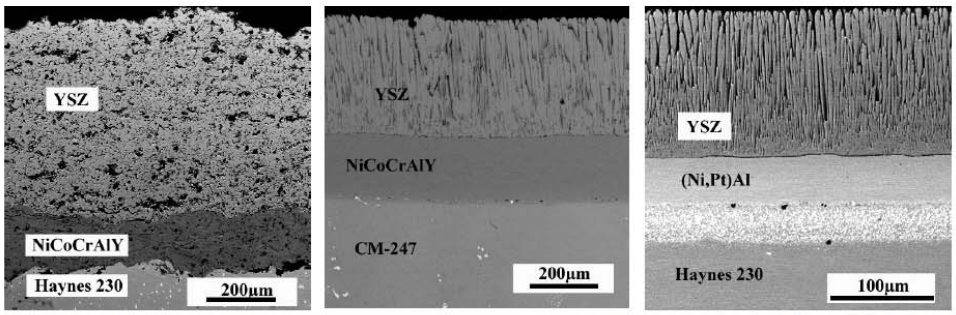

Fig. 1. Typical microstructure of as-processed TBCs with (a) APS YSZ and NiCoCrAlY bond coat; (b) EB-PVD YSZ and NiCoCrAlY bond coat; (c) EB-PVD YSZ and (Ni,Pt)Al bond coat.

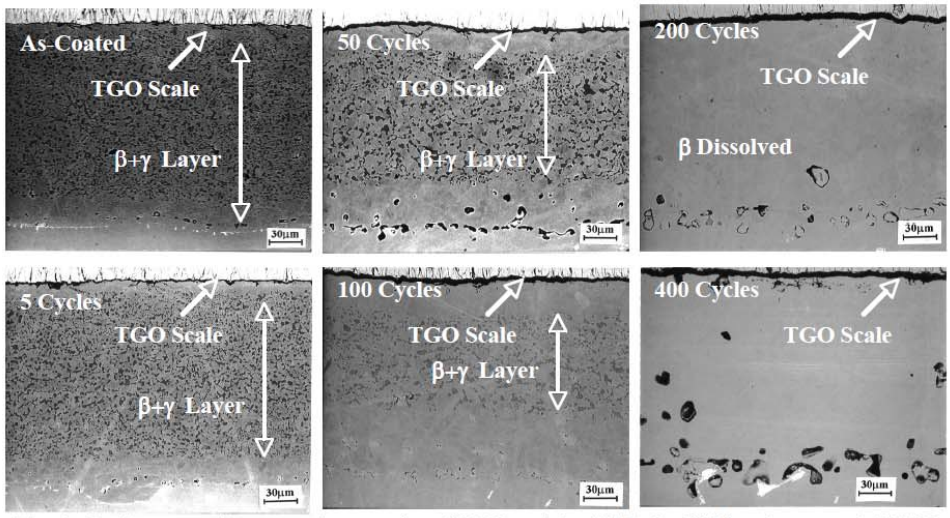

Fig. 2. Backscatter electron micrographs of TBCs with a NiCoCrAlY bond coat and IN738 superalloy substrate illustrating growth of TGO scale and dissolution of β-phase due to interdiffusion as a function of cyclic oxidation at 1121°C [6]. Each thermal cycling consists of 10-minute heat-up, 40-minute dwell at 1121°C and 10-minute forced-air-quench.

In a nuclear reactor environment, interdiffusion process with cladding and due to temperature gradient becomes critical in development and application of advanced metallic nuclear fuels (e.g., U-Pu-Zr and U-Mo). For example, a rod of U-19wt.%Pu-10wt.%Zr alloy under the gradient of temperature (220°C/cm for 41 days) develops a large-scale compositional changes and microstructure variation as a result of multicomponent thermotransport [7]. Also, interdiffusion between U-8~10wt.%Mo fuel-alloy with Al-cladding results in formation of Al-rich intermetallic compounds with low thermal conductivity [8,9] that degrade the rapid heat-extraction function of Al-cladding. Optimum performance and fuel stability require a detailed understanding of multicomponent-multiphase interdiffusion.

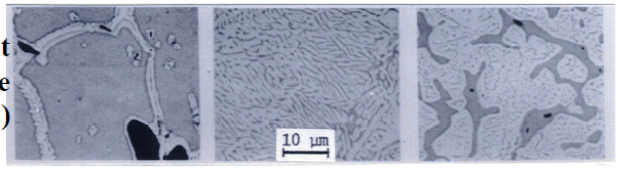

Fig. 3. Microstructural variation in U-19wt.%Pu-10wt.%Zr alloy after 41 days of thermotransport experiments. White and black regions correspond to ζ and Zr-rich precipitates, while gray region represents a fine mixture of α and δ phases [7].

Multicomponent Interdiffusion and Determination of Interdiffusion Fluxes

Isothermal interdiffusion flux of a component *i* in a multicomponent system can be defined as [10-12]:

$$\tilde{J}_i = -\sum_{j=1}^{n-1} \tilde{D}_{ij}^{n} \frac{\partial C_j}{\partial x} \quad (i = 1,2,...,n-1). \tag{1}$$

where $\tilde{J}_i$ is the interdiffusion flux of component *i*, $\tilde{D}_{ij}^{n}$ is the $(n-1)^2$ interdiffusion coefficient of component *i* with respect to the concentration gradient of *j* in an n-component system, and $\partial C_j/\partial x$ is the (n-1) independent concentration gradient. To assess interdiffusion fluxes of individual components during isothermal interdiffusion, Eq. (1) requires knowledge of (n-1) independent concentration gradients and composition-dependent $(n-1)^2$ interdiffusion coefficients that are generally determined using Boltzmann-Matano analysis. This analytical approach may require a large number of experimental diffusion couples, and becomes increasingly difficult to use for quaternary and higher order systems.

Alternatively, the interdiffusion fluxes of individual components may be determined directly from their concentration profiles without the need of the interdiffusion coefficients by [13]:

$$\tilde{J}_i = \frac{1}{2t} \int_{C_i^{\infty}}^{C_i(x)} (x - x_o)\, dC_i \quad (i = 1,2,...,n). \tag{2}$$

where t is the diffusion anneal time. Determination of interdiffusion fluxes using experimental concentration profiles via Eq. (2) can provide direct insight to magnitude and direction of interdiffusion fluxes of individual components, and has lead to noble observations such as zero-flux planes and flux reversals [13,14].

Integrated and Effective Interdiffusion Coefficients

A profile of interdiffusion flux for a component *i* can be integrated with respect to distance, and this accumulated interdiffusion flux for a component can be defined as an integrated interdiffusion coefficient, $\tilde{D}_i^{int}$ over a selected region, x_1 from x_2, as [15]:

$$\tilde{D}_{i,\Delta x}^{int} = \int_{x_1}^{x_2} \tilde{J}_i dx. \tag{3}$$

An effective interdiffusion coefficient, $\tilde{D}_i^{eff}$ over the corresponding composition range, $C_i^{x_2}$ to $C_i^{x_1}$ can be then defined as [15]:

$$\tilde{D}_{i,\Delta x}^{eff} = \frac{\tilde{D}_{i,\Delta x}^{int}}{C_i^{x_2} - C_i^{x_1}}. \tag{4}$$

The $\tilde{D}_i^{eff}$ incorporates multicomponent diffusional interactions for the system to provide an effective value for the interdiffusion of a component as defined by [15]:

$$\tilde{D}_i^{eff} = \tilde{D}_{ii}^{n} + \sum_j \frac{\tilde{D}_{ij}^{n} \partial C_j / \partial x}{\partial C_i / \partial x} \quad (j \neq i). \tag{5}$$

Since $\tilde{J}_i$ must be continuous at any location, and the effective interdiffusion coefficient can be defined on either side of any location (e.g., $\tilde{D}_{i,L}^{eff}$ and $\tilde{D}_{i,R}^{eff}$ for the left and right-hand-side of the selected plane, x_o), the following relation can be defined [16]:

$$\tilde{J}_i\Big|_{x=x_o} = \frac{\sqrt{\tilde{D}_{i,L}^{eff}}}{\alpha_{i,L}\sqrt{t}}\left(C_i^{-\infty} - C_i^{o}\right) = \frac{\sqrt{\tilde{D}_{i,R}^{eff}}}{\alpha_{i,R}\sqrt{t}}\left(C_i^{o} - C_i^{+\infty}\right). \tag{6}$$

where $\alpha_{i,L}$ and $\alpha_{i,R}$ are dimensionless parameters. Eq. (6) is true for any selected plane within the diffusion zone including the Matano plane. For example, based on the experimental concentration profile on one side of the Matano plane, Eq. (6) can be employed to predict the effective interdiffusion coefficient on the other side of the Matano interface provided that α_i does not deviate from $\sqrt{\pi}$ [16]. This would be a good assumption for concentration profile that can be modeled using error-function solutions, such as intrinsically fast-diffusing component (e.g., Al in superalloys). A similar equation for $\tilde{D}_i^{int}$ by substituting Eq. (4) into Eq. (6) can be defined as:

$$\frac{\tilde{D}_{i,R}^{int}}{\tilde{D}_{i,L}^{int}} = \left(\frac{C_i^{-} - C_i^{o}}{C_i^{o} - C_i^{+}}\right). \tag{7}$$

Average Interdiffusion Coefficients in Multicomponent Alloys

For ternary system, the interdiffusion flux $\tilde{J}_i$, determined from Eq. (7) as a function of x, can be multiplied by $(x-x_o)^p$ and integrated over a selected region, x_1 to x_2; in the light of Eq. (1), one gets [17]:

$$\int_{x_1}^{x_2} \tilde{J}_i (x - x_o)^p dx = -\overline{\tilde{D}}_{i1}^{3} \int_{C_1(x_1)}^{C_1(x_2)} (x - x_o)^p dC_1 - \overline{\tilde{D}}_{i2}^{3} \int_{C_2(x_1)}^{C_2(x_2)} (x - x_o)^p dC_2 \quad (i,j = 1,2). \tag{8}$$

where $\overline{\tilde{D}}_{ij}^{3}$ $(i,j = 1,2)$ coefficients are the average values of main and cross-interdiffusion coefficients treated as constants over the selected composition range. For values of p = 0 and 1, Eq. (8) yields [17] :

$$\int_{x_1}^{x_2} \tilde{J}_i dx = \overline{\tilde{D}}_{i1}^{3}\left[C_1(x_1) - C_1(x_2)\right] + \overline{\tilde{D}}_{i2}^{3}\left[C_2(x_1) - C_2(x_2)\right] \quad (i,j = 1,2). \tag{9}$$

and

$$\int_{x_1}^{x_2} \tilde{J}_i(x-x_o)dx = 2t\left\{\overline{\tilde{D}}_{i1}^{3}\left[\tilde{J}_1(x_1)-\tilde{J}_1(x_2)\right]+\overline{\tilde{D}}_{i2}^{3}\left[\tilde{J}_2(x_1)-\tilde{J}_2(x_2)\right]\right\} \quad (i,j=1,2). \tag{10}$$

Eqs. (9) and (10) provide four equations involving the $\overline{\tilde{D}}_{ij}^{3}$ interdiffusion coefficients and can be set up from interdiffusion fluxes calculated on the basis of Eq. (2) from the concentration profiles of a single diffusion couple in a ternary system. The $\overline{\tilde{D}}_{ij}^{3}$ coefficients, characteristic of the diffusion path, can be determined over selected composition ranges that include nonlinear segment of the profiles [17,18].

Average Interdiffusion Coefficients and Heat of Transport in Multicomponent Alloys

Under the gradients of temperature ($\partial T/\partial x$) and concentrations ($\partial C_j/\partial x$), Onsager's formalism for the interdiffusion flux $\tilde{J}_i$ of component i in a ternary system can be written as [7] :

$$\tilde{J}_i = -C_i\beta_i\tilde{Q}_i^{*}\frac{1}{T}\frac{\partial T}{\partial x}-\sum_{j=1}^{2}\tilde{D}_{ij}^{3}\frac{\partial C_j}{\partial x} \quad (i=1,2). \tag{11}$$

where β_i and $\tilde{Q}_i^{*}$ refer to the mobility and heat of transport, respectively. Eq. (11) can be integrated over a selected region, x_1 to x_2 to yield [7]:

$$\int_{x_1}^{x_2}\tilde{J}_i dx = -\overline{\beta_i\tilde{Q}_i^{*}}\int_{T(x_1)}^{T(x_2)} C_i\frac{dT}{T}-\overline{\tilde{D}}_i^{eff}\int_{C(x_1)}^{C(x_2)}dC_i \quad (i=1,2). \tag{12}$$

and

$$\int_{x_1}^{x_2}\tilde{J}_i(x-x_o)dx = -\overline{\beta_i\tilde{Q}_i^{*}}\int_{T(x_1)}^{T(x_2)} C_i\frac{(x-x_o)dT}{T}-\overline{\tilde{D}}_i^{eff}\int_{C(x_1)}^{C(x_2)}(x-x_o)dC_i \quad (i=1,2). \tag{13}$$

where

$$\overline{\tilde{D}}_i^{eff} = \overline{\tilde{D}}_{ii}^{3}+\overline{\tilde{D}}_{ij}^{3}\frac{\Delta C_j}{\Delta C_i} \quad (i\neq j). \tag{14}$$

Eqs. (12) and (13) provides four equations to determine the average thermotransport coefficients, $\overline{\beta_i\tilde{Q}_i^{*}}$, and average effective interdiffusion coefficients, $\overline{\tilde{D}}_i^{eff}$, over a selected concentration range ΔC_i in the diffusion zone from experimental concentration profiles. Substituting Eq. (14) into Eqs. (12) and (13) and utilizing the calculated values of $\overline{\beta_i\tilde{Q}_i^{*}}$, one can also evaluate average ternary interdiffusion coefficients $\overline{\tilde{D}}_{ij}^{3}$ (i,j = 1,2).

Selection of Ni-base Superalloys for Durable NiAl Coatings

Commercial superalloys have been developed with compositions and heat treatments to optimize high temperature strength, as well as resistance against creep, fatigue, oxidation and hot-corrosion [1]. Also, and somewhat in parallel, similar optimizations of the composition for Al_2O_3-forming NiCoCrAlY and NiAl-based coatings have been carried out to increase the oxidation and hot-corrosion resistance. Considering the significance of diffusional interactions in these systems, the lifetime of the coatings, defined by depletion of Al and dissolution of Al-rich B2 β-NiAl [5,6], may be enhanced by controlling the interdiffusion

fluxes of individual components, particularly for Al. A system selection/development should be optimized to control the interdiffusion fluxes of diffusing components, so that Al interdiffusion flux across the coating-superalloy interface is minimized.

Diffusion couples consisting of single-phase β-NiAl (hot-extruded with equiaxed-grain diameter of 30~50 μm) vs. various commercial superalloys, namely CM247™, GTD111™, IN738™, IN939™ and Waspalloy™ were examined. The measurement of concentration profiles (and thus interdiffusion fluxes and coefficients) by electron probe microanalysis (EPMA) is difficult for fine two-phase microstructures like that of the γ+γ' in Ni-base superalloys. Quantitative determination of interdiffusion fluxes and coefficients can only be carried out from concentration profiles measured in single-phase β-NiAl side of the couple. Then utilizing the general expression of average effective interdiffusion coefficient, Eq. (4), along with mass balance and local continuity of interdiffusion flux, Eq. (6), integrated interdiffusion coefficients and effective interdiffusion coefficients of individual components in superalloys can be predicted using Eqs. (2) through (7).

Backscatter electron micrographs of diffusion couples, NiAl vs. CM247™, GTD111™, IN738™, IN939™ and Waspalloy™ are shown in Fig. 4. Many small precipitates, such as TCP phases rich in refractory, were observed near the interface between NiAl and superalloys. These precipitates also prevent any meaningful determination of concentration profiles by EPMA in these zones, and subsequent analysis. The concentration profiles of the major elements obtained from the diffusion couples of NiAl vs. CM247, GTD111, IN738, IN939 and Waspalloy are shown in Fig. 5. In these profiles, as expected, concentrations determined on the single-phase β-NiAl side are consistent without any scatter, while those on the multiphase superalloy side, including the precipitates near the interface exhibit large scatters.

Integrated, $\tilde{D}^{int}_{Al,NiAl}$, and effective, $\tilde{D}^{eff}_{Al,NiAl}$, interdiffusion coefficients for Al in the NiAl side of the diffusion couples was calculated using Eqs. (3) and (4), and are reported in Table I. Then, Eqs. (6) and (7) were employed to predict $\tilde{D}^{eff}_{Al,SA}$ and $\tilde{D}^{int}_{Al,SA}$ for Al in the superalloy side of the couples as reported in Table I. The $\tilde{D}^{int}_{Al,total}$ provided in Table I is a measure of the integrated interdiffusion flux of Al in diffusion couples. The $\tilde{D}^{eff}_{Al,total}$ in Table I is an average effective interdiffusion coefficient of Al in the diffusion couples. In general, superalloys with higher concentration of Cr, Mo and Ti had higher $\tilde{D}^{eff}_{Al,SA}$, and higher concentrations of Ta, W and Al in the superalloys were related to lower $\tilde{D}^{eff}_{Al,SA}$. These values can be quantitatively employed to design and/or select appropriate compositions of coatings and/or superalloys to minimize degradation due to interdiffusion.

Table I. Integrated and effective interdiffusion coefficients of Al determined from experimental concentration profiles on the NiAl side of the diffusion couples. The integrated and interdiffusion coefficients of Al for the superalloy side of the diffusion couples were predicted based on Eqs. (6) and (7).

Superalloy	Constituent Element	$\tilde{D}^{int}_{NiAl}$	$\tilde{D}^{eff}_{NiAl}$	$\tilde{D}^{int}_{SA}$	$\tilde{D}^{eff}_{SA}$	$\tilde{D}^{int}_{Tot}$	$\tilde{D}^{eff}_{Tot}$
CM-247	Al	1.51	13.55	0.66	2.56	2.17	5.87
GTD-111	Al	1.50	9.87	0.80	2.80	2.30	5.30
IN-738	Al	1.91	12.72	1.06	3.90	2.97	6.92
IN-939	Al	1.56	9.56	0.84	2.74	2.40	5.14
Waspalloy	Al	2.34	16.16	1.02	3.10	3.36	7.15

Note: All interdiffusion coefficients are reported in 10^{-15} m^2/sec.

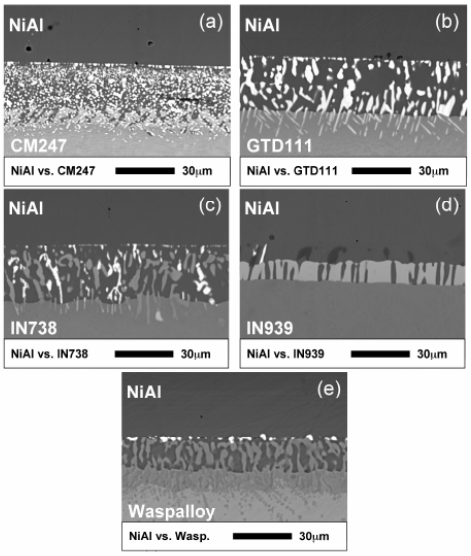

Fig. 4. Backscatter electron micrographs of diffusion microstructure observed in solid-to-solid diffusion couples, NiAl vs. (a) CM-247, (b) GTD-111, (c) IN-738, (d) IN-939 and (e) Waspalloy, annealed at 1050°C for 96 hours.

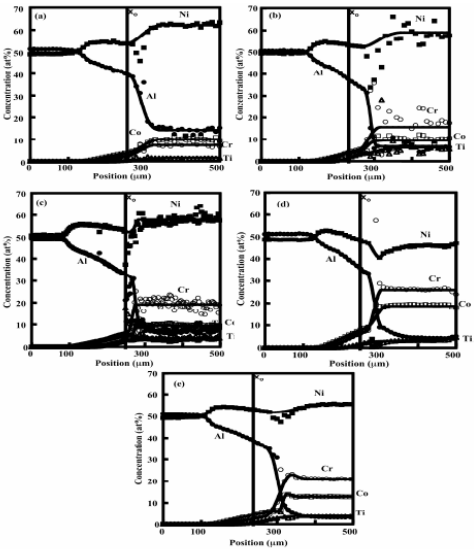

Fig. 5. Concentration profiles of major component in solid-to-solid diffusion couples, determined by EPMA for NiAl vs. (a) CM-247, (b) GTD-111, (c) IN-738, (d) IN-939 and (e) Waspalloy, annealed at 1050°C for 96 hours.

Assessment of Diffusional Interactions in Ni-Cr-X (X = Al, Si, Ge or Pd) using Average Interdiffusion Coefficients

Nickel-chromium base alloys are widely used a variety of high-temperature applications due to their combination of good oxidation resistance and excellent high-temperature strength, and are the basis for a number of commercial superalloy families [1,19,20]. Oxidation resistance in these alloys is derived from a continuous, slow-growing, adherent C_2O_3-base oxide scale [1,19,20]. In particular, composition in the range of Ni alloyed with 20~30 wt.% Cr have been extensively studied as a model material for Cr_2O_3 scale formation [19,20]. Minor alloying additions (< 5wt.%) can significantly improve the oxidation resistance of Ni-base Cr_2O_3-forming alloys [1,21,22]. Effects include: (1) establishment of continuous Cr_2O_3 scale formation at reduced Cr concentrations; (2) a decrease in the growth rate of Cr_2O_3; and (3) enhanced scale adherence. For example, the addition of Si in Ni-28wt.%Cr promoted formation of both Cr_2O_3 and SiO_2, in which a continuous inner SiO_2 layer acted as a diffusion barrier, and reduced the isothermal oxidation rate by suppressing cation transport through the Cr_2O_3 scale. However, the same inner SiO_2 layer can also reduce the spallation resistance, dependent on the level of Si and the continuity and thickness of the inner SiO_2 layer formed.

Diffusional effects of minor alloy additions may play a significant role in the initial establishment of a continuous protective oxide scale [19,23]. It can also play a significant role in maintaining protective scale growth. For example, the growth of Cr_2O_3 can locally deplete Cr from the alloy in the subsurface region. If the scale is locally damaged or spalled, such depletion can prevent reformation of the Cr_2O_3 scale, and result in a transition to less-protective or non-protective oxidation behavior. Understanding of diffusional interactions in Ni-Cr-X alloys where X represents minor alloying additions can help design Ni-base Cr_2O_3-forming alloys with improved resistance against environmental degradation [23].

In this work, interdiffusion in Ni-22at.%Cr-X (fcc γ phase) alloys with small additions of X (X = Al, Si, Ge, or Pd) was investigated using solid-to-solid diffusion couples annealed at 900°C for 168 hours. Binary and ternary alloys with compositions reported in Table II were prepared with 99.9% pure Ni, Cr, Al, Si, Ge and Pd by arc melting under an argon atmosphere. Table III presents ternary diffusion couples that were assembled and annealed at 900˚C in a horizontal Lindberg 3-zone furnace for 168 hours. The experimental concentration profiles measured by EPMA with pure standards were smoothened by spline-fit and used to calculate interdiffusion fluxes of individual components, and to determine average effective interdiffusion coefficients $\tilde{D}_i^{eff}$, and average ternary interdiffusion coefficients $\widetilde{\widetilde{D}}_{ij}^{Ni}$ (i, j = Cr, X). Values of $\tilde{D}_{Cr}^{eff}$ and $\widetilde{\widetilde{D}}_{CrX}^{Ni}$ are examined to assess the effects of alloying additions on the interdiffusion behavior of Cr, and the Cr_2O_3-forming ability in Ni-Cr-X alloys.

Table II. Compositions of Ni-Cr-X alloys employed for solid-to-solid diffusion couples.

Alloy	Composition (atom fraction)		
	Ni	Cr	X
Ni	100.0	-	-
NiCr (X = None)	78.0	22.0	-
NiCrAl (X = Al)	72.5	21.3	6.2
NiCrSi (X = Si)	74.0	22.0	4.0
NiCrGe (X = Ge)	76.3	22.1	1.6
NiCrPd (X = Pd)	76.1	22.3	1.6

Table III. List of Ni vs. Ni-Cr-X and NiCr vs. Ni-Cr-X solid-to-solid diffusion couples annealed at 900°C for 168 hours.

Series	Diffusion Couples
I	Ni vs. Ni-Cr
II	Ni vs. Ni-Cr-Al
	Ni vs. Ni-Cr-Si
	Ni vs. Ni-Cr-Ge
	Ni vs. Ni-Cr-Pd
III	Ni-Cr vs. Ni-Cr-Al
	Ni-Cr vs. Ni-Cr-Si
	Ni-Cr vs. Ni-Cr-Ge
	Ni-Cr vs. Ni-Cr-Pd

Fig. 6 presents examples of experimental and smoothened concentration profiles that were used for the determination of interdiffusion coefficients. Scatters in the concentration profiles for all diffusion couples were minimum and within the experimental uncertainty associated with EPMA. Table IV reports the average effective interdiffusion coefficients $\tilde{D}_i^{eff}$'s determined using Eq. (4) on either side of the Matano plane. In general, $\tilde{D}_i^{eff}$ was higher on the $\left(C_i^{\circ} \sim C_i^{+\infty}\right)$ composition range with higher Cr concentration relative to the other side of the Matano plane. In particular, Al addition to NiCr alloy was observed to increase or decrease the $\tilde{D}_{Cr}^{eff}$ as a function of composition. This indicates appreciable variation in interdiffusion coefficients as a function of composition: specifically, Al increased $\tilde{D}_{Cr}^{eff}$ on the $\left(C_i^{\circ} \sim C_i^{+\infty}\right)$ composition range with higher Cr concentration. $\tilde{D}_{Cr}^{eff}$ was observed to increase with Si addition to NiCr alloy especially on the $\left(C_i^{\circ} \sim C_i^{+\infty}\right)$ side with higher Cr concentration. According to Table IV, Ge does not change $\tilde{D}_{Cr}^{eff}$ significantly, while Pd addition to Ni-Cr alloy increased $\tilde{D}_{Cr}^{eff}$, quite significant on the $\left(C_i^{\circ} \sim C_i^{+\infty}\right)$ range with higher Cr concentration.

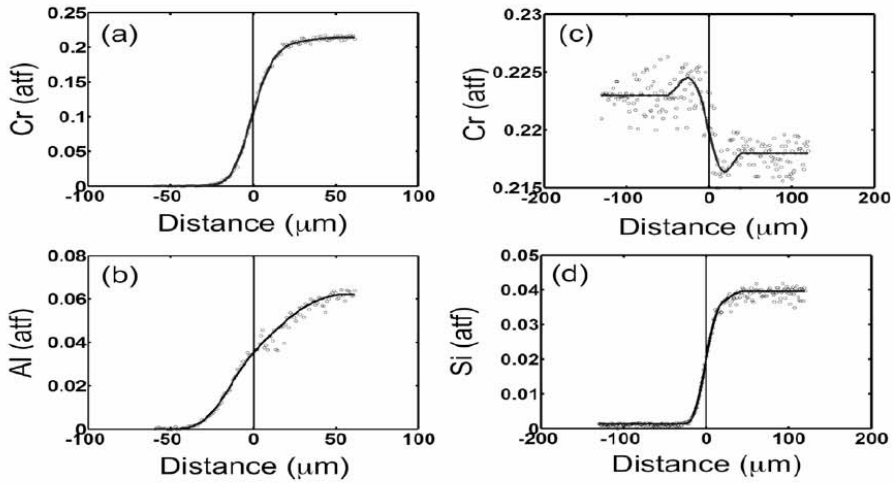

Figure 6. Typical experimental and smoothened concentration profiles measured from solid-to-solid diffusion couples (a,b) Ni vs. Ni-Cr-Al and (c,d) Ni-Cr vs. Ni-Cr-Si, annealed at 900°C for 168 hours annealed at 900°C for 168 hours.

Table IV. Average effective interdiffusion coefficients (10^{-16} m^2/s) determined from Ni vs. Ni-Cr-X diffusion couples annealed at 900°C for 168 hours.

Diffusion Couple	Composition Range	$\tilde{D}^{eff}_{Cr}$	$\tilde{D}^{eff}_{X}$	$\tilde{D}^{eff}_{Ni}$
Ni vs. Ni-Cr (X = None)	$(C_i^{-\infty} \sim C_i^{o})$	1.40	-	1.40
	$(C_i^{o} \sim C_i^{+\infty})$	1.53	-	1.53
Ni vs. Ni-Cr-Al (X = Al)	$(C_i^{-\infty} \sim C_i^{o})$	0.91	3.31	1.83
	$(C_i^{o} \sim C_i^{+\infty})$	1.58	4.68	2.19
Ni vs. Ni-Cr-Si (X = Si)	$(C_i^{-\infty} \sim C_i^{o})$	1.68	5.74	2.26
	$(C_i^{o} \sim C_i^{+\infty})$	3.00	6.91	3.57
Ni vs. Ni-Cr-Ge (X = Ge)	$(C_i^{-\infty} \sim C_i^{o})$	1.30	3.09	1.40
	$(C_i^{o} \sim C_i^{+\infty})$	1.44	3.47	1.61
Ni vs. Ni-Cr-Pd (X = Pd)	$(C_i^{-\infty} \sim C_i^{o})$	1.77	1.19	1.74
	$(C_i^{o} \sim C_i^{+\infty})$	4.09	2.07	3.92

Table V presents the average ternary interdiffusion coefficients, $\overline{\tilde{D}}^{Ni}_{ij}(i,j = Cr,X)$ determined on either side of the Matano plane using Eqs. (9) and (10). It should be noted that these diffusion couples were designed to yield the same sign of $\partial C_{Cr}/\partial x$ and $\partial C_X/\partial x$. Thus, positive and negative $\overline{\tilde{D}}^{Ni}_{CrX}$ indicates an increase and a decrease in $\tilde{J}_{Cr}$, respectively. In general, larger magnitude of $\overline{\tilde{D}}^{Ni}_{CrCr}$ and $\overline{\tilde{D}}^{Ni}_{XX}$ were observed on the $(C_i^{o} \sim C_i^{+\infty})$ composition range with higher Cr concentration. The Al addition in the Ni-Cr alloy yielded positive $\overline{\tilde{D}}^{Ni}_{CrAl}$, and increased $\tilde{J}_{Cr}$ in accordance with previous work [23]. The magnitude of $\overline{\tilde{D}}^{Ni}_{CrAl}$ was quite large as reported in Table V on the $(C_i^{o} \sim C_i^{+\infty})$ with higher Cr concentration. Similarly, Si, Ge

and Pd additions to Ni-Cr alloy increased $\tilde{J}_{Cr}$ with positive $\tilde{\tilde{D}}^{Ni}_{CrX}$. This effect was, again, stronger when Cr concentration is high on the $\left(C_i^{\circ} \sim C_i^{+\infty}\right)$ side particularly for Si and Pd. Diffusion couple series III was designed with initial $\partial C_{Cr}/\partial x = 0$, so that $\tilde{J}_{Cr}$ is largely due to $\partial C_X/\partial x$, and depends on the magnitude and sign of $\tilde{\tilde{D}}^{Ni}_{CrX}$. $\tilde{J}_X$ has caused an uphill-diffusion of Cr in the direction of $\tilde{J}_X$ with positive $\tilde{\tilde{D}}^{Ni}_{CrX}$ for Al and Si as presented in Table VI. On the other hand, $\tilde{J}_{Ge}$ and $\tilde{J}_{Pd}$ did not caused any measurable redistribution of Cr ($\tilde{J}_{Cr} \approx 0$). It should be noted that Ge and Pd have lower contents in the Ni-Cr-X alloys than Al and Si, as reported in Table II.

Based on average effective interdiffusion coefficients and average ternary interdiffusion coefficients determined in this study, alloying additions of Al, Si, Ge and Pd have all increased $\tilde{D}^{eff}_{Cr}$ and yielded positive $\tilde{\tilde{D}}^{Ni}_{CrX}$ particularly with high Cr content (~22at.%). Therefore, the Cr_2O_3-forming ability of Ni-20at.%Cr-base alloy should improve with these alloying additions by establishing Cr_2O_3 scale, maintaining protective Cr_2O_3 scale formation, and in reformation of Cr_2O_3 upon spallation. It should be noted that positive $\tilde{\tilde{D}}^{Ni}_{XCr}$ reported in Tables V and VI should also promote the formation of other scales (Al_2O_3, SiO_2) in the γ (fcc) Ni-Cr alloy, which may reduce the rate of scale growth and/or change the thermo-mechanical properties of the scale.

Table V. Average ternary interdiffusion coefficients (10^{-16} m^2/s) determined from Ni vs. Ni-Cr-X diffusion couples annealed at 900°C for 168 hours.

Diffusion Couple	Composition Range	$\tilde{\tilde{D}}^{Ni}_{CrCr}$	$\tilde{\tilde{D}}^{Ni}_{CrX}$	$\tilde{\tilde{D}}^{Ni}_{XCr}$	$\tilde{\tilde{D}}^{Ni}_{XX}$
Ni vs. Ni-Cr-Al (X = Al)	$\left(C_i^{-\infty} \sim C_i^{\circ}\right)$	0.78	0.31	0.40	1.99
	$\left(C_i^{\circ} \sim C_i^{+\infty}\right)$	1.11	1.72	0.43	2.84
Ni vs. Ni-Cr-Si (X = Si)	$\left(C_i^{-\infty} \sim C_i^{\circ}\right)$	1.23	0.15	0.44	2.92
	$\left(C_i^{\circ} \sim C_i^{+\infty}\right)$	2.05	4.88	0.57	3.35
Ni vs. Ni-Cr-Ge (X = Ge)	$\left(C_i^{-\infty} \sim C_i^{\circ}\right)$	1.08	0.36	0.07	1.73
	$\left(C_i^{\circ} \sim C_i^{+\infty}\right)$	1.24	0.89	0.10	1.99
Ni vs. Ni-Cr-Pd (X = Pd)	$\left(C_i^{-\infty} \sim C_i^{\circ}\right)$	1.43	4.06	0.01	0.98
	$\left(C_i^{\circ} \sim C_i^{+\infty}\right)$	3.49	4.86	0.01	1.76

Table VI. Average ternary interdiffusion coefficients (10^{-16} m^2/s) determined from Ni-Cr vs. Ni-Cr-X diffusion couples annealed at 900°C for 168 hours.

Diffusion Couple	Composition Range	$\tilde{\tilde{D}}^{Ni}_{CrCr}$	$\tilde{\tilde{D}}^{Ni}_{CrX}$	$\tilde{\tilde{D}}^{Ni}_{XCr}$	$\tilde{\tilde{D}}^{Ni}_{XX}$
Ni-Cr vs. Ni-Cr-Al (X = Al)	$\left(C_i^{-\infty} \sim C_i^{\circ}\right)$	0.23	0.12	0.01	0.67
	$\left(C_i^{\circ} \sim C_i^{+\infty}\right)$	1.20	0.44	0.13	1.17
Ni-Cr vs. Ni-Cr-Si (X = Si)	$\left(C_i^{-\infty} \sim C_i^{\circ}\right)$	2.58	1.73	0.01	0.68
	$\left(C_i^{\circ} \sim C_i^{+\infty}\right)$	1.39	0.63	1.78	1.97

$\Delta C_{Cr}/\Delta x = 0$ and could not be determined for Ni-Cr vs. Ni-Cr-Ge and Ni-Cr-Pd couples.

Non-isothermal Thermotransport in U-Pu-Zr Alloys

An U-19wt.%Pu-10wt.%Zr alloy rod was annealed under a temperature gradient of 220°C/cm with one end maintained at 740°C and the other end at 600°C for 41 days [7]. The observed redistribution of U, Pu and Zr was analyzed with due consideration of thermotransport and ternary diffusional interactions among the components. The concentration profiles of U, Pu and Zr in the γ(bcc) phase region of the alloy are shown in Fig. 7(a), from which interdiffusion fluxes of the components were determined by using Eq. (2).

Eqs. (12) and (13) provides four equations to determine the average thermotransport coefficients, $\overline{\beta_i \tilde{Q}_i^*}$, and average effective interdiffusion coefficients, $\overline{\tilde{D}}_i^{eff}$, over a selected concentration range ΔC_i in the diffusion zone from experimental concentration profiles. Substituting Eq. (14) into Eqs. (12) and (13) and utilizing the calculated values of $\overline{\beta_i \tilde{Q}_i^*}$, one can also evaluate average ternary interdiffusion coefficients $\overline{\tilde{D}}_{ij}^3 (i, j = 1,2)$. From the redistribution profiles of the constituents shown in Fig. 7(a), $\overline{\beta_i \tilde{Q}_i^*}$, $\overline{\tilde{D}}_i^{eff}$ and $\overline{\tilde{D}}_{ij}^3$ coefficients were determined over three selected regions, I, II, III, and are reported in Table VII.

Values of $\overline{\beta_i \tilde{Q}_i^*}$ and $\overline{\tilde{D}}_{ij}^3 (i, j = 1,2)$ coefficients presented in Table VII were employed for estimating the three flux contributions, $\tilde{J}_{i,\partial T/\partial x}$, $\tilde{J}_{i,\partial C_U/\partial x}$, $\tilde{J}_{i,\partial C_{Zr}/\partial x}$, arising from the gradients of temperature, U concentration, and Zr concentration, respectively [7]. In Fig. 7(b) are presented these contributions to the flux of Zr in the region I. The magnitude of the flux contributions arising from the gradients of U and Zr are much greater than that of the flux due to the temperature gradient. However, the $\tilde{J}_{i,\partial C_U/\partial x}$ and $\tilde{J}_{i,\partial C_{Zr}/\partial x}$ terms are opposite in sign and their sum is quite small compared to $\tilde{J}_{i,\partial T/\partial x}$ as seen in Fig 7(b). The net interdiffusion flux of Zr is negative and contributes to the build-up of Zr in the hot-end region of the sample during annealing of the U-Pu-Zr alloy under a temperature gradient.

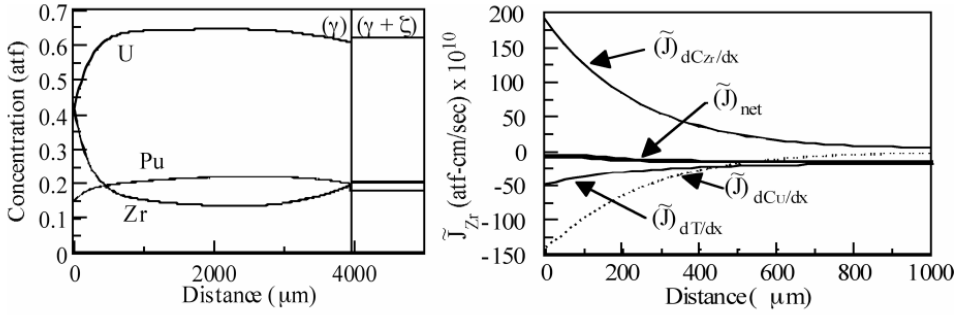

Fig. 7. (a) Experimental concentration profiles for U, Pu and Zr in the γ phase under the gradients of temperature and concentrations. (b) Estimated contributions from the gradients of temperature and concentrations of U and Zr to the interdiffusion flux of Zr in region I.

Table VII. $\overline{\beta_i \tilde{Q}_i^*}$, $\overline{\tilde{D}_i^{eff}}$ and $\overline{\tilde{D}_{ij}^{Pu}}$ (i, j = U, Zr) coefficients calculated from the redistribution of U, Pu and Zr under the gradients of temperature and concentrations.

Region in the γ	Location (μm)	$\overline{\beta_i \tilde{Q}_i^*}$ (10^{-8} cm^2/sec)			$\overline{\tilde{D}_i^{eff}}$ (10^{-10} cm^2/sec)			$\overline{\tilde{D}_{ij}^{Pu}}$ (i, j = U, Zr) (10^{-9} cm^2/sec)			
		U	Pu	Zr	U	Pu	Zr	$\overline{\tilde{D}_{UU}^{Pu}}$	$\overline{\tilde{D}_{UZr}^{Pu}}$	$\overline{\tilde{D}_{ZrU}^{Pu}}$	$\overline{\tilde{D}_{ZrZr}^{Pu}}$
I	0-1000	0.7	1.2	-5.5	0.8	0.9	4.5	7.5	6.0	1.6	1.7
II	1000-2450	0.7	1.7	-6.8	4.4	19.3	26.7	7.0	2.9	0.5	2.9
III	2450-4015	1.1	1.7	-8.6	-47.8	-24.6	-51.3	na*	na*	na*	na*

*not calculated due to uncertainties in the concentration profiles.

Refined Assessment of Average Interdiffusion Coefficients in Multicomponent Alloys

Although the use of Eqs. (9) and (10) for ternary systems is valid over a large composition range with non-linear segment of concentration profiles, use of Eq. (8) for the determination of average interdiffusion coefficients can be extended with multiple and higher "p" values for refined assessment of average multicomponent interdiffusion coefficients. It is evident that Eq. (8) can be written to provide $(n-1)^2$ equations involving the $(n-1)^2$ $\overline{\tilde{D}_{ij}^n}$ interdiffusion coefficients from (n-1) independent concentration profiles. Figs. 8 and 9 presents experimental (dotted lines) and calculated (solid lines) concentration profiles of Fe-Ni-Al diffusion couples, where $\overline{\tilde{D}_{ij}^n}$ coefficients were calculated using Eq. (8) with p = 0 and p = 1, 2,…, 50). Accurate $\overline{\tilde{D}_{ij}^n}$ coefficients that are consistent with Boltzmann-Matano analysis can be obtained using the following criteria in sequence:

1. $\overline{\tilde{D}_{ij}^n}$ at p = 0 (extrapolated) if $\frac{\partial \overline{\tilde{D}_{ij}^3}}{\partial p} \to 0$ as $p \to 0$ (for error-function profiles).
2. $\overline{\tilde{D}_{ij}^n}$ at p where $\frac{\partial \overline{\tilde{D}_{ij}^3}}{\partial p} = 0$ (see Fig. 8).
3. $\overline{\tilde{D}_{ij}^n}$ at p = 0 (extrapolated) if $\frac{\partial \overline{\tilde{D}_{ij}^3}}{\partial p} \neq 0$ at any p (see Fig. 9).

This refined approach for the determination of average multicomponent interdiffusion coefficients can be applied to near-linear segment of the concentration profiles (e.g., Fig. 8). Applicability of this technique is currently being examined for small composition ranges and higher-order systems.

Summary

Importance of multicomponent-multiphase interdiffusion was highlighted with selected examples from materials and coatings employed in gas turbines and nuclear fuels. Alternative methods to determine interdiffusion fluxes, integrated interdiffusion coefficients, effective interdiffusion coefficients, average multicomponent interdiffusion coefficients were presented along with their applications for components in advanced energy production systems including oxidation resistance/thermal barrier coatings, Cr_2O_3-forming Ni-Cr alloys, and U-Pu-Zr alloys. Alternative approach to accurately assess composition-dependent interdiffusion coefficients is continuously being examined for multicomponent alloys.

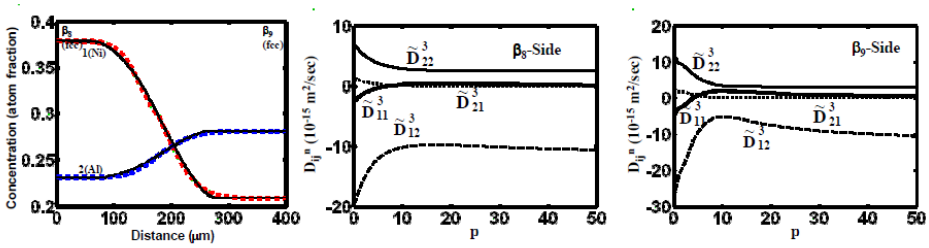

Fig. 8. Experimental (dotted lines) and calculated (solid lines) concentration profiles, and variation in $\tilde{D}_{ij}^3$ as a function of "p" on either side of the Matano plane for Fe-Ni-Al (B2) diffusion couples β_8 vs. β_9 annealed at 1000°C for 96 hours.

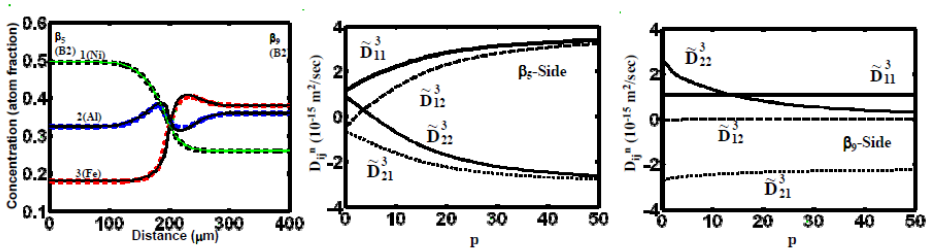

Fig. 9. Experimental (dotted lines) and calculated (solid lines) concentration profiles, and variation in $\tilde{D}_{ij}^3$ as a function of "p" on either side of the Matano plane for Fe-Ni-Al (B2) diffusion couples β_5 vs. β_9 annealed at 1000°C for 96 hours.

Acknowledgement

This paper highlights results obtained from programs that were financially supported by CAREER award from National Science Foundation (NSF-CAREER DMR-0238356), U.S. Department of Energy (DE-FC26-02NT41431 Subcontract No. 02-01-SR103), Idaho National Laboratory (DE-AC07-05ID14517 Subcontract No. 00051953), Solar Turbines Incorporated and Siemens Power Generation with technical assistance from Oak Ridge National Laboratory, General Electric Global Research Center, General Electric Aviation, Pratt & Whitney, and Howmet Research Corporation.

References

[1] C.T. Sims, N.S. Stoloff, W.C. Hagel: *Superalloys II* (John Wiley and Sons, 1987)
[2] R. Miller, J. Therm. Spray Technol. Vol. 6 (1997), p. 35
[3] A.G. Evans, D.R. Mumm, J.W. Hutchinson, G.H. Meier, F.S. Pettit: Prog. Mater. Sci. Vol. 46 (2001), p. 505
[4] N.P. Padture, M. Gell, E.H. Jordan: Science Vol. 296 (2002), p. 280
[5] R.D. Sisson, Jr., E.Y. Lee, Y.H. Sohn: Proc. PRICM-2, (1995), p. 1203
[6] Y.H. Sohn, J.H. Kim, E. Jordan, M. Gell: Surf. Coat. Technol. Vol. 146/7 (2001), p. 70
[7] Y.H. Sohn, M.A. Dayananda, G.L. Hofman, R.V. Strain, S.L. Hayes: J. Nucl. Mater. Vol. 279 (2000), p. 317
[8] D.D. Keiser, Jr., S.L. Hayes, M.K. Meyer, C.R. Clark: J. Metals (JOM) Vol. 55 (2003), p. 55

[9] H.J. Ryu, J.M. Park, C.K. Kim, Y.S. Kim, G.L. Hofman: J. Phase Equil. Diff. (2006) in Press
[10] L. Onsager: Ann. NY Acad. Sci. Vol. 46 (1965), p. 241
[11] J.S. Kirkaldy, D.J. Young: *Diffusion in Condensed State* (The Institute of Metals – London, 1987)
[12] J. Philibert: Atom Movements (Les Editions de Physique, 1991)
[13] M.A. Dayananda, C.W. Kim: Metall. Trans. A Vol. 10A (1979), p. 1333
[14] C.W. Kim, M.A. Dayananda: Metall. Trans. A Vol. 15A (1984), p. 649
[15] M.A. Dayananda, D.A. Behnke: Scripta Metall. Vol. 25 (1991), p. 2187
[16] M.A. Dayananda: Metall. Mater. Trans. A Vol. 27A (1996), p. 2504
[17] M.A. Dayananda, Y.H. Sohn: Metall. Mater. Trans. A Vol. 30A (1999), p. 535
[18] Y.H. Sohn, M.A. Dayananda: Acta Mater. Vol. 48 (2000), p. 1427
[19] P. Kofsted: *High Temperature Corrosion* (Elsevier – London, 1980)
[20] J.L. Smialek, C.A. Barret, J.C. Schaffer: *ASM Metals Handbook: Design for Oxidation Resistance* (ASM International, 1997)
[21] D.P. Whittle, J. Stringer: Trans. Royal Soc. London A Vol. 295 (1980), p. 309
[22] F.H. Stott, G.C. Wood, M.G. Hobby, Oxi. Metals Vol. 3 (1971), p. 103
[23] J.A. Nesbitt, R.W. Heckel, Metall. Trans. A Vol. 18A (1987), p. 2061

Oxid Met (2007) 68:97–111
DOI 10.1007/s11085-007-9063-0

ORIGINAL PAPER

Microstructure and Residual Stress of Alumina Scale Formed on Ti_2AlC at High Temperature in Air

J. W. Byeon · J. Liu · M. Hopkins · W. Fischer · N. Garimella · K. B. Park · M. P. Brady · M. Radovic · T. El-Raghy · Y. H. Sohn

Received: 22 December 2006 / Revised: 16 April 2007 / Published online: 7 June 2007

Abstract Ti_2AlC ternary carbide is being explored for various high temperature applications due to its strength at high temperatures, excellent thermal-shock resistance, and high electrical conductivity. A potential advantage of Ti_2AlC over conventional Al_2O_3-forming materials is the near-identical coefficient of thermal expansion (CTE) of Ti_2AlC and α-Al_2O_3, which could result in superior spallation resistance and make Ti_2AlC a promising option for applications ranging from bondcoats for thermal barrier coatings to furnace heating elements. In this study,

J. W. Byeon · J. Liu · M. Hopkins · N. Garimella · Y. H. Sohn (✉)
Advanced Materials Processing and Analysis Center and Department of Mechanical, Materials and Aerospace Engineering, University of Central Florida, Orlando, FL, USA
e-mail: ysohn@mail.ucf.edu

W. Fischer
University High School, Orange County Public Schools, Central Florida Space Science Institute through National Science Foundation (NSF) Research Experience for Teachers (RET) Program, Orlando, FL, USA

K. B. Park
Department of Materials Science and Engineering, Andong National University, Andong, Kyungbuk, Korea

M. P. Brady
Materials Science and Technology Division, Oak Ridge National Laboratory, Oak Ridge, TN, USA

M. Radovic
Deparment of Mechanical Engineering, Texas A&M University, College Station, TX, USA

T. El-Raghy
3-one-2, LLC, Voorhees, NJ, USA

Present Address:
J. W. Byeon
Materials Science and Engineerings, University of Ulsan, Ulsan, Kyungnam, Korea

isothermal and cyclic oxidation were performed in air to examine the oxidation behavior of Ti_2AlC. Isothermal oxidation was performed at 1000, 1200 and 1400 °C for up to 25 h and cyclic oxidation consisted of 1,000 1-hour cycles at 1200 °C. Characteristics of the oxide scale developed in air, including mass change, residual stress in the α-Al_2O_3 scale, phase constituents and microstructure, were examined as functions of time and temperature by thermogravimetry, photostimulated luminescence, x-ray diffraction, scanning electron microscopy, and transmission electron microscopy via focused ion beam in situ lift-out. Above a continuous and adherent α-Al_2O_3 layer, a discontinuous-transient rutile-TiO_2 scale was identified in the oxide scale developed at 1000 and 1200 °C, while a discontinuous-transient Al_2TiO_5 scale was identified at 1400 °C. The continuous α-Al_2O_3scale thickened to more than 15 μm after 25 h of isothermal oxidation at 1400 °C, and after 1,000 1-hour cycles at 1200 °C, yet remained adherent and protective. The compressive residual stress determined by photoluminescence for the α-Al_2O_3 scale remained under 0.65 GPa for the specimens oxidized up to 1400°C for 25 hours. The small magnitude of the compressive residual stress may be responsible the high spallation-resistance of the protective α-Al_2O_3 scale developed on Ti_2AlC, despite the absence of reactive element additions.

Keywords Ti_2AlC · Coefficient of thermal expansion · Ternary carbide · Oxidation · Residual stress · Photoluminescence spectroscopy · Transmission electron microscopy

Introduction

The MAX phases are ternary compounds such as Ti_3SiC_2, Ti_3AlC_2, Ti_2AlC, and Ti_2AlN that consist of an early transition metal (M), a IIIA or IVA element (A), and nitrogen or carbon as a third element (X). MAX phases can possess a combination of metallic and ceramic behaviors: good high temperature strength, machinability, excellent thermal shock resistance, good electrical/thermal conductivity, good oxidation resistance, low density and low thermal expansion coefficient [1–11]. Thus, fabrication processes and properties of various MAX phases are being explored for various high temperature applications ranging from bondcoats for thermal barrier coatings to furnace heating elements. Of the phases in the Ti–Al–C ternary system, Ti_2AlC has the lowest density, about 4.11 g/cm^3, and is one of the most thermodynamically stable [12]. Following the successful fabrication of fully-dense polycrystalline Ti_2AlC [13–15], its mechanical and electrical properties have been investigated with regard to high temperature applications [14, 15].

Oxidation resistance is one of the critical properties of MAX phases for high temperature applications [16–18]. Wang et al. [8, 19] reported that the oxidation resistance of Al_2O_3-forming Ti_3AlC_2 was superior to that of SiO_2-forming Ti_3SiC_2. Sundberg et al. [20] have also reported the oxidation kinetics and phase constituents of the scale.

In this paper, we examined the characteristics of the oxide scale formed during isothermal and cyclic oxidation of Ti_2AlC at high temperatures ranging from 1000 to 1400 °C in air. The characteristics of the oxide scale analyzed include: (1) mass-

gain continuously determined by thermo-gravimetric analysis as a function of time of oxidation; (2) residual stress in the α-Al_2O_3 scale determined by non-destructive photostimulated luminescence (PL) spectroscopy, and (3) microstructural development of the phase constituents in the oxide scale by x-ray diffraction (XRD) and cross-sectional electron microscopy including scanning electron microscopy (SEM) and transmission electron microscopy (TEM) via focused ion beam in situ lift-out (FIB-INLO) specimen preparation [21]. This study focused on how the relatively low CTE of Ti_2AlC, nearly identical to α-Al_2O_3, would affect the scale residual stress and spallation resistance. This was of particular interest because conventionally available Fe- and Ni-base Al_2O_3 forming alloys have relatively high CTE's and typically require reactive element additions to improve the spallation resistance [22].

Experimental Procedure

Rods of polycrystalline Ti_2AlC [13–15] with a diameter of 15 mm were supplied by 3-ONE-2^{TM}, LLC, USA (Vorhees, NJ, USA). Impurity content in Ti_2AlC was analyzed by glow-discharge mass spectroscopy and interstitial gas analysis (Shiva Technologies, Evans Analytical Group, Syracuse, NY 13211). Tabulated results are presented in Table 1. The Ti_2AlC rods were sectioned into 1 mm thick disks by using a low-speed diamond wafering blade. Both sides of each disk were polished with SiC paper (600 grit). Kinetics of oxidation was examined at 1000, 1200, and 1400 °C in air by thermo-gravimetric analysis (TGA) using TA Instrument^{TM} (New Castle, DE, USA) STS1100. Specimens were placed in an alumina crucible and were heated at a rate of 20 °C per minute to desired temperature while purging Ar at a rate of 100 mL per minute to minimize any oxidation during heating. Upon reaching the specified temperature, purging Ar was replaced with air. Mass change

Table 1 Impurity content in as-received Ti_2AlC analyzed by glow-discharge mass spectroscopy and interstitial gas analysis (Shiva Technologies, Evans Analytical Group, Syracuse, NY 13211)

Concentration	Impurity Constituents
2.5 wt.%	Sr
2.2 wt.%	O*
1.1 wt.%	Fe, Mo
< 1000 ppm wt.	N*, Si, Y,
< 100 ppm wt.	P, Cl, V, Cr, Mn, Ni, Ga, Cu, Zr, Nb, Hf, Ta, W
< 10 ppm wt.	B, S*, Mg, K, Ca, Co, As, Se, Rb, Ag, Sn, Sb, Ba, Pb
< 1.0 ppm wt.	Na, Ge, Br, Rh, Pd, Cd, La, Re, Pt, Bi
< 0.1 ppm wt.	F, Sc, Zn, Ru, Te, Ir, Au, Hg, U
< 0.01 ppm wt.	Li, Be, Cs, Ce, Pr, Nd, Sm, Eu, Gd, Tb, Dy, Ho, Er, Tm, Yb, Lu, Os, Tl, Th

Note: * denotes results from interstitial gas analysis

due to oxidation, normalized by the initial mass, was continuously recorded as a function of time at each temperature.

In addition, isothermal oxidation in air at 1000, 1200, and 1400 °C as a function of time, ranging from 30 s up to 25 h, was carried out using a CM^{TM} Rapid Temperature Furnace (Bloomfield, NJ, USA) where each temperature was forced-air-quenched to room temperature. Cyclic oxidation at 1200 °C in air was also carried out using specimens suspended by Pt wire in a vertical furnace. Mass change was measured as a function of number of thermal cycles up to 1,000 cycles. The 1-hour thermal cycle consists of 10-minute heat-up, 1-hour dwell at 1200 °C, and 10-minute forced-air-quench.

The residual stress in the α-Al_2O_3 scale developed after isothermal and cyclic oxidation was determined by PL spectroscopy [23]. A Renishaw (Gloucestershire, United Kingdom) 1000B Ramanscope^{TM} with Ar-ion laser source (wavelength of 514 nm) for the optical excitation, charge-coupled device (CCD) detectors, and a software package (GRAMS^{TM}) for spectrum analysis, was used. Luminescence spectra were collected at room temperature from over 15 randomly selected locations for each specimen. The magnitude of shift in luminescence was analyzed to determine the residual stress in the α-Al_2O_3 scale [23].

Microstructure of the oxide scale was characterized by XRD, SEM, TEM and scanning TEM (STEM). Detailed cross-sectional microstructure of the scale was observed by Philips/Tecnai (FEI Company, Hillsboro, OR, USA) F30^{TM} 300 KeV TEM using selected-area electron diffraction (SAD), high angle annular dark field (HAADF) imaging, and X-ray energy dispersive spectroscopy (XEDS). Focused ion beam in situ lift-out technique (FIB-INLO) was employed to prepare site-specific cross-sectional TEM specimens of thin and brittle oxide scale [21].

Results and Discussion

Overall Kinetics of Oxidation

Figure 1(a) shows normalized weight change of Ti_2AlC as a function of oxidation time at 1000, 1200C, and 1400 °C in air. Wang et al. [14] reported cubic-rate for the oxidation of Ti_2AlC for a temperature range from 1000 to 1300 °C in air, while Sunderberg et al. [15] reported parabolic rate of oxidation at 1100, 1200, 1300 °C in air. Our study finds that although a cubical growth rate of an oxide scale may best represent the overall oxide growth kinetics of Ti_2AlC as presented in Fig. 1(b), such a simple description of growth kinetics based on simple rate constant, regardless of whether it is parabolic or cubic, may not be sufficient since three oxide-phases co-exist in the scale (see Fig. 3).

Figure 2 shows the changes in specific mass gain of Ti_2AlC with 1-hour thermal cycling at 1200 °C in air compared with benchmark Al_2O_3-forming oxidation-resistant alloys. Although the rate of mass gain is the highest for Ti_2AlC, the observed rate under these aggressive test conditions is still low (and protective). More importantly, mass loss due to scale spallation was not observed during cyclic oxidation up to 1,000 cycles indicating a high degree of spallation resistance

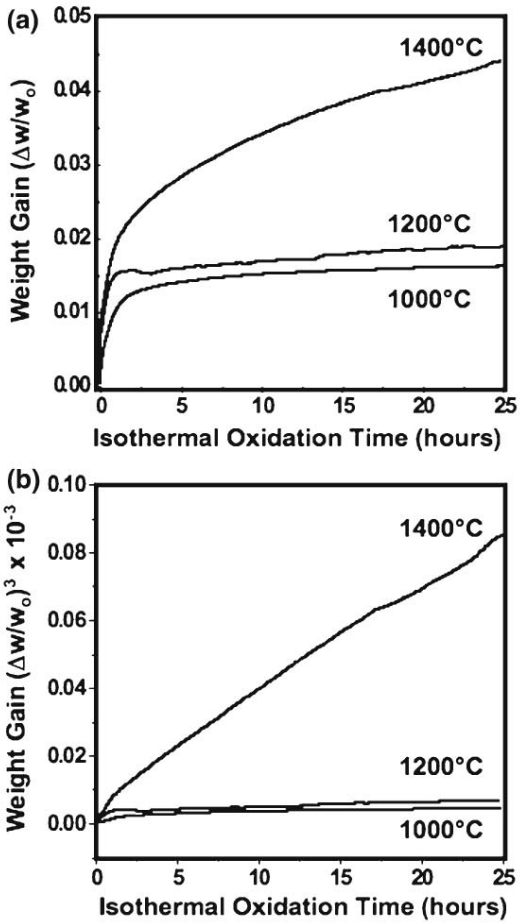

Fig. 1 (**a**) Normalized weight change of Ti_2AlC as a function of oxidation time at 1000, 1200 and 1400 °C. (**b**) Cubical growth rate of the oxide scale best describes the overall growth kinetics

superior to that of un-doped NiAl, Hf-doped Ni_3Al, Y/Hf-doped NiCrAl, as presented in Fig. 2 [24].

Phase Constituents and Microstructure of the Oxide Scale

Figure 3 presents XRD patterns from the oxide scale formed after isothermal oxidation at 1200 and 1400 °C. All specimens prior to oxidation consist of Ti_2AlC, although trace amounts of Ti_3AlC_2 were observed via electron microscopy. XRD patterns from the oxide scale formed at 1000 °C are similar to those obtained from specimens oxidized at 1200 °C with the main difference being the lower intensity from oxide phases. At 1000 and 1200 °C, both rutile-TiO_2 and α-Al_2O_3 scales formed in accordance with Wang et al. [19]. No residual meta-stable Al_2O_3 was detected even in the specimen oxidized for 30 min at 1200 °C as shown in Fig. 3(a). With an increase in time of oxidation, the intensity of XRD peaks associated with

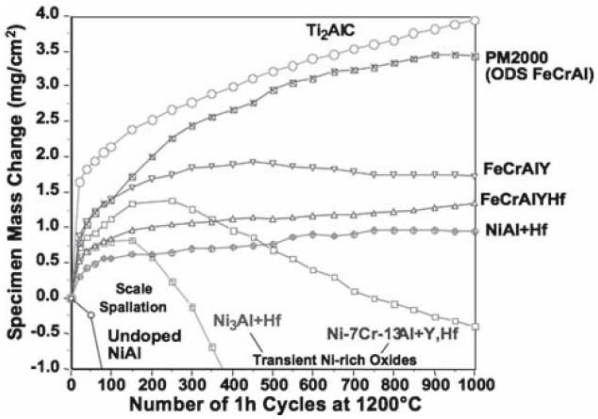

Fig. 2 Mass changes per unit area for various Al_2O_3-forming alloys during thermal cyclic oxidation at 1200 °C

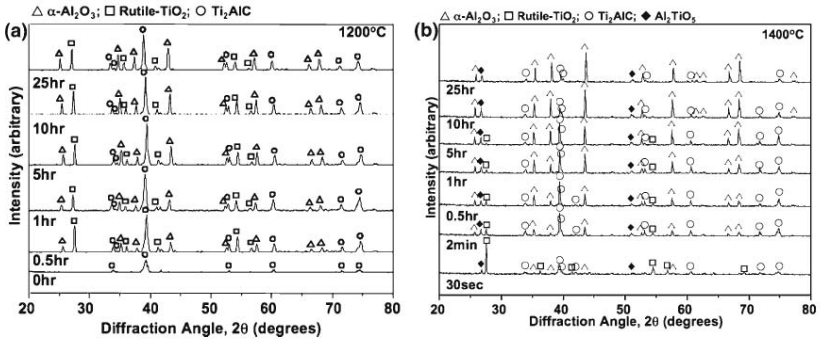

Fig. 3 X-ray diffraction patterns from the oxide scale formed on Ti_2AlC as a function of time of isothermal oxidation at (**a**) 1200 °C and (**b**) 1400 °C

α-Al_2O_3 increased while that of rutile-TiO_2 remained the same after transient formation during the initial stage of oxidation.

The Al_2TiO_5 phase in the oxide scale was observed in the specimens oxidized at 1400 °C as shown in Fig. 3(b). XRD peaks from rutile-TiO_2 decreased in intensity with time of oxidation at 1400 °C and disappeared after 10 h of oxidation at 1400 °C. The Al_2TiO_5 can form by a solid-state reaction of Al_2O_3 and TiO_2 with a very low free energy of formation at temperatures above 1300 °C [25]. Figure 4 shows the XRD pattern of Ti_2AlC after 1,000 1-hour thermal cycles at 1200 °C. Similar to the isothermal oxidation at 1200°C, formation of rutile-TiO_2 and α-Al_2O_3

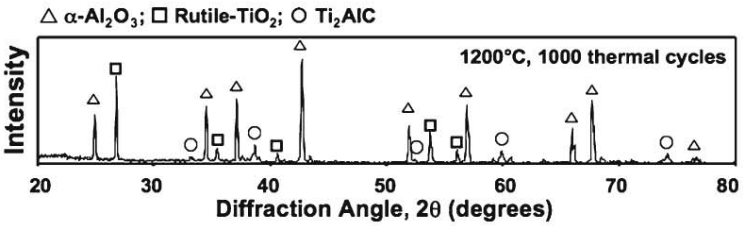

Fig. 4 X-ray diffraction pattern from the oxide scale formed on Ti_2AlC after 1,000 thermal cycles of oxidation at 1200 °C with the dwell time of 1 h

was observed. The diffraction peaks of α-Al_2O_3 were very intense relative to those of rutile-TiO_2 after prolonged growth of thick α-Al_2O_3 scale.

For Ti_2AlC, the oxide scale developed after isothermal oxidation at 1000 and 1200 °C consisted of an inner Al-rich continuous scale and an outer Ti-rich discontinuous scale as shown by backscatter electron micrographs in Fig. 5. Formation of Ti_3AlC_2 due to depletion of Al and a few localized regions of internal oxidation (presumably due to pores within Ti_2AlC) was observed near the surface. Based on EDS analysis of the scale, the lighter gray region below the epoxy mount is the Ti-rich discontinuous scale and the darker gray layer underneath is the Al-rich continuous scale as indicated in Fig. 5(c). The inner Al-rich scale looks dense and adherent to Ti_2AlC. Based on the XRD analysis presented in Fig. 3 and EDS analysis, the inner and outer scales can be identified as α-Al_2O_3 and rutile-TiO_2, respectively. Two distinctive morphologies of the oxide scale were observed from

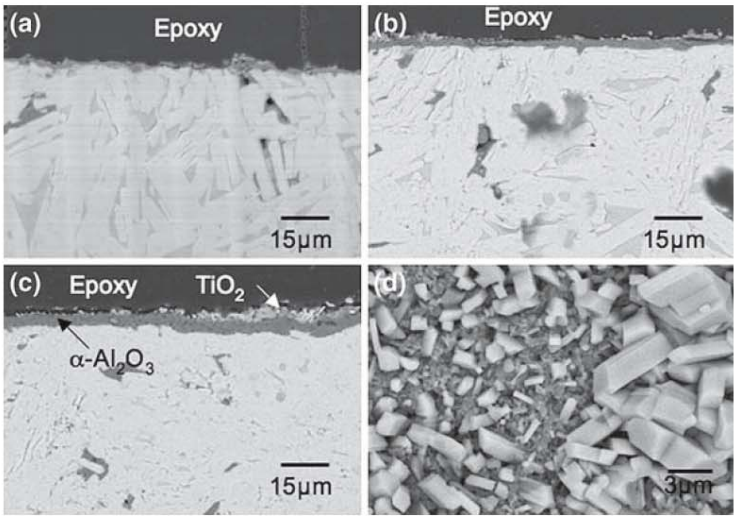

Fig. 5 Cross-sectional backscatter electron micrographs of oxide scale developed on Ti_2AlC after isothermal oxidation at 1200 °C for (**a**) 1 (**b**) 5 and (**c**) 25 h. (**d**) Two distinctive morphologies of the oxide scale were observed from the top surface of oxidized Ti_2AlC at 1200 °C for 25 h

the top surface of the specimens oxidized at 1200 °C for 25 h as presented in Fig. 5(d). Large bright grains on top and small dark ones underneath correspond to rutile-TiO_2 and α-Al_2O_3, respectively.

Cross-sectional backscatter electron micrographs and EDS from the oxide scale formed on the specimens oxidized at 1400 °C for 30 s up to 25 h are presented in Fig. 6. Like Ti_2AlC oxidized at 1000 and 1200 °C, the inner continuous scale was rich in Al. However, the outer discontinuous scale for specimens oxidized at 1400 °C consisted of Al/Ti-rich $TiAl_2O_5$ scale as presented in Fig. 6(d). The protective α-Al_2O_3 scale formed at 1400 °C was adherent and grew as thick as approximately 20 μm without apparent spallation after oxidation for 25 h as shown in Fig. 6(c). A few internally oxidized particles were observed at all temperatures as presented in Figs. 5 and 6.

No spallation was observed for the α-Al_2O_3 scale as thick as 15 μm formed during 1,000 1-hour thermal cycles at 1200 °C as presented by backscatter electron micrograph in Fig. 7. This microstructural observation supports the result of a continuous increase in mass with thermal cycling presented in Fig. 2.

Detailed cross-sectional microstructure of the oxide scale developed during the initial isothermal oxidation at 1400 °C for 30 s was examined by TEM as shown in Fig. 8. In accordance with XRD and SEM results, the oxide scale consisted of a continuous α-Al_2O_3 layer near to Ti_2AlC, and a mixed oxides layer of rutile-TiO_2 and Al_2TiO_5 phases above the protective α-Al_2O_3 scale. For the Ti_3AlC_2 sample oxidized at 1400 °C, it was reported [8] that voids and Al_2TiO_5 complex oxide particles formed at the interface between α-Al_2O_3 scale and Ti_3AlC_2 substrate. However, in this study, no void was observed along the interface between Ti_2AlC

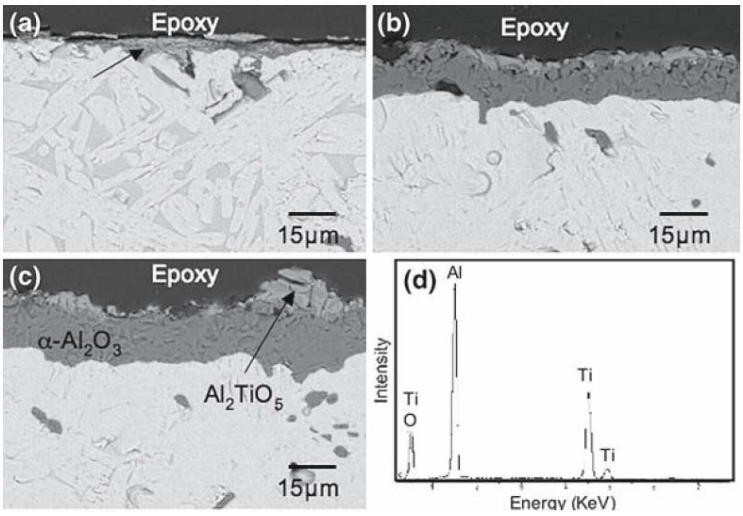

Fig. 6 Cross-sectional backscatter electron micrographs of oxide scale developed on Ti_2AlC after isothermal oxidation at 1400 °C for (**a**) 30 s (**b**) 5 and (c) 25 h. (d) The TiO_2 external scale reacted with Al_2O_3 to form Al_2TiO_5 based on EDS

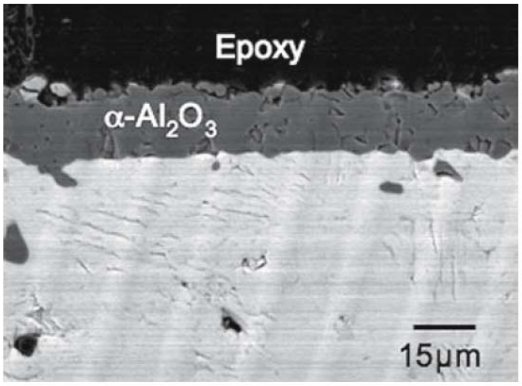

Fig. 7 Cross-sectional backscatter electron micrographs of oxide scale developed on Ti_2AlC after 1,000 thermal cycles of oxidation at 1200 °C with the dwell time of 1 h

and continuous α-Al_2O_3 scale, although chained-voids existed at the interface between continuous α-Al_2O_3 layer and the thin-transient mixed oxide layer. This work suggests that the oxidation resistance of Ti_2AlC may be better than that of Ti_3AlC_2 under the oxidation conditions employed in this study.

Photoluminescence and Residual Stress of the Oxide Scale

PL spectroscopy was utilized to determine the residual stress in the α-Al_2O_3 scale. For all oxidized Ti_2AlC specimens, ruby luminescence (R_1 and R_2) from α-Al_2O_3 was observed without any observable luminescence from metastable polymorphs (i.e., θ-Al_2O_3 and γ-Al_2O_3). Figure 9 shows typical PL spectra as a function of oxidation time at 1000 °C. The frequency of R_1 and R_2 shifted to lower wavenumber than those of standard ruby luminescence (i.e., 14402 and 14432 cm^{-1}, respectively). This indicates that the scale is under residual compression [23].

The magnitude of compressive residual stress within the α-Al_2O_3 scale was examined as a function of temperature and time of isothermal oxidation as reported in Table 2 and presented in Fig. 10. The magnitude of compressive residual stress within the α-Al_2O_3 scale determined after 1,000 thermal cycles at 1200 °C is also presented in Fig. 10. The method to calculate the magnitude of residual stress, based on frequency shift via piezospectrospic coefficients, has been developed for the α-Al_2O_3 scale without any presence of other oxides [23]. Thus, in this study, the calculation of the compressive residual stress determined for the α-Al_2O_3 assumes that the presence of other oxide phases such TiO_2 and Al_2TiO_5 does not effect the assumptions employed in calculation.

Overall, the magnitude of compressive residual stress was at most 0.65 GPa for Ti_2AlC specimen oxidized at 1400 °C as reported in Fig. 10. This value is much smaller than 2–5 GPa reported for other α-Al_2O_3-forming high temperature materials and coatings such as FeCrAlY [26] and NiAl [27]. The standard deviation in the magnitude of the compressive residual stress, based on minimum of 15 measurements at random locations, was very small for all specimens as reported in Table 2. The small (i.e., magnitude) and homogeneous (i.e., small standard

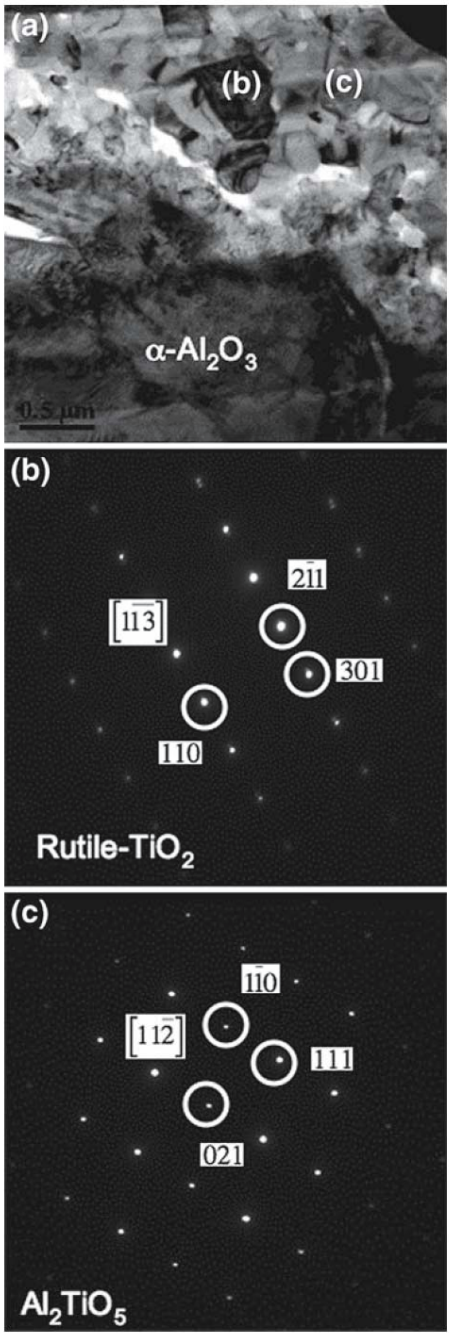

Fig. 8 (**a**) Cross-sectional bright-field image of oxide scale developed on Ti_2AlC after isothermal oxidation at 1400 °C for 30 s. The scale consisted of α-Al_2O_3, (**b**) rutile-TiO_2 and Al_2TiO_5

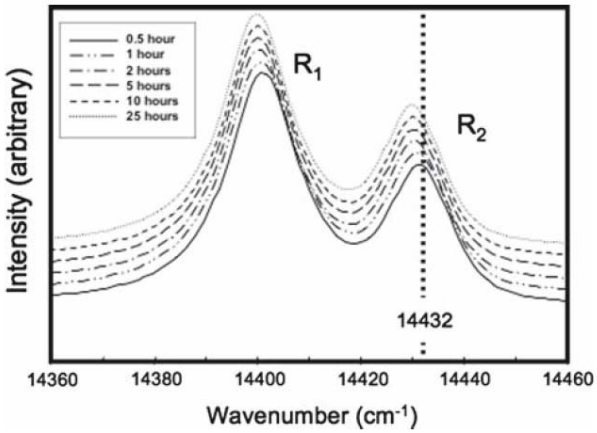

Fig. 9 Typical photoluminescence spectra from the α-Al_2O_3 scale on Ti_2AlC as a function of time of isothermal oxidation at 1000 °C

deviation) compressive residual stress of the α-Al_2O_3 scale is considered to play a significant role in the excellent adherence of the scale that has a thickness of over 15 μm after cyclic oxidation of 1,000 1-hour cycles at 1200 °C and isothermal oxidation of 25 h at 1400 °C.

The small magnitudes of compressive residual stress in the α-Al_2O_3 formed on Ti_2AlC may be explained by a simple estimation of thermal stress induced upon cooling due to thermal expansion mismatch between Al_2O_3 and Ti_2AlC substrate. Thermal stress within the oxide scale is estimated by [28]:

$$\sigma_{ox} = -\frac{E_{ox}}{(1-\upsilon_{ox})}\frac{(\alpha_{ox}-\alpha_s)\Delta T}{1+\frac{E_{ox}(1-\upsilon_s)}{E_s(1-\upsilon_{ox})}\frac{h_{ox}}{h_s}} \quad (1)$$

where, σ, E, υ, α, ΔT, and h represent thermal stress, Young's modulus, Poisson's ratio, thermal expansion coefficient, temperature difference upon cooling, and thickness, respectively. The subscripts ox and s refer to oxide scale and substrate, respectively. Thermal expansion coefficient of Ti_2AlC was determined as 9.62×10^{-6}/K from dilatometer measurement in the temperature range up to 1000 °C as shown in Fig. 11. This is significantly lower than conventional Fe- and Ni-base Al_2O_3-forming alloys, which can have CTE's in excess of 15×10^{-6}/K at high temperature [29]. Thermal expansion coefficients of α-Al_2O_3 available in the published literature range from 7×10^{-6}/K to 9×10^{-6}/K depending on the crystallographic direction, temperature range investigated, and investigator [30]. The temperature dependence of Young's modulus and Poisson's ratio and thermal expansion coefficient was not considered for this simple approximation. For the calculation, the selected values of $E_{ox} = 400$ GPa [26], $E_s = 210$ GPa [31], $v_{ox} = 0.25$ [26], $v_s = 0.2$ [31], $h_s = 1$ mm, $\alpha_{ox} = 8.5 \times 10^{-6}$/K [30] were used. The calculated values at $h_{ox} = 5$ μm as a function of temperature difference, ΔT is presented in

Table 2 Compressive residual stress determined based on photostimulated luminescence (PL) for α-Al_2O_3 scale developed on Ti_2AlC as a function of time and temperature

Temperature (°C)	Time (hours)	Compressive residual stress measured by PL (GPa)	
		Average	Stdev
1000	0.5	0.088	0.068
	1	0.179	0.107
	2	0.268	0.061
	5	0.287	0.042
	10	0.313	0.061
	25	0.357	0.036
1200	0.5	0.504	0.075
	1	0.536	0.078
	2	0.590	0.040
	5	0.495	0.059
	10	0.409	0.032
	25	0.370	0.032
	1000 (cyclic)	0.338	0.046
1400	0.008 (0.5 min)	0.274	0.064
	0.033 (2 min)	0.608	0.067
	0.167 (10 min)	0.621	0.060
	0.5	0.626	0.065
	1	0.614	0.058
	2	0.599	0.063
	5	0.541	0.069
	10	0.490	0.074
	25	0.510	0.084

Fig. 12. In general, the magnitude calculated by Eq. (1) is slightly greater than that measured by PL, but is still lower than 1 GPa. The magnitude of compressive residual stress determined by PL increased with temperature of oxidation as presented in Fig. 10. It should be noted that the magnitude of compressive residual stress was observed to increase abruptly during the initial oxidation as presented in Fig. 10. The changes in the magnitude of compressive residual stress may be related to the growth stress during oxidation and stress-relaxation by creep.

Since the magnitude of compressive residual stress measured by PL is always smaller than that calculated using Eq. (1), the difference in residual stress within the scale may be interpreted as tensile growth stress, assuming that the creep relaxation during the air-quench is negligible. The tensile growth stress within the oxidation scale has been related to θ-to-α Al_2O_3 transformations [32, 33], although PL in this study did not observe any presence of metastable form of Al_2O_3 at any time, and the difference in residual stress persists throughout high tempeature oxidation.

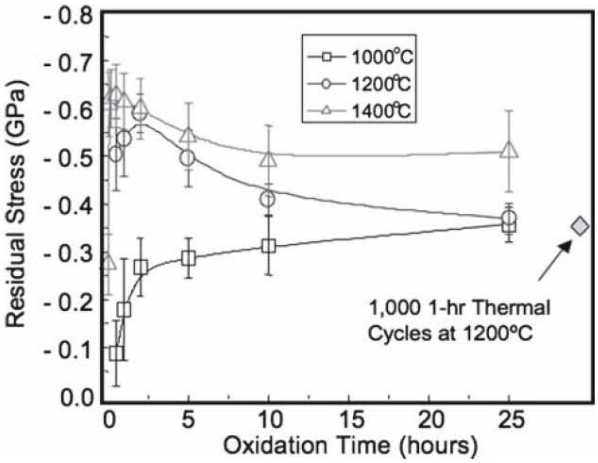

Fig. 10 Magnitude of compressive residual stress within the α-Al_2O_3 scale on Ti_2AlC determined based on luminescence-shift as a function of time of isothermal oxidation at 1000, 1200 and 1400 °C

Fig. 11 Thermal expansion coefficient as a function of temperature determined for Ti_2AlC using dilatometer measurement

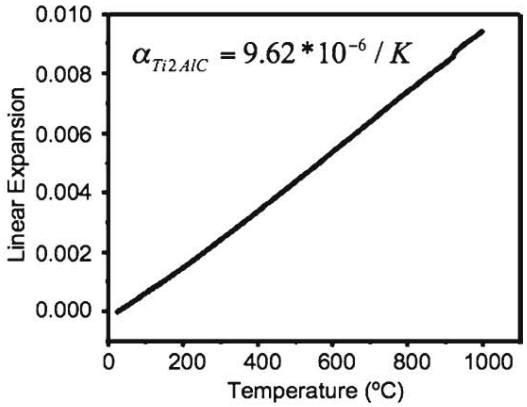

Summary

Oxide scales formed during isothermal and cyclic oxidation in air at 1000, 1200 and 1400 °C were characterized to examine the oxidation resistance of Ti_2AlC for high temperature applications. A continuous α-Al_2O_3 scale and a transient and isolated rutile-TiO_2 scale were found to form during isothermal oxidation in air at high temperature. At 1400 °C, transient Al_2TiO_5 phase was also observed. Protective α-Al_2O_3 scale exhibited excellent adherence with Ti_2AlC even after isothermal oxidation at 1400 °C for 25 h, and 1,000 1-hour thermal cycles at 1200 °C. This behavior is consistent with reports by Sundberg et al. [20] who also showed excellent spallation resistance and promise for furnace element applications.

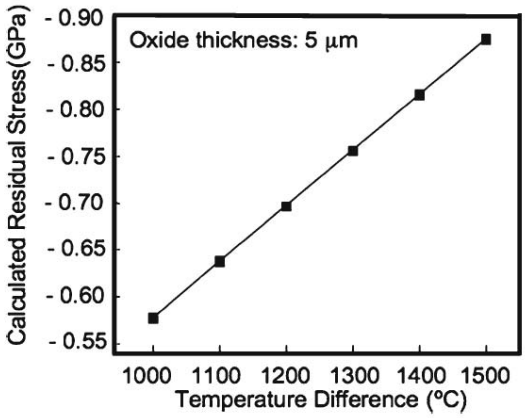

Fig. 12 Estimated magnitude of compressive residual stress within the α-Al_2O_3 scale on Ti_2AlC

No voids were observed at the interface between Ti_2AlC/α-Al_2O_3. The compressive residual stress for the α-Al_2O_3 scale determined by PL was homogeneous and very small in magnitude (less than 0.65 GPa) for both isothermal and cyclic oxidation likely due to similar thermal expansion coefficients of Ti_2AlC and α-Al_2O_3. These behaviors should make Ti_2AlC of particular interest for applications requiring oxidaton/spallation resistance. Recent work has also shown excellent adhesive strength of Al_2O_3 film on Ti_2AlC and Ti_3AlC_2 [34].

Acknowledgements The authors would like to thank Dr. B.A. Pint for assistance with cyclic oxidation testing and comparison data. J. Liu and W. Fischer have contributed to this study as an Amelia Earhart Fellow of Zonta International and a participant of NSF-RET program at UCF (EEC-0401926), respectively. M. P. Brady was funded at ORNL under the Fossil ARM program. ORNL is managed by UT-Battelle, LLC for the U.S. DOE under contract DE-AC05–00OR22725. Y. H. Sohn would also like to acknowledge financial support from NSF CAREER award (DMR-0238356). Assistant from Ms. Ashley Ewh, an undergraduate research assistant at UCF on manuscript preparation is sincerely appreciated.

References

1. M. W. Barsoum, and T. El-Raghy, *American Scientist* **89**, 334 (2001).
2. M. W. Barsoum, *Progress in Solid State Chemistry* **28**, 201 (2000).
3. M. W. Barsoum, and T. El-Raghy, *Journal of the American Ceramic Society* **79**, 1953 (1996).
4. M. W. Barsoum, T. El-Raghy, and L. U. J. Ogbuji, *Journal of the Electrochemical Society* **144**, 2508 (1997).
5. Z. M. Sun, Y. C. Zhou, and M. S. Li, *Corrosion Science* **43**, 1095 (2001).
6. Y. W. Bao, J. X. Chen, X. H. Wang, and Y. C. Zhou, *Journal of the European Ceramic Society* **24**, 855 (2004).
7. X. H. Wang, and Y. C. Zhou, *Acta Materialia* **50**, 3141 (2002).
8. X. H. Wang, and Y. C. Zhou, *Corrosion Science* **45**, 891 (2003).
9. Z. J. Lin, M. J. Zhuo, Y. C. Zhou, M. S. Li, and J. Y. Wang, *Scripta Materialia* **54**, 1815 (2006).
10. M. W. Barsoum, and M. Radovic, in Encyclopedia of Materials Science and Technology. K. H. J. Buschow, R. W. Cahn, M. C. Flemings, E. J. Kramer, S. Mahajan, P. Veyssiere, eds. (Elsevier Science).
11. R. Radovic, M. W. Barsoum, T. El-Raghy, S. Wiederhorn, and Luecke W, *Acta Materialia* **50**, 1297 (2002).
12. M. A. Pietzka, and J. C. Schuster, *Journal of Phase Equilibrium* **15**, 392 (1994).

13. M. W. Barsoum, D. Brodkin, and T. El-Raghy, *Scripta Materialia* **36**, 535 (1997).
14. M. W. Barsoum, M. Ali, and T. El-Raghy, *Metallurgical and Materials Transactions* A **A31**, 1857 (2000).
15. X. H. Wang, and Y. C. Zhou, *Zeitschrift fur MetaIlkunde* **93**, 66 (2002).
16. M. W. Barsoum, *Journal of the Electrochemical Society* **148**, C544 (2001).
17. M. W. Barsoum, N. Tzenov, A. Procopio, T. El-Raghy, and M. Ali, *Journal of the Eletrochemical Society* **148**, C551 (2001).
18. M. W. Barsoum, L. H. Ho-Duc, M. Radovic, andT. El-Raghy, *Journal of the Electrochemical Society* **150**, B166 (2003).
19. X. H. Wang, and Y. C. Zhou, *Oxidation of Metals* **59**, 303 (2003).
20. M. Sundberg, G. Malmqvist, A. Magnusson, and T. El-Raghy, *Ceramics International* **30**, 1899 (2004).
21. S. Laxman, B. Franke, B. W. Kempshall, Y. H. Sohn, L. A Giannuzzi, and K. S. Murphy, *Surface and Coatings Technology* **177–178**, 121 (2004).
22. B. A. Pint, *Oxidation of Metals* **45**, 1 (1996).
23. Q. Ma, and D. R. Clarke, *Journal of the American Ceramic Society* **77**, 298 (1994).
24. B. Pint, Unpublished Research.
25. B. Freudenberg, *Journal of the American Ceramic Society* **70**, 1 (1987).
26. V. K. Tolpygo, J. R. Dryden, and D. R. Clarke, *Acta Materialia* **46**, 927 (1998).
27. N. Mu, J. Liu, J. W. Byeon, Y. H. Sohn, and Y. L. Nava, *Surface and Coatings Technology* **188–189**, 27 (2004).
28. C. Liu, A. M. Huntz, and J. L. Lebrun, *Materials science & Engineering* A **A160**, 113 (1993).
29. I. G. Wright, B. A. Pint, and P. F. Tortorelli, *Oxidation of Metals* **55**, 333 (2001).
30. R. G. Munro, *Journal of the American Ceramic Society* **80**, 1919 (1997).
31. P. Finkel, M. W. Barsoum, and T. El-Raghy, *Journal of Applied Physics* **87**, 1701 (2000).
32. P. F. Tortorelli, K. L. More, E. D. Specht, B. A. Pint, and P. Zschack, *Materials at High Temperatures* **20**, 303 (2003).
33. B. W. Veal, A. P. Paulikas, and R. C. Birtcher, *Applied Physics Letters* **89**, 161916 (2006).
34. Z. J. Lin, M. J. Zhuo, Y. C. Zhou, M. S. Li, and J. Y. Wang, *Journal of the American Ceramic Society* **89**, 2964 (2006).

Defect and Diffusion Vol. 266 (2007) pp 191-198
online at http://www.scientific.net

Online available since 2007/Sep/04

Interdiffusion in (fcc) Ni-Cr-X (X = Al, Si, Ge or Pd) Alloys at 700°C

N. Garimella[1, a], M.P. Brady[2, b] and Y.H. Sohn[1, c]

[1]Advanced Materials Processing and Analysis Center and Department of Mechanical, Materials and Aerospace Engineering, University of Central Florida, Orlando, FL, USA.

[2]Metals and Ceramics Division, Oak Ridge National Laboratory, Oak Ridge, TN, USA.

[a]garimella_n@yahoo.com, [b] bradymp@ornl.gov, [c] ysohn@mail.ucf.edu

Keywords: Boltzmann/Matano analysis, diffusion couples, diffusion coefficients, experimental, interdiffusion, multicomponent alloys, ternary system.

Abstract. Interdiffusion at 700°C for Ni-22at.%Cr (fcc γ phase) alloys with small additions of Al, Si, Ge, or Pd was examined using solid-to-solid diffusion couples. Rods of Ni-22at.%Cr, Ni-21at.%Cr-6.2at.%Al, Ni-22at.%Cr-4.0at.%Si, Ni-22at.%Cr-1.6at.%Ge and Ni-22at.%Cr-1.6at.%Pd alloys were cast using arc-melt and homogenized at 900°C for 168 hours. The diffusion couples were assembled with alloy disks in Invar steel jig, encapsulated in Argon after several hydrogen flushes, and annealed at 700°C for 720 hours. Experimental concentration profiles were determined from polished cross-sections by using electron probe microanalysis with pure standards of Ni, Cr, Al, Si, Ge and Pd. Interdiffusion fluxes of individual components were calculated directly from the experimental concentration profiles, and the moments of interdiffusion fluxes were examined to determine average ternary interdiffusion coefficients. Effects of ternary alloying additions on the interdiffusional behavior of Ni-Cr-X alloys at 700°C are presented in the light of the diffusional interactions and the formation of protective Cr_2O_3 scale.

Introduction

Ni-Cr alloys have been extensively explored for a variety of high-temperature applications and form a basis for a numerous commercial superalloy families [1-3]. They possess a good oxidation resistance and excellent high-temperature strength. Oxidation resistance in these alloys is derived from a continuous, slow-growing, adherent Cr_2O_3 scale [1-3]. Minor alloying additions (< 6.2at.%) can significantly improve the oxidation resistance of these Cr_2O_3 forming alloys although the exact mechanism by which the improvement occurs requires further investigation [1,4-6]. Diffusional influence from minor alloying additions can play a significant role in assessing the oxidation behavior of these alloys [1-8]. Ternary interdiffusion coefficients are important parameters to elucidate the effects of minor alloying additions on the oxidation of Cr_2O_3-forming alloys.

In this work, interdiffusion in Ni-22at.%Cr-X (fcc γ phase) alloys (X = Al, Si, Ge, or Pd) was examined using solid-to-solid diffusion couples annealed at 700°C for 720 hours. The selection basis of minor alloying additions (e.g., Al, Si, Ge and Pd) has been described in previous interdiffusion study carried out at 900°C [9]. Experimental concentration profiles are employed to calculate interdiffusion fluxes of individual components, and to determine average effective interdiffusion coefficients and average ternary interdiffusion coefficients. Interdiffusion coefficients are examined to assess the influence of alloying additions on the interdiffusion behavior of Cr and the Cr_2O_3-forming ability in Ni-22at.%Cr alloys.

Determination of Interdiffusion Coefficients from Ternary Isothermal Diffusion Couples

On the basis of Onsager's formalism [10], the interdiffusion flux $\tilde{J}_i$ of a component i in a ternary system can be written as:

$$\tilde{J}_i = -\tilde{D}_{i1}^3 \frac{\partial C_1}{\partial x} - \tilde{D}_{i2}^3 \frac{\partial C_2}{\partial x} \quad (i, j = 1,2) \tag{1}$$

where $\partial C_1/\partial x$ and $\partial C_2/\partial x$ are the two independent concentration gradients, and $\tilde{D}_{i1}^3$ and $\tilde{D}_{i2}^3$ are the ternary interdiffusion coefficients. An experimental determination of the four concentration dependent interdiffusion coefficients requires the use of the Boltzmann-Matano analysis with two independent diffusion couples intersecting at a common composition in the diffusion zone.

Alternatively, the interdiffusion fluxes $\tilde{J}_i$ of all components can be determined directly from their concentration profiles of an infinite diffusion couple without the need of the interdiffusion coefficients using the expression [11]:

$$\tilde{J}_i = \frac{1}{2t} \int_{C_i^- \text{ or } C_i^+}^{C_i(x)} (x - x_o) dC_i \quad (i = 1, 2, ..., n) \tag{2}$$

where t is the time, C_i^- and C_i^+ are the terminal concentrations of the alloys employed for the couple and x_o refers to the location of the Matano plane. The interdiffusion flux $\tilde{J}_i$ can then be integrated with respect to position x to define average effective interdiffusion coefficient $\tilde{D}_i^{eff}$ [12]:

$$\tilde{D}_i^{eff} = \frac{\int_{x_1}^{x_2} \tilde{J}_i dx}{C_i^{x_2} - C_i^{x_1}} \quad (i = 1,2,3) \tag{3}$$

The effective interdiffusion coefficient is a chemical diffusion coefficient of individual species and it incorporates all multicomponent diffusional interactions within the system to provide an effective value for the interdiffusion of a component species as defined by:

$$\tilde{D}_i^{eff} = \tilde{D}_{ii}^n + \sum_j^{n-1} \frac{\tilde{D}_{ij}^n \partial C_j / \partial x}{\partial C_i / \partial x} (i \neq j) \tag{4}$$

The interdiffusion flux $\tilde{J}_i$ can be multiplied by $(x\text{-}x_o)^m$ and integrated over a selected region, x_1 to x_2 one gets [13]:

$$\int_{x_1}^{x_2} \tilde{J}_i (x - x_o)^m dx = -\overline{\tilde{D}}_{i1}^3 \int_{C_1(x_1)}^{C_1(x_2)} (x - x_o)^m dC_1 - \overline{\tilde{D}}_{i2}^3 \int_{C_2(x_1)}^{C_2(x_2)} (x - x_o)^m dC_2 \quad (i, j = 1,2) \tag{5}$$

where $\overline{\tilde{D}}_{ij}^3$ $(i, j = 1,2)$ coefficients are the average main and cross interdiffusion coefficients treated as constants over the selected composition range. For ternary interdiffusion with the independent components and infinitely possible moments (e.g., m=0, 1, 2, …), Eq. 5 can provide, at least, four equations involving the four interdiffusion coefficients $\overline{\tilde{D}}_{ij}^3$. The $\overline{\tilde{D}}_{ij}^3$ coefficients, characteristic

representations of the diffusion path, can be determined over selected composition ranges that include nonlinear segment of the profiles [13].

Experimental Procedure

Binary and ternary Ni-Cr-X alloys (fcc γ phase) with compositions reported in Table 1 were prepared with 99.9% pure Ni, Cr, Al, Si, Ge and Pd by arc melting under an argon atmosphere. The alloys were chill-cast by water-cooled copper mold into rods with approximately 12 mm in diameter. The alloy rods were placed in a quartz capsules, evacuated to a pressure less than 10^{-6} torr, and flushed several times with hydrogen. Ar was filled into the quartz capsules before the final sealing. All these alloy rods enclosed in quartz capsule assemblies, were homogenized at 900°C for 168 hours in a horizontal Lindberg™ 3-zone tube furnace, and water-quenched to preserve the high temperature microstructure. The microstructures and compositions of the alloys were examined by optical microscopy, scanning electron microscopy (SEM), energy dispersive spectroscopy (EDS) and electron microprobe analysis (EPMA). No measurable deviation in the alloy compositions was observed, and all alloys consisted of single phase fcc Ni solid solution (γ-phase).

Table 1. Nominal compositions of Ni-Cr-X alloys employed for solid-to-solid diffusion couples.

Alloy Identification	Composition (atom fraction)			Composition (weight fraction)		
	Ni	Cr	X	Ni	Cr	X
Ni	100.0	-	-	100	-	-
Ni-Cr (X = None)	78.0	22.0	-	80	20	-
Ni-Cr-Al (X = Al)	72.5	21.3	6.2	77	20	3
Ni-Cr-Si (X = Si)	74.0	22.0	4.0	78	20	2
Ni-Cr-Ge (X = Ge)	76.3	22.1	1.6	78	20	2
Ni-Cr-Pd (X = Pd)	76.1	22.3	1.6	77	20	3

Diffusion disks with approximate thickness of 2 mm were sliced from the alloy rods and prepared metallographically by polishing through 0.25 μm diamond paste. Table 2 presents ternary diffusion couples that were assembled with the disks held together in Invar™ steel jig consisting of two end plates and three threaded rods. The couples were placed in quartz capsules, which were sealed at one end, evacuated to a pressure less than 10^{-6} torr, and flushed with hydrogen several times. Ar was filled into a capsule before the final sealing. The capsules containing the couples were annealed at 700°C in a horizontal Lindberg 3-zone furnace for 720 hours. After the anneal, the couples were quenched in water to avoid any compositional and/or microstructural changes.

Table 2. List of solid-to-solid diffusion couples annealed at 700°C for 720 hours.

Series	Diffusion Couples
I	Ni vs. Ni-Cr
II	Ni vs. Ni-Cr-Al
	Ni vs. Ni-Cr-Si
	Ni vs. Ni-Cr-Ge
	Ni vs. Ni-Cr-Pd
III	Ni-Cr vs. Ni-Cr-Al
	Ni-Cr vs. Ni-Cr-Si
	Ni-Cr vs. Ni-Cr-Ge
	Ni-Cr vs. Ni-Cr-Pd

The diffusion couple assembly was then mounted, cross-sectioned, metallographically prepared for microstructural observations. Excellent bonding was observed with all diffusion couples. Then, cross-section surface was repolished with 1μm diamond paste for electron probe microanalysis (EPMA). The concentration profiles of elements Ni, Cr, Al, Si, Ge and Pd for the diffusion couples were determined with a JEOL 733 (Tokyo, Japan) EPMA by point-to-point counting techniques using pure Ni, Cr, Al, Si, Ge, and Pd as standards. Intensities of K_α X-radiations for Ni, Cr, Al, Si, Ge, and L_α X-radiations for Pd were measured and converted to their respective concentrations with appropriate ZAF (atomic number, Z; absorption, A; fluorescence, F) corrections.

Concentration profiles obtained from EPMA were smoothened by a smoothing-spline approximation using MatLab (The Math Works, Natick, MA). It is worth to mention that the analytical method used to determine interdiffusion coefficients in this study, is by the integration of interdiffusion fluxes (e.g., Eq. 5). This does not require the use of concentration gradients and therefore it significantly reduces the influence of a smoothening procedure on the determination of interdiffusion coefficients.

Results and Discussions

Excellent diffusion bonding was achieved in all diffusion couples. Fig. 1 presents a typical optical micrograph obtained by etching (Kalling's reagent) the polished surface of the diffusion couple.

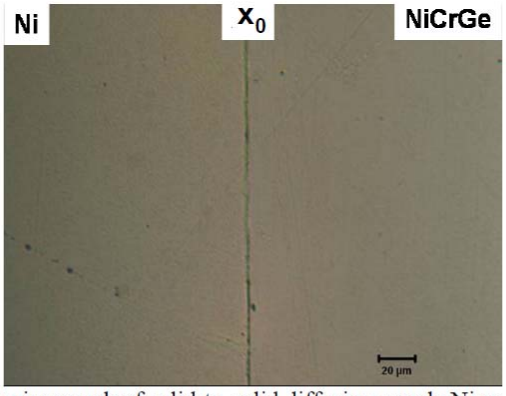

Fig. 1. Typical optical micrograph of solid-to-solid diffusion couple Ni vs. Ni-Cr-Ge annealed at 700°C for 720 hours.

Fig. 2 presents an example of experimental and smoothened concentration profiles that were used for the determination of interdiffusion fluxes and interdiffusion coefficients. The scatters in the concentration profiles for all diffusion couples were within the experimental uncertainty associated with EPMA. Experimental concentration profiles were smoothened with a smoothing-spline approximation by using MatLab. Consistency in experimental and smoothened concentration profiles of Cr in series III (see for example Fig. 2), owing to similar terminal concentration was examined by multiple EPMA acquisitions (e.g., independent Cr concentration) and by close examination of concentration profiles for Ni and X ternary alloying additions (e.g., dependent Cr concentrations). *Consistency in terms of repeatable assessment of all concentration profiles was obtained for determination of interdiffusion fluxes and interdiffusion coefficients.*

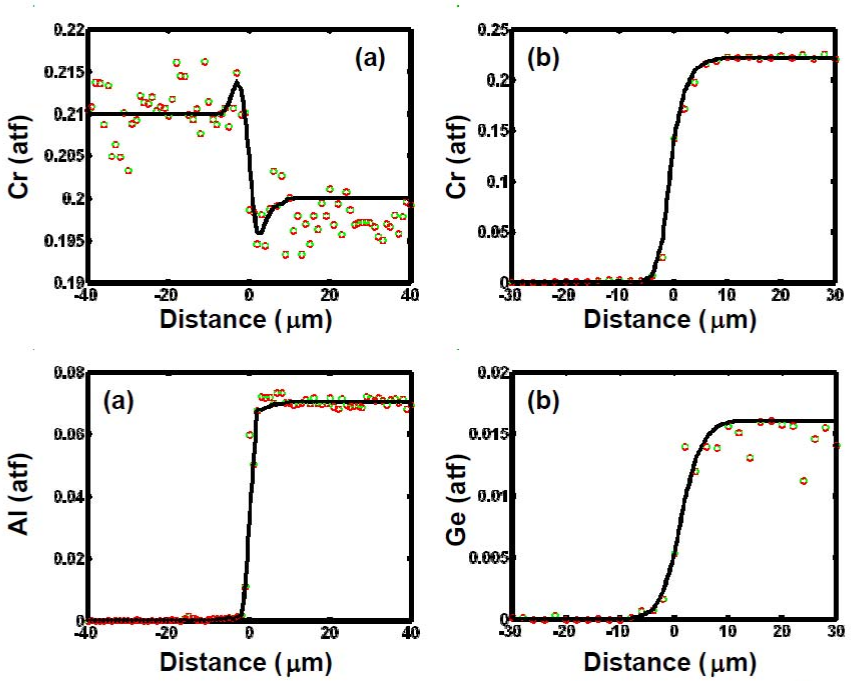

Fig. 2. Typical experimental and smoothened concentration profiles measured from solid-to-solid diffusion couples (a) Ni-Cr vs. Ni-Cr-Al and (b) Ni vs. Ni-Cr-Ge annealed at 700°C for 720 hours. Note that concentration is given in atf, which stands for atomic fraction.

Table 3. Average effective interdiffusion coefficients determined from Ni vs. Ni-Cr-X diffusion couples annealed at 700°C for 720 hours.

Diffusion Couple	Composition Range	$\tilde{D}^{eff}_{Cr}$ [10^{-18} m^2/s]	$\tilde{D}^{eff}_{X}$ [10^{-18} m^2/s]	$\tilde{D}^{eff}_{Ni}$ [10^{-18} m^2/s]
Ni vs. Ni-Cr (X = None)	$(C_i^{-\infty} \sim C_i^{o})$	1.98	-	1.98
	$(C_i^{o} \sim C_i^{+\infty})$	2.34	-	2.34
Ni vs. Ni-Cr-Al (X = Al)	$(C_i^{-\infty} \sim C_i^{o})$	0.50	0.40	0.47
	$(C_i^{o} \sim C_i^{+\infty})$	0.61	0.86	0.68
Ni vs. Ni-Cr-Si (X = Si)	$(C_i^{-\infty} \sim C_i^{o})$	1.22	2.08	1.27
	$(C_i^{o} \sim C_i^{+\infty})$	1.95	2.26	1.99
Ni vs. Ni-Cr-Ge (X = Ge)	$(C_i^{-\infty} \sim C_i^{o})$	1.39	2.38	1.43
	$(C_i^{o} \sim C_i^{+\infty})$	2.74	5.17	2.97
Ni vs. Ni-Cr-Pd (X = Pd)	$(C_i^{-\infty} \sim C_i^{o})$	6.91	6.06	6.85
	$(C_i^{o} \sim C_i^{+\infty})$	9.86	5.41	9.57

Using Eq. 3, average effective interdiffusion coefficients, $\tilde{D}_i^{eff}$'s on either side of the Matano plane were determined from the concentration profiles obtained from series I and II diffusion couples (i.e., Ni vs. Ni-Cr and Ni vs. Ni-Cr-X). They are reported in Table 3. These average effective interdiffusion coefficients are two orders lower in magnitude than those determined at 900°C [9]. $\tilde{D}_i^{eff}$ was generally higher on the $\left(C_i^{\circ} \sim C_i^{+\infty}\right)$ composition range with higher Cr concentration relative to the other side.

Table 3 also reports that Al, Si and Ge diffuse faster than Ni in γ-phase Ni-Cr-X alloys. In the case of Ni vs. Ni-Cr-Pd, $\tilde{D}_i^{eff}$'s for Ni, Cr and Pd are similar. These results are in general, analogues to previous work [9] carried out at 900°C. At 700°C, Table 3 shows that Al and Si additions to Ni-Cr alloy reduced $\tilde{D}_{Cr}^{eff}$, but Pd additions to Ni-Cr alloy increased $\tilde{D}_{Cr}^{eff}$ significantly, especially in the composition range of $\left(C_i^{\circ} \sim C_i^{+\infty}\right)$.

Concentration profiles obtained from diffusion couple series II and III (i.e., Ni vs. Ni-Cr-X and NiCr vs. Ni-Cr-X) were employed to determine average ternary interdiffusion coefficients, $\overline{\tilde{D}}_{ij}^{Ni}$ on either side of the Matano plane using Eq. 5. These are reported in Table 4 and 5. The magnitude of these interdiffusion coefficients is approximately two orders lower than those determined at 900°C [9]. The sign of the cross interdiffusion coefficients remained the same with those determined at 900°C.

Series II diffusion couples were designed to yield the same sign of $\partial C_{Cr}/\partial x$ and $\partial C_X/\partial x$ where a positive and negative $\overline{\tilde{D}}_{CrX}^{Ni}$ indicates an increase and a decrease in $\tilde{J}_{Cr}$, respectively. In general, higher magnitude of $\overline{\tilde{D}}_{CrCr}^{Ni}$ and $\overline{\tilde{D}}_{XX}^{Ni}$ was observed on the $\left(C_i^{\circ} \sim C_i^{+\infty}\right)$ composition range with higher Cr concentration. The Al addition in the Ni-Cr alloy yielded positive $\overline{\tilde{D}}_{CrAl}^{Ni}$, and increased $\tilde{J}_{Cr}$ in agreement with the previous work by Nesbitt [14], Thomson [15] and Garimella [9].

Table 4. Average ternary interdiffusion coefficients determined from Ni-Cr vs. Ni-Cr-X diffusion couples annealed at 700°C for 720 hours.

Diffusion Couple	Composition Range	$\overline{\tilde{D}}_{CrCr}^{Ni}$ [10^{-18} m^2/s]	$\overline{\tilde{D}}_{CrX}^{Ni}$ [10^{-18} m^2/s]	$\overline{\tilde{D}}_{XCr}^{Ni}$ [10^{-18} m^2/s]	$\overline{\tilde{D}}_{XX}^{Ni}$ [10^{-18} m^2/s]
Ni vs. Ni-Cr-Al (X = Al)	$\left(C_i^{-\infty} \sim C_i^{\circ}\right)$	0.48	0.53	0.06	0.42
	$\left(C_i^{\circ} \sim C_i^{+\infty}\right)$	0.54	0.02	0.10	0.35
Ni vs. Ni-Cr-Si (X = Si)	$\left(C_i^{-\infty} \sim C_i^{\circ}\right)$	0.96	0.58	0.03	1.20
	$\left(C_i^{\circ} \sim C_i^{+\infty}\right)$	1.42	0.05	0.05	1.30
Ni vs. Ni-Cr-Ge (X = Ge)	$\left(C_i^{-\infty} \sim C_i^{\circ}\right)$	0.67	5.44	Negligible	2.51
	$\left(C_i^{\circ} \sim C_i^{+\infty}\right)$	0.93	5.84	Negligible	2.88
Ni vs. Ni-Cr-Pd (X = Pd)	$\left(C_i^{-\infty} \sim C_i^{\circ}\right)$	6.49	4.92	Negligible	5.84
	$\left(C_i^{\circ} \sim C_i^{+\infty}\right)$	7.59	5.83	Negligible	5.58

The Si, Ge and Pd additions to Ni-Cr alloy also increased $\tilde{J}_{Cr}$ with positive $\overline{\tilde{D}}_{CrX}^{Ni}$. This effect was stronger when Cr concentration was high on the $\left(C_i^{\circ} \sim C_i^{+\infty}\right)$ side particularly for Ge and Pd. In previous work at 900°C [9], $\overline{\tilde{D}}_{CrGe}^{Ni}$ was not significant to this extent. The Si, Ge and Pd additions to

Ni-Cr alloy also increased $\tilde{J}_{Cr}$ with positive $\widetilde{\overline{D}}^{Ni}_{CrX}$. This effect was stronger when Cr concentration is high on the $\left(C_i^{\circ} \sim C_i^{+\infty}\right)$ side, particularly for Ge and Pd. In previous work at 900°C [9], $\widetilde{\overline{D}}^{Ni}_{CrGe}$ was not significant while $\widetilde{\overline{D}}^{Ni}_{CrSi}$ and $\widetilde{\overline{D}}^{Ni}_{CrPd}$ were significantly large. This study at 700°C finds that $\widetilde{\overline{D}}^{Ni}_{CrGe}$ and $\widetilde{\overline{D}}^{Ni}_{CrPd}$ are large positive values while $\widetilde{\overline{D}}^{Ni}_{CrSi}$ is not so significant.

Diffusion couple series III was designed so that the initial $\partial C_{Cr}/\partial x \approx 0$. Therefore, $\tilde{J}_{Cr}$ is mainly due to $\partial C_X/\partial x$, and the magnitude and sign of $\widetilde{\overline{D}}^{Ni}_{CrX}$. $\tilde{J}_{Al}$ and $\tilde{J}_{Si}$ have caused an uphill-diffusion of Cr owing to positive $\widetilde{\overline{D}}^{Ni}_{CrAl}$ and $\widetilde{\overline{D}}^{Ni}_{CrSi}$, respectively. On the other hand, $\tilde{J}_{Ge}$ and $\tilde{J}_{Pd}$ did not cause any measurable redistribution of Cr ($\tilde{J}_{Cr} \approx 0$). However, Ge and Pd are lower in concentration than those of Al and Si, in the Ni-Cr-X alloys, as reported in Table 1. Average ternary interdiffusion coefficients for series-III couples are reported in Table 5.

Table 5. Average ternary interdiffusion coefficients determined from Ni vs. Ni-Cr-X diffusion couples annealed at 700°C for 720 hours.

Diffusion Couple	Composition Range	$\widetilde{\overline{D}}^{Ni}_{CrCr}$ [10^{-18} m^2/s]	$\widetilde{\overline{D}}^{Ni}_{CrX}$ [10^{-18} m^2/s]	$\widetilde{\overline{D}}^{Ni}_{XCr}$ [10^{-18} m^2/s]	$\widetilde{\overline{D}}^{Ni}_{XX}$ [10^{-18} m^2/s]
Ni-Cr vs. Ni-Cr-Al (X = Al)	$\left(C_i^{-\infty} \sim C_i^{\circ}\right)$	1.98	0.73	1.97	0.78
	$\left(C_i^{\circ} \sim C_i^{+\infty}\right)$	2.65	1.00	1.01	0.76
Ni-Cr vs. Ni-Cr-Si (X = Si)	$\left(C_i^{-\infty} \sim C_i^{\circ}\right)$	6.91	5.87	0.11	0.62
	$\left(C_i^{\circ} \sim C_i^{+\infty}\right)$	2.59	2.22	0.16	1.35
Ni-Cr vs. Ni-Cr-Ge (X = Ge)	$\Delta C_{Cr}/\Delta x \approx 0$ and cannot be determined				
Ni-Cr vs. Ni-Cr-Ge (X = Ge)					

Based on average effective interdiffusion coefficients and average ternary interdiffusion coefficients determined in both the present study at 700°C and earlier study at 900°C [9], alloying additions of Al, Si, Ge and Pd have yielded positive $\widetilde{\overline{D}}^{Ni}_{CrX}$. Therefore, Cr_2O_3-forming ability of Ni-22at.%Cr alloy should improve with these alloying additions.

Summary

Experimental concentration profiles, measured after annealing at 700°C for 720 hours, were employed to determine interdiffusion fluxes, average effective interdiffusion coefficients and average ternary interdiffusion coefficients. The, $\widetilde{\overline{D}}^{Ni}_{CrX}$ were observed to be positive with the alloying additions of Al, Si, Ge, or Pd. These results indicate that these alloying additions can facilitate the formation of Cr_2O_3-scale after scale-spallation and Cr-depletion due to long-term oxidation.

Acknowledgements

This work was supported by the NSF CAREER Award under the grant DMR-0238356.

References

[1] J.L. Smialek and G.H.Meier, in: High temperature oxidation, edited by C.T. Sims, N.S. Stoloff, and W.C. Hagel, of Superalloy II, chapter 11, John Weley & Sons (1987).

[2] P. Kofsted, in: Growth and protective properties of Chromia (Cr_2O_3) and Alumina (Al_2O_3) scales, protective coatings, of High temperature Corrosion, Elsevier,London (1980) p. 389-404.

[3] J.L. Smialek, C.A. Barrett, J.C. Schaffer, in: Design for oxidation resistance, edited by George E. Dieter,Vol. 20 of ASM handbook, ASM International (1997).

[4] F.H. Stott, G.C. Wood, and J.Stringer : Oxi. Metals, Vol. 44 (1995), p. 113-145.

[5] D.P.Whittle and J.Stringer: Proc. R. Soc. Lond., Ser. A, Vol. 295 (1980), p.309-329.

[6] G.C. Wood and F.H.Stott: Mater. Sci. Technol., Vol.3 (1987), p. 519-530.

[7] W.C.Hagel: Corrosion, Vol. 21 (1965), p. 316-326.

[8] J.A. Nesbitt: Oxid. Metals, Vol. 44 (1995), p 309-338.

[9] N.Garimella, M.P. Brady and Y.H.Sohn: Journal of Phase Equilibria and Diffusion, Vol. 27, (2006), p. 665-670.

[10] L.Onsager, Ann. N.Y.Acad. Sci., Vol. 46 (1965), p. 241-265.

[11] M.A. Dayananda and C.W.Kim: Metall. Trans. A, Vol. 10A (1979), p. 1333-1339.

[12] M.A. Dayananda and Y.H.Sohn: Scr. Mater., Vol. 40 (1996), p. 683-688.

[13] M.A. Dayananda and Y.H.Sohn: Metall. Trans. A, Vol. 30A (1999), p 535-543.

[14] J.A. Nesbitt and R.W. Heckel: Metall. Trans. A, Vol.18A (1987), p 2075-2086.

[15] M.S.Thomson, J.E.Morral, and A.D.Roming Jr.: Metall. Trans. A, Vol. 21A, (1990), p. 2679-2685.

Defect and Diffusion Forum Vols. 273-276 (2008) pp 637-642
online at http://www.scientific.net

Online available since 2008/Feb/11

Ternary Interdiffusion in $L1_2$-Ni_3Al with Ir Alloying Addition

M. Ode[1a], N. Garimella[2b], M. Ikeda[3c], H. Murakami[1d], Y.H. Sohn[2e]

[1]National Institute of Materials Science, Tsukuba, Japan
[2]University of Central Florida, Orlando, FL, USA
[3]Kobe Steel, Co. Ltd. (Formally graduate student of the Univ. of Tokyo), Japan

[a] ODE.Machiko@nims.go.jp; [b] ga825540@pegasus.cc.ucf.edu
[c] ikeda.muneaki@steel.kobelco.co.jp; [d] murakami.hideyuki@nims.go.jp
[e] ysohn@mail.ucf.edu

Keywords: Ir, Ni_3Al, $L1_2$, intermetallics, high temperature alloys, ternary interdiffusion

Abstract. Average ternary interdiffusion coefficients in Ni_3Al with Ir additions have been determined using solid-to-solid diffusion couples annealed at 1200°C for 5 hours. Disc shaped alloy specimens were prepared by the vacuum arc melting at compositions of Ni-24Al, Ni-25Al, Ni-26Al, Ni-23.5Al-1Ir, Ni-24.5Al-1Ir, Ni-23Al-2Ir, Ni-23Al-2Ir, Ni-24Al-2Ir, Ni-23Al-3Ir (at.%). Surfaces of alloys were polished down to 1200 grit and diffusion couples were assembled in Si_3N_4 jig for initial bonding heat treatment at 1200°C for 0.5 hours. Additional diffusion anneal was carried out at 1200°C for 4.5 hours outside of Si_3N_4 jig so that diffusion couples can be water quenched. Concentration profiles of individual components were measured by electron probe microanalysis using pure standard of Ni, Al and Ir. Interdiffusion flux of individual component was determined directly from the experimental concentration profiles, and the moments of interdiffusion flux were examined to calculate the average ternary interdiffusion coefficients, $\widetilde{D}_{ij}^{k}$ either with Al or Ni as dependent component. Calculated interdiffusion coefficients suggest that Ir-alloyed Al_2O_3-forming oxidation resistant coatings would be beneficial to reduce the interdiffusion flux of Ni from superalloy substrates to the coating, and reduce the interdiffusion flux of Al from the coating to the superalloy substrate.

Introduction

Nickel-base superalloys are extensively used in both aviation and land-based gas turbine environments, and many studies have been devoted to improve their mechanical properties and microstructural stability. Ni-based superalloys are typically composed of $L1_2$ γ'-phase (Ni_3Al) coherently precipitated in a fcc γ-phase matrix. The diffusion mobility database for Ni-based superlloys is available for fcc phase [1]. However, a limited number of study [2,3] exist on interdiffusion of the γ'-phase, particularly with alloyed with other constituents in superalloys, although the γ' is the strengthening phase of the Ni-based superalloys. An understanding of multicomponent diffusion processes in these alloys is very important because it is essential to achieve durable microstructure for high-temperature strength and adequate high temperature oxidation resistance. This study is also fueled by recent conceptual development of γ+γ' coatings for optimized oxidation resistance, and reduced interdiffsion between the oxidation resistant coatings and structural superalloy substrate (e.g. formation of deleterious phases due to interdiffusion at the interface).

The diffusion mechanism in ordered alloys is recognized to be more complex than for disordered solid solutions [4]. In the case of $L1_2$ structure, the diffusion mechanism is even more complex than that for B2 structure. Diffusion can occur through the face-centered α-site where Ni atom mainly occupies, and the diffusion coefficient largely depends on the alloy composition, namely the degrees of order [5-7]. Tracer diffsion studies in γ' Ni_3Al is difficult since ^{26}Al is not easily available, although the self-diffusion of Ni and chemical/impurity diffusion in Ni_3Al binary and Ni_3Al-X ternary alloy (X= Co, Cu, Pt, Ti, Si, W, Ge, In, V, Mb, Cr, Fe, Mn) have been studied [2,3].

Murakami and coworkers have proposed Ir-based alloys for oxidation resistant coatings, either as stand-alone coatings or as bond coats [8-16], because Ir has the highest melting temperature (2716K) among platinum grope metals, excellent chemical stability and low oxygen diffusivity [17]. Ir addition also increases the melting temperature of Ni-based superalloys [18]. Furthermore, the Ir-Al phase diagram [19, 20] does not contain any intermediate phases between the B2 IrAl phase and the Ir-based fcc solid solution phase. Therefore, Ir-Al-based coatings are expected to be thermodynamically more stable during high temperature applications.

For better understanding of microstructural stability of Ni-base superalloys and potential development of Ir-Al-based oxidation resistant coatings, we examined the ternary diffusional interaction of Ir addition on the L12 Ni_3Al phase. Solid-to-solid diffusion couples were assembled and annealed at 1473K for 5 hours. Based on concentration profiles obtained by electron probe microanalysis, average ternary interdiffusion coefficients were determined to assess how Ir addition influences interdiffusion behavior of Ni and Al.

Experimental Details

Binary Ni-Al and ternary Ni-Al-Ir alloys were prepared by the vacuum arc melting of 99.97 wt.% Ni, 99.9 wt.% Al and 99.2 wt.% Ir according to the compositions presented in Table I. The alloys were cast into a semi-cylindrical mold with the diameter of 8 mm in the arc furnace. The alloy rods were homogenized at 1473K for 137 hours in the vacuum furnace evacuated to a pressure less than 10^{-2} Pa. The homogenized alloys were then sectioned into discs with the height of 1.5 mm. Surface of alloy discs were polished metallographically up to 1200-grit and cleaned thoroughly prior to diffusion couple assembly.

Table I. Nominal compositions of Ni-Al-Ir alloys employed for solid-to-solid diffusion couples.

Alloy Identification	Composition (atom percent)			Composition (weight percent)		
	Ni	Al	Ir	Ni	Al	Ir
Ni-24.5Al	76	24	0	59.3	40.7	0.0
Ni-25Al	75	25	0	58.0	42.0	0.0
Ni-26Al	74.5	25.5	0	57.3	42.7	0.0
Ni-23.5Al-1Ir	75.5	23.5	1	59.5	40.3	0.2
Ni-24.5Al-1Ir	74.5	24.5	1	58.2	41.6	0.2
Ni-23Al-2Ir	74.5	23.5	2	59.0	40.5	0.5
Ni-23Al-3Ir	74	23	3	59.2	40.0	0.7

Coupled alloys were put into a Si_3N_4 jig and were annealed at 1473K for 0.5 h in a vacuum furnace to promote initial bonding. Since the metal discs have larger thermal expansion coefficients than the Si_3N_4 jig, the discs can adhere to each other due to the compressive stress by the annealing treatment. A diffusion couple fabricated in this manner was then sealed in an evacuated transparent quartz capsule, and annealed at 1473K for 4.5 hours in an atmosphere furnace. All diffusion couples were water quenched after the high temperature anneal to preserve high temperature microstructure and concentration profiles. In this study, the time required for the diffusion bonding treatment (0.5 hours) was added to the total annealing time. Thus, concentration profiles from all diffusion couple were analyzed with diffusion anneal time of 5 hours.

Microstructures and concentration profiles of the annealed diffusion couples were analyzed by an JEOL-JXA-8900 electron probe microanalyzer (EPMA). The accelerating voltage of 20 kV, the beam current of 50 nA and the probe diameter of 1 μm were employed for data acquisition of Ni K_α x-radiation peak using LIF crystal, Al K_α x-radiation peak using TAP crystal, and Ir L_α x-radiation using LIFH crystal. Pure element standards of Ni, Al and Ir along with ZAF correction were used for quantification of concentrations.

Determination of Interdiffusion Coefficients in Ternary System

Based on Onsager's formalism [21], the phenomenological description of interdiffusion in ternary system requires four concentration-dependent interdiffusion coefficients: two main and two cross-coefficients [22]. For the classical experimental determination, two independent diffusion couples with intersecting diffusion paths are needed to determine four independent interdiffusion coefficient at the intersecting composition.

In the case of intermetallics, an alloying element often show site-preference. For example, Ir atoms mainly substituting for Ni atoms on the a-site in the $L1_2$ structure. This site prefefrence can lead to concentration profile where $\nabla C_{Ni} = -\nabla C_{Ir}$, and may pose a difficulty in determining the ternary interdiffusion coefficient for $(Ni,Ir)_3Al$ based on classical Boltzmann-Matano analysis.

On the basis of Onsager's formalism [21], the interdiffusion flux $\tilde{J}_i$ of a component i in a ternary system can be written as:

$$\tilde{J}_i = -\tilde{D}^3_{i1}\frac{\partial C_1}{\partial x} - \tilde{D}^3_{i2}\frac{\partial C_2}{\partial x} \quad (i, j = 1,2) \tag{1}$$

where $\partial C_1/\partial x$ and $\partial C_2/\partial x$ are the two independent concentration gradients, and $\tilde{D}^3_{i1}$ and $\tilde{D}^3_{i2}$ are the ternary interdiffusion coefficients. An experimental determination of the four concentration dependent interdiffusion coefficients requires the use of the Boltzmann-Matano analysis with two independent diffusion couples intersecting at a common composition in the diffusion zone [22].

Alternatively, the interdiffusion fluxes $\tilde{J}_i$ of all components can be determined directly from their concentration profiles of an infinite diffusion couple without the need of the interdiffusion coefficients using the expression [23]:

$$\tilde{J}_i = \frac{1}{2t}\int_{C_i^- \text{ or } C_i^+}^{C_i(x)} (x - x_o)\,dC_i \quad (i = 1, 2, ..., n) \tag{2}$$

where t is the time, C_i^- and C_i^+ are the terminal concentrations of the alloys employed for the couple and x_o refers to the location of the Matano plane.

The interdiffusion flux $\tilde{J}_i$ can be multiplied by $(x\text{-}x_o)^m$ and integrated over a selected region, x_1 to x_2 one gets [24]:

$$\int_{x_1}^{x_2} \tilde{J}_i (x - x_o)^m dx = -\overline{\tilde{D}}_{i1}^3 \int_{C_1(x_1)}^{C_1(x_2)} (x - x_o)^m dC_1 - \overline{\tilde{D}}_{i2}^3 \int_{C_2(x_1)}^{C_2(x_2)} (x - x_o)^m dC_2 \quad (i, j = 1,2) \tag{5}$$

where $\overline{\tilde{D}}_{ij}^3$ $(i, j = 1,2)$ coefficients are the average main and cross interdiffusion coefficients treated as constants over the selected composition range. For ternary interdiffusion with the independent components and infinitely possible moments (e.g., m = 0, 1, 2, …, n), Eq. 5 can provide, at least, four equations involving the four interdiffusion coefficients $\overline{\tilde{D}}_{ij}^3$. The $\overline{\tilde{D}}_{ij}^3$ coefficients, characteristic representations of the diffusion path, can be determined over selected composition ranges that include nonlinear segment of the profiles [24].

Results and Discussion

Figure 1 shows typical concentration profiles obtained by EPMA for diffusion couple Ni-25Al vs. Ni-23Al-1Ir annealed at 1437K for 5 hours. The x-axis represents the distance from the Matano plane, and the solid lines are smoothened concentration profiles.

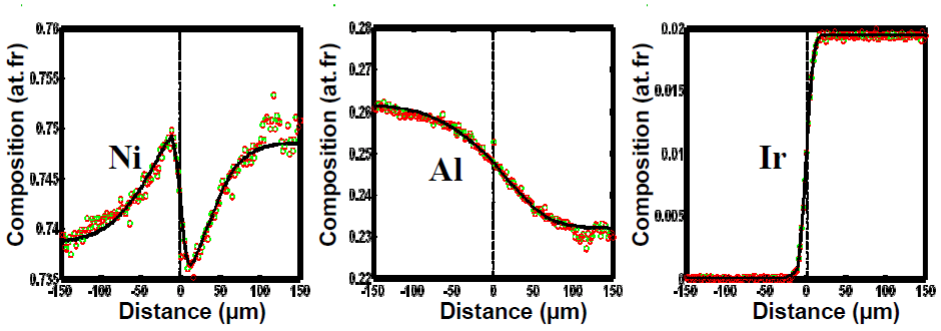

Fig. 1. Concentration profile of diffusion couple, Ni-25Al vs. Ni-23Al-1Ir annealed at 1437K for 5 hours.

The average ternary interdiffusion coefficients determined using Eq. [4] with m = 0 and m = 1 are presented in Table II. The magnitude of $\tilde{\overline{D}}_{AlAl}$ and $\tilde{\overline{D}}_{NiNi}$ is much larger than $\tilde{\overline{D}}_{IrIr}$. In Fig. 2, $\tilde{\overline{D}}_{IrIr}$ determined from of the diffusion couple Ni-25Al vs. Ni-23.5Al-1Ir (square dots) is compared with the reported interdiffusion coefficients in Ni_3Al [3]. The magnitude of $\tilde{\overline{D}}_{IrIr}$ is slightly smaller than that of the minimum diffusion coefficient, $\tilde{D}_{PtPt}$ among the Ni-substitute elements.

Table II. Average ternary interdiffusion coefficients determined from diffusion couples of $(Ni,Ir)_3Al$ alloys annealed at 1473K for 5 hours.

Diffusion Couple	Composition Range	$\tilde{\overline{D}}^{Ni}_{AlAl}$	$\tilde{\overline{D}}^{Ni}_{AlIr}$	$\tilde{\overline{D}}^{Ni}_{IrAl}$	$\tilde{\overline{D}}^{Ni}_{IrIr}$	$\tilde{\overline{D}}^{Al}_{NiNi}$	$\tilde{\overline{D}}^{Al}_{NiIr}$	$\tilde{\overline{D}}^{Al}_{IrNi}$	$\tilde{\overline{D}}^{Al}_{IrIr}$
Ni-25Al vs. Ni-23.5Al-1Ir	$C_i^{-\infty} \sim C_i^{o}$	783	-101	Ngl.	13	783	873	Ngl.	13
	$C_i^{o} \sim C_i^{+\infty}$	646	-101	Ngl.	13	644	73	Ngl.	13
Ni-24.5Al vs. Ni-24.5Al-1Ir	$C_i^{-\infty} \sim C_i^{o}$	541	-85	Ngl.	11	541	615	Ngl.	11
	$C_i^{o} \sim C_i^{+\infty}$	816	-76	Ngl.	19	816	871	Ngl.	22
Ni-26Al vs. Ni-23Al-2Ir	$C_i^{-\infty} \sim C_i^{o}$	873	-52	Ngl.	15	873	912	Ngl.	16
	$C_i^{o} \sim C_i^{+\infty}$	590	-117	Ngl.	13	590	690	Ngl.	12
Ni-25Al vs. Ni-23Al-2Ir	$C_i^{-\infty} \sim C_i^{o}$	522	-107	Ngl.	16	522	613	Ngl.	16
	$C_i^{o} \sim C_i^{+\infty}$	494	-117	Ngl.	16	494	594	Ngl.	16
Ni-25Al vs. Ni-23Al-3Ir	$C_i^{-\infty} \sim C_i^{o}$	440	-93	Ngl.	16	440	522	Ngl.	16
	$C_i^{o} \sim C_i^{+\infty}$	441	-136	Ngl.	19	441	548	Ngl.	19

The $\tilde{\overline{D}}^{Al}_{NiIr}$ coefficient is positive and large in magnitude. This suggests that Ir substitutes in Ni-site and influences the interdiffusion of Ni significantly. The $\tilde{\overline{D}}^{Ni}_{AlIr}$ coefficient is negative and large in magnitude as well. Based on magnitudes and sign of $\tilde{\overline{D}}^{Al}_{NiIr}$ and $\tilde{\overline{D}}^{Ni}_{AlIr}$, Ir can substitute Ni in oxidation resistant coatings (e.g., NiCoCrAlY and Ni-aluminides) to reduce the accumulated interdiffsion fluxes of Ni and Al. Ir addition in coatings would reduce the interdiffusion flux of Ni from superalloy substrates to the coating, and reduce the interdiffusion flux of Al from the coating to the superalloy substrate.

Conclusion

Ternary interdiffusional interaction of Ir addition on the L12 Ni_3Al phase was examined using solid-to-solid diffusion couples annealed at 1473K for 5 hours. Average ternary interdiffusion coefficients were determined from integration of interdiffusion fluxes for individual components. The $\tilde{\overline{D}}^{Al}_{NiIr}$ coefficient was determined to be positive and large in magnitude: Ir substitutes in Ni-site and influences the interdiffusion of Ni significantly. The $\tilde{\overline{D}}^{Ni}_{AlIr}$ coefficient was negative and appreciable in magnitude. Findings from this study finds that Ir addition in coatings would be beneficial to reduce the interdiffusion flux of Ni from superalloy substrates to the coating, and reduce the interdiffusion flux of Al from the coating to the superalloy substrate.

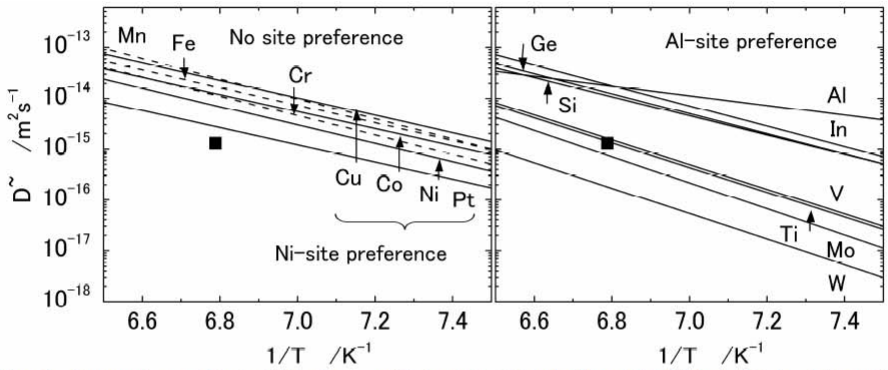

Fig. 2. Comparison of interdiffusion coefficients in Ni_3Al alloys [3]. Value obtained from this study is presented in square dots.

References

1. C. E. Campbell, W.J. Boettinger and U.R. Kattner: Acta Mater. Vol. 50 (2002), p. 775.
2. J. Cermak and V. Rothova: Acta Mater. Vol. 51 (2003), p. 4411.
3. Y. Minamino, H. Yoshida, S.B. Jung, K. Hirao and T. Yamane: Def. Diff. Forum Vol. 143 (1997), p. 257.
4. H. Mehrer: Mater. Trans. JIM Vol. 37 (1996), p. 1259.
5. H. Numakura, T. Ikeda, M. Koiwa and A. Almazouzi: Phil. Mag. A Vol. 77 (1998), p. 887.
6. S.V. Divinski, S. Frank, U. Sodervall and C. Herzig: Acta Mater. Vol. 46 (1998), p. 4369.
7. Numakura, T. Ikeda, H. Nakajima and M. Koiwa: Mater. Sci. Eng. A Vol. 312 (2001), p. 109.
8. P. Kuppusami, H. Murakami and T. Ohmura: J. Vac. Sci. Technol. A Vol. 22 (2004), p. 1208.
9. P. Kuppusami, H. Murakami and T. Ohmura: Surf. Eng. Vol. 21 (2005), p. 53.
10. H. Murakami, T. Yano and S. Sodeoka: Mater. Trans. Vol. 45 (2004), p. 2886.
11. Suzuki, M. Harada, Y.N. Wu and H. Murakami: Mater. Trans. Vol. 46 (2005), p. 1760.
12. Suzuki, F. Wu, H. Murakami and H. Imai: Sci. Technol. Adv. Mater. Vol. 5 (2004), p. 555.
13. F. Wu, H. Murakami and H. Harada: Mater. Trans. Vol. 44 (2003), p. 1675.
14. F. Wu, H. Murakami and A. Suzuki: Surf. Coat. Technol. Vol. 168 (2003), p. 62.
15. F. Wu, H. Murakami, Y. Yamabe-Mitarai, H. Harada, H. Katayama and Y. Yamamoto: Surf. Coat. Technol. Vol. 184 (2004), p. 24.
16. Y.N. Wu, A. Yamaguchi, H. Murakami and S. Kuroda: J. Mater. Res. Vol. 22 (2007), p. 206.
17. H. Hosoda, T. Takahashi, M. Takehara, T. Kingetsu and H. Masumoto: Mater. Trans. JIM Vol. 38 (1997), p. 871.
18. H. Murakami, T. Honma, Y. Koizumi and H. Harada: *Superalloys-2000*, T.M. Pollock, R.D. Kissinger and J.J. Schirra, Editors, (The Minerals, Metals and Materials Society Warrendale, Pennsylvania, USA, 2000) p. 747.
19. T.B. Massalski: *Binary Alloy Phase Diagrams. 2nd Ed.* (ASM International, Maerials Park, Ohio, USA, 1990) p. 164.
20. P.J. Hill, L.A. Cornish and M.J. Witcomb: J. Alloys Comp. Vol. 280 (1998), p. 240.
21. L. Onsager: Ann. Rev. NY Acad. Vol. 46 (1965), p. 241.
22. J.S. Kirkardy: Can. J. Phys. Vol. 36 (1958), p. 899.
23. M.A. Dayananda and C.W. Kim: Metall. Trans. A Vol. 10A (1979), p. 1333.
24. M.A. Dayananda and Y.H. Sohn: Metall. Mater. Trans. A Vol. 30A (1999), p. 535.

Materials Science Forum Vols. 595-598 (2008) pp 1145-1152
online at http://www.scientific.net

Online available since 2008/Sep/09

Ternary and Quaternary Interdiffusion in γ (fcc) Fe-Ni-Cr-X (X = Si, Ge) Alloys at 900°C

N. Garimella[1, a], M.P. Brady[2, b] and Y.H. Sohn[1, c]

[1]Advanced Materials Processing and Analysis Center and Department of Mechanical, Materials and Aerospace Engineering, University of Central Florida, Orlando, FL, USA.

[2]Metals and Ceramics Division, Oak Ridge National Laboratory, Oak Ridge, TN, USA.

[a]garimella_n@yahoo.com, [b] bradymp@ornl.gov, [c] ysohn@mail.ucf.edu

Keywords: Multicomponent diffusion, interdiffusion coefficients, Austenitic alloys

Abstract. Interdiffusion in Fe-Ni-Cr (fcc γ phase) alloys with small additions of Si and Ge at 900°C was studied using solid-to-solid diffusion couples. Alloy rods of Fe-24 at.%Ni, Fe-24 at.%Ni-22at.%Cr, Fe-24 at.%Ni-22at.%Cr-4at.%Si and Fe-24 at.%Ni-22at.%Cr-1.7at.%Ge were cast using arc-melt, and homogenized at 900°C for 168 hours. Sectioned alloy disks from the rods were polished, and diffusion couples were assembled with in Invar steel jig, encapsulated in Argon after several hydrogen flushes, and annealed atz 900°C for 168 hours. Polished cross-sections of the diffusion couples were characterized to determine experimental concentration profiles using electron probe microanalysis with pure elemental standards. Interdiffusion fluxes of individual components were calculated directly from the experimental concentration profiles, and the moments of interdiffusion flux profiles were examined to determine the average ternary and quaternary interdiffusion coefficients. Effects of alloying additions on the interdiffusional behavior of Fe-Ni-Cr-X alloys at 900°C are presented with due consideration for the formation of protective Cr_2O_3 scale.

Introduction

Austenitic (fcc-γ) Cr_2O_3 forming Fe-Ni-Cr alloys are of potential interest for many applications due to their combination of good oxidation/corrosion resistance and high temperature strength [1-7]. Minor alloying additions (< 5 wt.%) on these alloys are found to increase the oxidation resistance by forming a slowly growing, adherent, continuous and impervious layer of Cr_2O_3 [4,8,9]. In this work, effects of Si and Ge alloying additions on the interdiffusion behavior of quaternary Fe-Ni-Cr-X (X = Si, Ge) alloys (fcc γ-phase) were studied by using solid-to-solid diffusion couples with due respect for the formation and growth kinetics of protective Cr_2O_3 scale of these alloys.

Ternary and quaternary interdiffusion coefficients are important tools to explain the effects of minor alloying additions on the oxidation of Cr_2O_3-forming alloys. In this work, interdiffusion in Fe-24at.%Ni-22at.%Cr-X (fcc γ phase) alloys (X = Si, Ge) was examined using solid-to-solid diffusion couples annealed at 900°C for 168 hours. The selection criteria of minor alloying additions (e.g., Si, Ge) for the case of Ni-Cr alloys has been described in earlier interdiffusion studies carried out at 900°C and 700°C [10,11]. Experimental concentration profiles are employed to calculate interdiffusion fluxes of individual components, and determine average effective interdiffusion coefficients and average ternary and quaternary interdiffusion coefficients. Interdiffusion coefficients are examined to assess effects of alloying additions on the interdiffusion behavior of Cr in promoting Cr_2O_3-formation in Fe-24at.%Ni-22at.%Cr-X alloys.

Determination of Interdiffusion Coefficients from Ternary Isothermal Diffusion Couples

Onsager's formalism of Fick's law [12] provides the interdiffusion flux $\tilde{J}_i$ of a component i in a multicomponent system, written as:

$$\tilde{J}_i = -\sum_{j=1}^{n-1} \tilde{D}_{ij}^{n} \frac{\partial C_j}{\partial x} \quad (i = 1,2,...,n-1). \tag{1}$$

where, $\partial C_j/\partial x$ is the independent concentration gradient of component j, and $\tilde{D}_{ij}^{n}$'s are the $(n-1)^2$ composition-dependent interdiffusion coefficients. An experimental determination of 9 composition-specific quaternary interdiffusion coefficients requires the use of the Boltzmann-Matano analysis with three independent diffusion couples that develop a common composition in the diffusion zone. Alternatively, the interdiffusion fluxes $\tilde{J}_i$ of all components can be determined directly from their concentration profiles of an infinite diffusion couple without the availability of the interdiffusion coefficients using the expression [13]:

$$\tilde{J}_i = \frac{1}{2t} \int_{C_i^- \text{ or } C_i^+}^{C_i(x)} (x - x_o)\, dC_i \quad (i = 1, 2, ..., n). \tag{2}$$

where t is the time, C_i^- and C_i^+ are the terminal concentrations of the parent alloys employed for the couple and x_o refers to the location of the Matano plane.

The interdiffusion flux $\tilde{J}_i$, determined from Eq. 2 can then be integrated with respect to position x to define average effective interdiffusion coefficient, $\tilde{D}_i^{eff}$ [14]:

$$\tilde{D}_i^{eff} = \frac{\int_{x_1}^{x_2} \tilde{J}_i dx}{C_i^{x_2} - C_i^{x_1}} \quad (i = 1,2,3). \tag{3}$$

This average effective interdiffusion coefficient incorporates all multicomponent diffusional interactions for the system, and provides an effective value for the interdiffusion of a component as defined by:

$$\tilde{D}_i^{eff} = \tilde{D}_{ii}^{n} + \sum_{j} \frac{\tilde{D}_{ij}^{n} \partial C_j/\partial x}{\partial C_i/\partial x} \quad (i \neq j). \tag{4}$$

The interdiffusion flux $\tilde{J}_i$, determined from Eq. 2 as a function of x, can be multiplied by $(x-x_o)^n$ and integrated over a selected region, x_1 to x_2; in the light of Eq. 1, one gets [15],

$$\int_{x_1}^{x_2} \tilde{J}_i (x - x_o)^n dx = -\bar{\tilde{D}}_{i1}^{3} \int_{C_1(x_1)}^{C_1(x_2)} (x - x_o)^n dC_1 - \bar{\tilde{D}}_{i2}^{3} \int_{C_2(x_1)}^{C_2(x_2)} (x - x_o)^n dC_2 \quad (i = 1,2). \tag{5}$$

$$\begin{aligned} \int_{x_1}^{x_2} \tilde{J}_i (x - x_o)^n dx = &-\bar{\tilde{D}}_{i1}^{4} \int_{C_1(x_1)}^{C_1(x_2)} (x - x_o)^n dC_1 \\ &- \bar{\tilde{D}}_{i2}^{4} \int_{C_2(x_1)}^{C_2(x_2)} (x - x_o)^n dC_2 - \bar{\tilde{D}}_{i3}^{4} \int_{C_2(x_1)}^{C_2(x_2)} (x - x_o)^n dC_2 \quad (i = 1,2,3) \end{aligned} \tag{6}$$

for ternary and quaternary interdiffusion, respectively. Eq. 5 provides four equations involving the $\widetilde{\widetilde{D}}_{ij}^{3}$ interdiffusion coefficients (n = 0, 1) and can be set up from interdiffusion fluxes calculated using Eq. 2 from the concentration profiles of a single diffusion couple of the ternary system. Similarly, Eq. 6 provides nine equations involving the $\widetilde{\widetilde{D}}_{ij}^{4}$ interdiffusion coefficients (n = 0, 1 and 2) from the single diffusion couple of the quaternary system. The $\widetilde{\widetilde{D}}_{ij}^{k}$ coefficients, characteristic of the diffusion path, can be determined over selected composition ranges that include nonlinear segment of the profiles [15].

Experimental Procedure

Ternary and quaternary alloys of Fe-Ni-Cr-X (fcc γ phase) system with compositions reported in Table 1 were prepared with 99.9% pure Fe, Ni, Cr, Si and Ge by arc melting under an argon atmosphere. These alloys were chill-cast by water-cooled copper molds into rods with approximately 12 mm in diameter. The alloy rods were placed in a quartz capsule, evacuated to pressure below 10^{-6} torr, and flushed with hydrogen. The hydrogen-flush procedure was repeated several times, and Ar was finally filled into the capsule before the final encapsulation. They were homogenized at 900°C for 168 hours in a horizontal Lindberg™ 3-zone tube furnace, and water-quenched to retain the high temperature microstructure. The microstructures and compositions of the alloys were examined by optical microscopy, scanning electron microscopy (SEM), energy dispersive spectroscopy (EDS) and electron microprobe analysis (EMPA). No measurable variation in the alloy compositions was found, and all alloys consisted single-phase fcc solid solution (γ-phase).

Table.1 Nominal compositions of Fe-Ni-Cr-X alloys employed for solid-to-solid diffusion couple studies. Values in parenthesis are standard deviation.

Alloy Identification	Composition (atom percent)			
	Fe	Ni	Cr	X
Fe-Ni	76.3 (0.7)	23.7 (0.7)	-	-
Fe-Ni-Cr	55.5 (0.7)	23.1 (0.4)	21.4 (0.4)	-
Fe-Ni-Cr-Si (X = Si)	52.2 (0.7)	22.3 (0.4)	21.4 (0.3)	4.1 (0.4)
Fe-Ni-Cr-Ge (X = Ge)	53.4 (0.3)	22.3 (0.4)	21.9 (0.3)	1.4 (0.3)

Alloy disks of approximately 2 mm in thickness were sliced from the rods of alloys, and prepared metallographically by polishing through 0.25 μm diamond paste. Table 2 presents ternary and quaternary diffusion coupes that were assembled with the disks held together in Invar™ steel jig consisting of two end plates and three threaded rods. The couples were placed in quartz capsules, which were sealed at one end, and evacuated to a pressure less than 10^{-6} torr and flushed with hydrogen several times. Ar was filled into a capsule before the final sealing. The capsules containing the couples were annealed at 900˚C in a horizontal Lindberg 3-zone furnace for 168 hours. After the diffusion anneal, the couples were quenched in water to preserve the high temperature composition and/or microstructure.

The diffusion couple assembly was then mounted, sectioned and metallographically prepared for microstructural observations. Excellent diffusion bonding in all couples was observed. Then, cross-section surface was polished with 1μm diamond paste for electron microprobe analysis (EPMA). The concentration profiles of Fe, Ni, Cr, Si and Ge for the diffusion couples were determined with a

JEOL 733 (Tokyo, Japan) microprobe by point-to-point counting techniques using pure standards of all the constituent alloying elements. Intensities of K_α X-radiations were measured and converted to concentrations of Fe, Ni, Cr, Si and Ge with appropriate ZAF (atomic number, Z; absorption, A; fluorescence, F) corrections.

Table.2 List of solid-to-solid diffusion couples annealed at 900°C for 168 hours.

Series	Diffusion Couples
Fe-Ni vs. Fe-Ni-Cr-X (Si,Ge)	Fe-Ni vs. Fe-Ni-Cr
	Fe-Ni vs. Fe-Ni-Cr-Si
	Fe-Ni vs. Fe-Ni-Cr-Ge

Concentration profiles obtained from EPMA were smoothened by a smoothening-spline-tool using MatLab (The Math Works, Natick, MA). The analytical method used in this study to determine interdiffusion coefficients is by the integration of interdiffusion fluxes (e.g. Eqs. 5 and 6) only. It does not require the determination of concentration gradients that significantly reduces the influence of a smoothening procedure on the determination of interdiffusion coefficients.

Results and Discussion

Figs. 1 and 2 present examples of experimental and smoothened concentration profiles that were used for the determination of interdiffusion fluxes and interdiffusion coefficients. The scatters in the concentration profiles for all diffusion couples were minimal and within the experimental uncertainty associated with EPMA. Consistency in experimental and smoothened concentration profiles of Ni, owing to similar terminal concentration was examined by multiple EPMA acquisitions (e.g., independent Ni concentration) and by close examination of concentration profiles for Cr and X ternary alloying additions (e.g., dependent Ni concentrations).

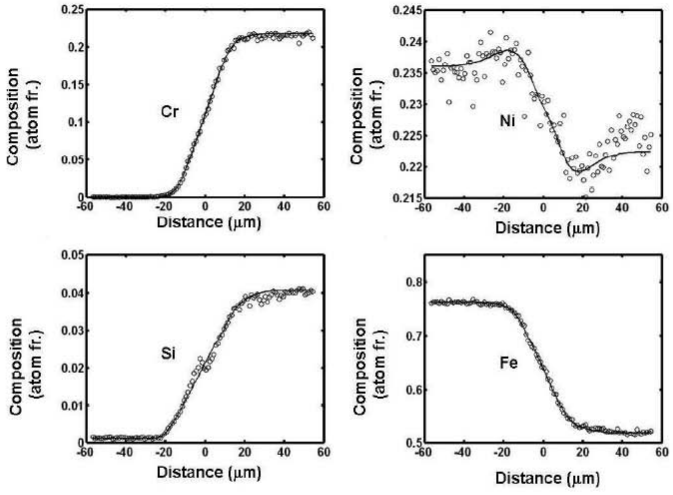

Fig. 1. Typical experimental and smoothened concentration profiles from solid-to-solid diffusion couple, Fe-Ni vs. Fe-Ni-Cr-Si annealed at 900°C for 168 hours.

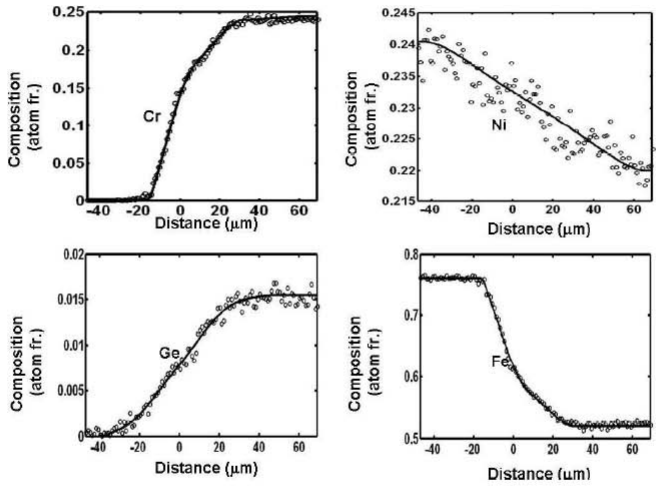

Fig. 2. Typical experimental and smoothened concentration profiles from solid-to-solid diffusion couple, Fe-Ni vs. Fe-Ni-Cr-Ge annealed at 900°C for 168 hours.

From concentration profiles obtained from diffusion couples, average effective interdiffusion coefficients $\tilde{D}_i^{eff}$'s on either side of the Matano plane were determined using Eq. 3, and are reported in Table 3. Fe-Ni vs. Fe-Ni-Cr is considered as a reference to compare and contrast the diffusional interactions of alloying elements Si and Ge. Average effective interdiffusion coefficients reported in Table 3 are comparable in magnitude to those determined for Ni-Cr-X (Si, Ge) alloys at 900°C [12]. Alloying additions have increased the magnitude of average effective interdiffusion coefficients of Cr and Fe on the $\left(C_i^{\circ} \sim C_i^{+\infty}\right)$ side with X (X = Si or Ge) alloying additions.

Table.3 Average effective interdiffusion coefficients determined from Fe-Ni vs. Fe-Ni-Cr-X (Si, Ge) diffusion couples annealed at 900°C for 168 hours. (Units: 10^{-16} m^2/s)

Diffusion Couple	Composition Range	$\tilde{D}_{Cr}^{eff}$	$\tilde{D}_{X}^{eff}$	$\tilde{D}_{Ni}^{eff}$	$\tilde{D}_{Fe}^{eff}$
Fe-Ni vs. Fe-Ni-Cr	$\left(C_i^{-\infty} \sim C_i^{\circ}\right)$	0.6	N/A	N/A	0.6
	$\left(C_i^{\circ} \sim C_i^{+\infty}\right)$	0.3	N/A	N/A	0.3
Fe-Ni vs. Fe-Ni-Cr-Si (X = Si)	$\left(C_i^{-\infty} \sim C_i^{\circ}\right)$	0.7	1.3	-2.8	0.9
	$\left(C_i^{\circ} \sim C_i^{+\infty}\right)$	0.8	1.2	-2.3	1.0
Fe-Ni vs. Fe-Ni-Cr-Ge (X = Ge)	$\left(C_i^{-\infty} \sim C_i^{\circ}\right)$	0.7	2.8	3.9	0.7
	$\left(C_i^{\circ} \sim C_i^{+\infty}\right)$	1.8	2.7	2.9	1.7

Note: $\tilde{D}_{Ni}^{eff}$ could not be determined since there was no observable development of concentration gradient (i.e., pseudo-binary).

Duh's [16] study for interdiffusion in Fe-Ni-Cr alloys at 1100°C reported a decrease in $\tilde{D}_{CrCr}^{Fe}$ values with an increase in Cr at constant Ni concentration. Similar observation was made in this study

from Fe-Ni vs. Fe-Ni-Cr diffusion couple where $\tilde{D}_{Cr}^{eff}$ was determined to decrease on the $\left(C_i^{\circ} \sim C_i^{+\infty}\right)$ region with higher Cr content. However, the influence of Si and Ge alloying additions on quaternary diffusion couples altered this trend by increasing the $\tilde{D}_{Cr}^{eff}$ on the $\left(C_i^{\circ} \sim C_i^{+\infty}\right)$ side where the contents of both Cr and X (X = Si or Ge) are higher. The $\tilde{J}_{Si}$ caused an uphill-diffusion of Ni as shown in Fig. 1, which yielded a negative average effective interdiffusion coefficients of Ni, $\tilde{D}_{Ni}^{eff}$, reported in Table 3. This indicates a significant diffusional interaction between Ni and Si in austenitic Fe-based alloys where $\tilde{J}_{Ni}$ would be significantly influence by the concentration gradient of Si, $\partial C_{Si}/\partial x$. There was no "noticeably-unusual" redistribution of Ni in Fe-Ni vs. Fe-Ni-Cr-Ge diffusion couple as shown in Fig. 2. However, a higher magnitude of $\tilde{D}_{Ni}^{eff}$ in Table 3 is noted for all concentration ranges within this diffusion couple.

Concentration profiles obtained from diffusion couples were employed to determine the average quaternary interdiffusion coefficients $\overline{\tilde{D}}_{ij}^{Fe}(i,j=Cr,Ni,X)$ on either side of the Matano plane using Eq. 5 and Eq. 6. They are reported in Table 4. Average ternary interdiffusion coefficients $\overline{\tilde{D}}_{ij}^{Fe}(i,j=Cr,Ni)$ could not be determined since there was no observable development of concentration gradient for Ni in Fe-Ni vs. Fe-Ni-Cr diffusion couple (i.e., pseudo-binary). Table 4 reports that the magnitude of these interdiffusion coefficients are comparable to those obtained for Ni-Cr-X alloys at 900°C [11]. These diffusion couples were designed with initial $\partial C_{Ni}/\partial x \approx 0$, and to yield the same sign of $\partial C_{Cr}/\partial x$ and $\partial C_X/\partial x$, so that a positive and negative $\overline{\tilde{D}}_{CrX}^{Fe}$ indicates an increase and a decrease in $\tilde{J}_{Cr}$, respectively. Also, the initial $\partial C_{Ni}/\partial x \approx 0$ implies that, $\tilde{J}_{Ni}$ is mainly due to $\partial C_{Cr}/\partial x$ and/or $\partial C_X/\partial x$, and the magnitude and sign of $\overline{\tilde{D}}_{NiCr}^{Fe}$ and/or $\overline{\tilde{D}}_{NiX}^{Fe}$.

Table.4 Average quaternary interdiffusion coefficients determined from Fe-Ni vs. Fe-Ni-Cr-X (X = Si or Ge) diffusion couples annealed at 900°C for 168 hours. (Units: 10^{-16} m^2/s)

Couple	Composition Range	$\overline{\tilde{D}}_{CrCr}^{Fe}$	$\overline{\tilde{D}}_{CrNi}^{Fe}$	$\overline{\tilde{D}}_{CrX}^{Fe}$	$\overline{\tilde{D}}_{NiCr}^{Fe}$	$\overline{\tilde{D}}_{NiNi}^{Fe}$	$\overline{\tilde{D}}_{NiX}^{Fe}$	$\overline{\tilde{D}}_{XCr}^{Fe}$	$\overline{\tilde{D}}_{XNi}^{Fe}$	$\overline{\tilde{D}}_{XX}^{Fe}$
Fe-Ni vs. Fe-Ni-Cr-Si (X=Si)	$\left(C_i^{-\infty} \sim C_i^{\circ}\right)$	1.1	0.3	-2.1	-0.1	2.7	2.7	0.2	Neg.	0.1
	$\left(C_i^{\circ} \sim C_i^{+\infty}\right)$	1.0	0.3	-1.1	-0.3	1.6	4.2	0.1	Neg.	0.3
Fe-Ni vs. Fe-Ni-Cr-Ge (X=Ge)	$\left(C_i^{-\infty} \sim C_i^{\circ}\right)$	0.8	-0.1	0.4	-0.3	4.3	4.3	0.1	-0.6	0.1
	$\left(C_i^{\circ} \sim C_i^{+\infty}\right)$	1.6	-0.4	2.9	-0.3	3.2	3.3	Neg.	-0.3	1.5

Note: "Neg." refers to magnitude less than 0.1 x 10^{-16} m^2/s.

The $\tilde{D}_{CrNi}^{Fe}$ and $\tilde{D}_{NiCr}^{Fe}$ cross coefficients have been reported small in magnitude and both positive and negative signs in literature [16-18] for Fe-Ni-Cr alloys. This holds true for quaternary cross coefficients, $\overline{\tilde{D}}_{CrNi}^{Fe}$ and $\overline{\tilde{D}}_{NiCr}^{Fe}$ reported in Table 4. This implies that there is no significant influence of Ni and Cr on each other in austenitic Fe alloys. The magnitude of $\overline{\tilde{D}}_{SiSi}^{Fe}$ is lower than that of both

$\overline{\tilde{D}}^{Fe}_{NiNi}$ and $\overline{\tilde{D}}^{Fe}_{CrCr}$ coefficients for Fe-Ni-Cr-Si alloys. However, the magnitude of $\overline{\tilde{D}}^{Fe}_{CrSi}$ and $\overline{\tilde{D}}^{Fe}_{NiSi}$ coefficients is comparable to that of $\overline{\tilde{D}}^{Fe}_{CrCr}$ and $\overline{\tilde{D}}^{Fe}_{NiNi}$ coefficients. The large magnitude of $\overline{\tilde{D}}^{Fe}_{NiSi}$ would have caused an uphill-diffusion of Ni. The magnitude of $\overline{\tilde{D}}^{Fe}_{GeGe}$ coefficient is comparable with that of $\overline{\tilde{D}}^{Fe}_{CrCr}$, and slightly lower than that of $\overline{\tilde{D}}^{Fe}_{NiNi}$ coefficient. Even though the magnitude of $\overline{\tilde{D}}^{Fe}_{NiGe}$ is large, an apparent uphill-diffusion of Ni is be absent due to a large $\overline{\tilde{D}}^{Fe}_{NiNi}$ despite a very small $\partial C_{Ni}/\partial x$.

Summary

Interdiffusion in Fe-Ni-Cr (fcc γ phase) alloys with small additions of Si and Ge was studied using solid-to-solid diffusion couples annealed at 900°C for 168 hours. Alloying addition of Si or Ge altered diffusional behavior of Ni and Cr in austenitic Fe-Ni-Cr alloys. Large magnitude of cross coefficients, $\overline{\tilde{D}}^{Fe}_{CrSi}$, $\overline{\tilde{D}}^{Fe}_{CrGe}$, $\overline{\tilde{D}}^{Fe}_{NiSi}$ and $\overline{\tilde{D}}^{Fe}_{NiGe}$ were observed in Fe-Ni-Cr-X (X=Si or Ge) alloys. The Si addition has caused on uphill-diffusion of Ni while there was no measurable uphill diffusion of Ni due to an increase in $\overline{\tilde{D}}^{Fe}_{NiNi}$ in Fe-Ni-Cr-Ge alloy, despite the large positive $\overline{\tilde{D}}^{Fe}_{NiGe}$.

Acknowledgements

This work was supported by the NSF CAREER Award under the grant DMR-0238356.

References

[1] J.L. Smialek and G.H.Meier, in: *High temperature oxidation*, edited by C.T. Sims, N.S. Stoloff, and W.C. Hagel, of Superalloy II, chapter 11, John Weley & Sons (1987) p. 293-323.

[2] P. Kofstad, in: *Growth and protective properties of Chromia and Alumina scales, protective coatings*, High temperature Corrosion, Elsevier, London (1980) p. 389-404.

[3] J.L. Smialek, C.A. Barrett, J.C. Schaffer, in: *Design for oxidation resistance*, edited by George E. Dieter,Vol. 20 of ASM handbook, ASM International (1997).

[4] F.H. Stott, G.C. Wood, and J. Stringer : Oxi. Metals, Vol. 44 (1995), p. 113-145.

[5] H.E. Evans, D.A. Hilton, R.A. Holm et al.: Oxi. Metals, Vol. 19 (No. 1-2), 1983, p. 1-18.

[6] S.N.Basu, G.J.Yurek: Oxi. Metals, Vol. 36 (No. 3-4), 1991, p. 281-315.

[7] A. Kumar, D.L. Douglass: Oxi. Metals, Vol. 10 (No. 1), 1976, p. 1-22.

[8] D.P. Whittle, J. Stringer: Proc. R. Soc. Lond., Ser. A, Vol. 295 (1980), p.309-329.

[9] G.C. Wood, F.H. Stott: Mater. Sci. Technol., Vol.3 (1987), p. 519-530.

[10] N. Garimella, M.P. Brady, Y.H. Sohn: Defects and Diffusion Forum, Vol. 266, (2007), p. 191-198.

[11] N. Garimella, M.P. Brady, Y.H. Sohn: Journal of Phase Equilibria and Diffusion, Vol. 27, (2006), p. 665-670.

[12] L.Onsager, Ann. N.Y.Acad. Sci., Vol. 46 (1965), p. 241-265.

[13] M.A. Dayananda, C.W. Kim: Metall. Trans. A, Vol. 10A (1979), p. 1333-1339.

[14] M.A. Dayananda, Y.H. Sohn: Scr. Mater., Vol. 40 (1996), p. 683-688.

[15] M.A. Dayananda, Y.H. Sohn: Metall. Trans. A, Vol. 30A (1999), p 535-543.

[16] J.G. Duh: Ph.D. Thesis, Purdue University, West Lafayette, IN, U.S.A. (1983).

[17] M.A. Krishtal, P.N. Zakharov, A.P. Mokrov et al.: Izv. Akad. Nauk SSSR, Met., No. 2 (1972) p. 75-78.

[18] A.P. Mokrov, V.K. Akimov and P.N. Zakharov: Izv. Akad. Nauk SSSR, Met., No. 1 (1979), p. 234- 238.

Intermetallics 16 (2008) 1095–1103

Contents lists available at ScienceDirect

Intermetallics

journal homepage: www.elsevier.com/locate/intermet

Effects of Ir or Ta Alloying Addition on Interdiffusion of $L1_2$–Ni_3Al

N. Garimella [a], M. Ode [b], M. Ikeda [c], H. Murakami [b], Y.H. Sohn [a,*]

[a] Advanced Materials Processing and Analysis Center, MMAE, University of Central Florida, 4000 Central Florida Boulevard, Orlando, FL 32816, USA
[b] National Institute of Materials Science, Tsukuba, Japan
[c] Kobe Steel, Co. Ltd., Japan

article info

Article history:
Received 18 December 2007
Received in revised form 8 May 2008
Accepted 24 June 2008
Available online 8 August 2008

Keywords:
A. Nickel aluminides, based on Ni_3Al
B. Diffusion
D. Site occupancy
F. Electron microprobe

abstract

Ternary interdiffusion in $L1_2$–Ni_3Al with ternary alloying additions of Ir and Ta was investigated at 1473 K using solid-to-solid diffusion couples. Average ternary interdiffusion coefficients were determined from an integration of interdiffusion fluxes calculated directly from experimental concentration profiles. The magnitude of $\bar{D}_{NiNi}$ and $\bar{D}_{AlAl}$ coefficients was determined to be much larger than that of $\bar{D}_{IrIr}$ and $\bar{D}_{TaTa}$ coefficients. Ir substituting in Ni-site influenced the interdiffusion of Ni significantly, and $\bar{D}^{Al}_{NiIr}$ coefficients were determined to be large and positive. On the other hand, Ta substituting for Al influenced the interdiffusion of Al significantly, and $\bar{D}^{Ni}_{AlTa}$ coefficients were determined to be large and positive. An excellent agreement was found with ternary interdiffusion coefficients determined by Boltzmann–Matano analysis. Profiles of concentrations and interdiffusion fluxes were also examined to estimate binary interdiffusion coefficients in Ni_3Al, and tracer diffusion coefficients of Ir (14.7 10 16 1.4 10 16 m^2/s) and Ta (2.6 10 16 2.4 10 16 m^2/s) in Ni_3Al.

1. Introduction

Nickel-base superalloys are extensively used in both aviation and land-based gas turbine environments, and many studies have been devoted to improve their mechanical properties and microstructural stability [1]. Ni-base superalloys are typically composed of $L1_2$ g′-phase (Ni_3Al) coherently precipitated in a fcc g-phase matrix. The diffusion mobility database for Ni-base superalloys is available for fcc phase [2]. Although g′ is the strengthening phase of Ni-base superalloys, a limited number of studies exists on interdiffusion of the g′-phase [3–9], particularly when alloyed with other constituents in superalloys. An understanding of multicomponent diffusion processes in these alloys is very important because it is essential to achieve a durable microstructure for strength and oxidation resistance at high temperature. This study is also fueled by recent conceptual development of refractory based superalloys with $L1_2$ precipitates and refractory-modified aluminide coatings [10–15] for optimized oxidation resistance along with reduced interdiffusion between oxidation resistant coatings and structural superalloy substrate (e.g., formation of deleterious phases due to interdiffusion at the interface).

The crystal structure of Ni_3Al is derived from an fcc based Cu_3Au prototype lattice with face centered sublattice sites (a-sites) occupied by Ni atoms and corner sublattice sites (b-sites) by Al-atoms. In general, highly electronegative substitutional elements (e.g., Pt, Cu and Co) occupy the a-sites, where as highly electropositive ones (e.g., Ti, Ta and Nb) occupy the b-sites in Ni_3Al [1]. The relative site-preference for some ternary alloying elements can be best illustrated from the direction of the solubility lobes for the g′-phase within the ternary isotherm of Ni–Al–X (X alloying addition) system at 1273 K as shown by Fig. 1 [16]. In Fig. 1, Pt (i.e., group VIII metal that includes Ir) and Ta are highlighted with circles. Site-preference of ternary alloying additions to Ni_3Al has attracted significant interest, as this true solid solution accepts considerable amount of third elements into solution [17–19].

The alloying phenomenon ultimately plays an important role in enhancing the mechanical properties and high-temperature oxidation resistance of this intermetallic [18–25]. The behavior of ternary substitutional alloying additions to Ni_3Al was first reported by Guard and Westbrook [17] as Ni-occupiers, Al-occupiers or both Ni- and Al-occupiers. Several studies [26–28] have predicted the change in site-preference of alloying elements as a function of temperature and chemical composition of Ni_3Al.

Diffusional interactions of a ternary alloying addition to Ni_3Al can be a tool to examine the site-preference. The diffusion mechanism in ordered alloys is recognized to be more complex than for disordered solid solutions [29]. In the case of $L1_2$ structure, the diffusion mechanism is even more complex than that for B2 structure. Diffusion can occur through a- or b-site where Ni or Al-atoms mainly occupy, respectively, and the diffusion coefficient

* Corresponding author. Tel.: 1 4078821181.
E-mail address: ysohn@mail.ucf.edu (Y.H. Sohn).

0966-9795/$ – see front matter
doi:10.1016/j.intermet.2008.06.011

largely depends on the alloy composition, namely the degrees of order [30–32]. While tracer diffusion studies in g′-Ni_3Al are difficult since ^{26}Al is not readily available, self-diffusion of Ni and chemical/impurity diffusion in Ni_3Al binary and Ni_3Al–X ternary alloys (X Pt, Ti, Cr, Fe, Nb, Ga, Mo) have been studied [3–5]. The temperature dependency of the diffusion for a ternary alloying addition is evident from Arrhenius rate law [5,33–35]. The b-site occupiers have been observed to diffuse slower than the a-site occupiers [29,36]. This is attributed to the fact that, in $L1_2$-ordered structure, each Ni atom is surrounded by 4 Al-atoms and 8 Ni atoms, where as an Al atom is surrounded by 12 Ni atoms. Therefore, the activation enthalpy of alloying element increases mainly due to the antisite-defect formation [36].

For an additional insight to understand the diffusion process in $L1_2$ structure, to enhance microstructural stability of Ni-base superalloys, and to develop refractory-modified aluminide oxidation resistant coatings, we examined the ternary diffusional interaction of Ir and Ta additions to the $L1_2$ Ni_3Al phase. Solid-to-solid diffusion couples were assembled and annealed at 1473 K for 5 h. Based on concentration profiles obtained by electron probe microanalysis, average ternary interdiffusion coefficients from an integration of interdiffusion fluxes, and ternary interdiffusion coefficients via Boltzmann–Matano analysis were determined to assess how Ir and Ta additions influence interdiffusion behavior of Ni and Al in $L1_2$ Ni_3Al phase. Additional estimates of binary interdiffusion coefficients in Ni_3Al, and tracer diffusion coefficients of Ir and Ta in Ni_3Al were made.

2. Determination of ternary interdiffusion coefficients

From Onsager's formalism [37,38] and Fick's law [39], the interdiffusion flux J_i of component i in a ternary system can be expressed in terms of two independent concentration gradients $\partial C_j/\partial x$ by:

$$J_i \quad \tilde{D}^3_{i1}\frac{\partial C_1}{\partial x} \quad \tilde{D}^3_{i2}\frac{\partial C_2}{\partial x} \quad i \quad 1;2 \tag{1}$$

where $\tilde{D}^3_{ij}$s refer to the ternary interdiffusion coefficients. An experimental determination of the four concentration-dependent interdiffusion coefficients is generally carried out by the use of Boltzmann–Matano analysis with two independent diffusion couples that develop a common composition in the diffusion zone where the interdiffusion coefficients can be evaluated [40,41].

Alternatively, the interdiffusion fluxes of individual components can be determined directly from their concentration profiles

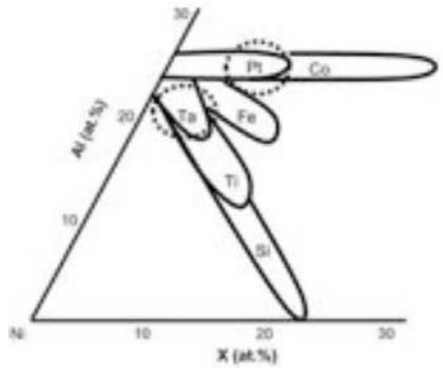

Fig. 1. Solubility ranges of selected ternary alloying additions in Ni_3Al (adopted from Ochiai et al. [16]) at 1273 K.

Table 1
Nominal composition of alloys employed for diffusion couple studies

Alloy identification	Composition (atom percent)			Composition (weight percent)		
	Ni	Al	Ir or Ta	Ni	Al	Ir or Ta
Ni–24.5Al	76.0	24.0	0	59.3	40.7	0.0
Ni–25Al	75.0	25.0	0	58.0	42.0	0.0
Ni–26Al	74.5	25.5	0	57.3	42.7	0.0
Ni–23.5Al–1Ir	75.5	23.5	1.0	59.5	40.3	0.2
Ni–24.5Al–1Ir	74.5	24.5	1.0	58.2	41.6	0.2
Ni–23Al–2Ir	74.5	23.5	2.0	59.0	40.5	0.5
Ni–23Al–3Ir	74.0	23.0	3.0	59.2	40.0	0.7
Ni–23Al–1.5Ta	75.5	23.0	1.5	59.9	39.7	0.4

without the need or use of the interdiffusion coefficients. The interdiffusion flux at any section x can be calculated directly from the concentration profile from the relation [42,43]:

$$J_i \quad \frac{1}{2t}\int_{C_i \text{ or } C_i}^{C_i\, x} x \quad x_o \, dC_i \quad i \quad 1;2; \ldots ;n \tag{2}$$

where t is the time, C_i and C_i are the terminal concentrations, and x_o refers to the location of the Matano plane. Based on the direct determination of interdiffusion fluxes, diffusional behavior of components can be examined, and observations of zero-flux-planes (ZFPs) and flux-reversals have been reported for individual components in isothermal ternary interdiffusion studies [42–45]. Furthermore, the calculated interdiffusion fluxes can be related to interdiffusion parameters which can be employed to generate and characterize concentration profiles developed in ternary diffusion couples [46–49].

The interdiffusion flux J_i determined from Eq. (2) as a function of x can be integrated over a selected region, x_1–x_2, to yield an expression based on Eq. (1) [49]:

$$\int_{x_1}^{x_2} J_i dx \quad \int_{C_1\,x_1}^{C_1\,x_2} \tilde{D}^3_{i1} dC_1 \quad \int_{C_2\,x_1}^{C_2\,x_2} \tilde{D}^3_{i2} dC_2 \quad i \quad 1;2$$
$$\bar{\tilde{D}}^3_{i1}\,C_1\,x_1 \quad C_1\,x_2 \quad \bar{\tilde{D}}^3_{i2}\,C_2\,x_1$$
$$C_2\,x_2 \quad i \quad 1;2 \tag{3}$$

where $\bar{\tilde{D}}^3_{ij}$s correspond to the average values of main and cross-interdiffusion coefficients.

With $\bar{\tilde{D}}^3_{ij}$s taken as constants, Eq. (1) is re-written as:

$$J_i \quad \bar{\tilde{D}}^3_{i1}\frac{\partial C_1}{\partial x} \quad \bar{\tilde{D}}^3_{i2}\frac{\partial C_2}{\partial x} \quad i \quad 1;2 \tag{4}$$

If both sides of Eq. (4) are multiplied by $x \quad x_o$ ^{m} and integrated over the diffusion zone between x_1 and x_2, one obtains in general [49]:

$$\int_{x_1}^{x_2} J_i \, x \quad x_o \,^m dx \quad \bar{\tilde{D}}^3_{i1} \int_{C_1\,x_1}^{C_1\,x_2} x \quad x_o \,^m dC_1 \quad \bar{\tilde{D}}^3_{i2}$$
$$\int_{C_2\,x_1}^{C_2\,x_2} x \quad x_o \,^m dC_2 \quad i \quad 1;2 \qquad 5$$

Table 2
Diffusion couples assembled and analyzed after anneal at 1473 K for 5 h

Series	Diffusion couples
Ni–Al vs. Ni–Al–Ir	Ni–25Al vs. Ni–23.5Al–1Ir
	Ni–24.5Al vs. Ni–24.5Al–1Ir
	Ni–26Al vs. Ni–23Al–2Ir
	Ni–24Al vs. Ni–24Al–2Ir
	Ni–25Al vs. Ni–23Al–3Ir
	Ni–25Al vs. Ni–23Al–2Ir
Ni–Al vs. Ni–Al–Ta	Ni–24Al vs. Ni–23Al–1.5Ta
	Ni–25Al vs. Ni–23Al–1.5Ta
	Ni–26Al vs. Ni–23Al–1.5Ta

If the exponent m is chosen to be zero, Eq. (5) becomes identical to Eq. (3). For m 1, Eq. (5) yields [49]:

$$\int_{x_1}^{x_2} J_i\,(x - x_0)\,dx = \bar{D}^3_{i1}\int_{c_1,x_1}^{c_1,x_2}(x - x_0)\,dC_1 + \bar{D}^3_{i2}\int_{c_2,x_2}^{c_2,x_1}(x - x_0)\,dC_2 = 2t\left[\bar{D}^3_{i1}\left(J_1(x_1) - J_1(x_2)\right) + \bar{D}^3_{i2}\left(J_2(x_1) - J_2(x_2)\right)\right] \quad i = 1;2 \qquad (6)$$

Eqs. (3) and (6) provide four equations involving the $\bar{D}^3_{11}$, $\bar{D}^3_{12}$, $\bar{D}^3_{21}$ and $\bar{D}^3_{22}$ interdiffusion coefficients and can be easily set up from experimental concentrations and the corresponding interdiffusion fluxes. Hence, from the concentration profiles of a single diffusion couple, $\bar{D}^3_{ij}$ $i;j = 1;2$ coefficients, characteristic of the diffusion path, can be determined by using Eqs. (3) and (6) over selected composition ranges in the diffusion zone [49]. Eqs. (3) and (6) provide independent relations when the composition ranges are selected to include non-linear segments of the profiles. This analysis method to determine average ternary interdiffusion coefficients has been directly employed in various studies [3,50–58]. In addition, the

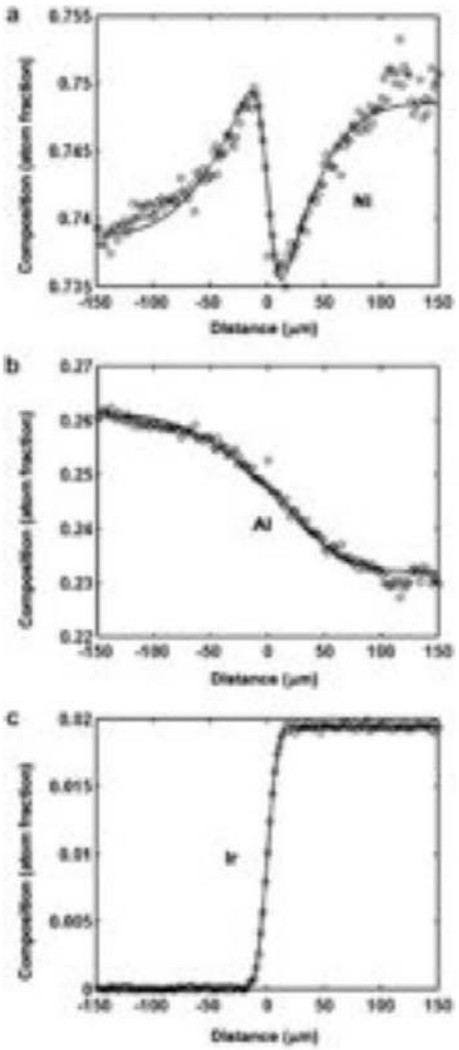

Fig. 2. Concentration profiles of (a) Ni, (b) Al and (c) Ir obtained from diffusion couple Ni–26Al vs. Ni–23Al–2Ir annealed at 1473 K for 5 h. Open circles and solid lines represent EPMA measurement and calculated concentration profiles, respectively.

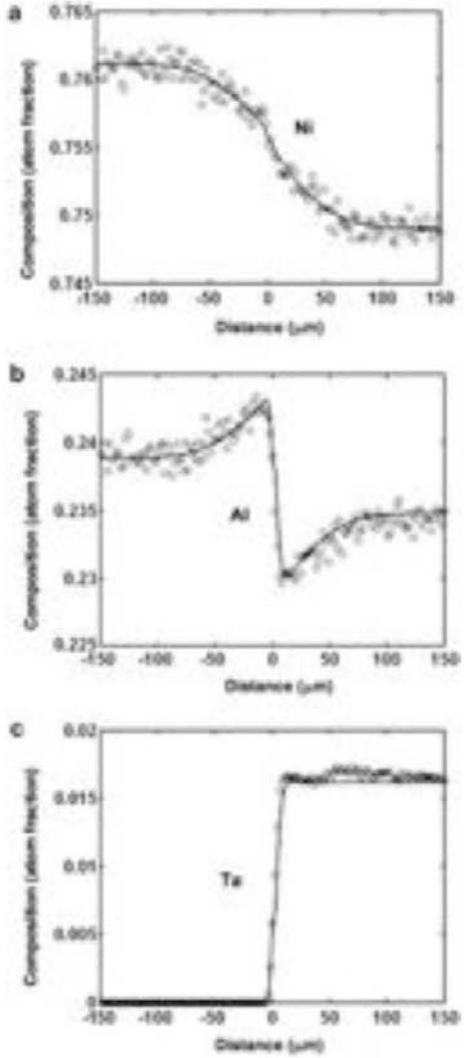

Fig. 3. Concentration profiles of (a) Ni, (b) Al and (c) Ta obtained from diffusion couple Ni–24.5Al vs. Ni–23Al–1.5Ta annealed at 1473 K for 5 h. Open circles and solid lines represent EPMA measurement and calculated concentration profiles, respectively.

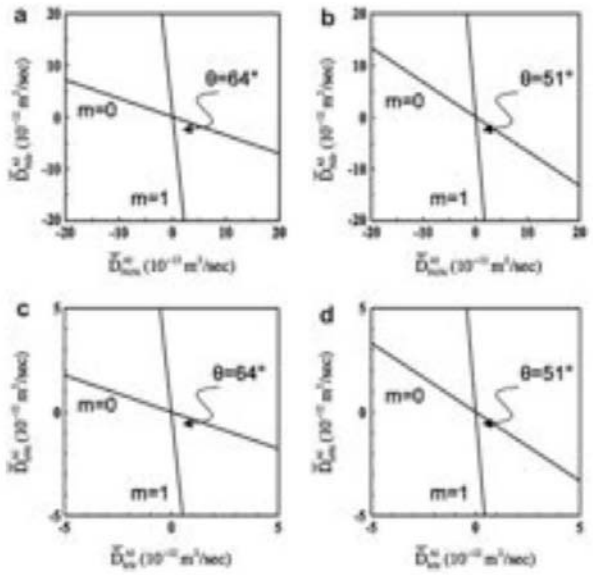

Fig. 4. Variation of $\bar{D}_{ij}^{Al}$ i;j Ni; Ir coefficients in Eq. (3), equivalent to Eq. (5) when m 0, and Eq. (6) equivalent to Eq. (5) when m 1. The two lines generated by Eqs. (3) and (6) are sufficiently independent to obtain an unique solution of $\bar{D}_{ij}^{Al}$ i;j Ni; Ir coefficients that are reported for the composition ranges of C_i C_i^o and C_i^o C_i in Table 3.

independence of Eqs. (3) and (6) in solving the average ternary interdiffusion coefficients for the concentration profiles obtained in this study is demonstrated in Section 4. In this paper, the analysis applied to the concentration profiles of experimental ternary diffusion couples in $L1_2$ Ni–Al–X (X Ir or Ta) intermetallics is carried out for 2 segments, one on either side of the Matano plane; the two chosen composition ranges are C_i C_i^o and C_i^o C_i, where C_i^o refers to the concentration at the Matano plane. The average ternary interdiffusion coefficients, $\bar{D}_{ij}^3$, determined on either side of the Matano plane are employed to simulate experimental concentration profiles using error-function solution for infinite ternary systems from Fujita and Gosting [59]. For Ni–Al vs. Ni–Al–Ir diffusion couples, the average ternary interdiffusion coefficients, $\bar{D}_{ij}^3$, are found to be consistent with ternary interdiffusion coefficients, D_{ij}^3, determined by Boltzmann–Matano analysis [40,41].

3. Experimental details

Ni–Al, Ni–Al–Ir and Ni–Al–Ta alloys were prepared by the vacuum arc melting of 99.97 wt.% Ni, 99.9 wt.% Al, 99.2 wt.% Ir, and 99.2 wt.% Ta, according to the compositions presented in Table 1. The alloys were cast into a semi-cylindrical mold with the diameter of 8 mm in an arc furnace. The alloy rods were homogenized at 1473 K for 137 h in the vacuum furnace evacuated to a pressure less than 10 ^{2} Pa. The homogenized alloys were then sectioned into discs with the height of 1.5 mm. The surfaces of alloy discs were polished metallographically up to 1200-grit and cleaned thoroughly prior to diffusion couple assembly.

Table 2 presents diffusion couples that were assembled and analyzed in this study. Coupled alloys were put into a Si_3N_4 jig and annealed at 1473 K for 0.5 h in a vacuum furnace to promote initial bonding. Since the metal discs have larger thermal expansion coefficients than the Si_3N_4 jig, the discs can adhere to each other due to the compression during the annealing treatment. Each diffusion couple fabricated in this manner was then sealed in an evacuated transparent quartz capsule, and annealed at 1473 K for 4.5 h in an atmosphere furnace. All diffusion couples were water quenched after the high-temperature anneal to preserve high-temperature microstructure and concentrations. In this study, the time required for the diffusion bonding treatment (0.5 h) was added to the total

Table 3
Average ternary interdiffusion coefficients (10 ^{16} m^2/s) determined from Ni–Al vs. Ni–Al–Ir diffusion couples annealed at 1473 K for 5 h

Diffusion couple	Composition range	$\bar{D}_{AlAl}^{Ni}$	$\bar{D}_{AlIr}^{Ni}$	$\bar{D}_{IrAl}^{Ni}$	$\bar{D}_{IrIr}^{Ni}$	$\bar{D}_{NiNi}^{Al}$	$\bar{D}_{NiIr}^{Al}$	$\bar{D}_{IrNi}^{Al}$	$\bar{D}_{IrIr}^{Al}$
Ni–25Al vs. Ni–23.5Al–1Ir	C_i ^{N} vv C_i^o	623.7	117.2	Ngl.	13.6	623.7	727.3	Ngl.	13.6
	C_i^o vv C_i ^{N}	511.6	166.6	Ngl.	11.2	511.6	667.0	Ngl.	11.2
Ni–24.5Al vs. Ni–24.5Al–1Ir	C_i ^{N} vv C_i^o	541.0	84.7	Ngl.	10.5	541.0	615.2	Ngl.	10.5
	C_i^o vv C_i ^{N}	816.9	75.7	Ngl.	19.1	816.9	873.5	Ngl.	19.1
Ni–26Al vs. Ni–23Al–2Ir	C_i ^{N} vv C_i^o	871.4	52	Ngl.	15.4	871.4	908.0	Ngl.	15.4
	C_i^o vv C_i ^{N}	591.5	117.3	Ngl.	13.0	591.5	695.8	Ngl.	13.0
Ni–25Al vs. Ni–23Al–2Ir	C_i ^{N} vv C_i^o	522	107.3	Ngl.	16.4	522	612.9	Ngl.	16.4
	C_i^o vv C_i ^{N}	494	116.6	Ngl.	15.9	494	594.7	Ngl.	15.9
Ni–25Al vs. Ni–23Al–3Ir	C_i ^{N} vv C_i^o	440.9	92.8	Ngl.	15.1	440.9	518.6	Ngl.	15.1
	C_i^o vv C_i ^{N}	441.2	135.5	Ngl.	19.3	441.2	557.4	Ngl.	19.3
Ni–24Al vs. Ni–24Al–2Ir	C_i ^{N} vv C_i^o	267.2	14.1	Ngl.	11.8	267.2	241.3	Ngl.	11.8
	C_i^o vv C_i ^{N}	318.0	9.8	Ngl.	14.8	318.0	293.4	Ngl.	14.8

Note: Ngl. refers to magnitude less than 0.1 10 ^{16} m^2/s.

Table 4
Average ternary interdiffusion coefficients (10^{-16} m^2/s) determined from Ni–Al vs. Ni–Al–Ta diffusion couples annealed at 1473 K for 5 h

Diffusion couple	Composition range	$\bar{D}^{Ni}_{AlAl}$	$\bar{D}^{Ni}_{AlTa}$	$\bar{D}^{Ni}_{TaAl}$	$\bar{D}^{Ni}_{TaTa}$	$\bar{D}^{Al}_{NiNi}$	$\bar{D}^{Al}_{NiTa}$	$\bar{D}^{Al}_{TaNi}$	$\bar{D}^{Al}_{TaTa}$
Ni–24.5Al vs. Ni–23Al–1.5Ta	$C_i^N \forall C_i^o$	561	501.3	Ngl.	3.2	561	56.5	Ngl.	3.2
	$C_i^o \forall C_i^N$	482.6	451.8	Ngl.	1.8	482.6	29	Ngl.	1.8
Ni–25Al vs. Ni–23Al–1.5Ta	$C_i^N \forall C_i^o$	810.4	807.1	Ngl.	3.4	810.4	Ngl.	Ngl.	3.4
	$C_i^o \forall C_i^N$	652.7	580.5	Ngl.	1.9	652.7	70.3	Ngl.	1.9
Ni–26Al vs. Ni–23Al–1.5Ta	$C_i^N \forall C_i^o$	313.2	333.6	Ngl.	3.7	313.2	24.1	Ngl.	3.7
	$C_i^o \forall C_i^N$	445	391.9	Ngl.	5.6	445	47.5	Ngl.	5.6

Note: Ngl. refers to magnitude less than 0.1 10^{-16} m^2/s.

annealing time. Thus, concentration profiles from all diffusion couples were analyzed with diffusion anneal time of 5 h.

Microstructures and concentration profiles of the annealed diffusion couples were analyzed by JEOL-JXA-8900 electron probe microanalyzer (EPMA). An accelerating voltage of 20 kV, a beam current of 50 nA, and a probe diameter of 1 μm were employed for data acquisition of Ni Kα x-radiation peak using LIF crystal, Al Kα x-radiation peak using TAP crystal, Ir Lα x-radiation using LIFH crystal, and Ta Lα x-radiation using LIFH crystal. Pure element standards of Ni, Al, Ir, Ta, along with ZAF correction [60], were used for quantification of concentrations via point-to-point count technique.

4. Results and analysis

4.1. Profiles of concentrations and interdiffusion fluxes

Figs. 2 and 3 present typical concentration profiles obtained by EPMA measurements from diffusion couples, Ni–26Al vs. Ni–23Al–2Ir and Ni–24.5Al vs. Ni–23Al–1.5Ta, respectively, annealed at 1473 K for 5 h. The x-axis represents the distance from the Matano plane and the open circles are EPMA measurement. Scatter in the concentration profiles for all diffusion couples was minimum and within the experimental uncertainty associated with EPMA. The interdiffusion fluxes of individual components were then determined using Eq. (2) from experimental concentration profiles that were smoothend with a series of weighted splines. While no zero-flux plane was observed, a significant diffusional interaction between Ni and Ir, and Al and Ta was observed when Ni_3Al was diffusion annealed against Ni_3Al alloyed with Ir and Ta, respectively, as shown in Figs. 2 and 3. Clearly, the interdiffusion of Ni was greatly enhanced by the interdiffusion of Ir down the Ir gradient, while Al exhibited an uphill diffusion against its own gradient due to the interdiffusion of Ta. However, diffusional influence of Ir on Al and Ta on Ni is difficult to ascertain from the profiles presented in Figs. 2 and 3. Determination of ternary interdiffusion coefficients can quantify the extent and magnitude of these diffusional interactions, and provide competent approaches to compositional design and modification of alloys and protective coatings.

4.2. Average ternary interdiffusion coefficients

From profiles of concentration and interdiffusion fluxes in Ni–Al vs. Ni–Al–Ir diffusion couples, average ternary interdiffusion coefficients, $\bar{D}^{Ni}_{ij}$ i; j Al; Ir and $\bar{D}^{Al}_{ij}$ i; j Ni; Ir , were determined on either side of the Matano plane using Eqs. (3) and (6). Use of Eqs. (3) and (6) provides independent relations for the determination of average ternary interdiffusion coefficients as presented in Fig. 4. In this figure, for diffusion couple Ni–26Al vs. Ni–23Al–2Ir whose

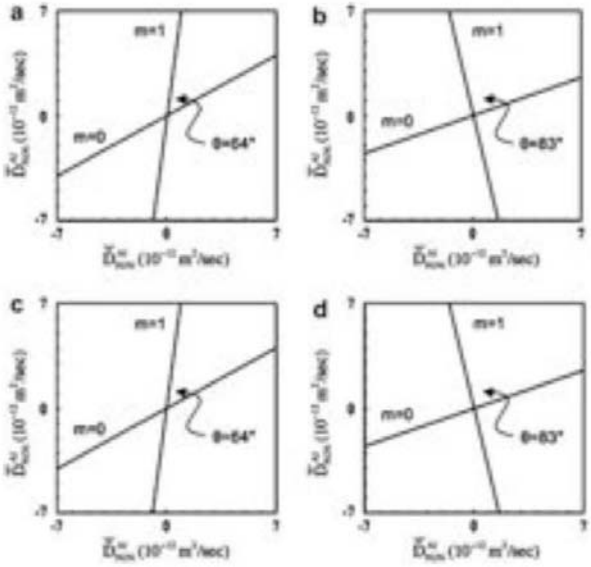

Fig. 5. Variation of $\bar{D}^{Ni}_{ij}$ i; j Al; Ta coefficients in Eq. (3), equivalent to Eq. (5) when m 0, and Eq. (6) equivalent to Eq. (5) when m 1. The two lines generated by Eqs. (3) and (6) are sufficiently independent to obtain an unique solution of $\bar{D}^{Ni}_{ij}$ i; j Al; Ta coefficients that are reported for the composition ranges of C_i C_i^o and C_i^o C_i in Table 4.

concentration profiles are presented in Fig. 2, the variation of $\bar{D}_{ij}^{Al}$ i;j Ni;Ir in Eq. (5) where m 0, equivalent to Eq. (3), and m 1, equivalent to Eq. (6), is presented. The two lines generated by Eqs. (3) and (6) are sufficiently independent to obtain an unique solution of $\bar{D}_{ij}^{Al}$ i;j Ni;Ir coefficients that are reported in Table 3.

The main diffusion coefficients, $\bar{D}_{AlAl}^{Ni}$ and $\bar{D}_{NiNi}^{Al}$, correspond well to the interdiffusion coefficients of Al and Ni reported in literature for binary Ni_3Al at 1473 K [3–9]. Estimation of binary interdiffusion coefficients from the ternary diffusion couples and the comparison to the interdiffusion coefficients of Al and Ni reported in literature for binary Ni_3Al are presented in detail in Section 4.4. The magnitudes of these main coefficients for Al and Ni are observed to be larger with higher Al content as well. The main interdiffusion coefficient of Ir, $\bar{D}_{IrIr}$, is 20–40 times lower in magnitude than the main coefficients of Ni and Al. Table 3 reports that $\bar{D}_{AlIr}^{Ni}$ coefficients are negative, and smaller in magnitude than $\bar{D}_{AlAl}^{Ni}$ coefficients, and $\bar{D}_{IrAl}^{Ni}$ coefficients are negligibly small (<0.1 10 ^{16} m^2/s). Thus the interdiffusion flux of Al can be influenced only slightly by the interdiffusion of Ir. However, $\bar{D}_{NiIr}^{Al}$ coefficients are positive and large (e.g., larger than the $\bar{D}_{NiNi}^{Al}$ coefficients in some cases), while $\bar{D}_{IrNi}^{Al}$ coefficients are negligibly small (<0.1 10 ^{16} m^2/s). The large positive $\bar{D}_{NiIr}^{Al}$ coefficient corresponds well with an enhanced interdiffusion of Ni (e.g., down the gradient of Ir). Against the concentration gradient of Ir, the large positive $\bar{D}_{NiIr}^{Al}$ coefficient can therefore reduce the interdiffusion of Ni. The average ternary interdiffusion coefficients reported in Table 3 indicate a strong diffusional interaction between Ni and Ir both occupying the a-site in $L1_2$ lattice structure.

The average ternary interdiffusion coefficients, $\bar{D}_{ij}^{Ni}$ i;j Al;Ta and $\bar{D}_{ij}^{Al}$ i;j Ni;Ta , determined on either side of the Matano plane for Ni–Al vs. Ni–Al–Ta couples are reported in Table 4. For diffusion couple Ni–24.5Al vs. Ni–23Al–1.5Ta whose concentration profiles are presented in Fig. 3, the variation of $\bar{D}_{ij}^{Ni}$ i;j Al;Ta in Eq. (3), equivalent to Eq. (5) where m 0, and Eq. (6), equivalent to Eq. (5) where m 1 is presented in Fig. 5. The two lines generated by Eqs. (3) and (6) are again sufficiently independent to obtain an unique solution of $\bar{D}_{ij}^{Ni}$ i;j Al;Ta coefficients that are reported in Table 4.

The main diffusion coefficients, $\bar{D}_{AlAl}^{Ni}$ and $\bar{D}_{NiNi}^{Al}$, again correspond well to the interdiffusion coefficients of Al and Ni reported in literature [3–9] for Ni_3Al at 1473 K. Aforementioned, estimation of binary interdiffusion coefficients from the ternary diffusion couples along with the comparison to the interdiffusion coefficients of Al and Ni reported in literature for binary Ni_3Al is presented in detail in Section 4.4. The main interdiffusion coefficient of Ta, $\bar{D}_{TaTa}$, is 10–40 times lower in magnitude than the main coefficients of Ni and Al. Table 4 reports that $\bar{D}_{AlTa}^{Ni}$ coefficients are positive, and comparable in magnitude to $\bar{D}_{AlAl}^{Ni}$ coefficients, while $\bar{D}_{TaAl}^{Ni}$ coefficients are negligibly small (<0.1 10 ^{16} m^2/s). Thus, the large positive $\bar{D}_{AlTa}^{Ni}$ coefficient corresponds well with an interdiffusion flux of Al (e.g., uphill diffusion) against the gradient of Ta. The $\bar{D}_{NiTa}^{Al}$ coefficients are positive, but much smaller than the $\bar{D}_{NiNi}^{Al}$ coefficients, and $\bar{D}_{TaNi}^{Al}$ coefficients are negligibly small (<0.1 10 ^{16} m^2/s). Thus the interdiffusion flux of Ni can be influenced only slightly by the interdiffusion flux of Ta. The average ternary interdiffusion coefficients reported in Table 4 indicate a strong diffusional interaction between Al and Ta both occupying the b-site in $L1_2$ lattice structure.

The average ternary interdiffusion coefficients reported in Tables 3 and 4 were employed to generate concentration profiles using error-function solution provided by Fujita and Gosting [59]. Excellent agreement between EPMA measurement and calculated concentration profiles were found for all couples. Typical examples are presented in Figs. 2 and 3 where open circles are the EPMA measurements and solid lines are the calculated concentration profiles.

4.3. Ternary interdiffusion coefficients determined by Boltzmann–Matno analysis

For the diffusion couples Ni–Al vs. Ni–Al–Ir, several intersecting compositions were found among the diffusion paths. Intersecting diffusion paths in Fig. 6 represent typical difficulties in determining interdiffusion coefficients by Boltzmann–Matano analysis for ordered intermetallics with ternary alloying addition. Two diffusion paths of interest can intersect at a shallow angle or with negligible Ir concentration gradient. These are due to site-preference of Ir and Ni on a-site in $L1_2$ lattice structure, and small interdiffusion

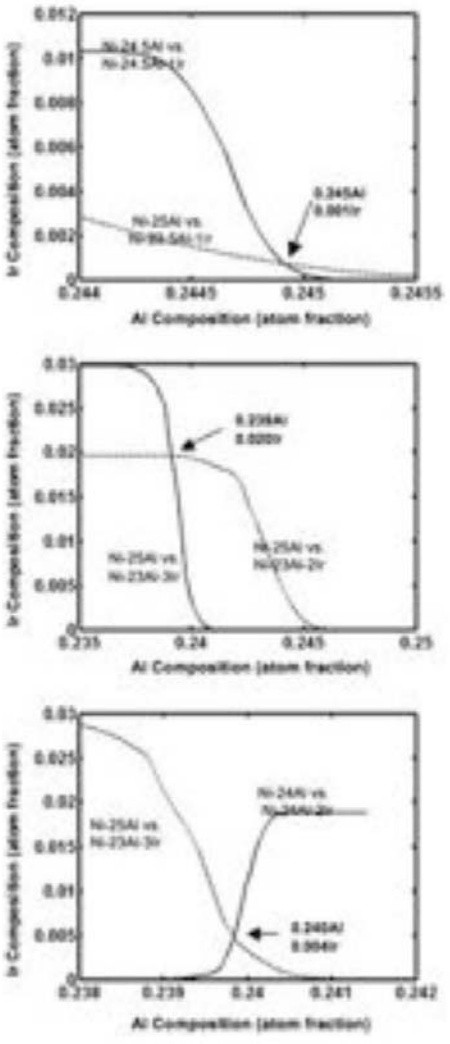

Fig. 6. Typical intersecting diffusion paths of Ni–Al vs. Ni–Al–Ir diffusion couples annealed at 1473 K for 5 h. Compositions at these intersections were employed for the determination of ternary interdiffusion coefficients based on Boltzmann-Matano analysis.

Table 5
Ternary interdiffusion coefficients (10 ^{16} m^2/s) determined by Boltzmann–Matano analysis from Ni–Al vs. Ni–Al–Ir diffusion couples annealed at 1473 K for 5 h

Diffusion couples with intersecting diffusion paths	Intersecting composition (atom fraction)	D^{Ni}_{AlAl}	D^{Ni}_{AlIr}	D^{Ni}_{IrAl}	D^{Ni}_{IrIr}	D^{Al}_{NiNi}	D^{Al}_{NiIr}	D^{Al}_{IrNi}	D^{Al}_{IrIr}
Ni–25Al vs. Ni–23Al–3Ir	Al: 0.24	1021.3	15.0	39.9	12.5	981.4	983.9	39.9	52.4
Ni–24Al vs. Ni–24Al–2Ir	Ir: 0.005								
Ni–25Al vs. Ni–23Al–2Ir	Al: 0.239	494.7	36.3	Ngl.	17.2	493.0	512.2	Ngl.	18.8
Ni–25Al vs. Ni–23Al–3Ir	Ir: 0.019								
Ni–26Al vs. Ni–23Al–2Ir	Al: 0.239	563.9	33.0	Ngl.	17.3	564.0	580.0	Ngl.	17.3
Ni–25Al vs. Ni–23Al–3Ir	Ir: 0.020								
Ni–24Al vs. Ni–24Al–2Ir	Al: 0.240	634.5	3.4	Ngl.	11.5	634.5	626.4	Ngl.	11.6
Ni–25Al vs. Ni–23.5Al–1Ir	Ir: 0.001								
Ni–24Al vs. Ni–24Al–2Ir	Al: 0.241	419.3	117.6	Ngl.	25.9	419.3	511.0	Ngl.	25.9
Ni–25Al vs. Ni–23Al–2Ir	Ir: 0.019								
Ni–25Al vs. Ni–23Al–2Ir	Al: 0.243	594.0	38.5	15.0	11.0	579.0	606.6	15.0	26.0
Ni–24.5Al vs. Ni–24.5Al–1Ir	Ir: 0.001								
Ni–25Al vs. Ni–23Al–2Ir	Al: 0.245	827.3	28.1	Ngl.	15.2	827.3	784.1	Ngl.	15.2
Ni–24.5Al vs. Ni–24.5Al–1Ir	Ir: 0.017								
Ni–25Al vs. Ni–23Al–3Ir	Al: 0.240	623.0	26.9	Ngl.	13.7	623.0	636.2	Ngl.	13.7
Ni–25Al vs. Ni–23.5Al–1Ir	Ir: 0.010								
Ni–25Al vs. Ni–23.5Al–1Ir	Al: 0.245	644.4	73.2	Ngl.	12.0	644.4	705.6	Ngl.	12.1
Ni–24.5Al vs. Ni–24.5Al–1Ir	Ir: 0.0002								

Note: Ngl. refers to magnitude less than 0.1 10 ^{16} m^2/s.

coefficient of Ir, respectively. In order to determine the ternary interdiffusion coefficients at these compositions, Boltzmann–Matano analysis was employed using a range of concentrations and distance that are certain with respect to EPMA measurement. The values of ternary interdiffusion coefficients determined in this study are reported in Table 5, and correspond well to the average ternary interdiffusion coefficients on either side of the Matano plane presented in Table 3.

Several relative maxima and minima in concentration profiles (e.g., vC_i=vx 0) were also observed for Ni in Ni–Al vs. Ni–Al–Ir couples and for Al in Ni–Al vs. Ni–Al–Ta couples as shown in Figs. 2 and 3. Ternary interdiffusion coefficients at these compositions were also determined since one of the terms in Eq. (1) becomes zero. These values are reported in Table 6 for Ni–Al vs. Ni–Al–Ir couples, and correspond well to the average ternary interdiffusion coefficients on either side of the Matano plane reported in Table 3, and ternary interdiffusion coefficients determined by Boltzmann–Matano analysis reported in Table 5. Unfortunately, for Ni–Al vs. Ni–Al–Ta couples, the concentration and its gradient for Ta, where the concentration gradient of Al becomes zero (e.g., relative maxima and minima of Al), were uncertain (e.g., $C_{Ta} \geq 0$ and vC_{Ta}=vx ≥ 0) to determine any ternary interdiffusion coefficients.

4.4. Estimation of binary interdiffusion coefficients in Ni_3Al

The ternary interdiffusion coefficients D^{Ni}_{AlAl} and D^{Al}_{NiNi} approach the binary D_i for Ni_3Al as the concentration of Ir or Ta decreases to zero. Hence, values of D_i i Ni or Al were estimated from ternary diffusion couples where Ir or Ta concentration was negligibly small in segments of the diffusion zone (e.g., Fick's law for substitutional binary alloys). Such regions were found in all couples since D_{IrIr} and D_{TaTa} coefficients are much smaller than D^{Ni}_{AlAl} and D^{Al}_{NiNi}. The D_i values extrapolated from the ternary couples with large enough concentration difference (e.g., DC_{Al} or $DC_{Ni} > 2$ at.%) in terminal alloys are presented in Fig. 7. The magnitude of D_i appears consistent with the available binary diffusion data [3–9] for Ni_3Al. However, the composition-dependence could not be evaluated correctly since this estimation is carried out near the terminal end of the concentration profiles with high uncertainty in the magnitude of concentration gradient for Al, and assumes that the Ir or Ta concentration, less than 2 at.%, do not influence the value of D_i.

4.5. Estimation of tracer diffusion coefficient of Ir and Ta in Ni_3Al

For component i diffusing into a binary alloy j–k, the cross-interdiffusion coefficient D^k_{ij} i≤j becomes negligible at infinite dilution of component i in a j–k alloy [61]. Then the value of the main coefficient D_{ii} approaches that of the tracer diffusion coefficient D^*_i for component i:

$$C_i \neq 0 \quad \tilde{D}_i \qquad D^k_{ii}\frac{vC_i}{vx} \quad D^*_{i\,jk}\frac{vC_i}{vx} \tag{7}$$

Thus, the tracer diffusion coefficients of Ir and Ta in Ni_3Al alloy can be estimated from the main interdiffusion coefficient of Ir, D^{Ni}_{IrIr}

Table 6
Ternary interdiffusion coefficients (10 ^{16} m^2/s) determined at relative maxima and minima of concentration profiles in Ni–Al vs. Ni–Al–Ir diffusion couples annealed at 1473 K for 5 h

Couple	Extrema composition (atom fraction)	Ternary interdiffusion coefficients at extrema		Extrema composition (atom fraction)	Ternary interdiffusion coefficients at extrema	
		D^{Al}_{NiIr}	D^{Al}_{IrIr}		D^{Al}_{NiIr}	D^{Al}_{IrIr}
Ni–25Al vs. Ni–23.5Al–1Ir	Al: 0.2452 Ir: 0.00037	737.4	12.5	Al: 0.2420 Ir: 0.0091	675	34.4
Ni–24.5Al vs. Ni–24.5Al–1Ir	Al: 0.2451 Ir: 0.00005	1190.4	12.0	Al: 0.2443 Ir: 0.0102	922.3	43.7
Ni–26Al vs. Ni–23Al–2Ir	Al: 0.2501 Ir: 0.001	656.5	18.9	Al: 0.245 Ir: 0.0186	617.6	22.2
Ni–25Al vs. Ni–23Al–2Ir	Al: 0.2453 Ir: 0.00045	552.2	12.4	Al: 0.2408 Ir: 0.0187	499.6	25.9
Ni–25Al vs. Ni–23Al–3Ir	Al: 0.2409 Ir: 0.00011	1195.6	8.8	Al: 0.2374 Ir: 0.0296	778.7	26.8

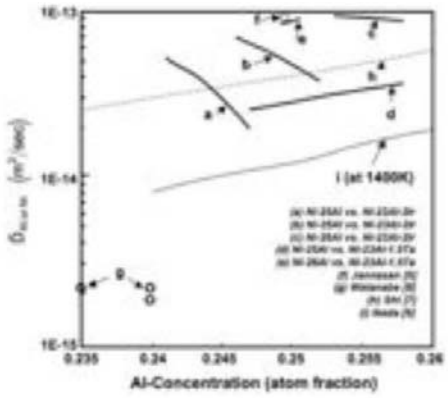

Fig. 7. Interdiffusion coefficients of Ni or Al in Ni_3Al at 1473 K compiled from this investigation and literature review.

or D^{Al}_{IrIr}, and Ta, D^{Ni}_{TaTa} or D^{Al}_{TaTa}, using Eq. (7), provided that the concentration of Ir or Ta approaches zero within the diffusion zone so that the cross-interdiffusion coefficients, D^{Ni}_{IrAl} or D^{Al}_{IrNi} and D^{Ni}_{TaAl} or D^{Al}_{TaNi}, become negligible. Such regions were found in all couples since D_{IrIr} and D_{TaTa} coefficients are much smaller than D^{Ni}_{AlAl} and D^{Al}_{NiNi}. Values of tracer diffusion coefficients of Ir, D^{*}_{Ir}, and Ta, D^{*}_{Ta}, were extrapolated from the main interdiffusion coefficients, D^{Ni}_{IrIr} or D^{Al}_{IrIr} and D^{Ni}_{TaTa} or D^{Al}_{TaTa}, as the concentration of Ir and Ta, respectively, becomes zero. The extrapolations for D^{*}_{Ir} and D^{*}_{Ta} from the ternary interdiffusion coefficients on the basis of Eq. (7) are presented in Figs. 8 and 9, respectively. The estimated values of D^{*}_{Ir} and D^{*}_{Ta} are reported in Table 7.

The estimated tracer diffusion coefficient for the b-site-occupying Ta (2.6 10 ^{16} 2.4 10 ^{16} m^2/s) is lower than that for the a-site-occupying Ir (14.7 10 ^{16} 1.4 10 ^{16} m^2/s). More importantly, at these dilute concentration of Ir and Ta, the magnitude of tracer diffusion coefficients of both Ir and Ta are very similar to ternary interdiffusion coefficients, namely D_{IrIr} (or $\tilde{D}_{IrIr}$) and D_{TaTa} (or $\tilde{D}_{TaTa}$).

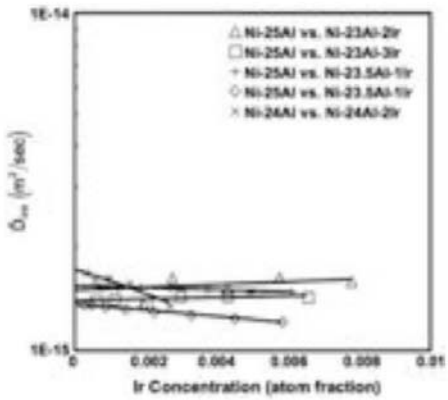

Fig. 8. Extrapolation of D_{IrIr} coefficient for the estimation of tracer diffusion coefficient of Ir in Ni_3Al at 1473 K.

Table 7
Tracer diffusion coefficients (10 ^{16} m^2/s) of Ir and Ta in Ni_3Al extrapolated from concentration profiles of ternary diffusion couples at 1473 K

Composition	Tracer component	D^{*}_{i} (10 ^{16} m^2/s)
75.4Ni–24.6Al	Ir	15.1
75.3Ni–24.7Al	Ir	14.6
75.5Ni–24.5Al	Ir	13.3
76.1Ni–24.1Al	Ir	13.6
76.2Ni–23.8Al	Ir	16.9
Average value for Ir		14.7 1.4
75.6Ni–24.3Al	Ta	0.6
75.1Ni–24.8Al	Ta	5.3
74.2Ni–25.8Al	Ta	2.0
Average value for Ta		2.6 2.4

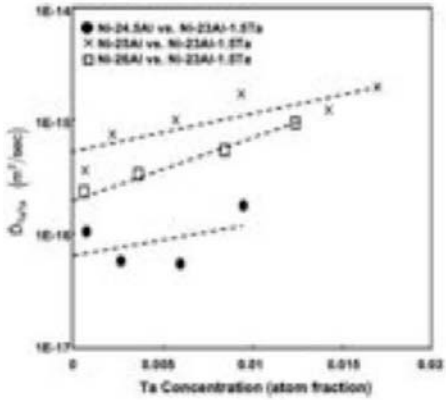

Fig. 9. Extrapolation of D_{TaTa} coefficient for the estimation of tracer diffusion coefficient of Ta in Ni_3Al at 1473 K.

5. Concluding remarks

Ternary interdiffusion interactions of Ir and Ta addition on the $L1_2$ Ni_3Al phase were examined using solid-to-solid diffusion couples annealed at 1473 K for 5 h. Average ternary interdiffusion coefficients were determined from an integration of interdiffusion fluxes for individual components. The magnitude of $\tilde{D}^{Al}_{NiNi}$ and $\tilde{D}^{Ni}_{AlAl}$ coefficients was determined to be much larger than that of $\tilde{D}_{IrIr}$ and $\tilde{D}_{TaTa}$ coefficients. The $\tilde{D}^{Al}_{NiIr}$ coefficient was determined to be positive and large in magnitude; Ir substitutes in Ni-site and influences the interdiffusion of Ni significantly. The $\tilde{D}^{Ni}_{AlTa}$ coefficient was positive and large in magnitude; Ta substitutes in Al-site and influences the interdiffusion of Al significantly. Ternary interdiffusion coefficients were also determined at compositions of intersecting diffusion paths, and at relative maxima and minima in concentration profiles for Ir-alloyed Ni_3Al. Consistency among ternary interdiffusion coefficients was observed. Profiles of concentrations were also examined to estimate binary interdiffusion coefficients in Ni_3Al. The results agreed well with published values. Tracer diffusion coefficients of Ir and Ta in Ni_3Al were also estimated as D^{*}_{Ir} 14.7 10 ^{16} 1.4 10 ^{16} m^2/s and D^{*}_{Ta} 2.6 10 ^{16} 2.4 10 ^{16} m^2/s at 1473 K.

The experiment and analysis reported herein demonstrate the practical use of analytical technique for multicomponent interdiffusion based on the determination and an integration of interdiffusion fluxes. The large magnitude of $\tilde{D}^{Al}_{NiIr}$ and $\tilde{D}^{Ni}_{AlTa}$ coefficients also signifies a correlation in ternary diffusional interactions and site-preference of ordered ternary intermetallic

alloys. In practical applications such as g′-Ni_3Al containing oxidation resistant coatings, Ir can substitute for Ni to reduce the interdiffusion fluxes of Ni from the Ni-rich superalloy substrate into the Al-rich oxidation resistant coatings [10–15]. Presence of Ta in Ni-base superalloy substrate can also reduce the interdiffusion fluxes of Al from the Al-rich coatings into the superalloy substrate. Microstructural stability of Ni-base superalloy can also improve by appropriate partitioning of Ir and Ta in g′-Ni_3Al precipitates and fcc-Ni matrix.

Acknowledgements

Financial support from CAREER Award of National Science Foundation (DMR-0238356) is gratefully acknowledged. Any opinions, findings, and conclusions or recommendations expressed in this manuscript are those of the authors and do not necessarily reflect the view of the National Science Foundation.

References

[1] Sims CT, Stoloff NS, Hagel WC. Superalloys II. New York, NY: John Wiley & Sons; 1987. p. 3–131.
[2] Campbell CE, Boettinger WJ, Kattner UR. Development of a diffusion mobility database for Ni-base superalloys. Acta Mater 2002;50:775–92.
[3] Cermak J, Rothova V. Concentration dependence of ternary interdiffusion coefficients in Ni_3Al/Ni_3Al–X couples with X Cr, Fe, Nb and Ti. Acta Mater 2003; 51:4411–21.
[4] Rothova V, Cermak J. Bulk and grain boundary diffusion of ^{67}Ga in Ni_3Al-cl influence of composition. Intermetallics 2005;13:113–20.
[5] Minamino Y, Yoshida H, Jung SB, Hirao K, Yamane T. Diffusion of platinum and molybdenum in Ni and Ni3Al. Defect Diffus Forum 1997;143–147:257–62.
[6] Janssen MMP. Diffusion in the nickel-rich part of the Ni–Al system at 1000 to 1300 C, Ni_3Al layer growth, diffusion coefficients and interface concentrations. Metall Trans 1973;4:1623–33.
[7] Shi Y, Frohberg G, Wever H. Diffusion of Ni and In in the g′-phase Ni_3Al. Phys Status Solidi A 1995;152:361–75.
[8] Watanabe M, Horita Z, Smith DJ, McCartney MR, Sano T, Nemoto M. Electron microscopy study of Ni/Ni[3]Al diffusion-couple interface. II: diffusivity measurement. Acta Metall Mater 1994;42:3389–96.
[9] Ikeda T, Almazouzi A, Numakura H, Koiwa M, Sprengel W, Nakajima H. Single-phase interdiffusion in Ni_3Al. Acta Mater 1998;46:5369–76.
[10] Wu YNA, Tsukuba J, Yamaguchi A, Tsukuba J, Kuroda S. Role of Iridium in hot corrosion resistance of Pt–Ir modified aluminide coatings with Na_2SO_4–NaCl salt at 1173 K. Mater Trans 2006;47:1918–21.
[11] Abe T, Ode M, Murakami H, Oh CS, Kocer C, Yamabe-Mitarai Y, et al. A thermodynamic description of the Al–Ir system. Mater Sci Forum 2007;539–543: 2389–94.
[12] Murakami H, Yamaguchi A, Wu YN, Kuroda S. Effect of Hf addition on high temperature properties of Ir-containing alloy coatings. Mater Sci Forum 2007; 546–549:1689–94.
[13] Wu YN, Yamaguchi A, Murakami H, Kuroda S. Hot corrosion behavior of Pt–Ir modified aluminide coatings on the nickel-base single crystal superalloy TMS-82 . J Mater Res 2007;22:206–16.
[14] Yamabe-Mitarai Y, Aoyagi T, Nishida K, Aoki H, Abe T, Murakami H. Phase equilibria between the B2, $L1_2$, and fcc phases in the Ir–Ni–Al system. Intermetallics 2007;15:479–88.
[15] Suzuki A, Wu YN, Yamaguchi A, Murakami H, Rae CMF. Oxidation behavior of Pt–Ir modified aluminized coatings on Ni-base single crystal superalloy TMS-82 . Oxi Metals 2007;68:53–64.
[16] Ochiai S, Oya Y, Suzuki T. Alloying behaviour of Ni_3Al, Ni_3Ga, Ni_3Si and Ni_3Ge. Acta Metall 1984;32:289–98.
[17] Guard RW, Westbrook JH. Alloying behaviour of Ni_3Al (g′phase). Trans TMS-AIME 1959;215:807–14.
[18] Decker RF, Mihalisin JR. Coherency strains in g hardened nickel alloys. Trans ASM 1969;62:481–9.
[19] Rawlings RD, Staton-Bevan AE. The alloying behaviour and mechanical properties of polycrystalline Ni_3Al (g′ phase) with ternary additions. J Mater Sci 1975;10:505–14.
[20] Chiba A, Shindo D, Watanabe S. Site occupation determination of Pd in Ni_3Al. Acta Metall Mater 1991;39:13–8.
[21] Chiba A, Hanada S, Watanabe S. Effect of g and g′ former doping on ductility of Ni_3Al. Scr Metall 1991;25:303–7.
[22] Chiba A, Hanada S, Watanabe S. Correlation between ductility and ordering energy of Ni_3Al. Mater Trans JIM 1990;31:824–7.
[23] Chiba A, Hanada S, Watanabe S. Ductilization of Ni_3 by microalloying with Ag. Scr Mater 1992;26:1031–6.
[24] Chiba A, Hanada S, Watanabe S. Improvement in ductility of Ni_3Al by g former doping. Mater Sci Eng A 1992;152:108–13.
[25] Gleeson B, Wang W, Hayashi S, Sordelet D. Effects of platinum on the interdiffusion and oxidation behavior of Ni–Al-based alloys. Mater Sci Forum 2004;461–464:213–22.
[26] Sluiter MHF, Kawazoe Y. Site preference of ternary additions in Ni_3Al. Phys Rev B 1995;51:4062–73.
[27] Ruban AV, Skriver HL. Calculated site substitution in ternary g′-Ni_3Al: temperature and composition effects. Phys Rev B 1997;55:8801–7.
[28] Enomoto M, Harada H. Analysis of g′/g equilibrium in Ni Al X alloys by the cluster variation method with the Lennard Jones potential. Metall Trans A 1989;20A:649–64.
[29] Mehrer H. Diffusion in intermetallics. Mater Trans JIM 1996;37:1259–80.
[30] Numakura H, Ikeda T, Koiwa M, Almazouzi A. Physics of condensed matter, structure, defects and mechanical properties. Philos Mag A 1998;77:887–909.
[31] Divinski SV, Frank S, Sodervall U, Herzig C. Solute diffusion of Al-substituting elements in Ni_3Al and the diffusion mechanism of the minority component. Acta Mater 1998;46:4369–80.
[32] Numakura H, Ikeda T, Nakajima H, Koiwa M. Diffusion in Ni_3Al, Ni_3Ga and Ni_3Ge. Mater Sci Eng A 2001;312:109–17.
[33] Minamino Y, Jung SB, Yamane T, Hirao K. Diffusion of cobalt, chromium, and titanium in Ni_3Al. Metall Trans A 1992;23:2783–90.
[34] Minamino Y, Yamane T, Saji S, Hirao K, Jung SB, Kohira T. Diffusion of copper, iron and silicon in $L1_2$-type intermetallic compound Ni_3Al. J Jpn Inst Metals 1994;58:397–403.
[35] Jung SB, Minamino Y, Yamane T. Diffusion of Mn in Ni and Ni_3Al. J Mater Sci Lett 1999;18:1063–6.
[36] Cermak J, Gazda A, Rothova V. Interdiffusion in ternary Ni_3Al/Ni_3Al–X diffusion couples with X Cr, Fe, Nb and Ti. Intermetallics 2003;11:939–46.
[37] Onsager L. Reciprocal relations in irreversible processes. Phys Rev 1931;37: 405–26;
Phys Rev 1932;38:2265–79.
[38] Onsager L. The diffusion of electrolytes and macromolecules in solution. Ann NY Acad Sci 1965;46:241–65.
[39] Fick A. Uber diffusion. Philos Mag 1855;10:30–9.
[40] Kirkaldy JS. Diffusion in multicomponent metallic systems. I. Phenomenological theory for substitutional solid-solution alloys. Can J Phys 1958;36: 899–906.
[41] Kirkaldy JS, Young DJ. Diffusion in the condensed state. London: The Institute of Metals; 1987. p. 226–72.
[42] Dayananda MA, Kim CW. Zero-flux planes and flux reversals in copper-nickel-zinc diffusion couples. Metall Trans A 1979;10A:1333–9.
[43] Dayananda MA. An analysis of concentration profiles for fluxes, diffusion depths, and zero-flux planes in multicomponent diffusion. Metall Trans A 1983;14A:1851–8.
[44] Kim CW, Dayananda MA. Identification of zero-flux planes and flux reversals in several studies of ternary diffusion. Metall Trans A 1983;14A:857–64.
[45] Kim CW, Dayananda MA. Zero-flux planes and flux reversals in the copper–nickel–zinc system at 775 . Metall Trans A 1984;15A:649–59.
[46] Dayananda MA, Behnke DA. Effective interdiffusion coefficients and penetration depths. Scr Metall 1991;25:2187–91.
[47] Dayananda MA. Average effective interdiffusion coefficients and the Matano plane composition. Metall Mater Trans A 1996;27A:2504–9.
[48] Dayananda MA, Sohn YH. Average effective interdiffusion coefficients and their applications for isothermal multicomponent diffusion couples. Scr Mater 1996;35:683–8.
[49] Dayananda MA, Sohn YH. A new analysis for the determination of ternary interdiffusion coefficients from a single diffusion couple. Metall Mater Trans A 1999;30A:535–43.
[50] Karunaratne MSA, Carter P, Reed RC. On the diffusion of aluminum and titanium in the Ni-rich Ni–Al–Ti system between 900 and 1200 C. Acta Mater 2001;49:861–75.
[51] Morimura T, Hasaka M, Nagata A. Ordered phase formation and diffusion composition path in Cu3Au/Pd couple. J Alloys Compd 2002;347:141–8.
[52] Bouchet R, Mevrel R. A numerical inverse method for calculating the interdiffusion coefficients along a diffusion path in ternary systems. Acta Mater 2002;50:4887–900.
[53] Bachorczyk R, Danielewski M, Filipek R. Interdiffusion under the chemical potential gradient; comparison of Onsager and Darken models. Defect Diffus Forum 2003;216–217:141–7.
[54] Moon J, Wynblatt P, Garoff S, Suter R. Pseudopartial wetting and precursor film growth in immiscible metal systems. Surf Sci 2004;559:149–57.
[55] Dawah-Tankeu P, Dorer L, Borchardt G, Gomann K, Pragnell WM, Evans HE, et al. Concentration dependence of the ternary interdiffusivities in the FeCrAl system at 1100 C. Mater High Temp 2005;22:375–84.
[56] Garimella N, Brady MP, Sohn YH. Interdiffusion in g (face-centered cubic) Ni–Cr–X (X Al, Si, Ge, or Pd) alloys at 900 C. J Phase Equilib Diffus 2006;27: 665–70.
[57] Kim S, Perepezko JH. Interdiffusion kinetics in the Mo_5SiB_2 (T_2) phase. J Phase Equilib Diffus 2006;27:605–13.
[58] Ram-Mohan LR, Dayananda MA. A transfer matrix method for the calculation of concentrations and fluxes in multicomponent diffusion couples. Acta Mater 2006;54:2325–34.
[59] Fujita H, Gosting LJ. An exact solution of the equations for free diffusion in three-component systems with interacting flows, and its use in evaluation of the diffusion coefficients. J Am Chem Soc 1956;78:1099–106.
[60] Pouchou JL, Pchoir F. A new model for quantitative X-ray microanalysis. I application to the analysis of homogeneous samples. Rech Aerosp (English Edition) 1984;3:13–38.
[61] Ziebold TO, Ogilvie RE. Ternary diffusion in copper–silver–gold alloys. Trans TMS-AIME 1967;239:942–53.

Journal of
PHASE EQUILIBRIA and DIFFUSION

Interdiffusion in L12-Ni3Al Alloyed with Re

ournal:	*Journal of Phase Equilibria and Diffusion*
anuscriptMID:M	MrautM
ManuscriptMDpe:M	MesearciMrticeM
DateMtui p itteMMDMi eM t uti sr:M	naaM
Msp peeteMistMuMuti srs:M	Marip eeatMiaraDana;NUniversitDMuMentraeMFesriMatMMut MrMMt EM MMetMiaci iEs;MiatisnaeMnstituteMsrMateriaesMcienceM IEeMatMiuraEap i;MKsi eMcteeeMs.tMtMM MuraEap itNEiMeDuEi;MiatisnaeMnstituteMsrMateriaesMcienceM csi ntMsnti s;NUniversitDMuMentraeMFesriMatMMut MrMMt EM
KeDu srMs:M	Msetsp annaMatansMnaeDsistMnterMiuusisntMeectrsnMprsi eM p icrsanaeDsisMeEuMt ;tMMiuusisnMcsupeestMMiuusivitDMcseuicienttM p ueicsp psnentMMiuusisntMi i3t eM

Interdiffusion in $L1_2$-Ni_3Al Alloyed with Re

N. Garimella[1], M. Ode[2], M. Ikeda[3], H. Murakami[2], Y.H. Sohn[1,*]

[1] Advanced Materials Processing and Analysis Center

Department of Mechanical, Materials and Aerospace Engineering

University of Central Florida, Orlando, FL, USA

[2] National Institute for Materials Science, Tsukuba, Japan

[3] Kobe Steel, Co. Ltd., Japan

* Corresponding Author

Keywords: Re, Ni_3Al, $L1_2$, intermetallics, high temperature alloys, ternary interdiffusion

Abstract

Ternary interdiffusion in $L1_2$-Ni_3Al with ternary alloying addition of Re was investigated at 1473K using solid-to-solid diffusion couples. Interdiffusion flux of Ni, Al and Re were directly calculated from experimental concentration profiles, and integrated for the determination of average ternary interdiffusion coefficients. The magnitude of main interdiffusion coefficients $\widetilde{\widetilde{D}}^{Al}_{NiNi}$ and $\widetilde{\widetilde{D}}^{Ni}_{AlAl}$ was determined to be much larger than that of the main interdiffusion coefficient $\widetilde{\widetilde{D}}^{Al\,(or\ Ni)}_{ReRe}$. A moderate tendency for Re to substitute for Al-sites was reflected by its influence on interdiffusion of Al, quantified by large and positive $\widetilde{\widetilde{D}}^{Ni}_{AlRe}$ coefficients. An excellent agreement was found with ternary interdiffusion coefficients determined by Boltzmann-Matano analysis. Profiles of concentrations and interdiffusion fluxes were also examined to estimate binary interdiffusion coefficients in Ni_3Al, and tracer diffusion coefficients of Re ($5.4 \times 10^{-16} \pm 2.3 \times 10^{-16}$ m^2/sec) in Ni_3Al.

1. Introduction

Ni_3Al precipitation and the associated coherency through tetragonal distortion with the γ-matrix is the key point behind the extensive use of Ni-base superalloys for high temperature applications [1]. Multicomponent diffusion plays an important role in processing and degradation of these alloys that must possess exceptional high temperature strength, microstructural stability and oxidation resistance. Multicomponent diffusion mobility database [2] for γ-phase, together with the alloying studies [3-10] to modify coherent precipitate (γ′) have yielded an excellent design criteria to develop advanced superalloys. Recent development of refractory-based superalloys with $L1_2$ precipitates, and refractory-modified aluminide coatings [11-16] warrant a better understanding of interdiffusion in Ni_3Al with alloying additions.

The ordered crystal structure of Ni_3Al consists of face-centers (α-sites) occupied by Ni-atoms and corners (α-sites) of the unit cell occupied by Al-atoms. Highly electronegative substitutional elements (e.g. Pt, Cu and Co) occupy the α sites, whereas highly electropositive ones (e.g. Ti, Ta and Nb) occupy the α sites in Ni_3Al [1]. The relative site-preference for a ternary alloying element can be best illustrated from the direction of the solubility lobes for the α phase on the ternary isotherm of Ni-Al-X (X = alloying addition) system at 1273K as shown by Figure 1 [17]. Site preference of ternary alloying additions to Ni_3Al has attracted significant interest as this true solid solution accepts considerable amount of third elements into solution [18-22].

The alloying phenomenon ultimately plays an important role in enhancing the thermomechanical properties and high temperature oxidation resistance of this intermetallic phase [19-26]. The substitutional ternary alloying additions to Ni_3Al was first classified by Guard and Westbrook [18] as Ni-occupiers or Al-occupiers or those with no preference. Several

studies [27-29] have examined the change in site preference of alloying elements as a function of temperature and chemical composition of Ni_3Al.

The diffusion mechanism in ordered alloys is more complex than disordered solid solutions [30]. Diffusion can occur preferentially through β or β site where Ni or Al atoms mainly occupy, respectively, and the diffusion coefficient largely depends on the alloy composition related to the degree of order [31-33]. While tracer diffusion studies in β' Ni_3Al are difficult since ^{26}Al is not readily available, self-diffusion of Ni and chemical/impurity diffusion in Ni_3Al binary and Ni_3Al-X ternary alloys (X= Ir, Ta, Pt, Nb, Mo, Cr, Fe, Ti) have been studied [3-6]. The temperature dependency of the diffusion for a ternary alloying addition is evident from Arrhenius rate law [34-36]. The β-site occupiers have been observed to diffuse slower than the β-site occupiers [30,37]. In $L1_2$-ordered structure each Ni atom is surrounded by 4 Al and 8 Ni atoms as nearest neighbors, where as an Al atom is surrounded by 12 Ni atoms as nearest neighbors. The β-sublattice forms a continuous network of nearest neighbors while the β-sublattice does not. Consequently, the activation enthalpy of alloying element can change due to the antisite-defect formation [37].

To further understand the diffusion process in $L1_2$ structure, to help improve the microstructural stability of Ni-base superalloys, and to help develop refractory-modified aluminide oxidation resistant coatings, we examined the ternary diffusional interaction of Re additions to the $L1_2$ Ni_3Al phase. Solid-to-solid diffusion couples were assembled with various Ni_3Al-Re alloys, and annealed at 1473K for 5 hours. Average ternary interdiffusion coefficients from an integration of interdiffusion fluxes, and ternary interdiffusion coefficients via Boltzmann-Matano analysis were determined from concentration profiles obtained by electron

probe microanalysis (EPMA). In addition, binary interdiffusion coefficients in Ni_3Al, and tracer diffusion coefficients of Re in Ni_3Al were estimated.

2. Determination of ternary interdiffusion coefficients

Based on Onsager's formalism [38,39] and Fick's law [40], the interdiffusion flux $\tilde{J}_i$ of component i in a ternary system can be expressed in terms of two independent concentration gradients, $\partial C_j/\partial x$ by:

$$\tilde{J}_i = -\tilde{D}^3_{i1}\frac{\partial C_1}{\partial x} - \tilde{D}^3_{i2}\frac{\partial C_2}{\partial x} \quad (i = 1,2) \tag{1}$$

where $\tilde{D}^3_{ij}$'s refer to the ternary interdiffusion coefficients. An experimental determination of the four concentration-dependent interdiffusion coefficients can be carried out by the use of Boltzmann-Matano analysis with two independent diffusion couples that develop a common composition in the diffusion zone where the interdiffusion coefficients can be evaluated [41,42].

Instead, the interdiffusion flux at any section x can be calculated directly from the concentration profile from the relation [43,44]:

$$\tilde{J}_i = \frac{1}{2t}\int_{C_i^- \text{ or } C_i^+}^{C_i=x=} (x - x_o)\, dC_i \quad (i = 1,2, \ldots, n) \tag{2}$$

where t is the time, C_i and C_i^{∞} are the terminal concentrations, and x_o refers to the location of the Matano plane. Use of Eq. (2) allows quantitative assessment of diffusional behavior for any components including zero-flux-planes (ZFPs) and flux-reversals that can develop during

multicomponent interdiffusion [43-46]. In addition, the calculated interdiffusion fluxes can be related to interdiffusion parameters that can be employed to model and characterize concentration profiles [47-50].

The interdiffusion flux $\tilde{J}_i$ determined from Eq. (2) can be integrated over a selected region, x_1 to x_2, to yield an expression based on Eq. (1) [50]:

$$\int_{x_1}^{x_2} \tilde{J}_i dx = -\int_{C_1(x_1)}^{C_1(x_2)} \tilde{D}_{i1}^3 dC_1 - \int_{C_2(x_1)}^{C_2(x_2)} \tilde{D}_{i2}^3 dC_2 \quad (i=1,2)$$
$$= \overline{\tilde{D}}_{i1}^3 \left[C_1(x_1) - C_1(x_2)\right] + \overline{\tilde{D}}_{i2}^3 \left[C_2(x_1) - C_2(x_2)\right] \quad (i=1,2) \tag{3}$$

where $\overline{\tilde{D}}_{ij}^3$'s correspond to the average values of main and cross interdiffusion coefficients. With $\overline{\tilde{D}}_{ij}^3$'s taken as constants, Eq. (1) is re-written as:

$$\tilde{J}_i = -\overline{\tilde{D}}_{i1}^3 \frac{C_1}{x} - \overline{\tilde{D}}_{i2}^3 \frac{C_2}{x} \quad (i=1,2) \tag{4}$$

If both sides of Eq. (4) are multiplied by $(x - x_o)^m$ and integrated over the diffusion zone between x_1 and x_2, one obtains in general [50]:

$$\int_{x_1}^{x_2} \tilde{J}_i (x - x_o)^m dx = -\overline{\tilde{D}}_{i1}^3 \int_{C_1(x_1)}^{C_1(x_2)} (x - x_o)^m dC_1 - \overline{\tilde{D}}_{i2}^3 \int_{C_2(x_1)}^{C_2(x_2)} (x - x_o)^m dC_2 \quad (i=1,2) \tag{5}$$

If the exponent m is chosen to be zero, Eq. (5) becomes identical to Eq. (3). For m=1, Eq. (5) becomes [50]:

$$\int_{x_1}^{x_2} \tilde{J}_i\,x\,x_o\,dx = \tilde{\bar{D}}_{i1}^{3} \int_{C_1(x_1)}^{C_1(x_2)} x\,x_o\,dC_1 + \tilde{\bar{D}}_{i2}^{3} \int_{C_2(x_1)}^{C_2(x_2)} x\,x_o\,dC_2$$

$$= 2t\left[\tilde{\bar{D}}_{i1}^{3}\left[\tilde{J}_1(x_1)\;\tilde{J}_1(x_2)\right] + \tilde{\bar{D}}_{i2}^{3}\left[\tilde{J}_2(x_1)\;\tilde{J}_2(x_2)\right]\right] \quad (i=1,2) \tag{6}$$

Eqs. (3) and (6) provide four equations to solve for $\tilde{\bar{D}}_{11}^{3}$, $\tilde{\bar{D}}_{12}^{3}$, $\tilde{\bar{D}}_{21}^{3}$ and $\tilde{\bar{D}}_{22}^{3}$ interdiffusion coefficients, and can be easily set up from experimental concentrations and the corresponding interdiffusion fluxes. Thus, from the concentration profiles of a single diffusion couple, $\tilde{\bar{D}}_{ij}^{3}$ (i,j = 1,2) coefficients, characteristic of the diffusion path, can be determined over selected composition ranges in the diffusion zone [50]. This analysis method has been directly employed in various studies [51-59] to determine average ternary interdiffusion coefficients. In this paper, this analysis applied to the experimental concentration profiles for 2 segments, one on either side of the Matano plane; the two chosen composition ranges are $(C_i' - C_i^o)$ and $(C_i^o - C_i'')$, where C_i^o refers to the concentration at the Matano plane. The average ternary interdiffusion coefficients, $\tilde{\bar{D}}_{ij}^{3}$'s, determined on either side of the Matano plane are employed to model experimental concentration profiles using error-function solution for infinite ternary system given by Fujita and Gosting [60].

3. Experimental details

Ni-Al and Ni-Al-Re alloys were prepared by the vacuum arc melting of 99.97 wt.% Ni, 99.9 wt.% Al, and 99.2 wt.% Re, according to the compositions presented in Table I. The alloys were cast into a semi-cylindrical mold with the diameter of 8 mm. The alloy rods were homogenized at 1473K for 137 hours in the vacuum furnace that was evacuated to a pressure lower than 10^{-2} Pa. The homogenized alloys were then sectioned into discs with an approximate height of 1.5 mm. The surfaces of alloy discs were ground metallographically down to 1200-grit and cleaned thoroughly prior to diffusion couple assembly.

Table II presents diffusion couples that were assembled and analyzed in this study. To promote initial bonding, coupled alloys were placed in a Si_3N_4 jig and annealed at 1473K for 0.5 hour in a vacuum furnace. The metal discs have larger thermal expansion coefficients than the Si_3N_4 jig, and the discs can adhere to each other due to the compression during the annealing treatment. Each diffusion couple fabricated in this manner was then sealed in an evacuated transparent quartz capsule, and annealed at 1473K for 4.5 hours in an atmosphere furnace. All diffusion couples were water quenched after the high-temperature anneal to preserve high temperature microstructure and concentrations. In this study, the time required for the diffusion bonding treatment (0.5 hour) was added to the total annealing time. Thus, concentration profiles from all diffusion couples were analyzed with diffusion anneal time of 5 hours.

Microstructural analysis by optical microscopy confirmed excellent bonding in all diffusion couples without any precipitation of other phases. Concentration profiles of the annealed diffusion couples were analyzed by JEOL-JXA-8900 EPMA. An accelerating voltage of 20 KeV, a beam current of 50 nA, and a probe diameter of 1 μm were employed for data acquisition of Ni K_μ x-radiation peak using LIF crystal, Al K_μ x-radiation peak using TAP

crystal, and Re L_{μ} x-radiation using LIFH crystal. Elemental standards of Ni, Al and Re along with ZAF [61] correction were employed for quantification of concentrations via point-to-point count technique.

4. Results and analysis

4.1. Profiles of concentrations and interdiffusion fluxes

Figure 2 presents typical concentration profiles obtained by EPMA from the diffusion couple, Ni-25Al vs. Ni-23.5Al-0.5Re annealed at 1473K for 5 hours. The x-axis is the distance from the Matano plane and the open circles represent EPMA measurement. Scatter in the concentration profiles for all diffusion couples were minimum and within the experimental uncertainty associated with EPMA. The interdiffusion fluxes of individual components were then determined using Eq. (2) from experimental concentration profiles that were smoothened with a series of weighted splines. Although no zero-flux plane was observed, a significant diffusional interaction between and Al and Re was observed when Ni_3Al was diffusion annealed against Ni_3Al alloyed with Re. As shown in Figure 2, interdiffusion of Al was reduced by the interdiffusion of Re against the gradient of Al. But, the diffusional influence of Re on Ni is difficult to ascertain from the profiles presented in Figure 2. Determination of ternary interdiffusion coefficients can quantify the extent of these diffusional interactions, and provide competent approaches to compositional design and modification of alloys and protective coatings.

4.2 Average ternary interdiffusion coefficients

From profiles of concentration and interdiffusion fluxes in Ni-Al vs. Ni-Al-Re diffusion couples, average ternary interdiffusion coefficients, $\overline{\tilde{D}}_{ij}^{Ni}(j=Al,Re)$ and $\overline{\tilde{D}}_{ij}^{Al}(j=Ni,Re)$, were determined on either side of the Matano plane using Eqs. (3) and (6). They are reported in Table III. The magnitudes of main diffusion coefficients, $\overline{\tilde{D}}_{AlAl}^{Ni}$ and $\overline{\tilde{D}}_{NiNi}^{Al}$ are similar to the interdiffusion coefficients of Al and Ni reported in literature for binary Ni_3Al at 1473K [3-10]. Estimation of binary interdiffusion coefficients from the ternary diffusion couples and the comparison to the interdiffusion coefficients of Al and Ni reported in literature for binary Ni_3Al are presented in detail in section 4.4. The main interdiffusion coefficient, $\overline{\tilde{D}}_{ReRe}$ is approximately 100 times smaller in magnitude than $\overline{\tilde{D}}_{AlAl}^{Ni}$ and $\overline{\tilde{D}}_{NiNi}^{Al}$. Table III reports that $\overline{\tilde{D}}_{AlRe}^{Ni}$'s are positive and comparable to the magnitude of $\overline{\tilde{D}}_{AlAl}^{Ni}$, while $\overline{\tilde{D}}_{ReAl}^{Ni}$ coefficients are negligibly small ($< 0.1 \times 10^{-16}$ m^2/sec). Thus the interdiffusion of Al can be strongly influenced by the interdiffusion of Re. The $\overline{\tilde{D}}_{NiRe}^{Al}$ coefficients are also positive, but 2 to 13 times smaller in magnitude than the $\overline{\tilde{D}}_{NiNi}^{Al}$'s.

The average ternary interdiffusion coefficients reported in Table III were employed to generate concentration profiles using error-function solution provided by Fujita and Gosting [60]. Excellent agreement between EPMA measurement and calculated concentration profiles were found for all couples. Typical examples are presented in Figure 2 where open circles are the EPMA data, and solid lines are the calculated concentration profiles.

4.3. Ternary interdiffusion coefficients determined by Boltzmann-Matno analysis

From the diffusion couples Ni-Al vs. Ni-Al-Re listed in Table II, several intersecting compositions were found within the diffusion paths. Intersecting diffusion paths in Figure 3 represent typical diffusion paths with one of the paths intersecting with its terminal end. In other

words, Re concentration of that end remained constant with no concentration gradient. These intersection composition points may be used for the determination of interdiffusion coefficients using Boltzmann-Matano analysis. The values of ternary interdiffusion coefficients determined in this study are reported in Table IV, and correspond well to the average ternary interdiffusion coefficients presented in Table III. Slight deviation in values and change in signs of the $\widetilde{\widetilde{D}}^{Al}_{NiRe}$ coefficients are attributed to the uncertainty in concentration gradient of Re.

4.4. Estimation of binary interdiffusion coefficients in Ni_3Al

The ternary interdiffusion coefficients $\tilde{D}^{Ni}_{AlAl}$ and $\tilde{D}^{Al}_{NiNi}$ approach the binary $\tilde{D}_i$ for Ni_3Al as the concentration of Re decreases to zero. Hence, values of $\tilde{D}_i$ (i μ Ni or Al) were estimated from ternary diffusion couples where Re concentration was negligibly small in segments of the diffusion zone (e.g., Fick's law for substitutional binary alloys). Such regions were found in all couples since $\widetilde{\widetilde{D}}_{ReRe}$ coefficients are much smaller than $\widetilde{\widetilde{D}}^{Ni}_{AlAl}$ and $\widetilde{\widetilde{D}}^{Al}_{NiNi}$. The $\widetilde{D}_i$'s extrapolated from the ternary couples with large enough concentration difference (e.g., μC_{Al} or $\mu C_{Ni} > 2$ at. %) in terminal alloys is presented in Figure 4. These values appear consistent with the available binary interdiffusion data [3-10] for Ni_3Al.

4.5. Estimation of tracer diffusion coefficient of Re in Ni_3Al

For a ternary component i diffusing into a binary alloy j-k, the cross interdiffusion coefficient $\widetilde{D}^{k}_{ij}$ (i μ j) becomes negligible at infinite dilution of component i in a j-k alloy [62]. Then the value of the main coefficient $\tilde{D}_{ii}$ approaches that of the tracer diffusion coefficient D^{μ}_{i} for component i:

$$C_i * 0 \quad \tilde{J}_i * \} \tilde{D}_{ii}^{k} \frac{*C_i}{*x} * \} D_{i*jk*}^{*} \frac{*C_i}{*x} \tag{7}$$

Thus, the tracer diffusion coefficients of Re in Ni_3Al alloy can be estimated from the main interdiffusion coefficient of Re, $\tilde{D}_{ReRe}^{Ni\ (or)\ Al}$, using Eq. (7), provided that the concentration of Re approaches zero within the diffusion zone so that the cross interdiffusion coefficients, $\tilde{D}_{ReAl}^{Ni}$ or $\tilde{D}_{ReNi}^{Al}$, become negligible. Such regions were found in all couples since $\tilde{\tilde{D}}_{ReRe}$ coefficients are much smaller than $\tilde{\tilde{D}}_{AlAl}^{Ni}$ and $\tilde{\tilde{D}}_{NiNi}^{Al}$. Values of tracer diffusion coefficients of Re, D_{Re}^{*} were extrapolated from the main interdiffusion coefficients, $\tilde{D}_{ReRe}^{Ni}$ or $\tilde{D}_{ReRe}^{Al}$ as the concentration of Re, becomes zero. The extrapolations for D_{Re}^{*} from the ternary interdiffusion coefficients on the basis of Eq. (7) are presented in Figure 5 for Ni-24.4 to 24.8 at.% Al. The estimated values of D_{Re}^{*} are reported in Table V.

5. Concluding remarks

Ternary interdiffusion interactions of Re addition on the $L1_2$ Ni_3Al phase was examined by using solid-to-solid diffusion couples annealed at 1473K for 5 hours. Average ternary interdiffusion coefficients were determined from an integration of interdiffusion fluxes for individual components. The magnitude of $\tilde{\tilde{D}}_{NiNi}^{Al}$ and $\tilde{\tilde{D}}_{AlAl}^{Ni}$ coefficients was determined to be much larger than that of $\tilde{\tilde{D}}_{ReRe}$ coefficients. The $\tilde{\tilde{D}}_{AlRe}^{Ni}$ coefficient was determined to be positive and large in magnitude; Re substitutes in Al-site and influences the interdiffusion of Al significantly. The $\tilde{\tilde{D}}_{NiRe}^{Al}$ coefficient was also positive but relatively low in magnitude; Re shows

a lower tendency to occupy Ni-sites. Consistency among ternary interdiffusion coefficients was observed from ternary interdiffusion coefficients determined by Boltzmann-Matano analysis. Profiles of concentrations were also examined to estimate binary interdiffusion coefficients in Ni_3Al. The results agreed well with published values. Tracer diffusion coefficient of Re at 1473K was also estimated as $D^{\rightarrow}_{Re} = 5.4 \times 10^{-16} \pm 2.3 \times 10^{-16}$ m^2/sec for Ni_3Al phase with Al concentration range of 24.4 to 24.8 at.%.

Acknowledgements

This study was financially supported by CAREER Award of National Science Foundation (DMR-0238356). Any opinions, findings, and conclusions or recommendations expressed in this manuscript are those of the authors and do not necessarily reflect the view of the National Science Foundation.

References

1. C.T. Sims, N.S. Stoloff and W.C. Hagel: Superalloys II, John Wiley & Sons, 1987.
2. C.E. Campbell, W.J. Boettinger and U.R. Kattner, Development of a diffusion mobility database for Ni-base superalloys, Acta Mater., 2002, **50**(4), p 775–92.
3. N. Garimella, M. Ode, M.Ikeda, H.Murakami and Y.H.Sohn, Effects of Ir and Ta alloying addition on interdiffusion of $L1_2$-Ni_3Al, Intermetallics., 2008, **16**(9), p 1095–1103.
4. J. Cermak and V. Rothova, Concentration dependence of ternary interdiffusion coefficients in Ni_3Al/Ni_3Al–X couples with X=Cr, Fe, Nb and Ti, Acta Mater., 2003, **51**(15), p 4411–21.
5. V. Rothova, J. Cermak and Bulk and grain boundary diffusion of ^{67}Ga in Ni_3Al—influence of composition , Intermetallics., 2005, **13**(1), p 113-20.
6. Y. Minamino, H. Yoshida, S.B. Jung and K. Hirao, T. Yamane, Diffusion of platinum and molybdenum in Ni and Ni_3Al, Defect Diff. Forum. 1997, 143-147, p 257–62.
7. M.M.P. Janssen, Diffusion in the Nickel-rich part of the Ni-Al system at 1000° to 1300°C, Ni_3Al layer growth, diffusion coefficients and interface concentrations, Metall. Trans., 1973, **4**(6), p 1623–33.
8. Y.Shi, G. Frohberg and H. Wever, Diffusion of Ni and In in the γ′-phase Ni_3Al, Phys.

Status Solidi A. 1995, **152**(2), p 361–375.
9. M. Watanabe, Z. Horita, D. J. Smith, M. R. McCartney, T. Sano and M. Nemoto, Electron microscopy study of Ni/Ni[3]Al diffusion-couple interface. II: Diffusivity measurement, Acta Metall. Mater., 1994, **42**(10), p 3389–96.
10. T. Ikeda, A. Almazouzi, H. Numakura, M. Koiwa and W. Sprengel, H. Nakajima, Single-phase interdiffusion in Ni_3Al, Acta Mater., 1998, **46**(15), p 5369–76.
11. Y.N.A. Wu, J. Tsukuba, A. Yamaguchi, J. Tsukuba and S. Kuroda, Role of Iridium in hot corrosion resistance of Pt-Ir modified aluminide coatings with Na_2SO_4-NaCl Salt at 1173 K, Mater. Trans., 2006, **47**(8), p 1918–21.
12. T. Abe, M. Ode, H. Murakami, C.S. Oh, C. Kocer, Y. Yamabe-Mitarai and H. Onodera, A thermodynamic description of the Al-Ir system, Mater. Sci. Forum, 2007, **539–543**(3), p 2389–94.
13. H. Murakami, A. Yamaguchi, Y.N. Wu and S. Kuroda, Effect of Hf addition on high temperature properties of Ir-containing alloy coatings, Mater. Sci. Forum. 2007, 546–**549**(3), p 1689–94.
14. Y.N. Wu, A. Yamaguchi, H. Murakami and S. Kuroda, Hot corrosion behavior of Pt-Ir modified aluminide coatings on the nickel-base single crystal superalloy TMS-82+, J. Mater. Res., 2007, **22**(1), p 206–16.
15. Y. Yamabe-Mitarai, T. Aoyagi, K. Nishida, H. Aoki, T. Abe and H. Murakami, Phase Equilibria between the B2, $L1_2$, and fcc phases in the Ir-Ni-Al System. Intermetallics. 2007, **15**(4), p 479–88.
16. A. Suzuki, YN. Wu, A. Yamaguchi, H. Murakami and C.M.F. Rae, Oxidation Behavior of Pt–Ir Modified Aluminized Coatings on Ni-base Single Crystal Superalloy TMS-82+, Oxi. Metals. 2007, **68**(1-2), p 53–64.
17. S. Ochiai, Y. Oya and T. Suzuki, Alloying behaviour of Ni_3Al, Ni_3Ga, Ni_3Si and Ni_3Ge, Acta Metall., 1984, **32**, p 289–98.
18. R.W. Guard and J.H. Westbrook, Alloying behaviour of Ni_3Al (γ'phase), Trans. TMS-AIME. 1959, **215**, p 807–14.
19. R. F. Decker and J. R. Mihalisin, Coherency strains in γ hardened nickel alloys, Trans. ASM, 1969, **62**, p 481–89.
20. R. D. Rawlings and A. E. Staton-Bevan, The alloying behaviour and mechanical properties of polycrystalline Ni_3Al ($\gamma\gamma$ phase) with ternary additions, J. Mater. Sci. 1975, **10**(3), p 505–14.
21. A. Chiba, D. Shindo and S. Watanabe, Site occupation determination of Pd in Ni_3Al, Acta. Metall. et Mat., 1991, **39**(1), p13–18.
22. A. Chiba, S. Hanada and S. Watanabe, Effect of γ and γ' former doping on ductility of Ni_3Al, Scripta Metall., 1991, **25**(2), p 303–07.
23. A. Chiba, S. Hanada and S. Watanabe, Correlation between ductility and ordering energy of Ni_3Al, Materials Transactions, JIM. 1990, **31**(9), p 824–27.
24. A. Chiba, S. Hanada and S.Watanabe, Ductilization of Ni_3Al by microalloying with Ag, Scripta Mater., 1992, **26**(7), p 1031–36.
25. A. Chiba, S. Hanada and S.Watanabe, Improvement in ductility of Ni_3Al by γ former doping, Mater. Sci. Eng. A, 1992, **152**(1-2), p108–13.
26. B. Gleeson, W. Wang, S. Hayashi and D. Sordelet, Effects of Platinum on the interdiffusion and oxidation behavior of Ni-Al-based alloys, Mater. Sci. Forum, 2004, **461-464**, p 213-22.

27. MHF Sluiter and Y. Kawazoe, Site preference of ternary additions in Ni_3Al, Phys. Rev. B, 1995, **51**(7), p 4062–73.
28. A.V. Ruban and H.L. Skriver, Calculated site substitution in ternary $\gamma\gamma$-Ni_3Al: Temperature and composition effects. Phys. Rev. B, 1997, **55**(14), p 8801–07.
29. M. Enomoto and H. Harada, Analysis of $\gamma\gamma'\gamma$ equilibrium in Ni Al X alloys by the Cluster Variation Method With the Lennard Jones Potential, Met. Trans. A. 1989, **20**(4), p 649–64.
30. H. Mehrer, Diffusion in intermetallics, Mater. Trans. JIM, 1996, **37**(6), p 1259–80.
31. H. Numakura, T. Ikeda, M. Koiwa and A. Almazouzi, Physics of condensed matter, structure, defects and mechanical properties, Phil. Mag. A, 1998, **77**(4), p 887–909.
32. S. V. Divinski, S. Frank, U. Sodervall and C. Herzig, Solute diffusion of Al-substituting elements in Ni_3Al and the diffusion mechanism of the minority component, Acta Mater., 1998, **46**(12), p 4369-80.
33. H. Numakura, T. Ikeda, H. Nakajima and M. Koiwa, Diffusion in Ni_3Al, Ni_3Ga and Ni_3Ge, Mater. Sci. Eng. A, 2001, **312**(1-2), p109–17.
34. Y. Minamino, S. B. Jung, T. Yamane and K. Hirao, Diffusion of Cobalt, Chromium, and Titanium in Ni_3Al. Met. Trans. A. 1992, **23**(10), p 2783–90.
35. Y. Minamino, T. Yamane, S. Saji, K. Hirao, S. B. Jung and T. Kohira, Diffusion of Copper, Iron and Silicon in $L1_2$-Type intermetallic compound Ni_3Al, J. Jap. Inst. Metals. 1994, **58**(4), p 397–403.
36. S.B. Jung, Y. Minamino and T. Yamane, Diffusion of Mn in Ni and Ni_3Al, J. Mater. Sci. Lett. 1999, **18**(13), p 1063-66.
37. J. Cermak, A. Gazda and V. Rothova, Interdiffusion in ternary Ni_3Al/Ni_3Al-X diffusion couples with X=Cr, Fe, Nb and Ti, Intermetallics, 2003, **11**(9), p 939–46.
38. L. Onsager, Reciprocal relations in irreversible processes, Phys. Rev. 1931, **37**, p 405–26 and 1932, **38**, p 2265–79.
39. L. Onsager, The Diffusion of Electrolytes and Macromolecules in Solution, Ann. NY Acad. Sci., **46** (1965) 241–65.
40. A. Fick, Uber Diffusion,Ann. Phys., 1855,**170**(1), p 59–86.
41. J.S. Kirkaldy, Diffusion in multicomponent metallic systems. I. Phenomenological theory for substitutional solid-solution alloys, Can. J. Phys. 1958, **36**, p 899–906.
42. J.S. Kirkaldy and D.J. Young, Diffusion in the Condensed State, The Institute of Metals, London, 1987, p 226–272.
43. M.A. Dayananda and C.W. Kim, Zero-flux planes and flux reversals in copper-nickel-zinc diffusion couples, Metall. Trans. A. 1979, **10**(9), p1333–39.
44. M.A. Dayananda, An analysis of concentration profiles for fluxes, diffusion depths, and zero-flux planes in multicomponent diffusion, Metall. Trans. A, 1983, **14A**(9), p 1851–58.
45. C.W. Kim and M.A. Dayananda, Identification of zero-flux planes and flux reversals in several studies of ternary diffusion, Metall. Trans. A. 1983, **14A**(5), p 857–64.
46. C.W. Kim and M.A. Dayananda, Zero-flux planes and flux reversals in the copper-nickel-zinc system at 775°, Metall. Trans. A. 1984, **15A**(4), p 649–59.
47. M.A. Dayananda and D.A. Behnke, Effective interdiffusion coefficients and penetration depths, Scripta Metall., 1991, **25**(9), p 2187–91.
48. M.A. Dayananda, Average effective interdiffusion coefficients and the Matano plane composition, Metal. Mater. Trans. A. 1996, **27**(9), p 2504–09.

49. M.A. Dayananda and Y.H. Sohn, Average effective interdiffusion coefficients and their applications for isothermal multicomponent diffusion couples, Scripta Mater., 1996, **35**(6), p 683–88.
50. M.A. Dayananda and Y.H. Sohn, A new analysis for the determination of ternary interdiffusion coefficients from a single diffusion couple, Metall. Mater. Trans. A. 1999, **30**(3), p 535-43.
51. M. S. A. Karunaratne, P. Carter and R. C. Reed, On the diffusion of Aluminum and Titanium in the Ni-rich Ni–Al–Ti system between 900 and 1200° C, Acta Mater., 2001, **49**(5), p 861-75.
52. R. Bouchet and R. Mevrel, A numerical inverse method for calculating the interdiffusion coefficients along a diffusion path in ternary systems, Acta Mater., 2002, **50**(19), p 4887-900.
53. T. Morimura, M. Hasaka and A. Nagata, Ordered Phase Formation and Diffusion Composition Path in Cu_3Au/Pd Couple, J. Alloys and Compounds, 2002, **347**(1-2), p 141-48.
54. R. Bachorczyk, M. Danielewski and R. Filipek, Interdiffusion under the Chemical Potential Gradient; Comparison of Onsager and Darken Models, Defect Diff. Forum. 2003, 216-217, p 141-47.
55. J. Moon, P. Wynblatt, S. Garoff and R. Suter, Pseudopartial wetting and precursor film growth in immiscible metal systems, Surf Sci., 2004, **559**(2-3), p 149-57.
56. P. Dawah-Tankeu, L. Dorer, G. Borchardt, K. Gomann, W.M. Pragnell, H.E. Evans and J. L. Coze, Concentration dependence of the ternary interdiffusivities in the FeCrAl System at 1100C, Mater. High Temp., 2005, **22**(3-4), p 375-84.
57. N. Garimella, M.P. Brady and Y.H. Sohn, Interdiffusion in γ (face-centered cubic) Ni-Cr-X (X =Al, Si, Ge, or Pd) alloys at 900 °C, J. Phase. Equil. Diff. 2006, **27**(6), p 665-70.
58. S. Kim, JH Perepezko, Interdiffusion kinetics in the Mo_5SiB_2 (T_2) phase, J. Phase. Equil. Diff., 2006, **27**(6), p 605-13.
59. L.R. Ram-Mohan and M.A. Dayananda, A transfer matrix method for the calculation of concentrations and fluxes in multicomponent diffusion couples, Acta Mater., 2006, **54**(9), p 2325-34.
60. H. Fujita and L.J. Gosting, An exact solution of the equations for free diffusion in three-component systems with interacting flows, and its use in evaluation of the diffusion coefficients, J. Am. Chem. Soc., 1956, **78**(6), p 1099–106.
61. J. L. Pouchou and F. Pchoir, A new model for quantitative X-ray microanalysis. I Application to the analysis of homogeneous samples, Recherche Aerospatiale, 1984, (3), p 13-38.
62. T.O. Ziebold and R.E. Ogilvie, Ternary diffusion in copper-silver-gold alloys, Trans. TMS-AIME., 1967, **239**(7), p 942–53.

List of Tables

1. Nominal composition of alloys employed for diffusion couple studies.
2. Diffusion couples assembled and analyzed after anneal at 1473K for 5 hours.
3. Average ternary interdiffusion coefficients (10^{-16} m^2/s) determined from Ni-Al vs. Ni-Al-Re diffusion couples annealed at 1473K for 5 hours.
4. Ternary interdiffusion coefficients (10^{-16} m^2/s) determined by Boltzmann-Matano analysis from Ni-Al vs. Ni-Al-Re diffusion couples annealed at 1473K for 5 hours.
5. Tracer diffusion coefficients (10^{-16} m^2/s) of Re in Ni_3Al extrapolated from ternary interdiffusion coefficients of diffusion couples annealed at 1473K.

List of Figures

Table I: Nominal composition of alloys employed for diffusion couple studies.

Alloy Identification	Composition (atom percent)			Composition (weight percent)		
	Ni	Al	Re	Ni	Al	Re
Ni-24.5Al	75.5	24.5	0.0	58.6	41.4	0.0
Ni-25Al	75.0	25.0	0.0	57.9	42.1	0.0
Ni-26Al	74.0	26.0	0.0	56.7	43.3	0.0
Ni-23.5Al-0.5Re	76.0	23.5	0.5	59.7	40.2	0.1
Ni-23.5Al-0.7Re	75.8	23.5	0.7	59.6	40.2	0.2

Table II: Diffusion couples assembled and analyzed after an anneal at 1473K for 5 hours.

Diffusion Couples
Ni-24.5Al vs. Ni-23.5Al-0.5Re
Ni-24.5Al vs. Ni-23.5Al-0.7Re
Ni-25Al vs. Ni-23.5Al-0.5Re
Ni-26Al vs. Ni-23.5Al-0.7Re

Table III. Average ternary interdiffusion coefficients (10^{-16} m^2/s) determined from Ni-Al vs. Ni-Al-Re diffusion couples annealed at 1473K for 5 hours.

Diffusion Couple	Composition Range	$\tilde{D}^{Ni}_{AlAl}$	$\tilde{D}^{Ni}_{AlRe}$	$\tilde{D}^{Ni}_{ReAl}$	$\tilde{D}^{Ni}_{ReRe}$	$\tilde{D}^{Al}_{NiNi}$	$\tilde{D}^{Al}_{NiRe}$	$\tilde{D}^{Al}_{ReNi}$	$\tilde{D}^{Al}_{ReRe}$
Ni-24.5Al vs. Ni-23.5Al-0.5Re	$-C_i^{-\infty} \sim C_i^{o}-$	417.7	380.2	Ngl.	3.8	417.7	33.7	Ngl.	3.8
	$-C_i^{o} \sim C_i^{-\infty}-$	265.1	191.0	Ngl.	4.0	265.1	70.1	Ngl.	4.0
Ni-24.5Al vs. Ni-23.5Al-0.7Re	$-C_i^{-\infty} \sim C_i^{o}-$	509.9	463.4	Ngl.	4.5	509.9	42.0	Ngl.	4.5
	$-C_i^{o} \sim C_i^{-\infty}-$	362.8	304.1	Ngl.	3.4	362.8	55.3	Ngl.	3.4
Ni-25Al vs. Ni-23.5Al-0.5Re	$-C_i^{-\infty} \sim C_i^{o}-$	463.2	294.6	Ngl.	3.8	463.2	164.8	Ngl.	3.8
	$-C_i^{o} \sim C_i^{-\infty}-$	668.3	477.4	Ngl.	2.4	668.3	188.5	Ngl.	2.4
Ni-26Al vs. Ni-23.5Al-0.7Re	$-C_i^{-\infty} \sim C_i^{o}-$	449.9	336.6	Ngl.	5.8	449.9	107.5	Ngl.	5.8
	$-C_i^{o} \sim C_i^{-\infty}-$	298.9	123	Ngl.	4.7	298.9	171.2	Ngl.	4.7

Note: Ngl refers to magnitude less than 0.1 x 10-16 m2/sec.

Table IV. Ternary interdiffusion coefficients (10^{-16} m^2/s) determined by Boltzmann-Matano analysis from Ni-Al vs. Ni-Al-Re diffusion couples annealed at 1473K for 5 hours.

Diffusion Couples with Intersecting Diffusion Paths	Intersecting Composition (atom fraction)	$\tilde{D}^{Ni}_{AlAl}$	$\tilde{D}^{Ni}_{AlRe}$	$\tilde{D}^{Ni}_{ReAl}$	$\tilde{D}^{Ni}_{ReRe}$	$\tilde{D}^{Al}_{NiNi}$	$\tilde{D}^{Al}_{NiRe}$	$\tilde{D}^{Al}_{ReNi}$	$\tilde{D}^{Al}_{ReRe}$
Ni-24.5Al vs. Ni-23.5Al-0.5Re Ni-25Al vs. Ni-23.5Al-0.5Re	Al: 0.239 Re: 0.005	832.5	926.5	Ngl.	2.8	832.5	-96.8	Ngl.	2.8
Ni-24.5Al vs. Ni-23.5Al-0.5Re Ni-24.5Al vs. Ni-23.5Al-0.7Re	Al: 0.2382 Re: 0.005	244.2	216.0	Ngl.	3.1	244.2	25.0	Ngl.	3.1
Ni-25Al vs. Ni-23.5Al-0.5Re Ni-24.5Al vs. Ni-23.5Al-0.7Re	Al: 0.2393 Re: 0.005	726.1	734.9	Ngl.	3.1	726.1	-11.9	Ngl.	3.1

Note: Ngl refers to magnitude less than 0.1 x 10^{-16} m^2/sec.

Table V. Tracer diffusion coefficients (10^{-16} m^2/s) of Re in Ni_3Al extrapolated from ternary interdiffusion coefficients of diffusion couples annealed at 1473K.

Composition	Tracer Component	D_i^* (10^{-16} m^2/sec)
75.2Ni-24.8Al	Re	4.0
75.6Ni-24.4Al	Re	8.1
75.5Ni-24.5Al	Re	4.1
Average Values		5.4 ± 2.3

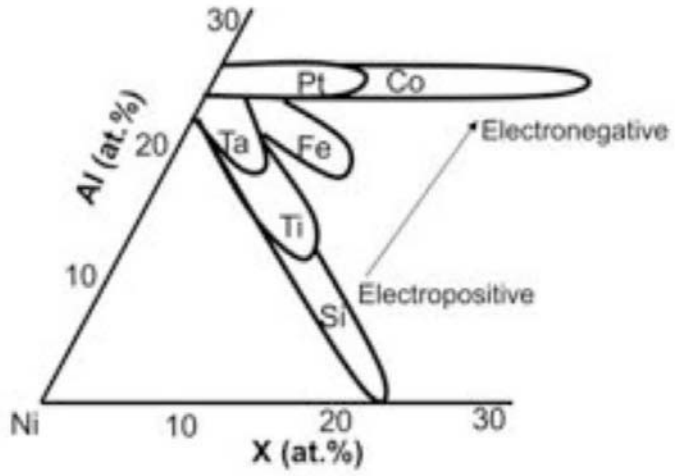

Solubility ranges of selected ternary alloying additions in yir al at 1f 7r K [11]d
1o1ubi mm yr oo u r oo 7PK)

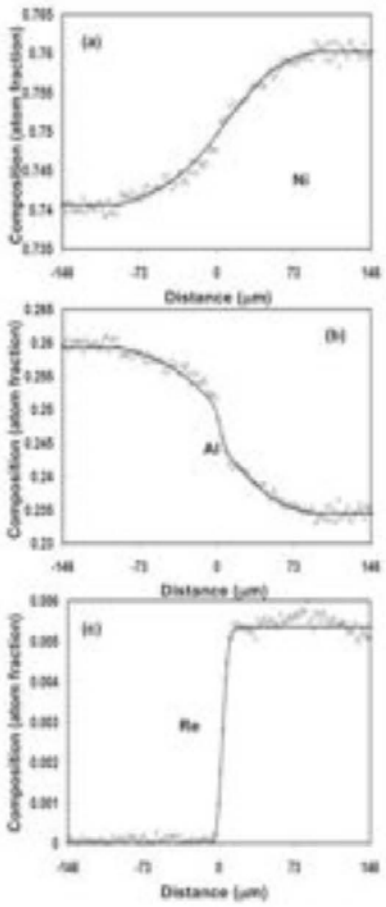

Concentration profiles of (a) Ni, (b) Al and (c) Re obtained fro diffl sion col ple Ni-b5Al vs. Ni-bo.5Al-r .5Re annealed at 1(7oK for 5 hol rs. Open circles and solid lines represent , P- A easl re ent and calcl lated concentration profiles, respectively.
1r 1cbor (orr c orr s PI)

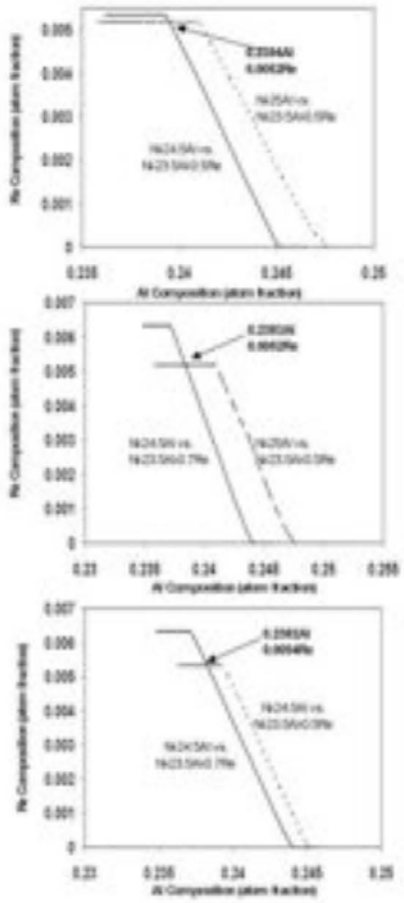

Typixagrinte0Dextingrdiffgd3nrpathDr3frNiMAgrwD.rNiMAgNRerdiffgD3nrx3gpgeDrannegedratrn473Krf30r5m
h3g0D.rf3mp3Dti3nDratrtheDerinte0Dexti3nDrde0erempg3yedrf30rtherndete0minati3nr3frte0ra0ym
inte0diffgD3nrx3effixientDr3aDedrn3nrh3gzmannNMatan3ranagyDD.rm
101x21t mmn4300rxrn300rDPI)rm

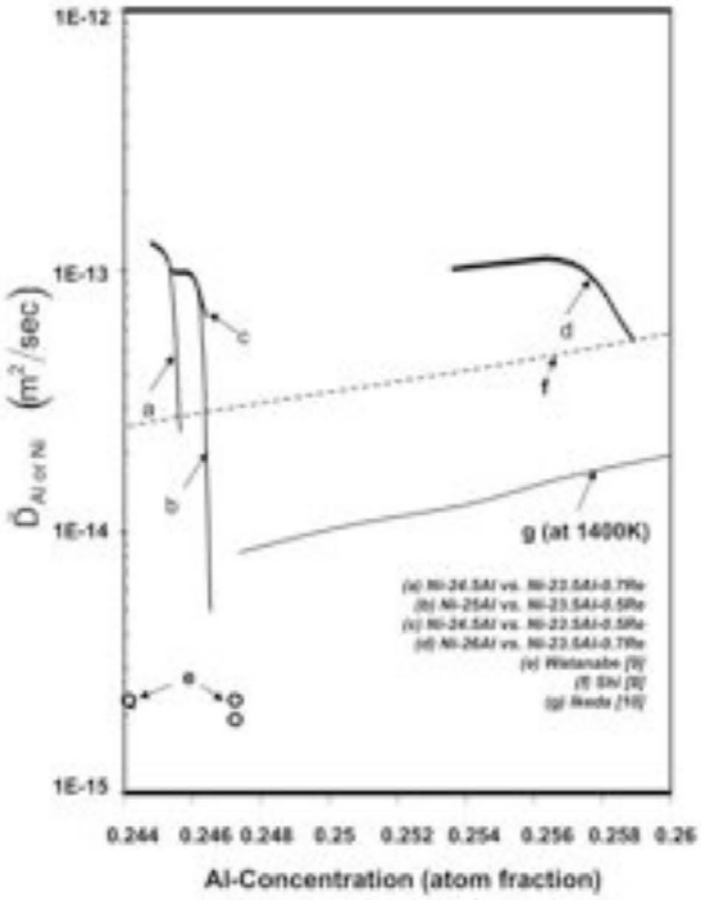

Inte0diffgD3nm3effixientDimrNi3Agatm1473Km3mpigedrf03mrthiDinveDtigati3nrandngte0atg0er0evied.m
101x130mmn4300nn300nDPI)rm

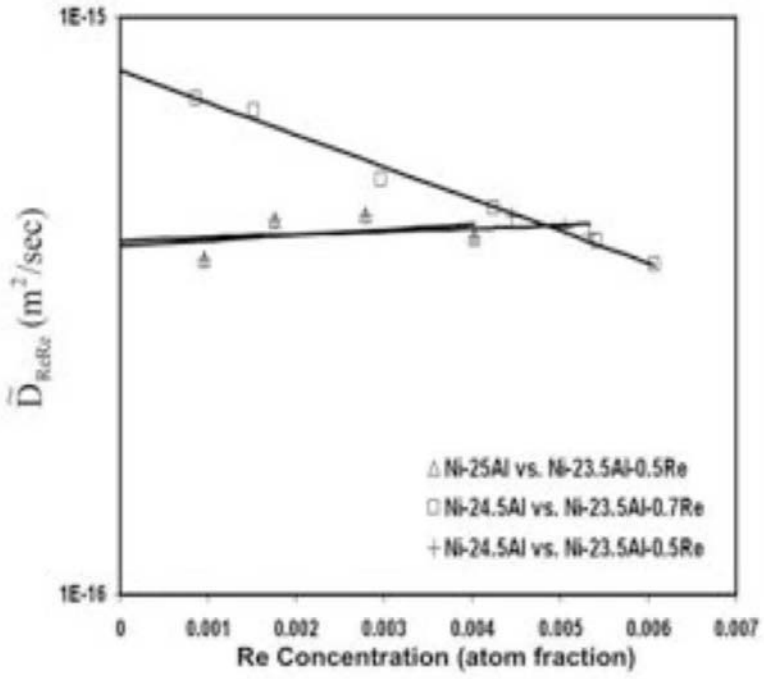

Ext0ap3gati3nr3frD0ReRem3effixientrf30rthemaDtimati3nr3frt0axe0rdiffgDi3nr3effixientr3frRerinrNi3Agatm
1473K.rm
101xt 1mmrA300nrn300rDPI)rm

APPENDIX B : MATLAB PROGRAM FOR INTERDIFFUSION ANALYSIS

B.1 Matano Plane Determination

```
% EXPORT TEXT FILE%
% NAME THAT DATA FILE AS 'A'%
% SPECIFY 'DF'. THAT IS LENGTH OF THE DATA POINTS DF= NUMBER %
DF1=DF-1;
rev=DF+1;
for i=1:DF;
   D(i,1)=i-1;
end;
for i=2:DF;
D1(i,1)=0;E1(i,1)=0;
D1(i,1)=(D(i)-D(i-1))*((C1(i))+(C1(i-1)))/2;
E1(i,1)=(D(i)-D(i-1))*((C2(i))+(C2(i-1)))/2;
end;
F1=(sum(D1(1:DF))-(D1(DF)*D(DF)))/(C1(1)-C1(DF));
F2=(sum(E1(1:DF))-(E1(DF)*D(DF)))/(C2(1)-C2(DF));
xx=(F1+F2)/2;
ND=D-xx;
for i=1:DF;
   x(i,1)=xx;
c1(i,1)=C1(rev-i);
c2(i,1)=C2(rev-i);
end;
for i=2:DF;
d1(i,1)=0;e1(i,1)=0;
d1(i,1)=(D(i)-D(i-1))*((c1(i))+(c1(i-1)))/2;
e1(i,1)=(D(i)-D(i-1))*((c2(i))+(c2(i-1)))/2;
end;
f1=(sum(d1(1:DF))-(d1(DF)*D(DF)))/(c1(1)-c1(DF));
f2=(sum(e1(1:DF))-(e1(DF)*D(DF)))/(c2(1)-c2(DF));
xr=(f1+f2)/2;
nd=D-xr;
```

B.2 Diffusion Coefficients Determination

```
%INPUT TIME OF THE ANNEAL IN HOURS, AS e.g. time=168 %
% INPUT MULTI TO DISPLAY DIFFUSION COEFFICIENT VALUES IN MULTI TIMES 10^-8
% cm^2/sec' e.g. multi=10000;%
for i=2:DF;
for n=1:100; G(1,n)=0;
G(i,n)=(C1(i)-C1(i-1))*((ND(i)^n)+(ND(i-1)^n))/2;
end;
end;
for i=2:DF;
for n=1:100; H(1,n)=0;
H(i,n)=(C2(i)-C2(i-1))*((ND(i)^n)+(ND(i-1)^n))/2;
end;
end;
for i=1:DF;
G1(i,1)=G(i,1);
H1(i,1)=H(i,1);
end;
for i=2:DF; J1(1)=0+(G1(1)*(1/(2*time*3600)));
J1(i,1)=J1(i-1)+(G1(i)*(1/(2*time*3600)));
end;
for i=2:DF; J2(1)=0+(H1(1)*(1/(2*time*3600)));
J2(i,1)=J2(i-1)+(H1(i)*(1/(2*time*3600)));
end;
for i=2:DF;J1d(1)=0;J2d(1)=0;
J1d(i,1)=(ND(i)-ND(i-1))*((J1(i))+(J1(i-1)))/2;
J2d(i,1)=(ND(i)-ND(i-1))*((J2(i))+(J2(i-1)))/2;
end;
for i=2:DF;
for n=1:100;O(1,n)=0;P(1,n)=0;
O(i,n)=(ND(i)-ND(i-1))*((J1(i)*ND(i)^n)+(J1(i-1)*ND(i-1)^n))/2;P(i,n)=(ND(i)-
ND(i-1))*((J2(i)*ND(i)^n)+(J2(i-1)*ND(i-1)^n))/2;
end;
end;
for i=2:DF;
for n=1:100; g(1,n)=0;
g(i,n)=(c1(i)-c1(i-1))*((nd(i)^n)+(nd(i-1)^n))/2;
end;
end;
for i=2:DF;
for n=1:100; h(1,n)=0;
h(i,n)=(c2(i)-c2(i-1))*((nd(i)^n)+(nd(i-1)^n))/2;
end;
end;
for i=1:DF;
g1(i,1)=g(i,1);
h1(i,1)=h(i,1);
end;
for i=2:DF; j1(1)=0+(g1(1)*(1/(2*time*3600)));
j1(i,1)=j1(i-1)+(g1(i)*(1/(2*time*3600)));
end;
for i=2:DF; j2(1)=0+(h1(1)*(1/(2*time*3600)));
```

```
j2(i,1)=j2(i-1)+(h1(i)*(1/(2*time*3600)));
end;
for i=2:DF;j1d(1)=0;j2d(1)=0;
j1d(i,1)=(nd(i)-nd(i-1))*((j1(i))+(j1(i-1)))/2;
j2d(i,1)=(nd(i)-nd(i-1))*((j2(i))+(j2(i-1)))/2;
end;
for i=2:DF;
for n=1:100;o(1,n)=0;p(1,n)=0;
o(i,n)=(nd(i)-nd(i-1))*((j1(i)*nd(i)^n)+(j1(i-1)*nd(i-1)^n))/2;p(i,n)=(nd(i)-
nd(i-1))*((j2(i)*nd(i)^n)+(j2(i-1)*nd(i-1)^n))/2;
end;
end;
for n=1:100;
D12R(n,1)=multi*((((sum(o(1:k1,n))/     sum(-g(1:k1,n)))-(     sum(j1d(1:k1))/
(c1(1)-c1(k1))))/((  (sum(-h(1:k1,n)))/  (sum(-g(1:k1,n))))-(  (c2(1)-c2(k1))/
(c1(1)-c1(k1))))));
end;
for n=1:100;
D11R(n,1)=multi*((((sum(o(1:k1,n))/     sum(-h(1:k1,n)))-(     sum(j1d(1:k1))/
(c2(1)-c2(k1))))/((  (sum(-g(1:k1,n)))/  (sum(-h(1:k1,n))))-(  (c1(1)-c1(k1))/
(c2(1)-c2(k1))))));
end;
for n=1:100;
D21R(n,1)=multi*((((sum(p(1:k1,n))/     sum(-h(1:k1,n)))-(     sum(j2d(1:k1))/
(c2(1)-c2(k1))))/((  (sum(-g(1:k1,n)))/  (sum(-h(1:k1,n))))-(  (c1(1)-c1(k1))/
(c2(1)-c2(k1))))));
end;
for n=1:100;
D22R(n,1)=multi*((((sum(p(1:k1,n))/     sum(-g(1:k1,n)))-(     sum(j2d(1:k1))/
(c1(1)-c1(k1))))/((  (sum(-h(1:k1,n)))/  (sum(-g(1:k1,n))))-(  (c2(1)-c2(k1))/
(c1(1)-c1(k1))))));
end;
for n=1:100;
D12(n,1)=multi*((((sum(O(1:k,n))/  sum(-G(1:k,n)))-(  sum(J1d(1:k))/  (C1(1)-
C1(k))))/((  (sum(-H(1:k,n)))/  (sum(-G(1:k,n))))-(  (C2(1)-C2(k))/  (C1(1)-
C1(k))))));
end;
for n=1:100;
D11(n,1)=multi*((((sum(O(1:k,n))/  sum(-H(1:k,n)))-(  sum(J1d(1:k))/  (C2(1)-
C2(k))))/((  (sum(-G(1:k,n)))/  (sum(-H(1:k,n))))-(  (C1(1)-C1(k))/  (C2(1)-
C2(k))))));
end;
for n=1:100;
D21(n,1)=multi*((((sum(P(1:k,n))/  sum(-H(1:k,n)))-(  sum(J2d(1:k))/  (C2(1)-
C2(k))))/((  (sum(-G(1:k,n)))/  (sum(-H(1:k,n))))-(  (C1(1)-C1(k))/  (C2(1)-
C2(k))))));
end;
for n=1:100;
D22(n,1)=multi*((((sum(P(1:k,n))/  sum(-G(1:k,n)))-(  sum(J2d(1:k))/  (C1(1)-
C1(k))))/((  (sum(-H(1:k,n)))/  (sum(-G(1:k,n))))-(  (C2(1)-C2(k))/  (C1(1)-
C1(k))))));
end;
```